ASTRONOMICAL OBSERVATORY for SHUTTLE

Phase A Study

FINAL REPORT

January 1973

Prepared for

NATIONAL AERONAUTICS AND SPACE ADMINISTRATION
Manned Spacecraft Center
Houston, Texas

BALL BROTHERS RESEARCH CORPORATION
SUBSIDIARY OF BALL CORPORATION
BOULDER, COLORADO

BALL BROTHERS RESEARCH CORPORATION

BOULDER, COLORADO

ASTRONOMICAL OBSERVATORY for SHUTTLE

Phase A Study

FINAL REPORT

January 1973

Prepared for the
Manned Spacecraft Center
Houston, Texas
Under Contract
NAS9-13094

PREPARED

D. L. Guthals
Program Manager

APPROVED

R. H. Gablehouse
Director,
Space Sciences

Page Intentionally Left Blank

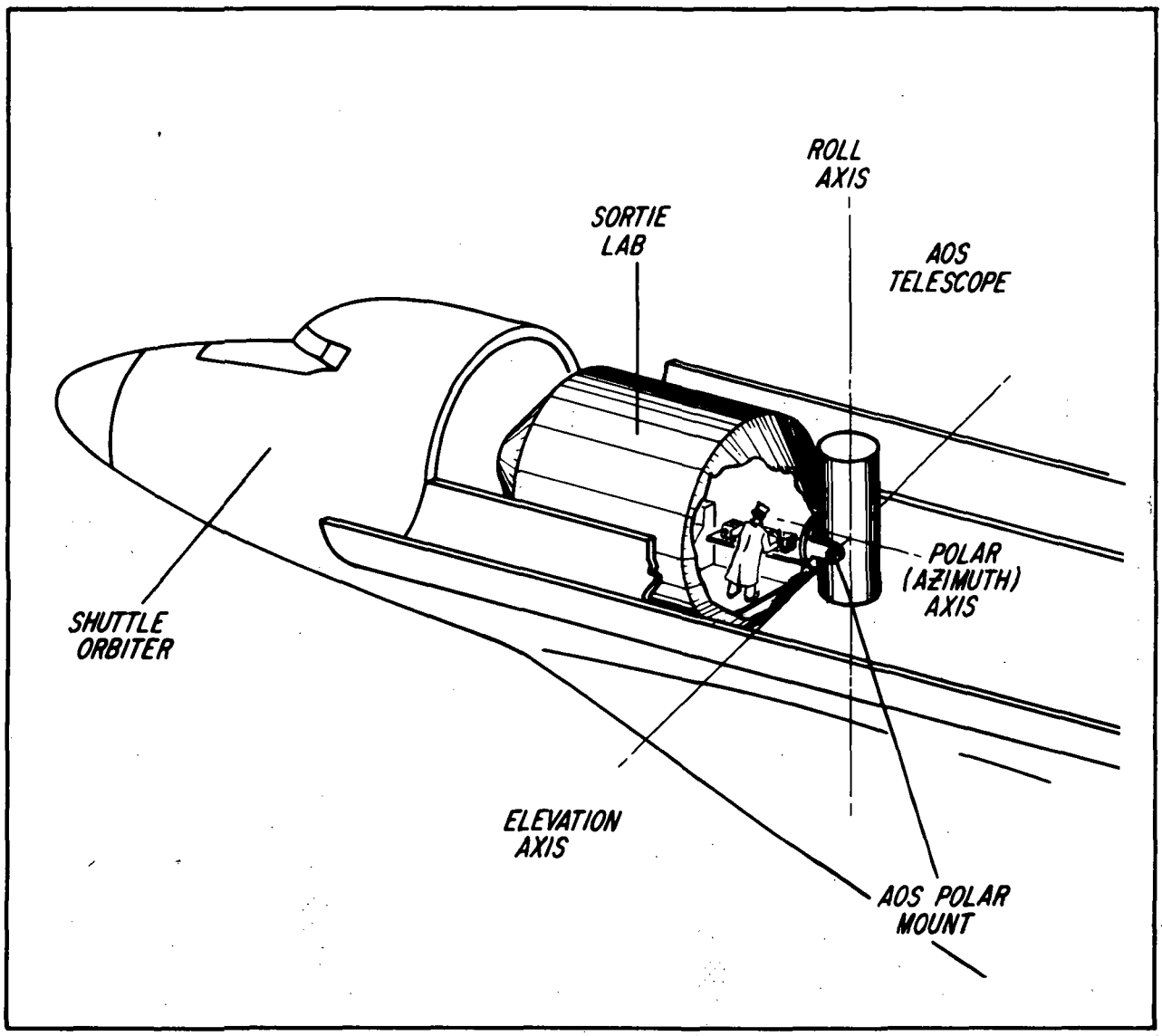

Astronomical Observatory for Shuttle

PREFACE

This Study for the Astronomical Observatory for Shuttle was performed with the NASA/Manned Spacecraft Center by Ball Brothers Research Corporation under Contract NAS9-13094. The BBRC Program Manager was Mr. D. L. Guthals, and the NASA direction of the Study was effected through a working group of MSC astronomers comprising

Dr. R. T. Guili (Co-Chairman)

Dr. H. M. Heckathorn

Dr. K. G. Henize

Dr. Y. Kondo (Chairman)

Dr. T. L. Page

Dr. R. A. Parker

CONTENTS

CONTENTS (Cont.)

ILLUSTRATIONS

ILLUSTRATIONS (Cont.)

ILLUSTRATIONS (Cont.)

ILLUSTRATIONS (Cont.)

ILLUSTRATIONS (Cont.)

TABLES

Section 1
INTRODUCTION

The proposed Astronomical Observatory for Shuttle (AOS) is conceived with the objective of providing an observatory from which astronomers can conduct *in situ* observations. The AOS study has resulted in a concept definition of the major hardware components for this observatory.

The AOS concept utilizes a pointed and stabilized one-meter telescope with the capability of operating at two focal ratios, f/10 and f/25. The study presents a preliminary design of such a telescope and identifies the inherent advantages and disadvantages associated with it. In addition, the study conceptually defines a variety of basic spectroscopic and image recording instruments and detectors which will permit a large variety of astronomical observations to be made in the wavelength range of 900 to 7000 Å.

The AOS concept requires that only current technology be incorporated at any time, but that future technological developments may easily be incorporated. This requirement produces reliability and minimizes cost.

The AOS concept of modular instrumentation combines laboratory incremental growth capability with incremental funding. This permits flexible growth with the current economy.

The study guidelines were established by MSC. Among these were:

- The AOS is to use a 1-meter aperture telescope in two f-ratio configurations.
- An airlock will be available in which the various instruments can be mounted.

- The payload and mission specialists will be in a "shirtsleeve" environment and will have access to the telescope focal plane.
- The spectral range to be covered is 900 - 7000 Å.
- A Sortie Lab is considered available and can be appropriately modified to accept the AOS.
- Baseline instrument spectral resolution capability is to be 0.1 Å for spectral imagery and 0.01 Å for spectrography.
- Near diffraction-limited performance should be achieved over as wide a field as possible.
- A team of mission specialists will be on hand to assist the payload specialists during AOS operation.
- Spectroscopy of point sources and extended objects shall be performed with the baseline instruments.
- Bandpass photometry instrumentation is desired.
- Visual access to the telescope focal plane must be permitted.
- Photometric calibration is to be accomplished in real time wherever possible.
- The AOS is not to depend on detached or erected payload operation or on EVA.

- The study should utilize the results of previous study efforts wherever possible.

In addition, certain assumptions were provided by MSC regarding mission operations:

- The study is to assume dedicated missions for astronomy.
- There will be no restrictions to shuttle vehicle orientations in or relative to the orbital plane.
- Mission-dependent data will not be a part of this study. (i.e., orbital altitudes, solar and lunar proximities, etc., will be considered elsewhere.)
- Up and down communication links will be provided.

Section 2 summarizes the results of the study.

Page Intentionally Left Blank

Section 2
AOS SUMMARY

2.1 STUDY OBJECTIVES

The Astronomical Observatory for Shuttle (AOS) study is a Phase A effort which culminates in a preliminary conceptual design of a shuttle-borne astronomy observatory operational concept, and preliminary developmental schedules and costs. The study baselines and constraints were established by a working group of astronomers at the NASA Manned Spacecraft Center in Houston, Texas.

The AOS concept is a shuttle-borne observatory which is provisioned with an inventory of general purpose instrumentation for use *in situ* by members of the scientific community. The inventory instruments shall provide moderate performance for imaging and spectroscopy at ultraviolet and visible wavelengths. Other instruments which are designed for special purposes may also be employed for a particular observing program. Maximum flexibility and simplicity of operation is obtained by providing the observer with direct access to the focal plane of the telescope in a "shirt-sleeve" environment.

The use of general purpose instrumentation and the operating philosophy of the AOS are comparable to that used at ground-based observatories. The astronomer will be in orbit with the instrumentation and will be an integral part of the operation. The AOS utilizes man to functionally control target acquisition, accomplish precise image positioning, evaluate the data in real time, make decisions affecting the observing program, and provide routine calibration and servicing of the instrumentation.

2.2 CONFIGURATION

The major components for the AOS consist of: Telescope, echelle spectrograph, imaging spectrograph, SEC vidicon and electronographic detector systems, offset guidance system, and an optical bench. The performance of the AOS instrumentation is summarized in Table 2-1. Performance is based on computer ray traces and preliminary pointing control studies. The AOS configuration is shown in Figure 2-1. The telescope is mounted outside the Sortie Lab, whereas the focal plane and instrumentation are accessible to the observer inside the Sortie Lab.

The telescope, which is supplied with two secondary mirrors for either f/10 or f/25 operation, is bearing-mounted to the aft bulkhead of the Sortie Lab. The mount permits telescope motion within a 90° arc about the "azimuth" axis and a 30° arc about the "elevation" axis (see Figure 2-1).

Internal to the telescope, between the primary and secondary mirrors, is a tertiary mirror. A bearing-driven intermediate servo coarsely positions the tertiary mirror cell to reflect the beam into the airlock. Within the cell is the fine position servo for the tertiary mirror. This is a two axis servo which performs the final positioning of the image at the telescope focal plane.

Internal to the Sortie Lab and aligned to the azimuth axis of the telescope is an optical bench on which the various instrumentation packages and the fine guidance error sensor are mounted. The optical bench is bearing-mounted and provides image roll position control as well as telescope focus adjustment. Roll position error information is derived from a sensor which is mounted orthogonally to the telescope optical axis.

Table 2-1
AOS TELESCOPE AND SPECTROGRAPH PERFORMANCE

Telescope

Type - Ritchey Chrétien at f/25/Modified Coudé

Aperture - 1 meter

f/Ratios - f/25 or f/10

Useful Field Diameter -- 30 arc-min at f/25
-- 34 arc-min at f/10

Image Diameter - 0.4 arc-sec at -- 11.0 arc-min at f/25 (80 mm dia.)
0.3 arc-sec at -- 13.75 arc-min at f/10 (40 mm dia.)

Pointing Accuracy - 0.028 arc-sec rms, f/25
0.077 arc-sec rms, f/10

Echelle Spectrograph

Spectral Range - 1150-7000 Å (3 ranges)

Resolving Power - 1.2×10^5

Imaging Spectrograph

Spectral Range - 1150-7000 Å (multiple ranging)

Resolving Power - 10^4

Lyman Spectrometer

Spectral Range - 900-1200 Å

Resolving Power - 10^4

2.3 AOS OPTICAL SYSTEM

2.3.1 Telescope Assembly

The telescope assembly chosen for the AOS is designed to form ~0.2 arc-second images over a 14 arc-minute field. A one-meter primary is used in combination with one of two selectable secondary mirrors to give the assembly an effective focal length of either 10 or 25 meters. The figure of the mirrors is chosen so that

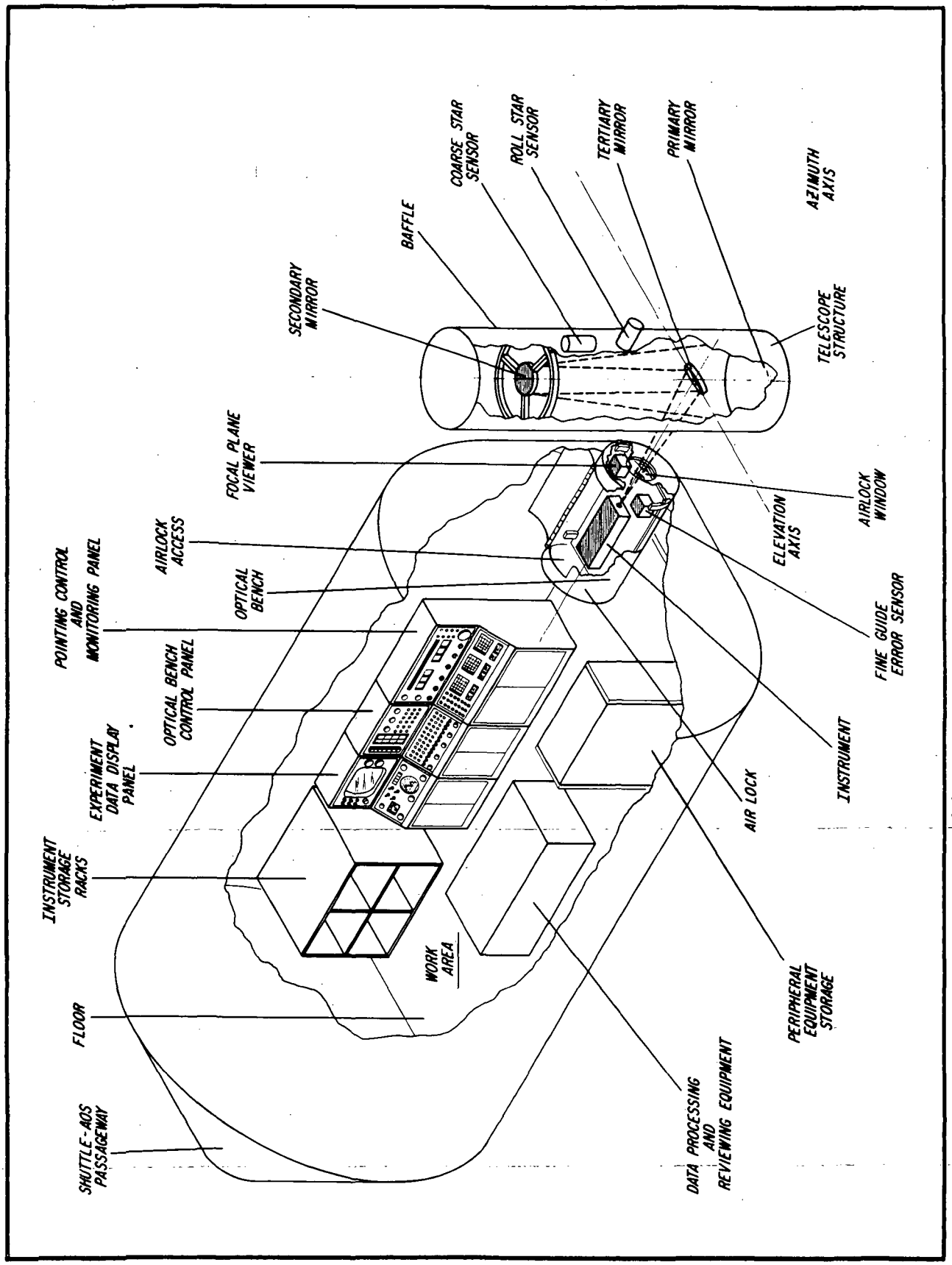

Figure 2-1 AOS Configuration

the Ritchey-Chretien criteria are satisfied at f/25 and spherical aberration is corrected at f/10. A plane, tertiary mirror redirects the beam from the telescope axis to the focal plane within the Sortie Lab. The telescope is thus a Coudé in effect, but the two rigidly mounted mirrors of the Coudé are replaced in the AOS by a single mirror which must be accurately and actively aligned in two axes, thus compensating for both azimuth and elevation errors in the telescope axis which result from vehicle motion.

Although a specific structural concept has not been selected, a monocoque structure appears to have certain advantages from a thermal stability viewpoint. The thermal analysis run indicates that a combined insulation/ heater package will be required. The monocoque structure concept is more adaptable to this type of thermal control.

Several mirror materials and coatings were examined. The trade-offs indicate that a primary of fused silica and a secondary of Cervit C-101, both flashed with aluminum and overcoated with magnesium fluoride, will be required.

Telescope performance is determined by the combination of residual aberrations and smearing due to guidance errors. Preliminary guidance studies indicate that this latter effect dominates in all cases at the shorter wavelengths. At the longer wavelengths, ray traces show that the image degradation due to coma in the f/10 configuration becomes a significant contributor near the edge of the fields. Table 2-2 gives the Rayleigh criterion resolution of the system as determined from computer ray tracing and includes optical quality and pointing accuracy considerations.

Table 2-2
SYSTEM RAYLEIGH RESOLUTION
(Includes Pointing Error)

Configuration	Field Half Angle (arc-min/mm)	Resolution on Flat Plane (arc-sec)	
		1216Å	6563Å
f/10	0/0	0.21	0.25
	2.0/5.8	0.21	0.25
	6.875/20	0.23	0.28
	10.0/29	--	0.72
	13.75/40	--	0.78
	17.0/49.5	--	0.80
f/25	0/0	0.09	0.16
	2.75/20	0.13	0.16
	5.5/40	0.15	0.17
	10.0/72.7	--	*2.6
	15.0/109.1	--	*5.6

*Resolution degraded primarily due to curved focal surface.

2.3.2 Echelle Spectrograph

The design for an echelle spectrograph provides a resolving power of ~10^5 over the 1150 - 7000 Å range in approximately one octave segments. The design is similar to the one proposed for LST but has no aspherical elements. An approximately one-meter focal length is used.

When configured for high resolution, an f/10 camera is used, and the spectrum is recorded with an SEC vidicon. A second configuration is available using a fast electronographic camera. The cameras can be interchanged during flight. Table 2-3 gives limiting magnitudes of the spectrograph when viewing different star types.

Table 2-3

AOS LIMITING MAGNITUDES (m_v)*

Wavelength (Angstroms)	Telescope Efficiency	SEC Quantum Efficiency	SEC-Echelle** (0.01 Å resolution)			SEC Imaging** (0.1 Å resolution)			Film*** D=.6 (500 Å band)		
			O5V	A0V	G2V	O5V	A0V	G2V	O5V	A0V	G2V
1200	.55	.09	13.3	9.1	-4.5	17.7	13.5	-0.1	---	---	---
2500	.64	.20	14.9	12.1	8.2	17.9	15.2	11.3	22.6	22.4	16.0
4000	.70	.20	14.0	13.7	11.2	17.0	16.7	14.2	21.0	20.8	18.3
6000	.66	.07	11.4	11.6	10.1	14.4	14.6	13.1	18.9	19.1	17.6

* The O5V fluxes are taken from Hickok and Morton, Ap.J. 152, 203, 1968.
The A0V fluxes are taken from Mihalas, Ap.J. Suppl. 114, 1966.
The G2V (solar) fluxes are taken from Brinkman, et al., JPL Technical Report No. 32-951.

** For the SEC a signal to noise ratio of 5:1 is used. Also, the table does not take into account the effect of pre-amplifier noise. It is assumed that optimum photocathode materials are used at each wavelength. A single photocathode is not appropriate at all wavelengths.

*** The table is for exposure times of 30 minutes on un-reddened stars.
103a-J is used at 2500 Å and 4000 Å. 103a-E is used at 6000 Å.

Note: Electronographic echelle and imaging spectrographs with 0.05 Å and 1.0 Å spectral resolutions, respectively, attain effectively the same limiting magnitudes as those given above for the SEC spectrographs.

2.3.3 Imaging Spectrograph

An imaging spectrograph has been designed to provide a spectral resolving power of ~10^4 over the full field in the dispersion direction, and 0.35 arc-seconds spatial resolution along the slit. An f/10 camera is provided for operation with an SEC vidicon. A fast electronographic camera can be used at f/1. The cameras and spectral segments are interchangeable in flight. Spectrograph limiting magnitude performance is given in Table 2-3.

2.4 OPERATION

The AOS is to be operated by a crew of mission and payload specialists. Although the AOS has many automated features, the presence of man will reduce laboratory cost by reducing the number of automated systems required to maintain a large variety of operational modes.

2.4.1 Equipment Installation and Removal

To perform a specific experiment, the payload specialist will select the appropriate equipment and install it on the optical bench inside the airlock. The optical bench will have a set of registration surfaces and locks to which the equipment will have been previously aligned. Fine alignment may be accomplished in vacuum by motor driven lead screws positioning the optical bench. This may be done by remote control from the Optical Bench Control Panel, or by direct access to the instrumentation package.

2.4.2 Data Handling

Data will be either electronically stored or stored in emulsions. Spectral or imaging data that is electronically derived will be processed and stored in an on-board recorder and may also be telemetered to the ground. In addition to being stored, the data can be displayed on the Experiment Data Display Monitor for real time interaction and evaluation by the payload specialist. It is also possible that proven "wet or dry" developing systems will be developed which will permit *in situ* evaluation of emulsions.

2.4.3 Focus Checks

The payload specialist will have the capability of checking and adjusting telescope focus from the Optical Bench Control Panel. A mirror is inserted in the light path directing energy to an SEC vidicon. The output of the vidicon is processed by a scan converter and displayed on the TV monitor. In addition, he will be able to make test exposures in the focal plane. Automatic focus for the AOS was considered but discarded since the presence of man made for a less costly and simpler approach.

2.4.4 Acquisition and Guidance

The AOS telescope will use offset guiding. Offset guidance is chosen so that all wavelengths above 900 Å from a selected target can be presented at the science focal plane and so that dim or diffuse targets can be observed.

Targets are acquired and tracking is initiated by the payload specialist at the Pointing Control and Monitoring Panel. First the telescope is slewed to within 30 arc-minutes of the selected

target. A shuttle-provided, on-board inertial platform is used for reference and the appropriate azimuth and elevation angles are determined by the computer. Coarse guidance is then initiated using a coarse star sensor mounted on the telescope. This sensor automatically acquires a bright star in its 5° circular field of view and initiates tracking. The star can then be identified and the offset trimmed. The active servo can then hold the telescope to within approximately 1 arc-minute of the target. An intermediate servo system then rotates the tertiary mirror cell so that the mirror normal bisects the airlock-tertiary-target angle.

Fine error sensing is accomplished with a star sensor mounted on the optical bench in the airlock. It tracks a guide star located in the off-axis region of the telescope's field of view. Dynamic corrections are applied to the tertiary mirror in two axes to keep the target on axis to within 0.077 arc-seconds rms at f/10 or 0.028 arc-seconds rms at f/25.

Image roll control is also required and is accomplished by rotating the optical bench in response to error signals generated by a second coarse star sensor mounted orthogonally to the first.

Section 3
TELESCOPE ASSEMBLY

3.1 SYSTEM REQUIREMENTS

In order to perform the anticipated experiments with the desired accuracy, the AOS telescope should:

- Have a 1 meter diameter collecting aperture.
- Be capable of operation at both f/10 and f/25, using the same primary mirror and with a fixed image plane location that is accessible in a shirtsleeve environment.
- Provide as high a spatial resolution as possible over a 40 mm diameter image format at both f-numbers without refractive correctors. A resolution of 0.2 arc-second is the design goal. At f/10, reduced resolution is preferable to reduced ultraviolet response.
- Have at least a 34 arc-minute total unvignetted field of view at f/10 and 30 minute field at f/25, to allow the fine tracker to observe off-axis guide stars.
- Maintain the minimum practical central obscuration.
- Be stable in the shuttle environment although periodic refocusing is assumed.
- Be baffled against direct star light outside the field.

- Incorporate a folding (tertiary) mirror, located at the telescope center of gravity, for fine guidance control.

The configuration selected is summarized in Table 3-1.

3.2 CONFIGURATION

Figure 3-1 is a layout of the f/25 telescope. Figure 3-2 is a layout of the f/10 telescope. They use a common primary mirror, a common primary mirror baffle, a common telescope tube, a common tertiary mirror, and a common image location. The tertiary mirror articulates to stabilize the image.

To switch the f-number of the telescope, the secondary mirror and secondary mirror baffle are exchanged and the telescope is realigned optically. This conversion is presently conceived as a ground-based operation.

Details of the telescopes are presented in their appropriate sections.

3.3 OPTICAL DESIGN

3.3.1 Obscuration Considerations and Primary Mirror Focal Ratio

Refer to Table 3-2 for a summary of the notation used in this discussion. When designing a telescope a balance must be reached between several conflicting parameters in order to optimize its performance and its manufacturability. These parameters include obscuration ratio, baffled field, primary mirror focal ratio, back focal distance, tertiary mirror location, and mirror surface figure. To optimize performance a small central obscuration is required. Figures 3-3 and 3-4 show the effect on MTF of apodization by the central obscuration. The obscuration should be minimized but

Table 3-1

TELESCOPE PARAMETERS

Two different f/numbers available with common primary mirror, primary baffle, and tertiary mirror, and different secondary mirrors and secondary baffles.

	f/25	f/10
Type:	Ritchey-Chretien(within manufacturing tolerance of a true Cassegrain, with paraboloidal primary and hyperboloidal secondary)	Secondary selected to yield zero third order spherical aberration
Clear Aperture:	1.0 meter diameter	1.0 meter diameter
Stop Location:	At primary mirror	At primary mirror
f/Number Primary:	f/3	f/3
f/Number Telescope:	f/25	f/10
Resolution:	Better than 0.2 arc-sec over 40 mm diameter field	Better than 0.3 arc-sec over 40 mm diameter field
Wavelength Range-Science Field:	1200 Å - 7000 Å	1200 Å - 7000 Å
Resolution-Tracker Field:	0.5 arc-sec over 30 arc-min diameter field	3.3 arc-sec over 34 arc-min diameter field
Tracker Refracting Corrector:	Yes	No
Wavelength Range Used-Tracker Field:	3650 Å - 7000 Å	2000 Å - 4000 Å
Primary Mirror Material:	Fused Silica	Fused Silica
Primary Mirror Construction:	Honeycomb Weight-Relieved Structure	Honeycomb Weight-Relieved Structure
Figure Tolerance, Primary Mirror:	λ/10 peak-to-peak λ = 6328 Å	λ/10 peak-to-peak λ = 6328 Å
Secondary Mirror Material:	Cer-Vit C-101 or ULE 7971	Cer-Vit C-101 or ULE 7971
Figure Tolerance, Secondary Mirror:	λ/10 peak-to-peak λ = 6328 Å	λ/10 peak-to-peak λ = 6328 Å

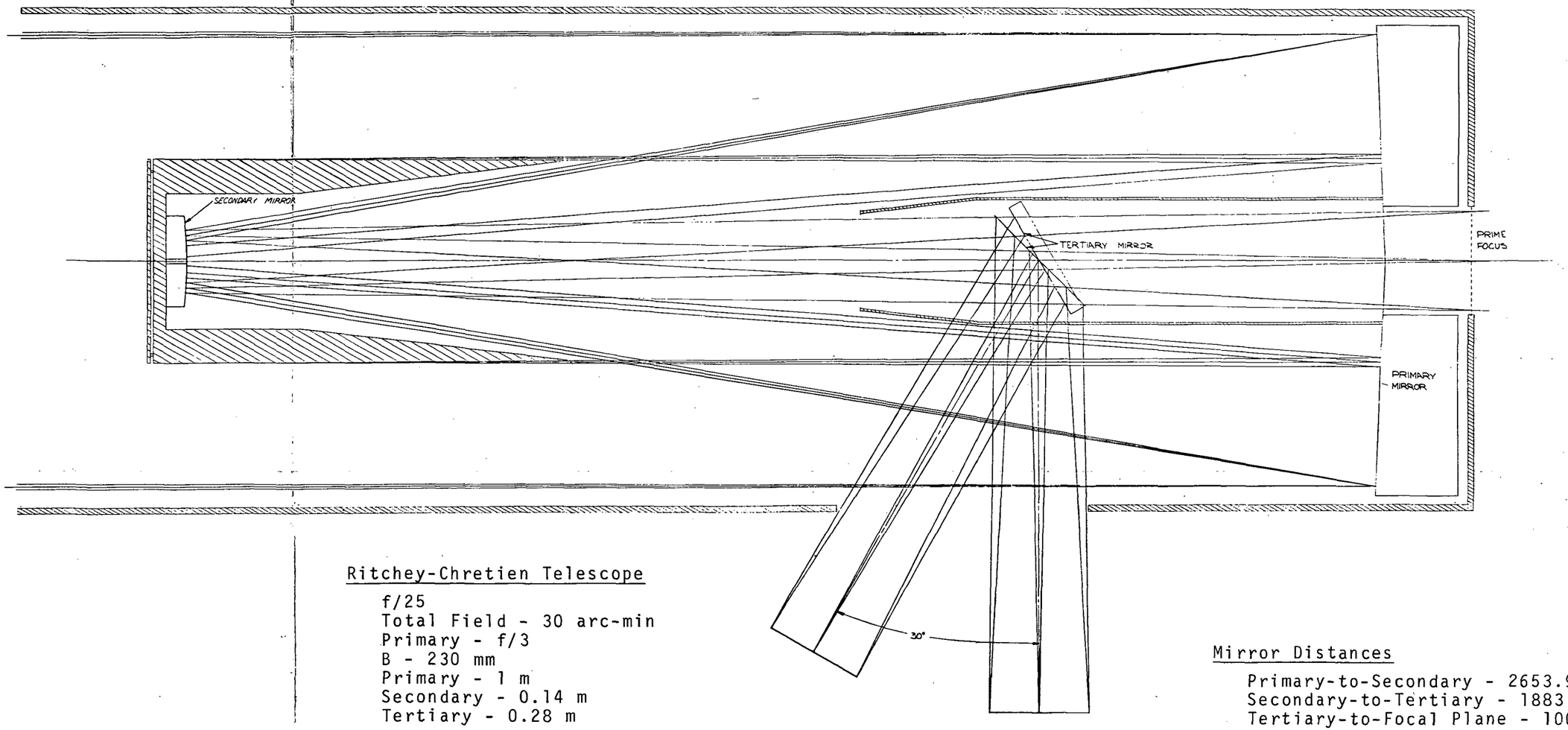

Ritchey-Chretien Telescope

f/25
Total Field - 30 arc-min
Primary - f/3
B - 230 mm
Primary - 1 m
Secondary - 0.14 m
Tertiary - 0.28 m

Mirror Distances

Primary-to-Secondary - 2653.93 mm
Secondary-to-Tertiary - 1883.93 mm
Tertiary-to-Focal Plane - 1000 mm

Figure 3-1 Telescope Layout - f/25

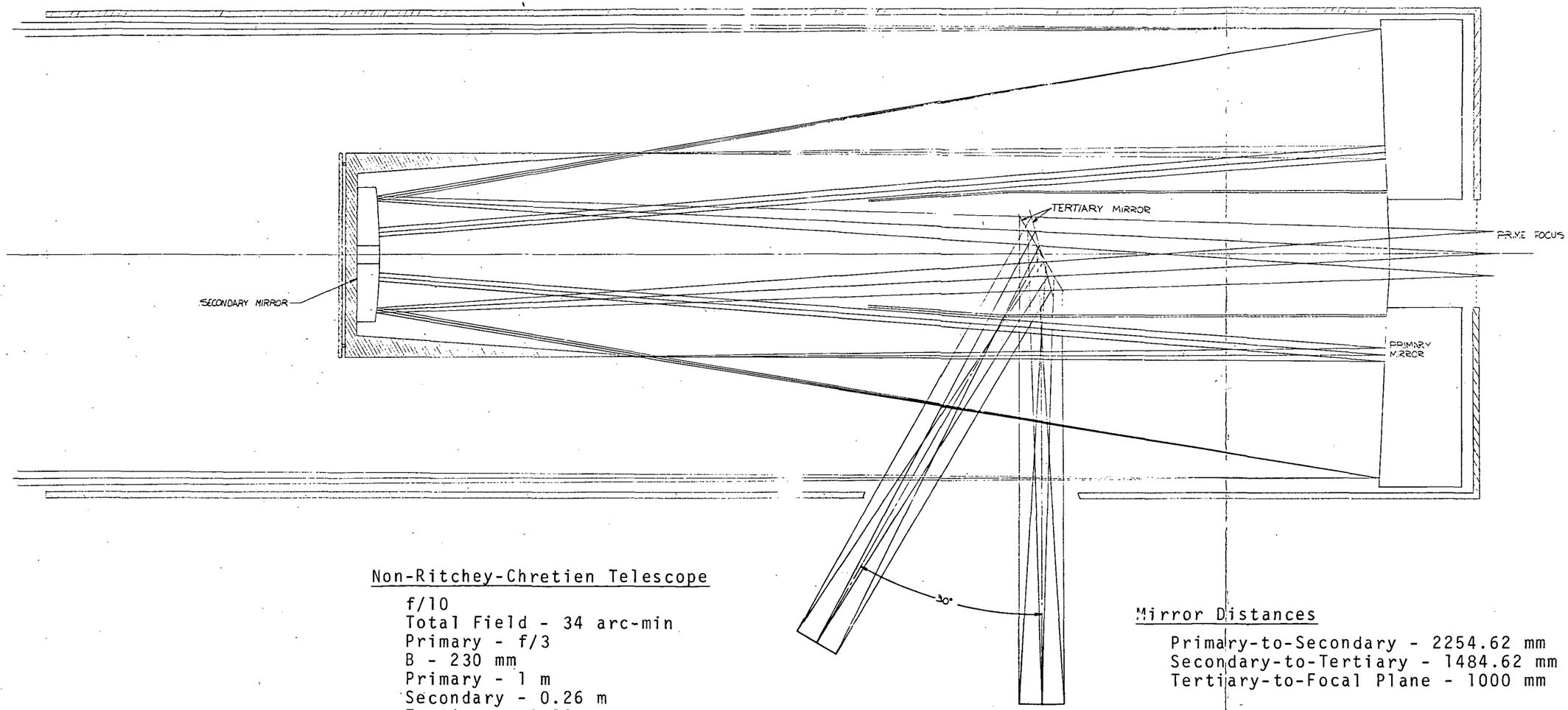

Non-Ritchey-Chretien Telescope

f/10
Total Field - 34 arc-min
Primary - f/3
B - 230 mm
Primary - 1 m
Secondary - 0.26 m
Tertiary - 0.28 m

Mirror Distances

Primary-to-Secondary - 2254.62 mm
Secondary-to-Tertiary - 1484.62 mm
Tertiary-to-Focal Plane - 1000 mm

Figure 3-2 Telescope Layout - f/10

Table 3-2
NOTATION

D: Diameter - clear aperture of primary mirror

f_p: Focal length of primary mirror

F_p: f/number of primary mirror

α: Object semi-field angle, measured in $\theta = 0$ plane

ε: Central obscuration ratio formed by secondary mirror baffle; diameter of baffle is εD

B: Telescope back focal distance, distance from vertex of primary mirror to image

p: Object distance of secondary mirror

q: Image distance of secondary mirror

f: Focal length of telescope

F: F/number of telescope

γ: Obscuration ratio, $\gamma = -p/f_p = q/f$

ℓ: Distance from tertiary mirror to image

(ρ,θ): Polar coordinates on plane tangent to vertex of primary mirror

(ξ,η): Cartesian coordinates of third order aberration in paraxial focal plane. The η axis is parallel to the $\theta = 0$ plane

e_1: Conic coefficient of primary mirror, measures deviation of surface from a paraboloid of revolution, $e-1 = -(\text{eccentricity})^2$

e_2: Conic coefficient of secondary mirror

d: Mirror separation, primary to secondary

t: Ratio of mirror separation to focal length, $t = -d/f$

m: Secondary mirror magnification, $m = q/p$

s: Ratio of image distance to mirror separation, $s = q/d$

a_1: Secondary mirror third order spherical aberration coefficient

a_2: Secondary mirror third order coma coefficient

MTF: Modulation transfer function, a function of ν

ν,ν_x,ν_y: Spatial frequency in line pair((cycles) per millimeter at which the MTF is measured. Subscript x refers to the sinusoidal object variation in the x direction(i.e., the object's bars lie parallel to the y axis); subscript y refers to a sinusoidal object variation in the y direction. (NOTE: All field angles are taken to lie in the y-z plane.)

Table 3-2
NOTATION (Continued)

δ: Tilt angle of secondary mirror relative to the optical axis of the primary mirror which yields a field angle change of K where $\delta = -K/2\gamma$

λ: Wavelength of light

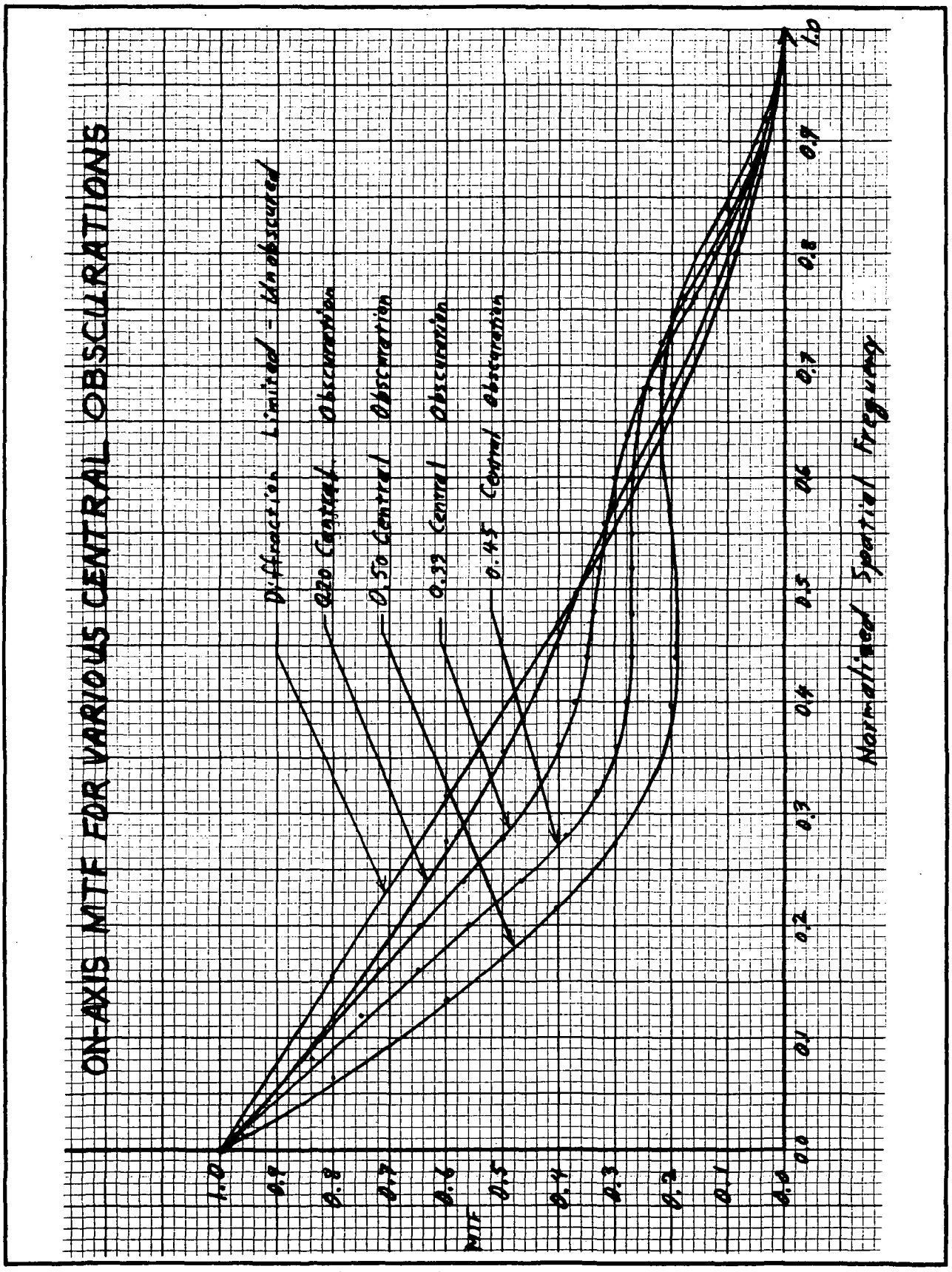

Figure 3-3 MTF Versus Spatial Frequency

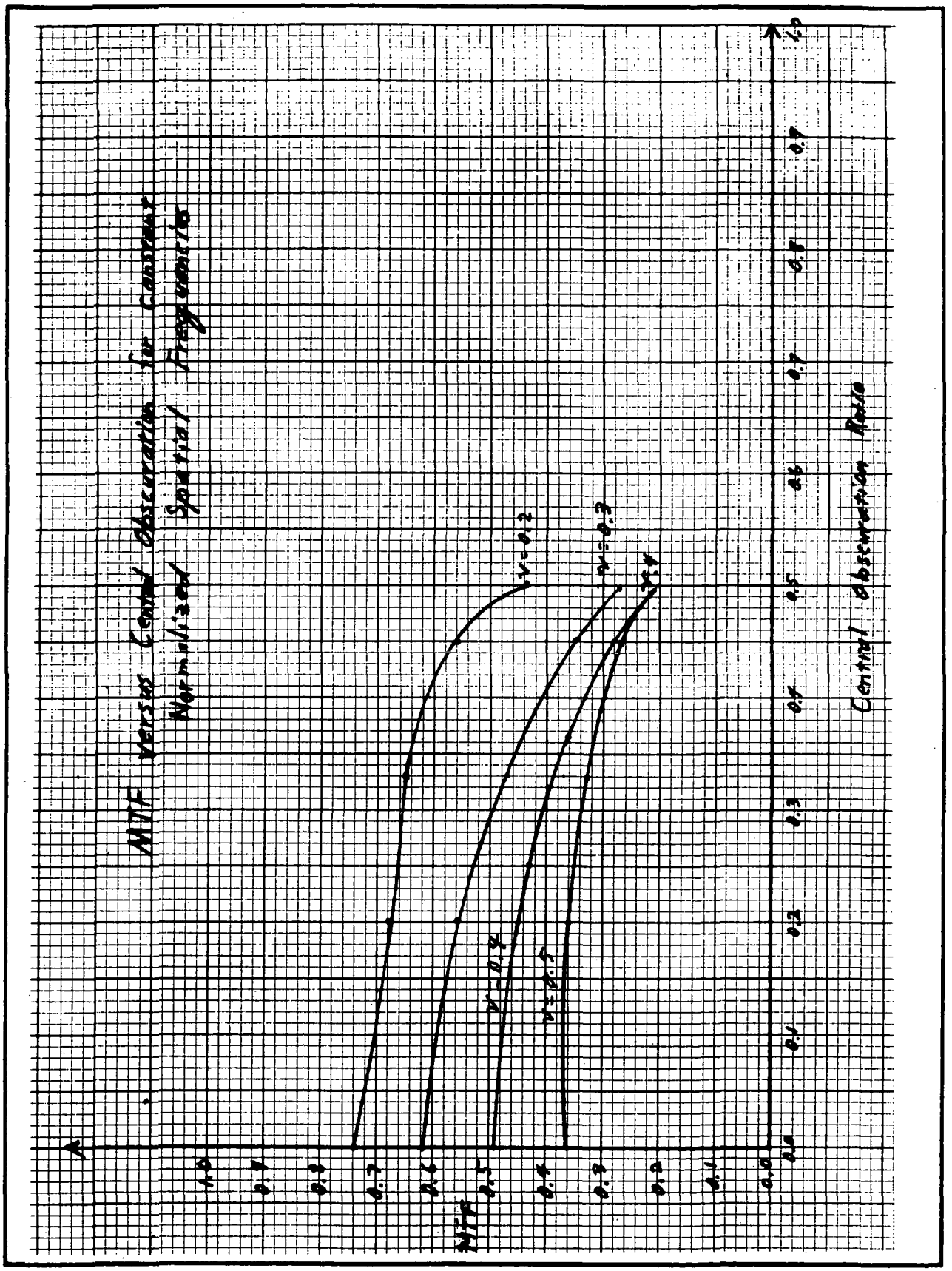

Figure 3-4 MTF Versus Central Obscuration Ratio

if at all possible kept below $\varepsilon = 0.33$.[1] To baffle the telescope from stray radiation efficiently, a large central obscuration is required. At minimum obscuration, the relationship between the field size and the focal ratio of the primary is given in Figure 3-5, showing that as the required field is increased, the primary mirror must become faster and, as a result, more difficult to manufacture.

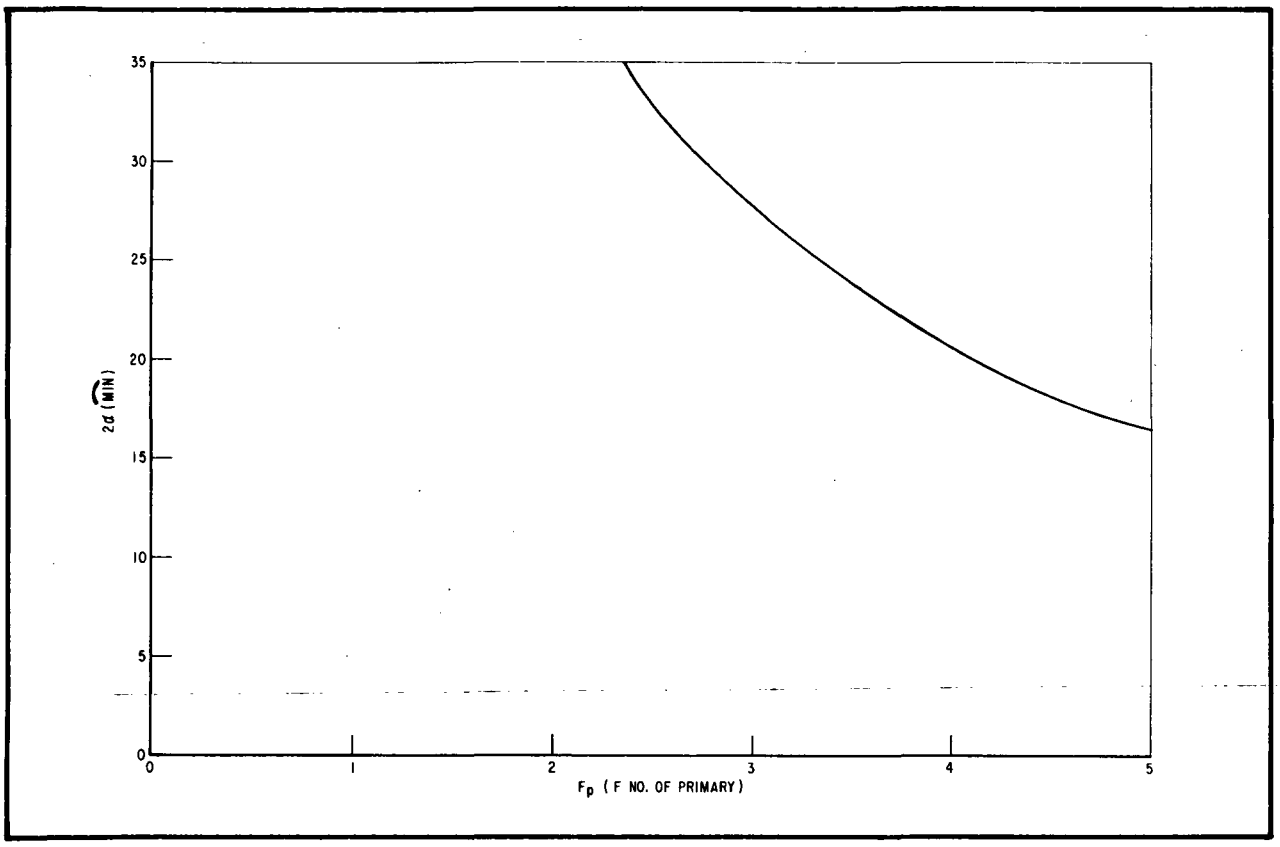

Figure 3-5 Baffle Field Size Versus Primary Focal Ratio

In general, one should select the fastest primary consistent with manufacturing constraints, since this minimizes the obscuration for a given field and telescope focal ratio and also minimizes the overall length of the telescope. For AOS, $F_p/3$ was selected, although Wetherall reports that $F_p/2.5$ is practical. The $F_p/3$

primary will reduce manufacturing costs and should allow better figure tolerance and better polish (i.e., lower scattered light) to be maintained. Both become increasingly important when working in the vacuum ultraviolet. Having specified $F_p/3$, Figure 3-5 provides the corresponding value of the baffled field for minimum obscuration. The field of view value is 27.5 arc-minutes, which is less than that required for the star sensor field. The combination of star sensor field requirements and telescope mounting constraints requires a deviation from the minimum obscuration condition.

The slowest of the two telescope focal ratios determines the final obscuration value. Figure 3-6 shows the relation between the back focal distance B and focal length of the primary for constant γ for the f/10 telescope. Layouts show that $\gamma < 0.25$ is required when using an f/3 primary in order to baffle the tracking field

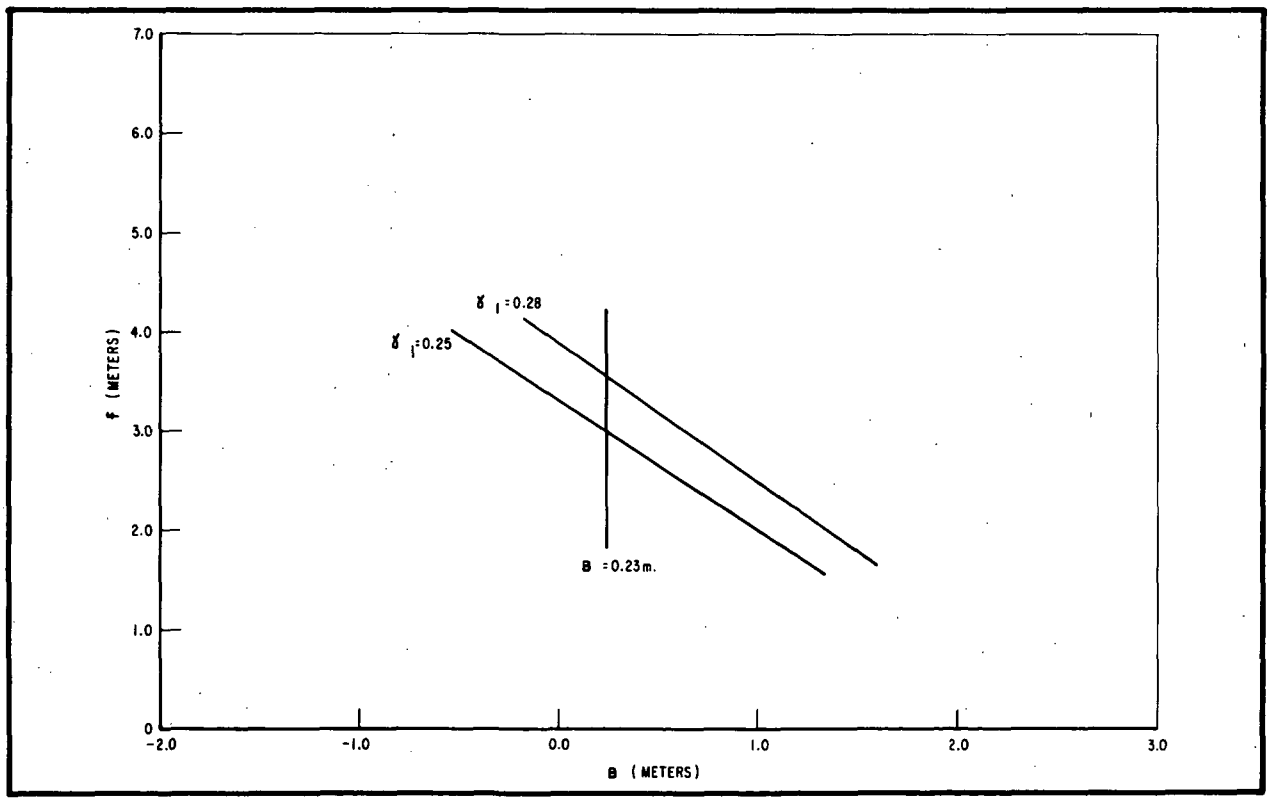

Figure 3-6 Primary Focal Length Versus Backworking Distance (f/10 Telescope)

while maintaining the total obscuration $\varepsilon < 0.5$ ($\varepsilon = 0.45$ is achieved). A slower primary with small obscuration forces B to be less than zero with the result that access to the focal plane becomes more difficult to achieve.

3.3.2 Tertiary Mirror Location

Fine guidance is to be done by the offset technique. Mirror eccentricities can be chosen to allow the secondary mirror to be used as a low moment-of-inertia telescope motion corrector; but the field of such a telescope is relatively small, being limited by coma.[2] Therefore, the approach adopted for the AOS is one of inserting a tertiary mirror in the converging beam. Two possible locations for the tertiary mirror were considered and the decision was made to locate it in front of the primary. The trade-offs between the two choices are summarized below.

Case A: Tertiary Located Behind Primary. The advantage of placing the tertiary behind the primary mirror is that it does not place tight envelope constraints on the tertiary mirror mount and gimbal. A strong disadvantage is that the tertiary mirror is not near the telescope natural center of gravity. Since the gimbaling system must be centered on the tertiary mirror, mounting behind the primary mirror would produce a configuration that would be difficult to balance and hence would adversely affect ground testing. In addition, servo and mechanical design would be adversely affected by the offset rotational mass of the telescope.

Case B: Tertiary Located in Front of Primary. The advantage of this location is that it allows the tertiary to be placed more nearly at the natural center of gravity of the telescope, it minimizes obscuration of the beam, and it facilitates mounting to the shuttle. The only disadvantage is one of restricting the envelope available for mounting and articulating the tertiary. The advantages

of this configuration outweigh the disadvantages; thus, the decision was made to locate the tertiary in front of the primary, as shown in Figures 3-1 and 3-2.

3.3.3 Position of Focal Plane Relative to Primary Mirror

It would be convenient to have the Cassegrain focus slightly behind the primary mirror as this is a possible location for instruments (like polarimeters) and this feature would be useful during alignment. Since the thickness of the primary is ~170 mm (1/6 of diameter) and ~60 mm is required for structure, the distance from the back surface of the primary mirror to the focal plane B is 0.23 meters.

If the tertiary mirror is mounted as shown in Figure 3-1, the distance from the tertiary mirror to the focal plane is 1.0 meter, which is sufficient to provide space for mounting the star tracker and allows telescope motion of 30 degrees. Layouts of several possible arrangements show that due to the large required field of 30 arc-minutes, the tertiary mirror and gimbal size sets the obscuration rather than the relationship between field and focal ratio of the primary. Therefore, the design requires deviation from the minimum obscuration case ($\varepsilon = 0.33$) and a final value for ε of 0.45 was selected.

3.3.4 Selection of Mirror Eccentricities

The eccentricity of the primary mirror is chosen to make the telescope Ritchey-Chretien at one of the two focal ratios. The figure of the secondary mirror is chosen to correct third order spherical aberration at the other focal ratio. A choice of whether the telescope should be corrected to Ritchey-Chretien in the f/10 configuration or in the f/25 configuration must be made. Considerations that enter into the choice include scientific requirements, refractive corrector constraints, and fine error sensor requirements.

Figures 3-7 and 3-8 summarize computer generated ray trace data on four possible telescope designs without refractive correction. This data gives only an indication of telescope resolution for they do not include diffraction effects. Point spread functions, including diffraction effects, presented in Section 3.7.1 are used to determine telescope resolution.

Refractive correctors for the non-Ritchey-Chretien cases are impractical, whereas the f/10 Ritchey-Chretien cases can be corrected with refractive correctors to 0.3 arc-second resolution over the required field in the spectral interval from λ3650 Å to λ7000 Å. The trade-offs between the two cases follow:

Case A: f/10 Ritchey-Chretien, f/25 non-Ritchey-Chretien. An f/10 Ritchey-Chretien without corrector will provide 0.5 arc-second resolution over a 40 mm data format. It could be corrected with refractors beyond a 40 mm format and would provide 0.3 arc-second resolution to the star tracker. The resolution over a 40 mm data format could be increased to 0.3 arc-second through the use of a refractive corrector but would limit the wavelength range to λ3500 Å - λ7000 Å.

An f/25 non-Ritchey-Chretien cannot be corrected over the field with a practical corrector. The uncorrected resolution over a data format of 40 mm is about 0.9 arc-second. Star tracker and corrector constraints make the choice unattractive.

Case B: f/25 Ritchey-Chretien, f/10 non-Ritchey-Chretien. An f/25 Ritchey-Chretien will provide better than 0.25 arc-second resolution without a refractive corrector over a 40 mm diameter data format.

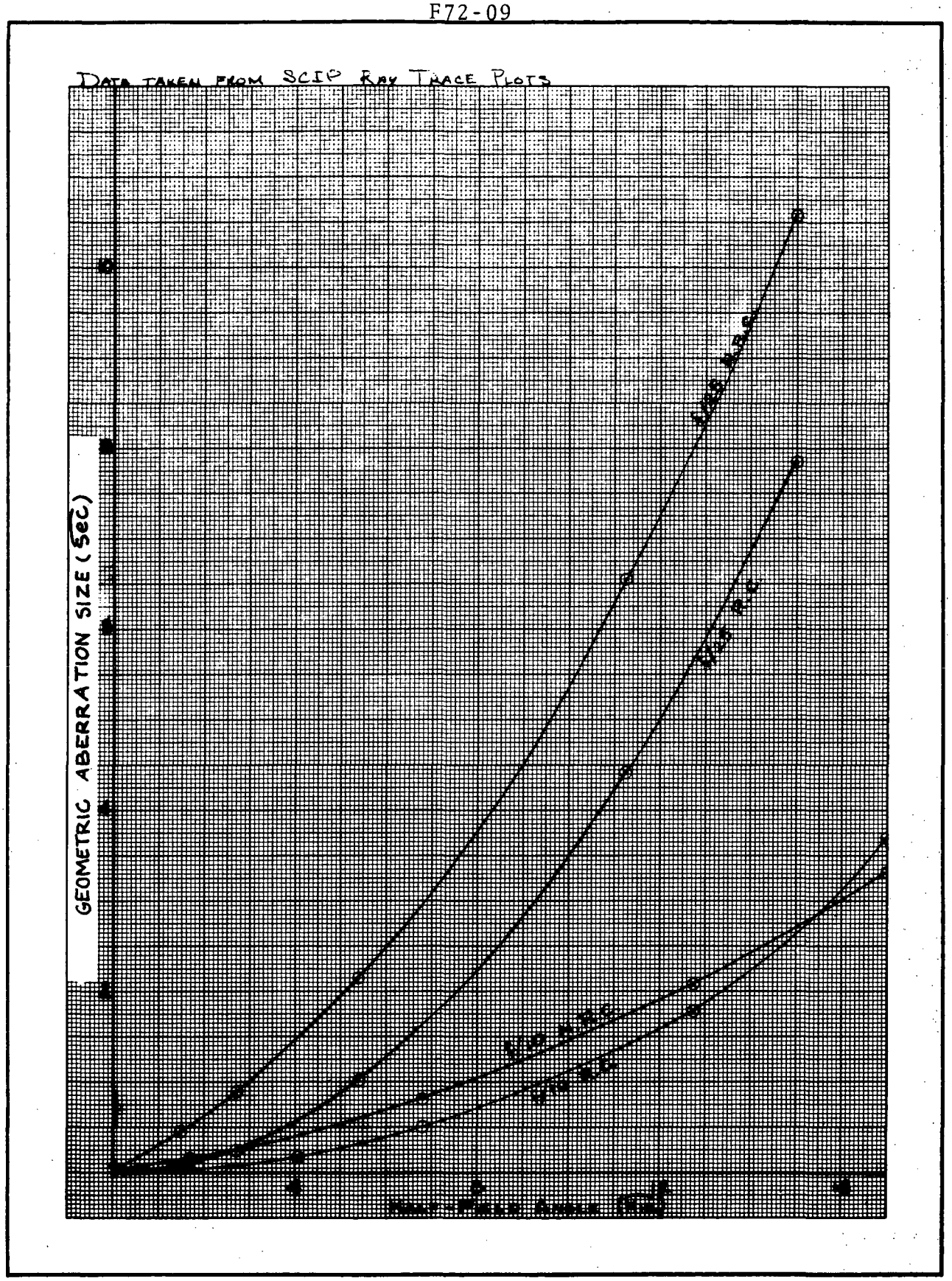

Figure 3-7 Aberration Size Versus Field Half-Angle (0-16 Arc-Minutes)

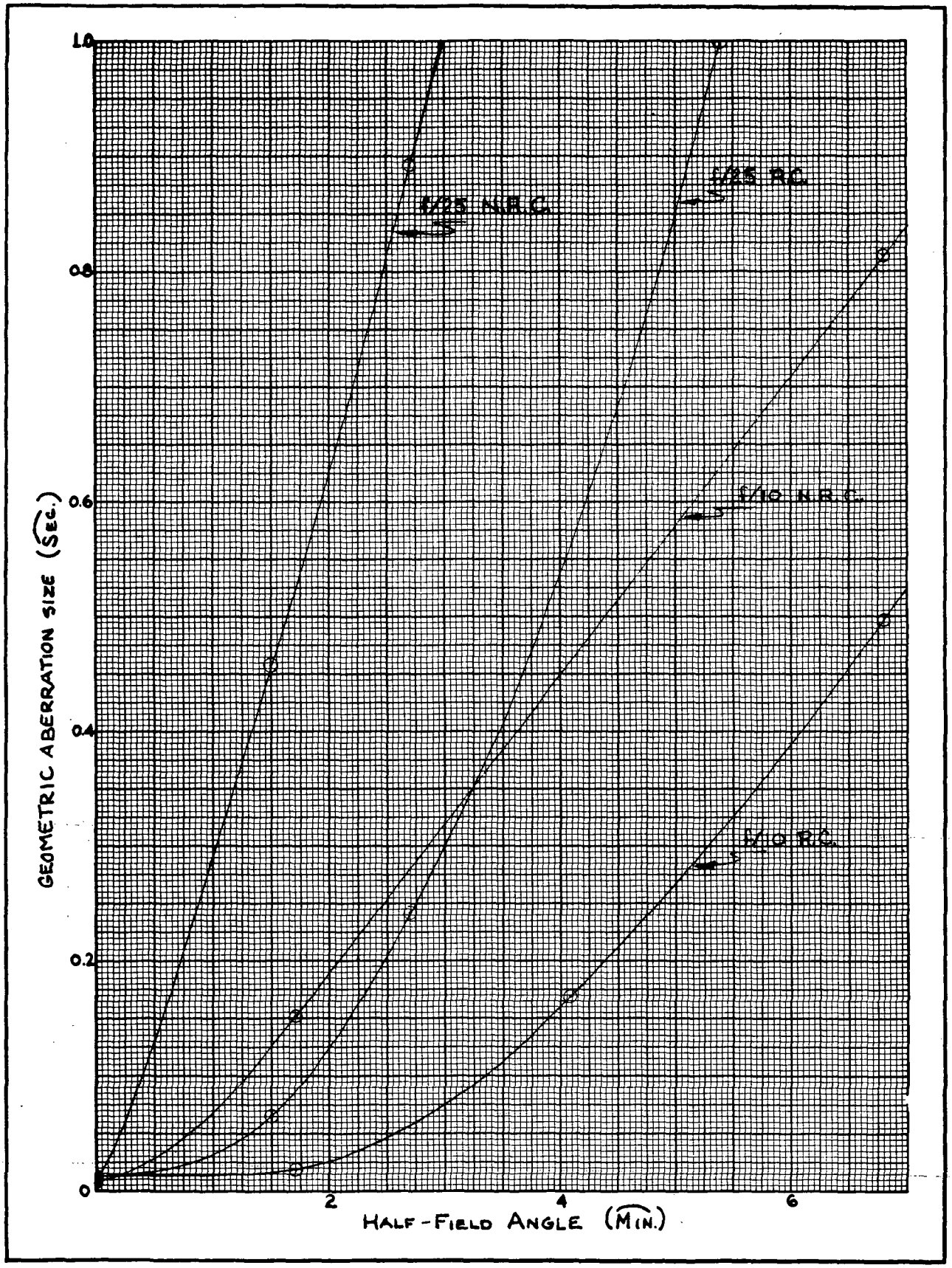

Figure 3-8 Aberration Size Versus Field Half-Angle (0-6 Arc-Minutes)

Refractive correction can be accomplished outside a 40 mm data format over the 30 arc-minutes field required by the star tracker. The primary of this telescope is a parabola within manufacturing tolerances. Hence a null test using a collimated light source can be used during manufacturing and alignment.

An f/10 non-Ritchey-Chretien will provide sufficient resolution to allow the star tracker to track, with reduced accuracy, without the need of a refractive corrector. Also, the data field will not need a refractive corrector and will have better than 0.25 arc-second resolution over a 40 mm data format.

Detailed optical parameters for each case are summarized in Table 3-3. Since Case B provides the best compromise between scientific and guidance constraints, it has been selected for the AOS.

3.4 TELESCOPE STRUCTURE

During the AOS study, two basic structure concepts were considered: a monocoque, which is a cylinder of sheet metal with circumferential structural rings added for strength at points of attachment; and a cylindrical framework consisting of a series of rings connected by trusswork.

In both cases, the primary mirror assembly would be mounted at one end and the secondary mirror assembly mounted near the other. Aluminum, titanium, and Invar have been considered as structural materials. The approximate size of the structure is 47 inches outside diameter maximum, 44 inches inside diameter minimum, and 140 inches long. Although no firm conclusion was reached during the study concerning a recommended structure configuration, at this point there is a slight preference for the monocoque structure.

Table 3-3

OPTICAL PARAMETERS FOR POSSIBLE MIRROR FIGURE COMBINATIONS

CASE A

	f/10 RC	f/25-Primary of f/10 RC
Focal length, primary (f_p)	-3000.0 mm	-3000.0 mm
Secondary magnification (m)	3.333	8.333
Focal length, telescope (f)	10,000.0 mm	25,000.0 mm
Mirror separation (d)	-2254.62 mm	-2653.93 mm
Back focal distance (B)	230.0 mm	230.0mm
Tertiary to image (ℓ)	1000.0 mm	1000.0 mm
Diameter-entrance pupil (D)	1000.0 mm	1000.0 mm
Object distance, secondary (p)	745.38 mm	346.07 mm
Image distance, secondary (q)	2484.62 mm	2883.93 mm
Optical obscuration ratio (γ)	0.248	0.115
Effective obscuration ratio (ε)	0.45	0.45
Conic coefficient, primary (e_1)*	-0.05951	-0.05951
Conic coefficient, secondary (e_2)*	-3.1473	-1.3768
Focal length, secondary (f_2)	-1064.84 mm	-393.26 mm
Effective total baffled field (θ_t)	34 min of arc	30 min of arc

CASE B

	f/25 RC	f/10-Primary of f/25 RC
Focal length, primary (f_p)	-3000.0 mm	-3000.0 mm
Secondary magnification (m)	8.333	3.333
Focal length, telescope (f)	25,000.0 mm	10,000.0 mm
Mirror separation (d)	-2653.93 mm	-2254.62 mm
Back focal distance (B)	230.0 mm	230.0 mm
Tertiary to image (ℓ)	1000.0 mm	1000.0 mm
Diameter-entrance pupil (D)	1000.0 mm	1000.0 mm
Object distance, secondary (p)	346.07 mm	745.38 mm
Image distance, secondary (q)	2883.93 mm	2484.62 mm
Optical obscuration ratio (γ)	0.115	0.248
Effective obscuration ratio (ε)	0.45	0.45
Conic coefficient, primary (e_1)*	-0.00376	-0.00376
Conic coefficient, secondary (e_2)*	-0.6676	-2.493
Focal length, secondary (f_2)	-393.26 mm	-1064.84 mm
Effective total baffled field (θ_t)	30 min of arc	34 min of arc

A final decision will require more in-depth tradeoff studies. The following sections summarize the results of the present structure studies.

3.4.1 Thermal Considerations

The thermal stability of the telescope structure is important for several reasons:

- Primary-secondary and -tertiary mirror spacing must be held within the adjustment range of the internal alignment system. (Focus only, at the detector.)

- If the telescope structure is temperature-compensated, the internal focus alignment system requires less frequent adjustments. In case of partial thermal control system failure, the quality of the data would be better if the telescope were kept close to the aligned state.

- Structural gradients side to side must be kept small, 21.1 ± 2.3°C (70.0 ± 4.1°F), so that co-alignment of the primary, secondary, and tertiary mirrors stays within 1.0 arc-second of the initial alignment.

- A thermal shroud can be used to stabilize structure temperature and gradients, but its partial or total failure should still leave the structure partially usable.

Invar was selected as the structural material for the monocoque cylinder because of its low expansion coefficient. When Invar has been annealed and stabilized, it has a creep rate of 15×10^{-6} inch per inch over a six-month period. For a 140 inch long structure,

this is 0.0021 inch total creep, which is acceptable in the AOS telescope if an active focus system is used at the detector. A truss structure using aluminum rings and Invar truss tubes with aluminum end fittings can be made to have zero thermal expansion along the optical axis, even less than an all-Invar structure. The radial expansion of the rings spreads the base of the truss tubes apart, which counteracts the expansion of the tubes. By selecting the proper ratio of aluminum to Invar for the trusses, the net effect is zero thermal expansion. This situation occurs when the temperatures of all sides of a truss triangle are equal, which means there is no temperature gradient across the diameter of the structure. Even with a transverse temperature gradient, the first approximation of the bending distortion of this "compensating" aluminum ring and Invar truss structure indicates that it is less than that for an all-Invar structure. Calculations of the compensating truss are shown in later paragraphs.

It should be noted that other combinations of materials can also be made self-compensating; for example, titanium rings and Invar trusses. If the strength analysis were to indicate a strength problem with aluminum rings, the titanium-Invar combination would be considered.

Sunlight never falls on the structure through the aperture, and the external insulation prevents thermal gradients from occurring. Hence, there is little distortion due to thermal asymmetry, and a one-material structure could be used. However, the compensating truss would help maintain alignment in the event of partial thermal control system failure.

Longitudinal expansion would not be a problem with either aluminum or titanium, but Invar requires the smallest movement of the focus device. In case of total thermal control system failure, structure temperature will fall to extremely low temperatures, approaching

absolute zero, because there are no heat sources in the telescope. In the event of partial thermal control system failure, temperature excursions might be 30°F, resulting in length changes of 0.056, 0.024, and 0.004 inch for aluminum, titanium and Invar structures respectively, all within the range of the focus system.

On the basis of the arguments above, the choice was narrowed to Invar monocoque versus compensating truss. These concepts were then compared and the conclusions reached are summarized below.

Thermal Distortion. The truss appears to give less thermal distortion because of the compensating triangle effect, although the distortion of both concepts is within acceptable limits.

Mounting. The truss structure can use the ring for convenient mounting points. However, the monocoque structure also requires the addition of rings at all concentrated load points to distribute the load around the skin.

Acoustic Effects. Either concept will survive the acoustic environment without damage. In the case of the monocoque structure, it would be necessary to evaluate the possibility of skin resonances that might require the addition of some extra rings to stiffen the skin.

Fabrication and Assembly Comparison. The fabrication and assembly requirements for the monocoque and truss structures are appreciably different; however, there do not appear to be any major fabrication obstacles with either concept.

The monocoque concept involves machining end rings, cutting and bending Invar sheet, and riveting the sheets together. The riveting operation would have to be done accurately and would require an assembly fixture. After assembly, the end rings would

probably require machining. Since Invar sheet is a specialty material and only rolled to order, there may be limitations on the size of sheet that can be obtained. A sheet size limitation would compromise the cylinder design to some extent. The bending operation would introduce stresses which could later cause creep and warping. These effects could be removed only by heat-treating, which could itself cause warping.

The truss concept involves machining rings, machining tube fittings, cutting tubes to length, and riveting or bolting these items together. The assembly operation would require some type of fixture. The joints could have no play. The assembly, however, would be stress free.

Since the two concepts require different types of manufacturing equipment and skills, the choice of concept from the fabrication viewpoint might vary from one manufacturer to another. For manufacturing purposes, the preference is for the truss concept because of past experience with similar structures and the availability of facilities for that approach.

3.4.2 Strength and Weight Considerations

The weight of the aluminum ring-Invar truss structure is estimated to be 110 pounds, which includes a thick inner aluminum liner to which the thermal control system heaters are bonded. It appears that the weight of a monocoque structure would be about 135 pounds, for a skin thickness of 0.040 inch, which is believed to be the minimum practical thickness for this size structure. The monocoque has no weight advantage in this case, but it would be about 50 percent stiffer. Since weight, at present, is not a deciding factor, weight comparisons should not be a primary basis for selecting a structure concept.

3.4.3 Compensating Structure

The compensating truss provides zero axial length change with uniform temperature change, providing only that the temperature coefficients of expansion are constant over the desired temperature range. This is demonstrated by the following example.

A truss structure is comprised of six rings, each connected by twelve tubes arranged to form a truss between adjacent rings, (see Figure 3-9). The cross section of the truss member is tubular for maximum column load capacity and highest lateral natural frequency-to-weight ratio. The material of the truss members is Invar, heat treated after forming for dimensional stability.

The ring material is aluminum and the cross-section is an I-beam. The resulting loads are in the plane of the ring, so the most efficient section is one which has the highest stiffness to weight ratio in this plane. An aluminum I-beam ring can give adequate stiffness with low weight.

Consider a right triangle whose base is one-half the chord of the aluminum ring sector, whose height is the distance between rings, and whose hypotenuse is one truss length. Since the ring sector is 60 degrees, the chord is equal to the mean radius of the ring, or 17 inches. Assuming a ring spacing of 20 inches, the triangle has the following dimensions:

$$\text{Base} = A = 8.5 \text{ inches}$$
$$\text{Ring Spacing} = C = 20.0 \text{ inches (constant)}$$
$$\text{Truss Length} = D = (A^2 + C^2)^{1/2} = 21.7 \text{ inches}$$

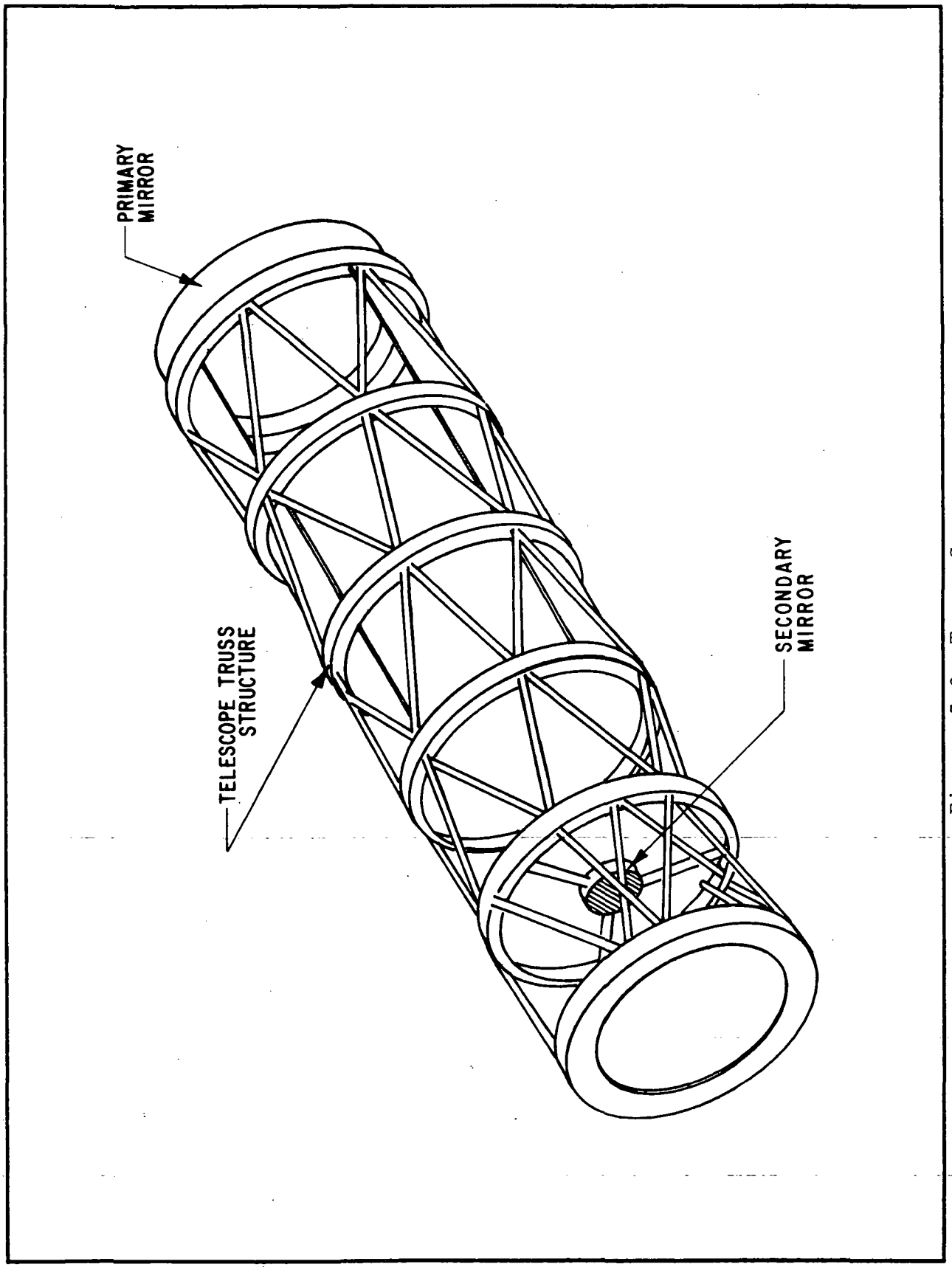

Figure 3-9 Truss Structure

Using $\alpha_{alum} = 12.0 \times 10^{-6}$ in/in/°F

$\alpha_{Invar} = 0.5 \times 10^{-6}$ in/in/°F

and $\Delta t = 10°F$:

$$\Delta A = A\alpha_{alum}\Delta t = 0.00102 \text{ inch}$$

$$\Delta D = [(A + \Delta A)^2 + C^2]^{1/2} - D = 0.000399$$

From this it is determined that the required α_{Invar} that produces no change in C is:

$$\alpha_{Invar} = \frac{\Delta D}{D\Delta t} = \frac{0.000399}{21.7 \times 10} = 1.8 \times 10^{-6} \text{ in/in/°F}$$

This is too high for Invar, but by combining Invar and a material with a higher α, in the correct length proportions, one can produce the required α of 1.8×10^{-6} in/in/°F in the truss member.

For example, if the fittings were made of titanium:

$$\alpha_{Ti} = 5.0 \times 10^{-6} \text{ in/in/°F}$$

The desired α is attained for Invar tubes 15.3 inches long with titanium fittings 6.4 inches long. It can be shown that, in general, axial expansion is zero if

$$\frac{\alpha_A}{\alpha_D} = \frac{4D^2}{A^2}$$

where α_A is the effective temperature coefficient of the base, and α_D that of the truss.

Next examine warping, as opposed to extension, for a representative set of temperatures. To see what happens with laterial temperature gradient, consider a two-dimensional example:

The angle between sides A and B is defined as $\gamma = \alpha - \beta$. From the law of cosines,

$$-\cos\beta = \frac{E^2 - D^2 - B^2}{2BD}$$

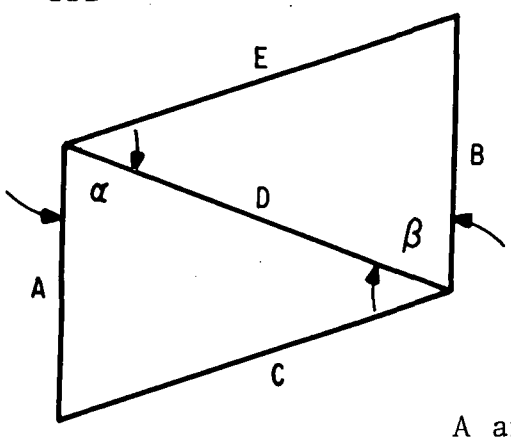

A and B are of one material; C, D and E of another.

Take derivatives

$$\sin\beta\ d\beta > \frac{1}{BD}\left[EdE - DdD - BdB - 1/2(E^2 - D^2 - B^2)\left(\frac{dD}{D} + \frac{dB}{B}\right)\right] \qquad (1)$$

Similarly,

$$\sin\alpha\ d\alpha = \frac{1}{AD}\left[CdC - DdD - AdA - 1/2(C^2 - D^2 - A^2)\left(\frac{dD}{D} + \frac{dA}{A}\right)\right] \qquad (2)$$

Subtracting Equation (1) from Equation (2), substituting $\sin\beta \simeq \sin\alpha$, $A \simeq B$, $C \simeq D \simeq E$, and $\cos\alpha = \frac{A}{2D}$:

$$d\alpha = \frac{1}{\sin\alpha}\left[\frac{1}{A}(dC-dE)-\frac{1}{D}(dA-dB)+\left(\frac{A}{2D}\right)\left(\frac{dA}{A}-\frac{dB}{B}\right)\right]$$

$$= \frac{1}{\sin\alpha}\left[\frac{1}{A}(dC-dE)-\frac{1}{2D}(dA-dB)\right]$$

Assume a linear temperature gradient vertically on the page, and let t_c = reference temperature.

Then
$$dC = 0$$
$$dD = \alpha_D D\delta$$
$$dE = 2\alpha_D\delta$$
$$dA = 1/2\alpha_A A\delta$$
$$dB = 3/2\alpha_A A\delta$$

and

$$d\alpha = \frac{1}{\sin\alpha}\left[\frac{1}{A}(0-2\alpha_D D\delta)-\frac{1}{2D}(1/2\alpha_A A\delta - 3/2\alpha_A A\delta)\right]$$

$$= \frac{\delta\alpha_D}{\sin\alpha}\left[-\frac{2D}{A} + \frac{\alpha_A}{\alpha_D}\frac{A}{2D}\right]$$

The angular change is zero if the bracketed term is zero:

$$\frac{\alpha_A}{\alpha_D}\frac{A}{2D} - \frac{2D}{A} = 0$$

or

$$\frac{\alpha_A}{\alpha_D} = \frac{4D^2}{A^2}$$

This is the same condition as that for zero axial expansion.

3.5 THERMAL CONTROL DESIGN

The preliminary thermal control design concept is based upon the requirement to maintain the AOS telescope near the calibration temperature of approximately 21°C (70°F), throughout the orbital life of the instrument. This requirement stems from the fact that active alignment mechanisms will not be incorporated into the optical design except at the focal plane. It is desirable, therefore, to operate the telescope at the alignment temperature, i.e., near room temperature. Additionally, large variations of the primary mirror temperature from the manufacturing temperature would cause focal length changes and possibly other distortion factors that could not be compensated for by the detector adjustments.

The goal of the thermal design is to maintain the instrument mean temperature at all times within the design limits 21 ± 7°C (70° ± 12.6°F)*, reduce orbital variations to a minimum, and limit thermal gradients to acceptable levels.

3.5.1 Thermal Control Subsystem

The AOS missions encompass a wide range of orbital parameters and spacecraft orientations. These factors result in widely varying environmental conditions. For this reason, the conceptual design includes a passive multilayer insulation shield enclosing the telescope and mounting yoke. The purpose of this shield is to null out the environmental heat fluxes from solar and Earth radiation and radiant exchange with the spacecraft. The telescope temperature can then be controlled by heaters bonded to the shroud which compensate for the radiant heat loss out of the aperture. Figure 3-10 depicts the conceptual thermal design.

*Based on the expansion of an Invar structure.

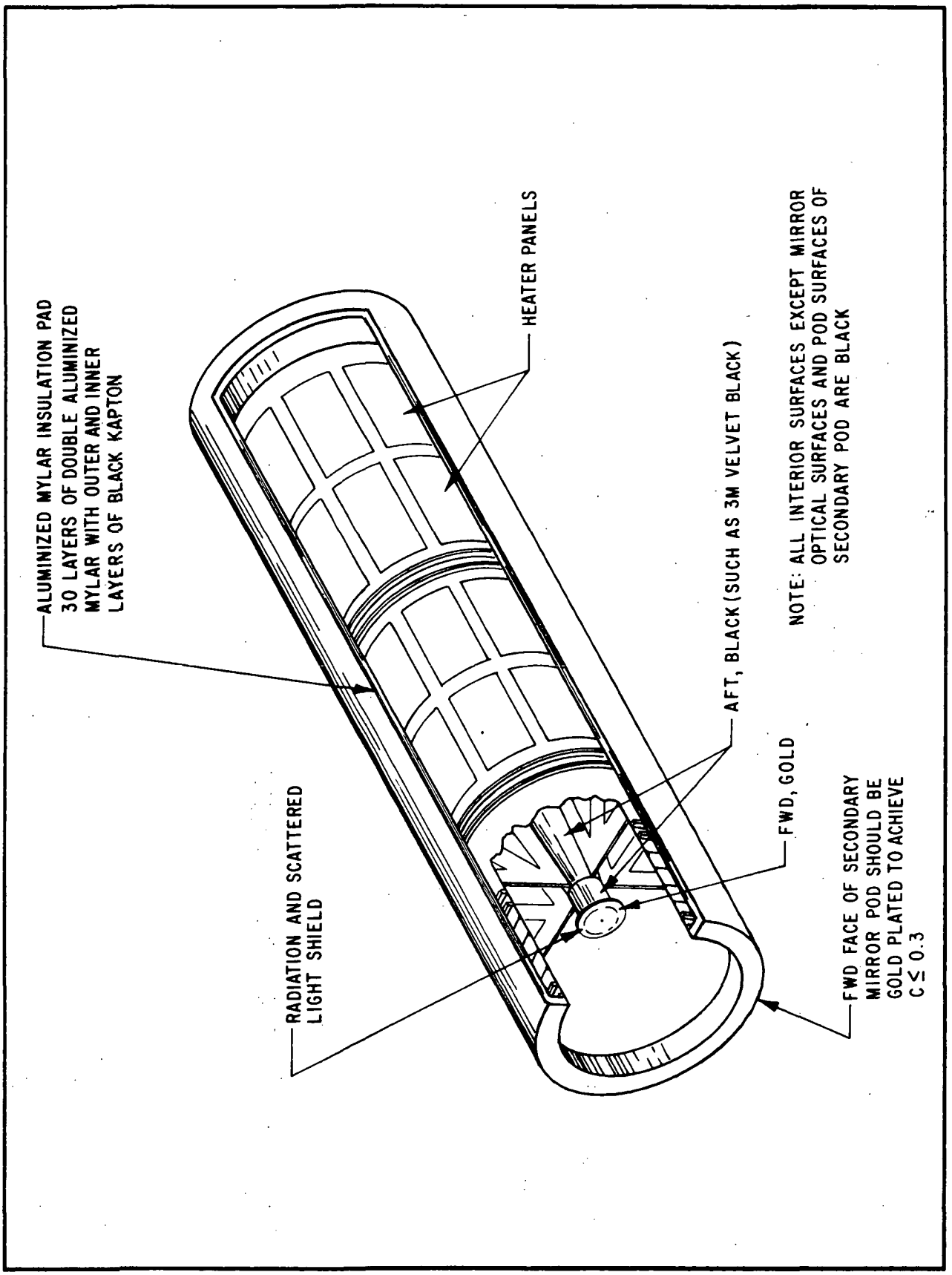

Figure 3-10 Thermal Control

Passive Control. The passive component of the thermal control system consists of an insulation blanket composed of 30 layers of one-quarter mil thick, doubly aluminized Mylar with outer and inner layers of one-half mil thick black Kapton. The heat leak through the insulation blanket to space is estimated to be less than 15 watts. (See Section 3.5.2.) The outer black Kapton layer provides an absorptivity to emissivity ratio of 1 -- thus limiting the maximum exterior surface temperature to 121°C (250°F) when exposed to direct solar radiation. This is an acceptable exposure temperature for Mylar or Kapton.* It is possible for the insulation outer layer to exceed the allowable lower limit for Mylar or Kapton, -166°C (-300°F), if continuously exposed to deep space and if other environmental fluxes are blocked. A more detailed study of the exposure temperatures can be made in the detailed design phase of the AOS. At worst, restrictions requiring spacecraft rotation or orientation change could be imposed to prevent the insulation from exceeding its lower limit temperature.

Active Control. The average heater power required to compensate the heat loss out of the aperture and through the insulation is less than 450 watts (see Section 3.5.2). Reduction in the required average power can be achieved by providing an aperture door which can be closed during nonoperating periods. The heaters should be sized to allow a duty cycle no greater than 50 percent to guarantee adequate temperature control using simple on-off controllers. Therefore, the peak heater power requirement could be 1000 watts, twice the average power.

Figure 3-10 shows the conceptual heater configuration. The heaters are Kapton encapsulated, etched film bonded to the telescope shroud.

*Schjeldoehl Company, Northfield, Minn., Black Kapton film (1/2 mil) No. C403000.

It is sometimes undesirable to bond thermal control heaters to the structure being controlled, particularly if the structure is massive and simple on-off control is used. Such systems generally result in thermal overshoot on temperature cycling. In the conceptual design, the monococque structure proposed for the telescope avoids these problems by providing a thin-wall, low thermal capacitance shroud to which the heaters are bonded. Since the control sensors are essentially mounted on the heaters, simple on-off control can be used with negligible overshoot. A similar narrow (1°F) on-off temperature control band, low thermal capacitance heater system is used on the Skylab/ATM instruments built by BBRC.

The heater system's primary function is to maintain the mean structure temperature within the design limits of 21° ± 7°C (70° ± 12.6°F), thus maintaining the spacing and alignment of the optical elements. The temperatures of the optical elements are maintained at the desired level by radiation exchange with the heated structure. An exception may be the secondary mirror pod and spider, since its view of space is large relative to its view of the heated structure. Direct heating of the secondary mirror mount and spider structure may be required. The secondary mirror, being Cervit (an ultra-low expansion coefficient material), can withstand a wide range of temperature without resulting distortion.

The radiation exchange factor between the primary mirror and the heated structure is large relative to its view of space because the edge and rear surfaces are thermally black, with emissivity (ε) > 0.8 and the forward face is aluminized (ε < 0.1). Furthermore, the geometric view factor between the mirror and space through the aperture is small relative to its view of the heated structure. Although the primary mirror is well coupled radiatively to the heated shroud, the time required to change the mean temperature of the mirror after being hot or cold soaked would be excessive because of its large thermal mass and low conductance (see Section 3.5.2). (The thermal time constant for the mirror is approximately

4 hours.) For this reason, the primary mirror temperature and therefore the telescope mean temperature must be maintained within its operating limits through the prelaunch, boost, and orbital phases of the mission.

3.5.2 Thermal Computations

Heat Loss Computation

Aperture

$$Q_A = \varepsilon A \sigma T^4$$

$\varepsilon = 1$ view from aperture to space

$A = .7854\ D^2$

$= \frac{.7854(44)^2}{144} = 10.56\ ft^2$

$\sigma = .1714 \times 10^{-8}$ Btu/hr-ft^2-°R^4
Stefan-Boltzmann constant

T = telescope interior temperature

$= 70°\ F = 530°\ R$

$$Q_A = \frac{(1).7854(44)^2}{144}(.1714 \times 10^{-8})(530)^4$$

$= 1428.1$ BTU/hr.

$= 418$ watts

Insulation

$$Q_I = AF\sigma T^4$$

$$A = \frac{.7854\ D^2 + \pi DL}{144}\ ft^2$$

$$= \frac{.7854(44)^2 + 3.14(44)(140)}{144} = 144.9\ ft^2$$

$$F = \frac{1}{30(\frac{1}{.05} + \frac{1}{.05} - 1) + (\frac{1}{.8} + \frac{1}{.8} - 1)} = \frac{1}{1171.5}$$

$\sigma = .1714 \times 10^{-8}$ Btu/hr-ft^2-°R^4

T = telescope shroud temperature

= 70° F = 530° R

$$Q_I = \frac{.7854(44)^2 + 3.14(44)(140)}{144(1171.5)} (.1714 \times 10^{-8})(530)^4$$

= 16.7 BTU/hr

= 4.9 watts

If the insulation factor is degraded by a factor of 3 to account for compression and contact conductance, the heat loss ~ 15w.

Total Heat Loss

$$Q_T = Q_A + Q_I$$

= 418 + 15 watts

= 433

Maximum Insulation Outer Layer Temperature

Assume solar radiation impinges directly on the aft (primary mirror) end of the telescope insulation. This area behaves essentially as an insulated flat plate.

$$\alpha q = A\varepsilon\sigma T^4$$

or $$T = \sqrt[4]{\frac{\alpha q}{A\varepsilon\sigma}}$$

$\alpha = 0.8$ Black Kapton
$q = 443$ Btu/hr-ft^2 (Solar flux)
$A = 1$ ft^2
$\varepsilon = 0.8$ Black Kapton
$\sigma = .1714 \times 10^{-8}$ Btu/hr-ft^2-°R^4

$$T = \sqrt[4]{\frac{.8(443)}{1(.8)(.1714 \times 10^{-8})}} = 713 \ °R$$

$= 253°$ F $= 122.8°$ C

The maximum insulation outer layer temperature is 122.8° C (253° F), which is within the allowable temperature limits for Kapton of +176.7°C(+ 350°F).

Thermal Time Constant - Primary Mirror

$$\theta = \frac{WC_p}{h_r A}$$

$W = 187$ lbs

$C_p = 0.2$ BTU/lb-°F

$$A = \frac{.7854\ D^2 + \pi Dh}{144}$$

$$= \frac{.7854(39.37)^2 + 3.14(39.37)(7)}{144}$$

$$= 14.47\ ft^2$$

$$h_r = \sigma(T_M^3 + T_S T_M^2 + T_S^2 T_M + T_S^3)F$$

$F = (1)(.8)(.8) = 0.64$

where $T_M \approx T_S \approx 530°R$,

and $\sigma(4T^3) \approx 1$.

$h_r = 0.64$

$$\theta = \frac{187(.2)}{(0.64)14.47} = 4.04 \text{ hrs.} \quad \text{time constant.}$$

Time required to change the temperature of the primary mirror from 60° F to 70° F in an 80° F environment:

$$\theta = \frac{WC_p}{2T_E^3 FA\sigma}\left\{\frac{1}{2}\left[\ln\left|\frac{T_E+T_M}{T_E-T_M}\cdot\frac{T_E-T_O}{T_E+T_O}\right|\right] + \left[\tan^{-1}\frac{T_M}{T_E} - \tan^{-1}\frac{T_O}{T_E}\right]\right\}$$

where $T_E = 80° F = 540° R$ Environment temperature

$T_M = 70° F = 530° R$ Final temperature of mirror

$T_O = 60° F = 520° R$ Initial temperature of mirror

$W = 187$ lbs

$C_p = 0.2$ Btu/lb-°F

$F = 0.8(0.8) = 0.64$

$A = 14.47$ ft^2

$\sigma = .1714 \times 10^{-8}$ Btu/hr-ft^2-°R^4

$$\theta = \frac{187(.2)}{2(540)^3(.64)(14.47)(.1714 \times 10^{-8})} \left\{ \frac{1}{2}\left[\ln \left| \frac{540+530}{540-530} \cdot \frac{540-520}{540+520} \right| \right] + \right.$$

$$\left. + \left[\tan^{-1} \frac{530}{540} - \tan^{-1} \frac{520}{540} \right] \right\}$$

$= 5.38$ hrs.

3.6 MIRROR COATINGS

The telescope has three mirrors. Two mirrors are used near normal incidence, whereas for the third, the angle of incidence varies from 30° to 45°. Each spectrometer contains a number of reflective surfaces. Individual mirror reflectance (R) must be maximized if the system efficiency is to be reasonable. For example, if R = 0.9, the system "transmission" (T) for five surfaces is $T = (0.9)^5 = 0.59$; if R = 0.8, $T = (0.8)^5 = 0.33$ and if R = 0.4, $T = (0.4)^5 = 0.01$.

Figures 3-11 and 3-12 show reflectances for various metals and overcoatings. The only coating which comes close to covering the wavelength range λ900 Å to λ7000 Å is overcoated aluminum. Highly reflecting mirrors for the vacuum ultraviolet can be made by immediately overcoating freshly deposited aluminum with MgF_2[3,4] or LiF.[5,6] These overcoat materials prevent the oxidation of Al to Al_2O_3, which absorbs strongly below 1600 Å, and preserve the intrinsically high reflectance of Al.[7] The spectral region is then limited by the absorption region of the overcoat, which is below 1100 Å for MgF_2 and below 1000 Å for LiF. The spectral reflectance depends on the overcoat film thickness since the overcoat acts as an interference film.

During the study, several types of overcoatings were investigated in detail. These coatings included:

- LiF
- MgF_2 (Research)
- MgF_2 (Commercial)

For the AOS, the combination of aluminum overcoated with MgF_2 is recommended.

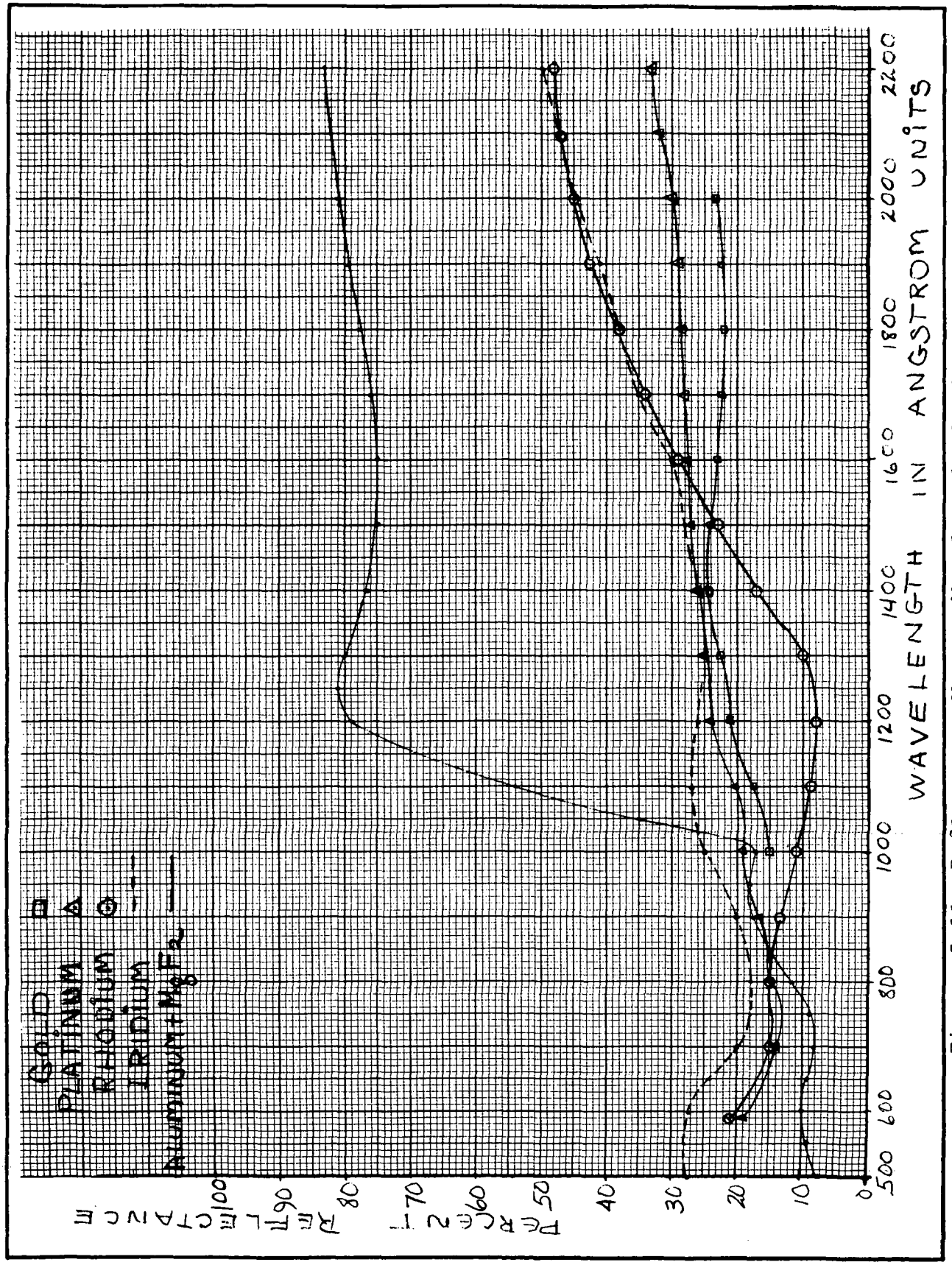

Figure 3-11 Reflectance Versus Wavelength, Various Materials

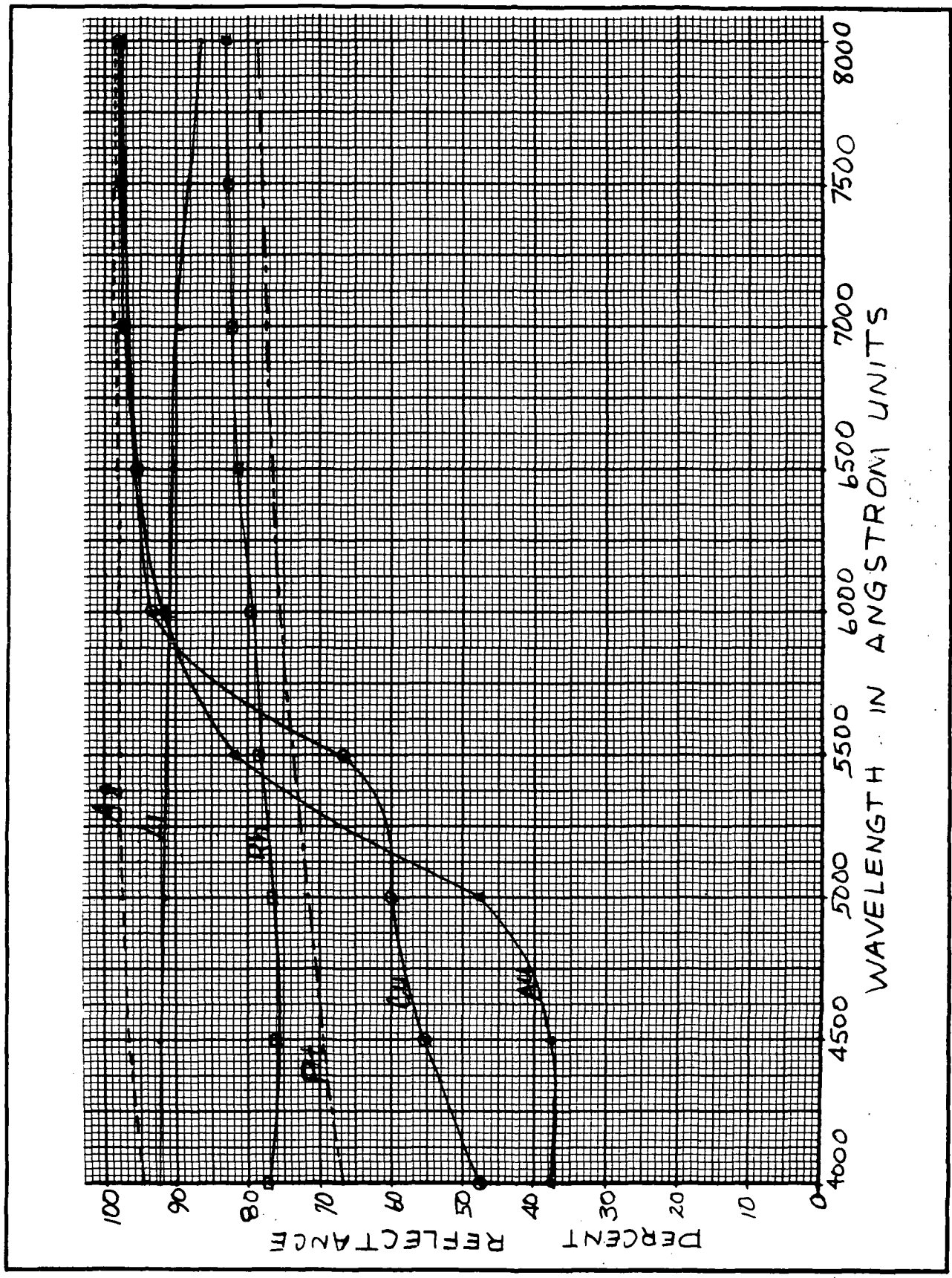

Figure 3-12 Reflectance Versus Wavelength, Various Materials

3.6.1 Aluminum Coated with LiF

Recent near normal incidence measurements[8] have demonstrated reflectances greater than 20 percent for $\lambda > 950$Å. Values of 55 to 65 percent have been obtained in the λ1025Å - 1600Å region using a 140Å thick layer of LiF, which is $\lambda/2$ thick at $\lambda = 1026$Å (Figure 3-13). A 250Å thick layer penalizes the region $\lambda < 1050$Å but increases the reflectance in the region $\lambda > 1200$Å to nearly 70 percent (Figure 3-14). More recent measurements[9] made on films prepared at the optimum substrate temperature of 100°C show much higher reflectances (Figure 3-15).

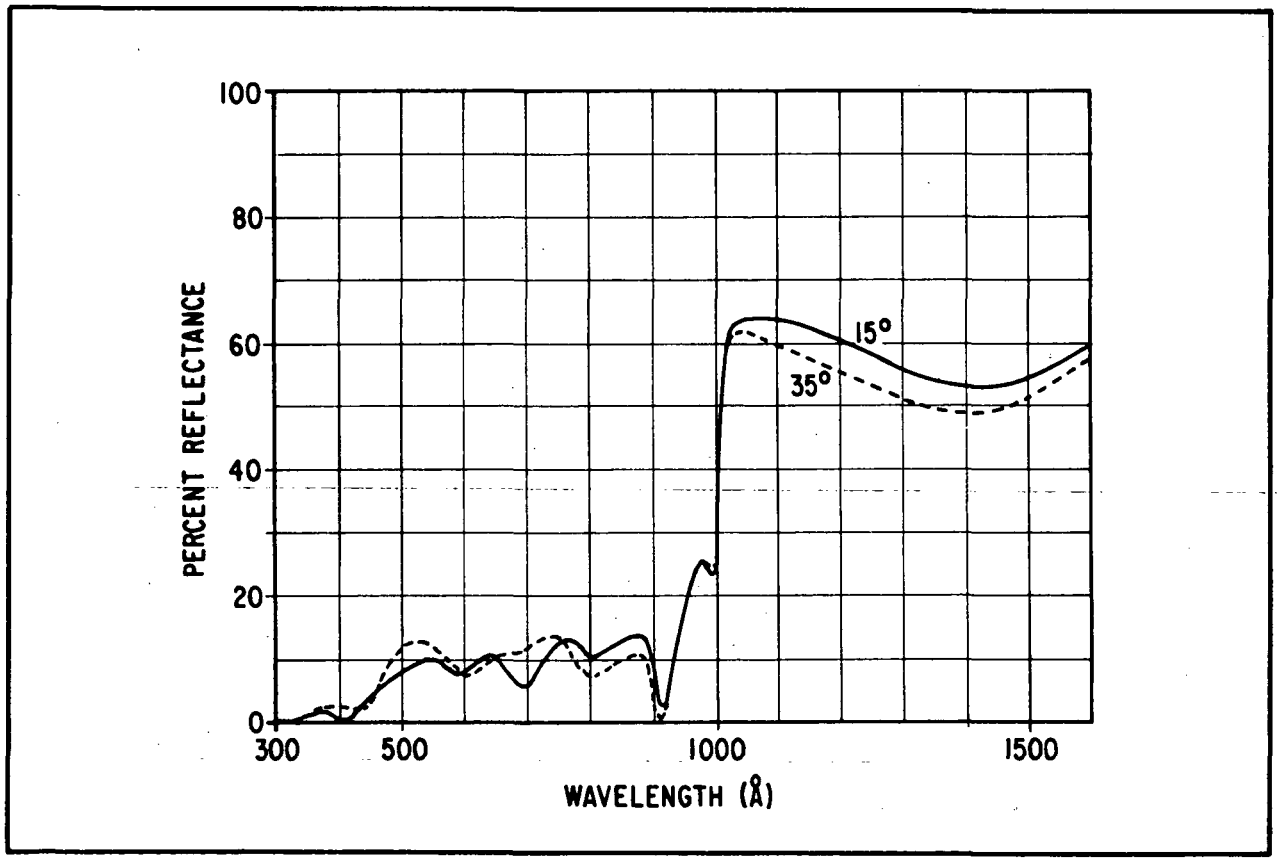

Figure 3-13 Measured Reflectance of an Al + LiF Mirror From 300Å to 1600Å (140Å Thick)

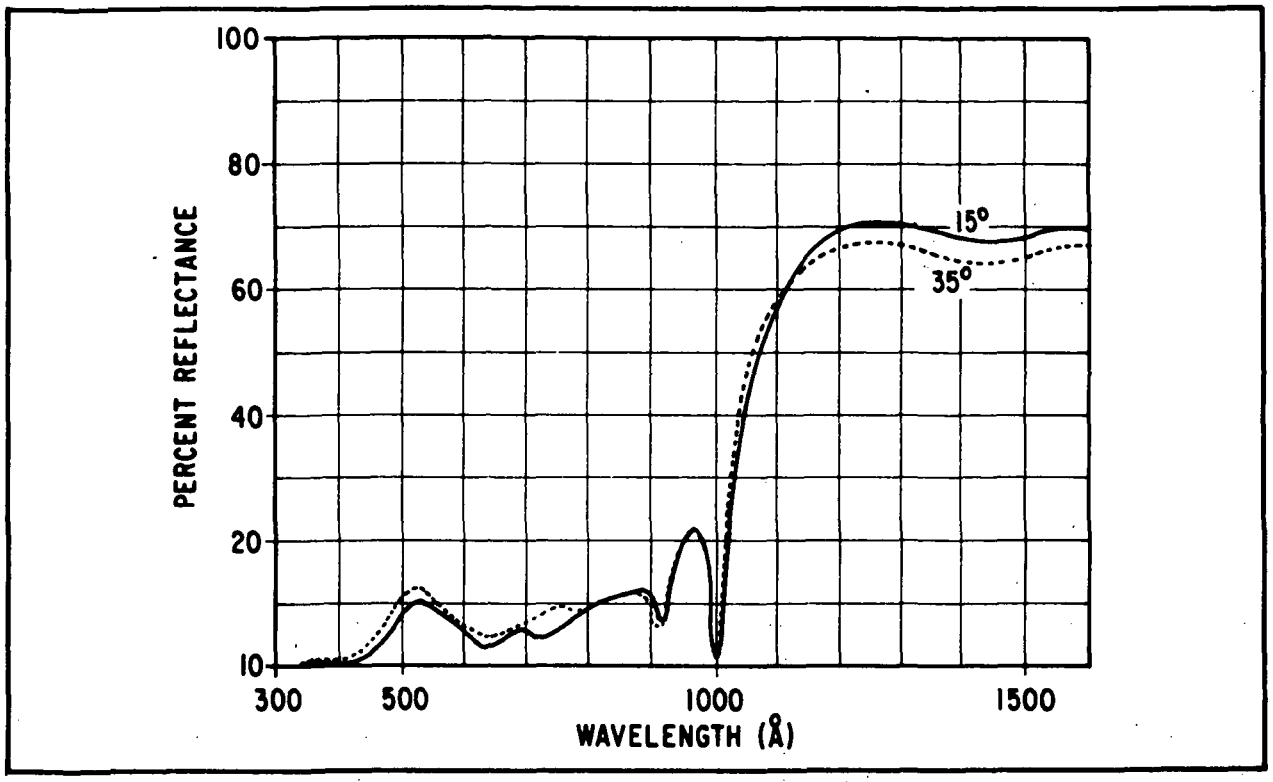

Figure 3-14 Measured Reflectance of an Al + LiF Mirror From 300Å to 1600Å (250Å Thick)

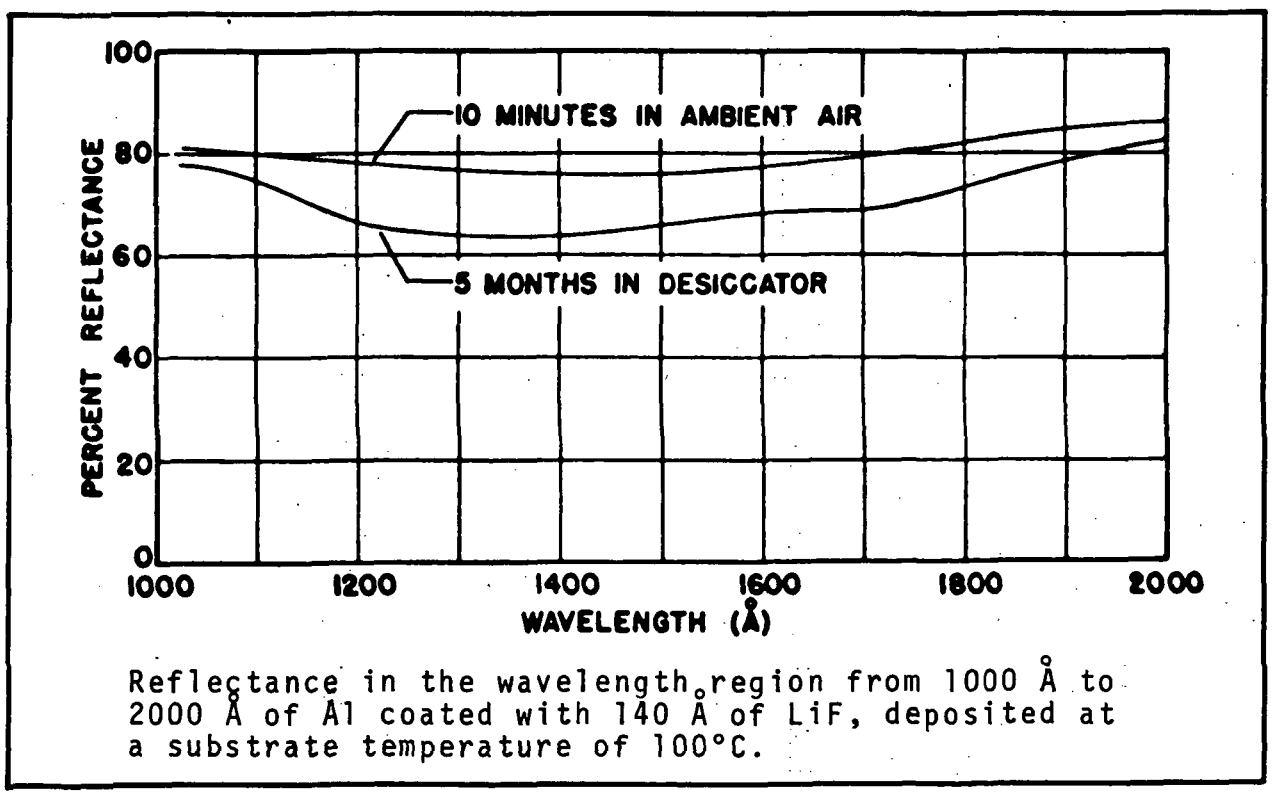

Figure 3-15 Effect of Aging on Mirror Reflectance

The optical properties of LiF are very sensitive to atmospheric water vapor, and therefore its performance is strongly influenced by the environment it is stored in.

This study[9] also examined the aging effects of LiF coated mirrors. The results of five months storage in a desiccator are shown in Figure 3-15. Even more drastic effects occur if the mirror is stored in an ambient air environment (Table 3-4).

Table 3-4

COMPARISON OF EFFECTS OF AGING ON VACUUM ULTRAVIOLET REFLECTANCE OF Al + LiF COATINGS MADE AT 40°C

	Ambient Air		Desiccator	
λ(Å)	Fresh	Aged 2 months (Percent reflectance)	Fresh	Aged 5 months
1026	74.0	41.6	74.4	63.4
1216	71.6	43.6	72.4	65.6
1609	74.5	46.9	73.0	62.3
2000	86.1	50.5	85.2	81.2

Because of its aging characteristics, Al + LiF is not recommended.

3.6.2 Aluminum Coated with MgF_2

These coatings do not show any significant degradation of vacuum ultraviolet reflectance with aging even after storage either in a desiccator or in ambient air for periods as long as five months.[9] These mirrors are very stable and are not generally affected by

exposure to atmosphere or even ultraviolet or electron irradiation.[4] The mirrors can be successfully cleaned by rinsing with ether, acetone, freon TF,or by colloidion cleaning.[4] For the AOS application, Hunter et al[8] indicate a film thickness of 250 Å is about optimum. It would have a reflectance of 15 to 20 percent between λ900 Å and λ1080 Å, increasing to 40 percent at λ1100 Å (Figure 3-16). Hutcheson et al[9] using optimized deposition conditions, show about the same reflectance below λ1250 Å but improved reflectance above λ1250 Å (Figure 3-17).

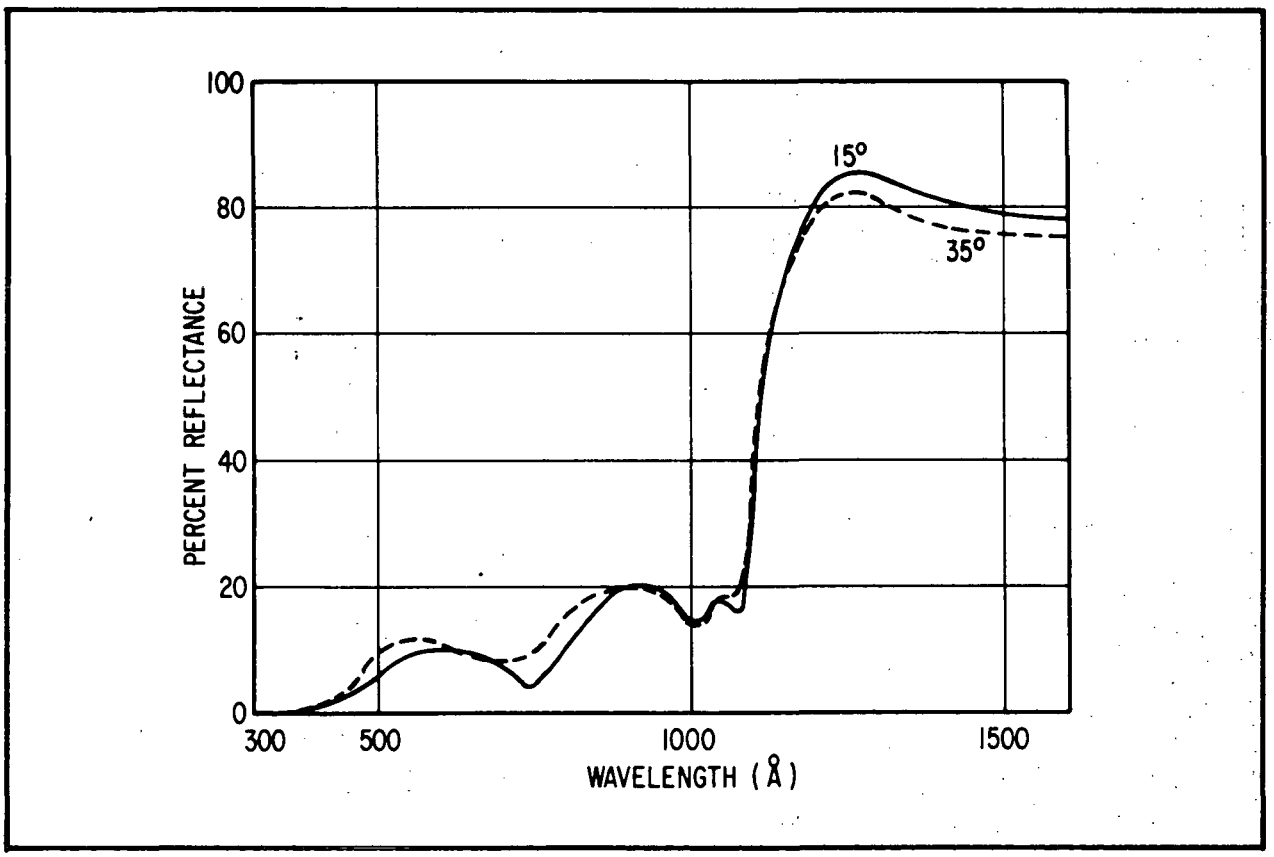

Figure 3-16 Measured Reflectance of an Al Mirror with MgF_2 Thickness of 250 Å

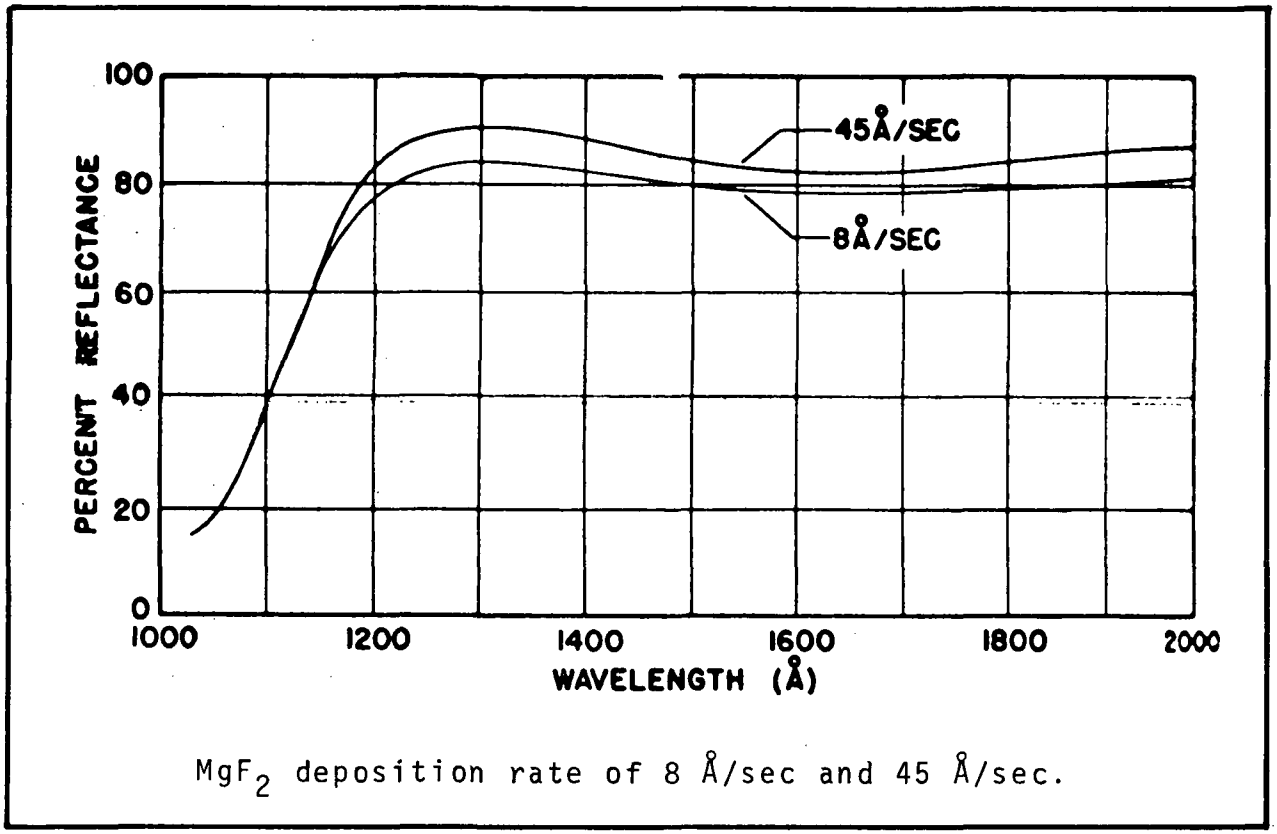

Figure 3-17 Reflectance in 1000 Å to 2000 Å Wavelength Region of Al Coated with 250 Å of MgF_2

The coated tertiary mirror, used between 30 degrees and 45 degrees angle of incidence, will introduce polarization into the beam. Its magnitude at λ1216 Å can be estimated from data presented in reference 8 which gives $R_1 \approx 83$ percent and $R_{11} \approx 75$ percent at 45° angle of incidence, where R_1 and R_{11} are the reflectances of light polarized with its electric vector perpendicular to and parallel to the plane of incidence. The corresponding degree of polarization (ρ) is given by

$$\rho = \frac{R_1 - R_{11}}{R_1 + R_{11}}$$

Substituting the values of R_1 and R_{11} for MgF_2 gives $\rho \approx 5\%$.

Commercially Available Al + MgF_2 Coatings. A search of the commercial community with coating capability revealed several sources that were capable of coating optics of the size used in the AOS. In general, though, it was found that the coatings available did not quite meet the high reflectance previously stated. Figure 3-18 is a graph showing reflectance actually attained by one commercial firm. While it is inferior to that reported in the literature, it is still quite high. One could reasonably expect commercial firms to improve their coating substantially in the next few years by adopting the recently discovered optimum coating conditions.

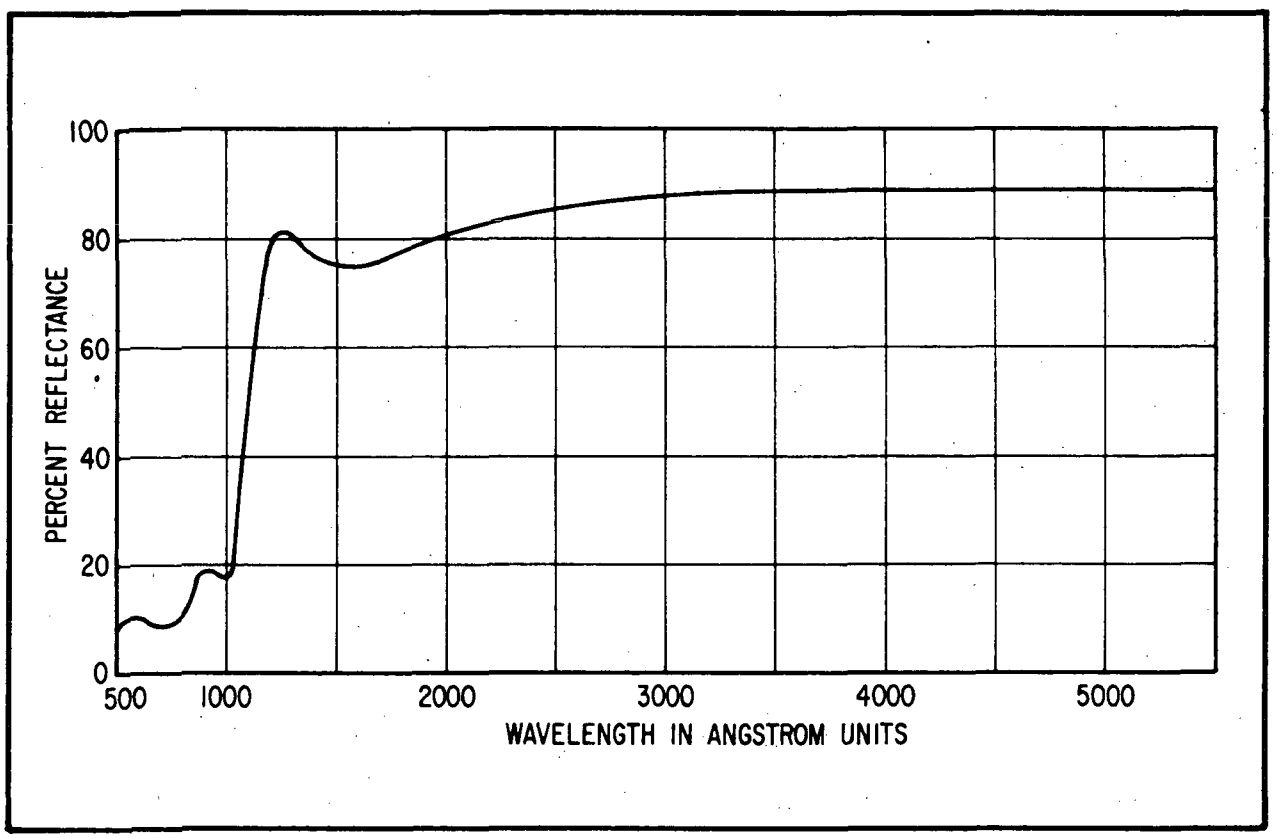

Figure 3-18 Coating of Al and MgF_2 Optimized for the 1200 Å Region

3.6.2 Refractive Correctors

The telescope offset guiding technique for the AOS requires that the field not available for science be corrected to provide image sizes compatible with the fine guide error sensor resolution element. In the f/10 configuration the tracking field image size can be adequately corrected in either of two ways: with the corrector after the folding mirror, or ahead of it. Vignetting of the tracker field results if the corrector is placed after the folding mirror, and spectral range is limited if it is placed ahead of it. See Figure 3-19. The decision was made not to limit the spectral range to the science and to accept decreased pointing performance in the f/10 configuration. Hence, the f/10 configuration will not use a corrector. The f/25 configuration does permit the addition of a corrector without adverse effects, and the

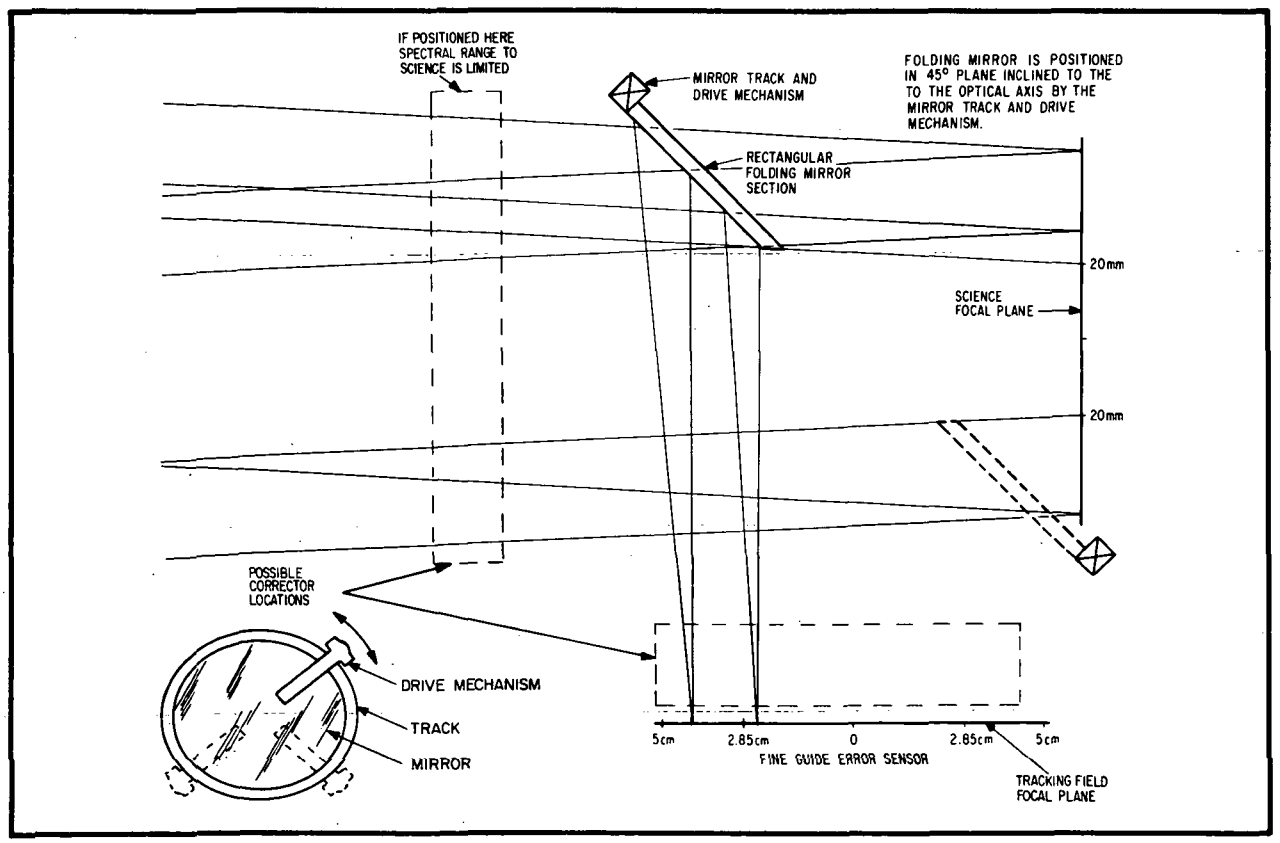

Figure 3-19 Refractive Corrector Locations

following discussion presents its preliminary design. The fields for both the f/10 and f/25 configurations are tabulated as follows:

Telescopes Fields of View

	f/10	f/25
FOV for 40 mm diameter detector	13.75 arc-min	5.5 arc-min
Tracking FOV	34 arc-min	30 arc-min

Corrector for f/25 Ritchey-Chretien. An f/25 40 mm diameter science field is well corrected without additional optics, but the tracking field must be corrected to provide a better image for the fine guide tracker. A steep meniscus corrector, mentioned by Wilson[10] was examined. It proved to have so much lateral color that it was abandoned. However, by splitting the meniscus into two elements, one curved each way, the color shift was fairly well balanced. Additional manipulation of the parameters provided adequate correction for the guidance system. A consequence is that the fine error sensor drive must have a third drive axis to follow the rather steep curvature of field. Figure 3-20 is a layout of the corrector and its prescription.

Ray traces were run to evaluate the f/25 tracking field corrector. The requirement is to correct the image to produce a spot not to exceed 60 μm in diameter across the tracking field. Figure 3-21 shows the results of the ray tracking. Trace A is the spot size at the inner edge of the tracking field, Trace B is near the middle of the tracking field, and Trace C is out at the edge of the tracking field. It can be seen that the 60 μm image diameter requirement is met for the two inner field positions and is very nearly met at the very edge of the field. Further optimization during detail design can bring the field edge into proper limits.

SURFACE	RADIUS	AXIAL SEPARATION	MATERIAL	DESCRIPTION
①	∞			UNCORRECTED IMAGE
		-320 mm	air	
②	-328.560mm			
		15.2 mm	FK50	
③	-343.056mm			
		0.01mm	AIR	
④	343.056mm			
		15.2mm	FK50	
⑤	328.560			
		299.76mm	AIR	
⑥	∞			MEAN POSITION OF CORRECTED FIELD
⑦	69.1mm			ACTUAL POSITION OF CORRECTED FIELD

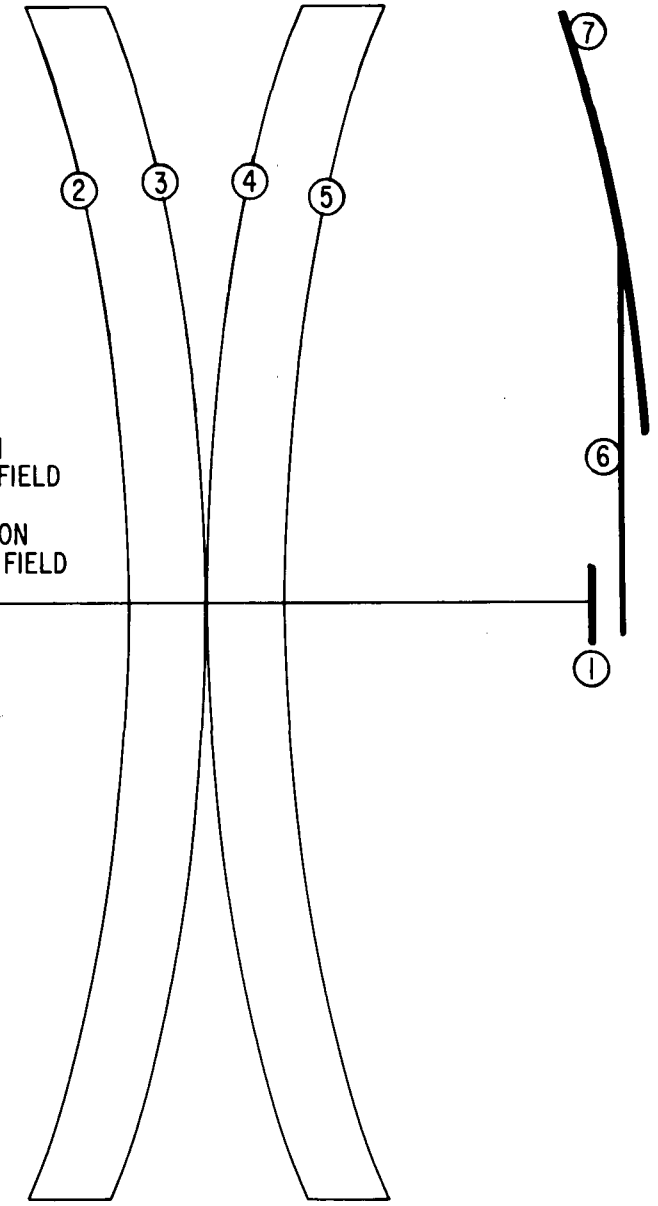

Figure 3-20 f/25 Corrector Layout and Prescription

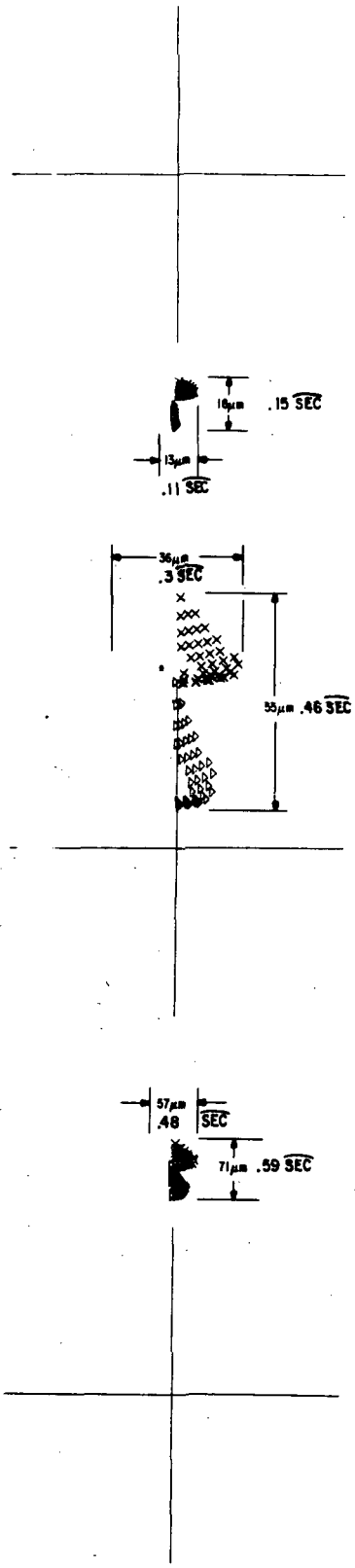

(A) INNER EDGE OF TRACKING FIELD.

(B) MIDDLE OF TRACKING FIELD.

(C) OUTER EDGE OF TRACKING FIELD.

X 4000Å

▷ 7000Å

Figure 3-21 Corrector Ray Traces

3.7 AOS TELESCOPE PERFORMANCE AND SPECIFICATIONS

3.7.1 Point Spread Functions

Monochromatic point spread functions (PSF) of the telescope were computed using BBRC's computer program POLYPAGOS which includes diffraction effects in its calculations. The results are presented in this section. These point spread functions were convolved with the anticipated pointing error to yield system resolution. The degraded point spread functions as a result of pointing error are presented in Section 3.7.3.

No detailed tolerancing was attempted, but to degrade the λ1216 Å on-axis performance from a pure unaberrated point spread function each mirror's figure was warped by an additive factor A cos $\frac{\pi r'}{D'}$, where r' is the radial coordinate on the element, D' is the diameter of the element, and A = 500 Å was arbitrarily chosen. This function has its only mode at the outer edge of the mirror in question. Test cases with λ = 4000 Å were computed with and without the surface error introduced. It caused only minor changes to the PSF and MTF. On-axis PSF's were unchanged. The off-axis of f/25 case had a slight increase in its secondary maximum value. The off-axis f/10 case was unchanged. More detailed design, which must include all other tolerancing, perhaps should consider a larger surface error than the above value.

The plots that follow show sharp spikes, which are artifacts introduced because the PSF sampling plot interval was too coarse to remove them.

3.7.1.1 f/25 Telescope PSF

Figure 3-22 is the Y slice through the PSF for the f/25 telescope operated on-axis for λ = 6563 Å. It is similar to an Airy disk except the central maxima has a 34 μm diameter and the secondary maxima relative height is 9 percent. An Airy disk would have a diameter of 20 μm and a secondary maxima relative amplitude of about 2 percent. The difference is due to the presence of the central obscuration and is reflected in the MTF by reduced MTF at mid-spatial frequencies and improved MTF at higher spatial frequencies. Resolution is approximately 0.16 arc-seconds.

Figure 3-23 shows slices through the PSF for the f/25 telescope operated at the edge of a 40 mm diameter field for λ = 6563 Å. The field angle is along the Y axis as it is in all cases. As compared to the on-axis case, the X slice is unchanged and the central spike and secondary maxima relative amplitudes for the Y slice are washed out slightly. The X MTF values are therefore unchanged and the Y MTF values are only slightly lowered. The performance is still basically determined by diffraction of the obscured aperture.

Figure 3-24 shows X and Y slices and the three dimensional plot of the PSF for the f/25 telescope operated at 5.5 arc-minutes field at λ = 6563 Å. This field corresponds to an image format of 80 mm diameter. The central maxima of the X slice is basically unchanged in shape and size. The central maxima of the Y slice is broadened. Energy has been relocated into the outer rings. Resolution will be degraded to around 0.17 arc-second according to the Rayleigh criteria.

Figure 3-25 is a Y PSF slice for the same telescope operated on-axis at λ = 1216 Å. Scaling Figure 3-22 linearly with wavelength, the first minima of Figure 3-25 should lie at 1.5 μm and the secondary maxima at 4.9 μm. Since the PSF sampling was done in 1 μm increments, starting from zero, it would have missed the minima and caught the maxima. The secondary maxima is at the same relative height as for

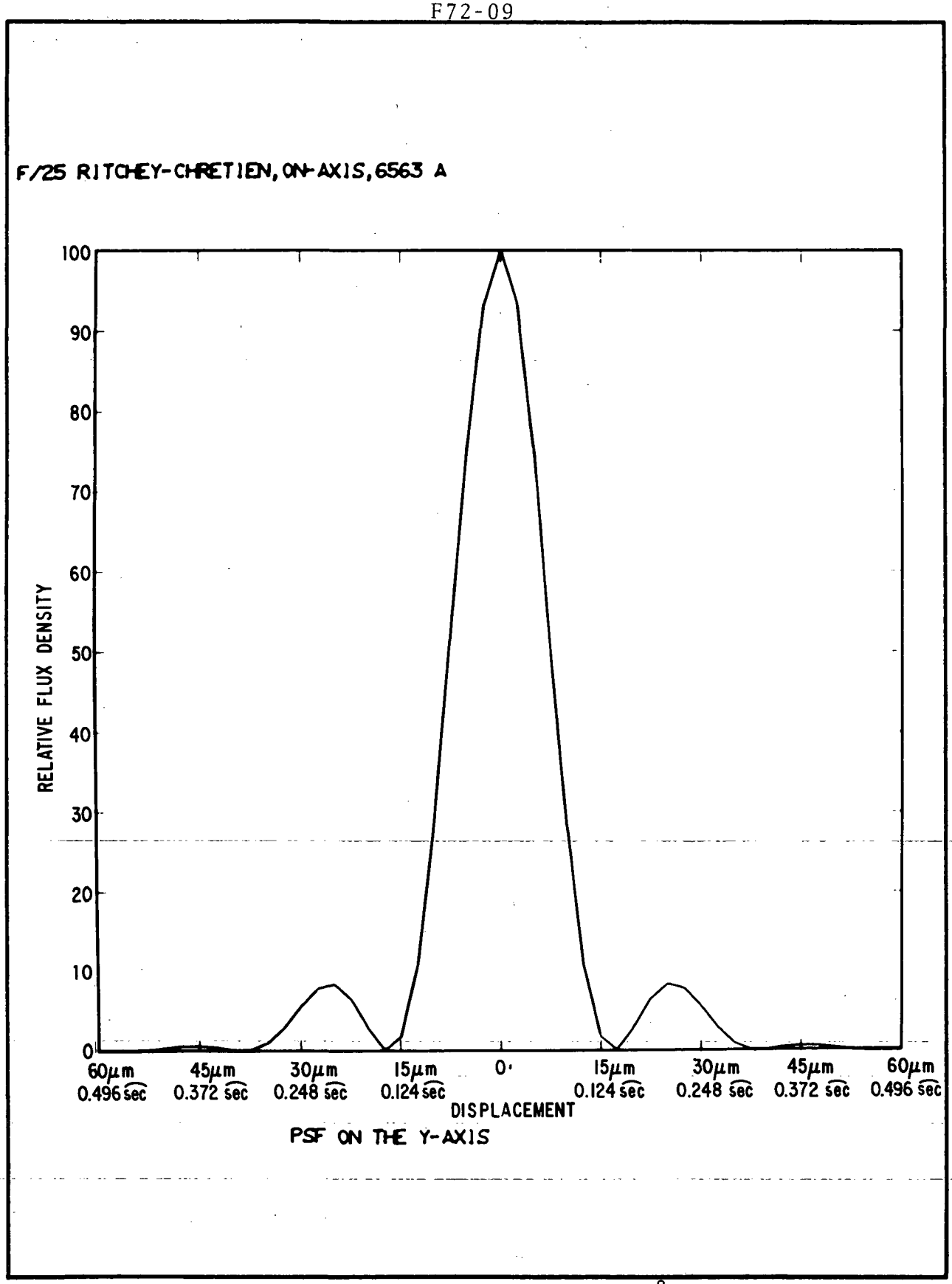

Figure 3-22 PSF, f/25, On-Axis, 6563 Å, Y Slice

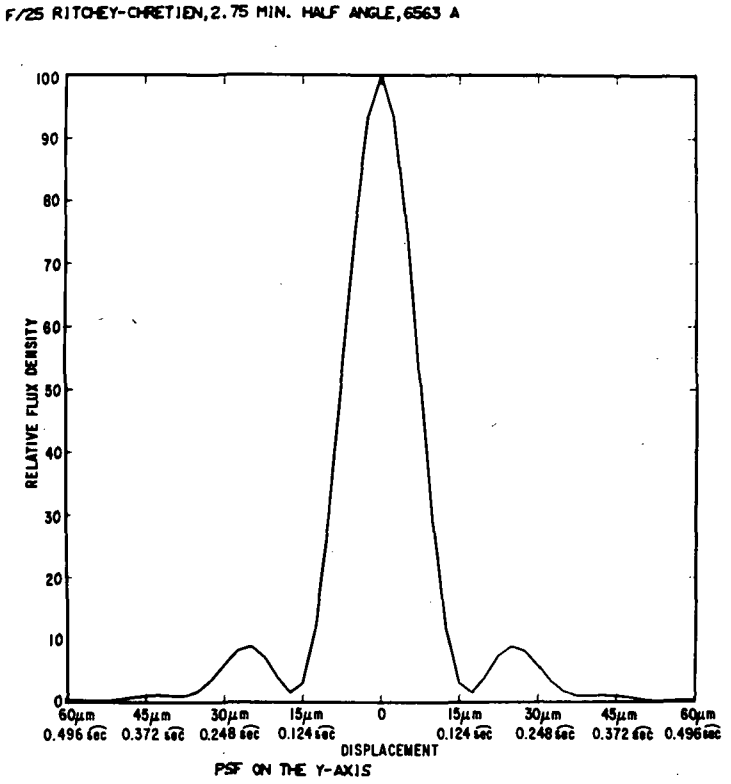

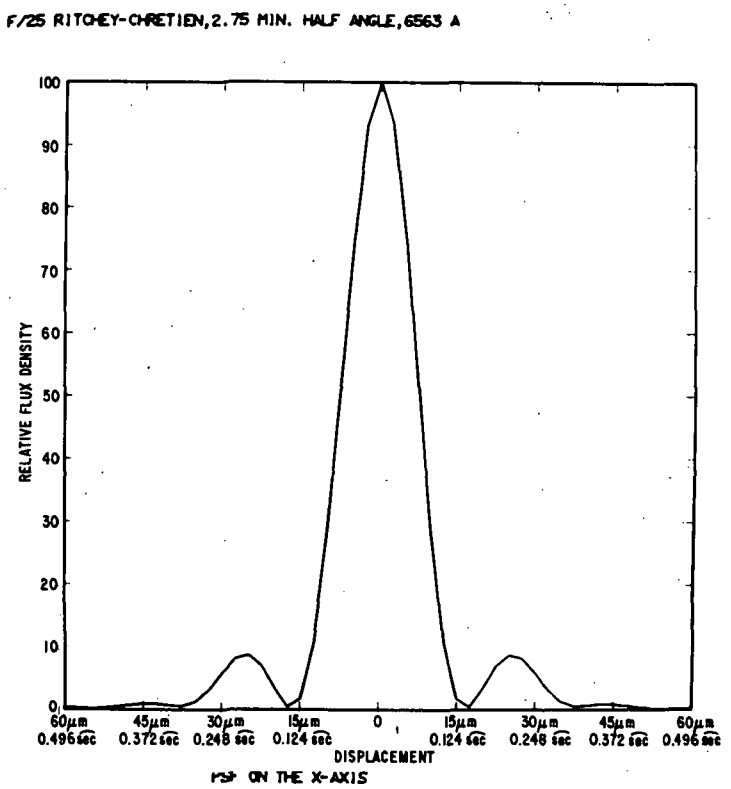

Figure 3-23 PSF, f/25, Off-Axis, 6563 Å, X and Y Slices

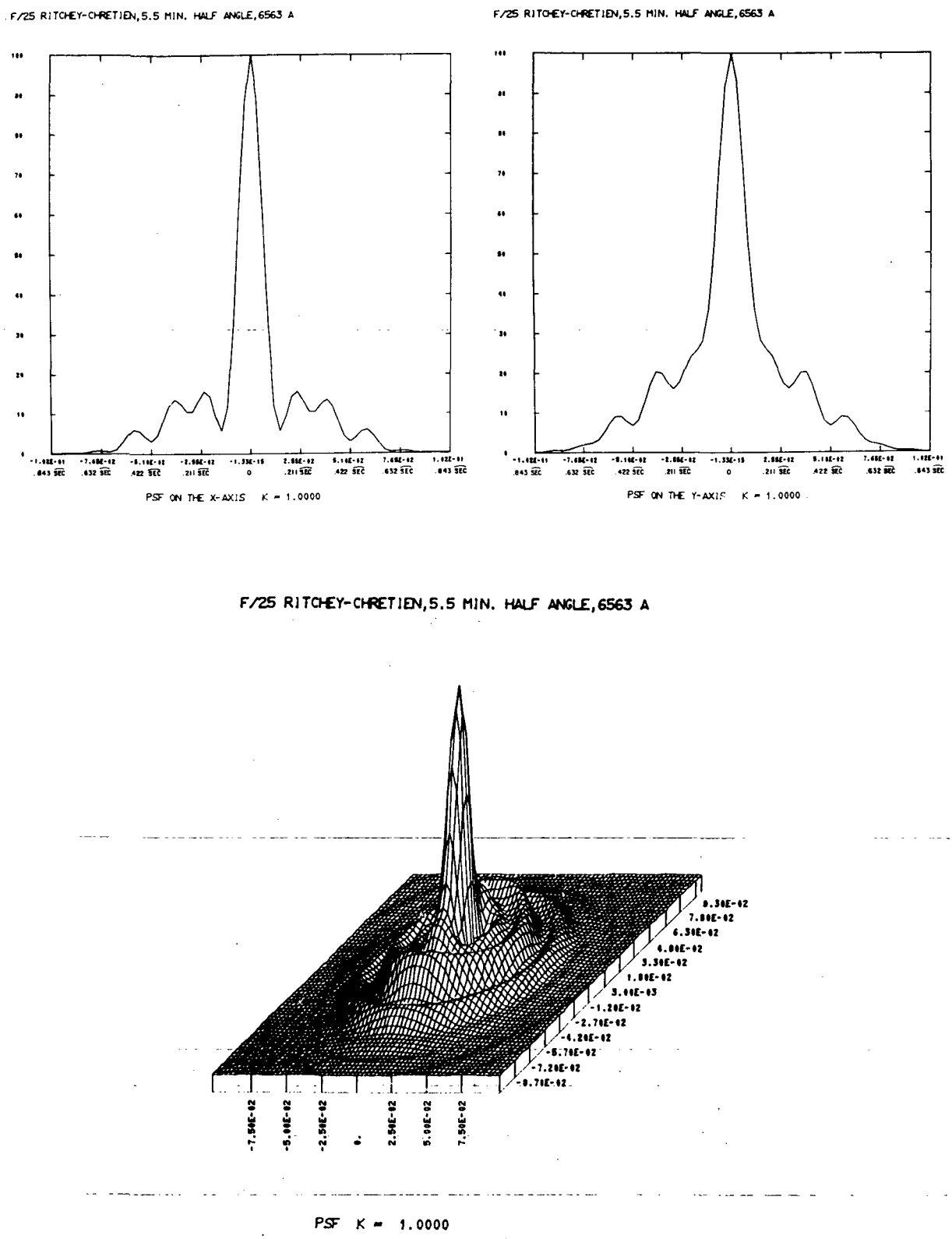

Figure 3-24 PSF, f/25, Off-Axis, 6563 Å, X and Y Slices and 3-D Plot

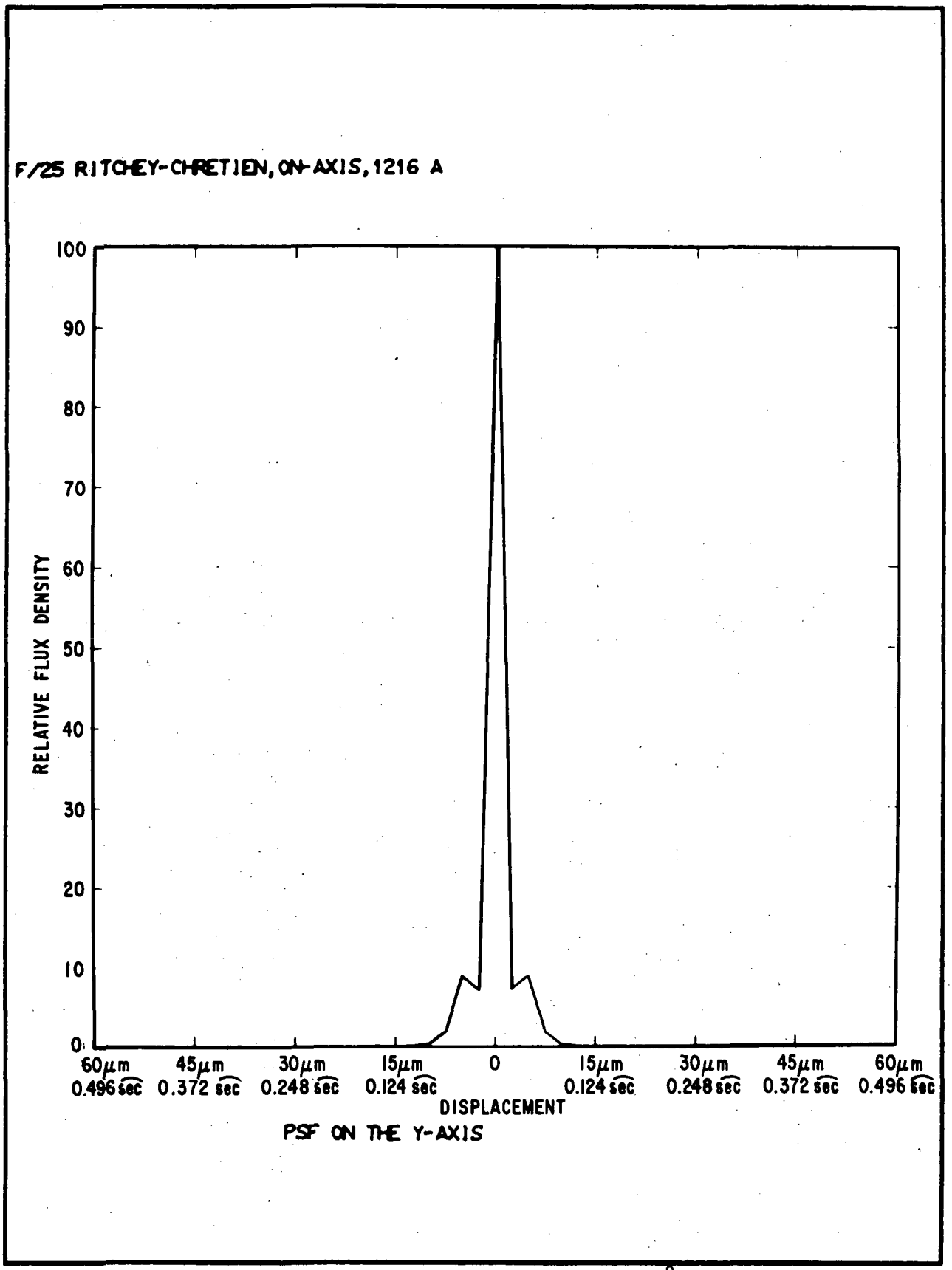

Figure 3-25 PSF, f/25, On-Axis, 1216 Å, Y Slice

λ = 6563 Å. Thus the absence of the first zero is undoubtedly an artifact of the computer. The mirror surface errors had a minimal effect on the PSF.

Figure 3-26, plots A and B are PSF slices at the edge of a 40 mm diameter science field at λ = 1216 Å. Vertical lines have been superimposed to show the size predicted by third order theory. In third order theory the region labeled "obscuration" would be void of energy. The PSF's show diffraction effects (and artifacts) in the obscured region and beyond the predicted third order aberration size, but the basic aberration (third order astigmatism) is large enough compared to diffraction limit (Figure 3-24) that the aberration is well described by the third order theory. Figure 3-26, plot C is the three-dimensional plot from which plots A and B are taken.

The above PSF's show that the f/25 telescope will provide spatial resolution of better than 0.25 arc-seconds over a 40 mm diameter field over the entire wavelength range used.

3.7.1.2 f/10 Telescope PSF

The f/10 telescope performance is shown in Figures 3-27 and 3-28 for the on-axis case at the wavelengths λ = 6563 Å and λ = 1216 Å. These are formed strictly by diffraction by the obscured aperture and are identical, in angular units, to Figures 3-22 and 3-24 for the f/25 on-axis cases. Resolution is approximately 0.16 arc-seconds.

Figure 3-29 plots PSF's for the f/10 telescope at 2 arc-minutes field angle. The central peak is essentially unchanged. Energy is shifted in the second ring along the Y direction, as is typical of the aberration caused by a small amount of coma. At this wavelength one Rayleigh limit (optical path difference = $\lambda/4$) of sagittal coma is $\pm \lambda F = \pm 6.5$ µm.[11] Third order sagittal coma amounts to 3.3 µm at 2 µm arc-minutes, which is about one-half of one Rayleigh limit; hence, at this field the system is essentially diffraction-limited (0.16 arc-second). This can also be seen in Figure 3-30 where the

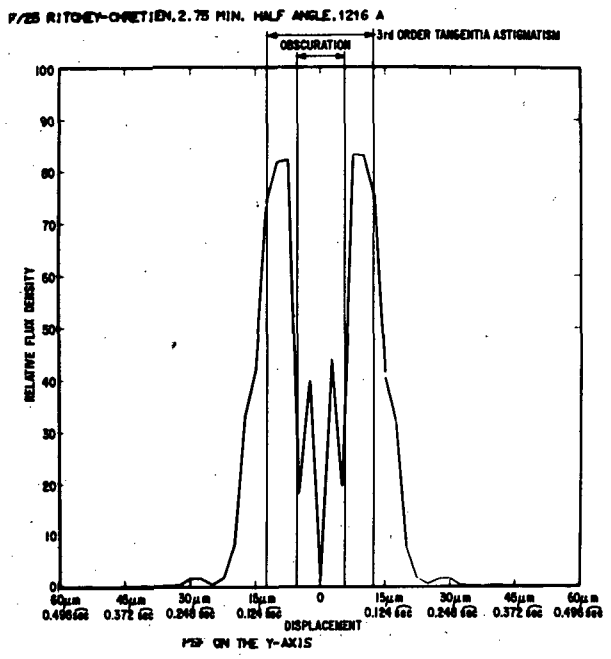

(A)

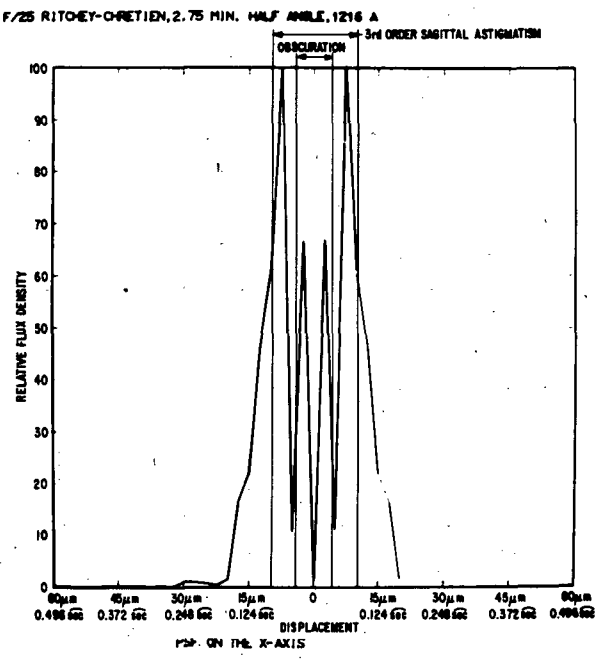

(B)

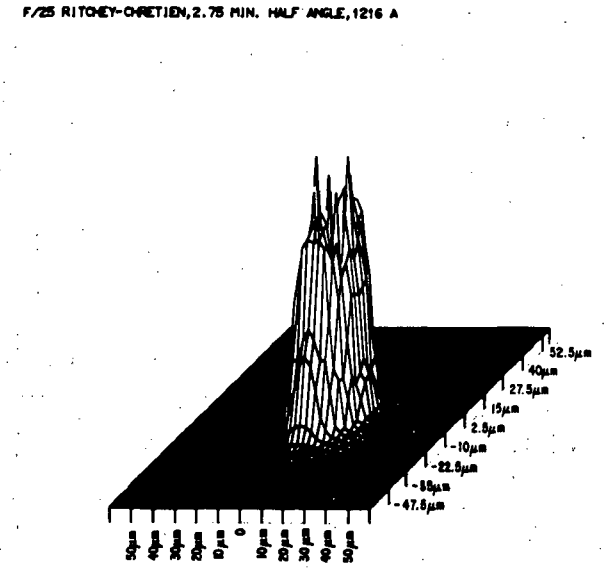

(C)

Figure 3-26 PSF, f/25, Off-Axis, 1216 Å, X and Y Slices and 3-D Plot

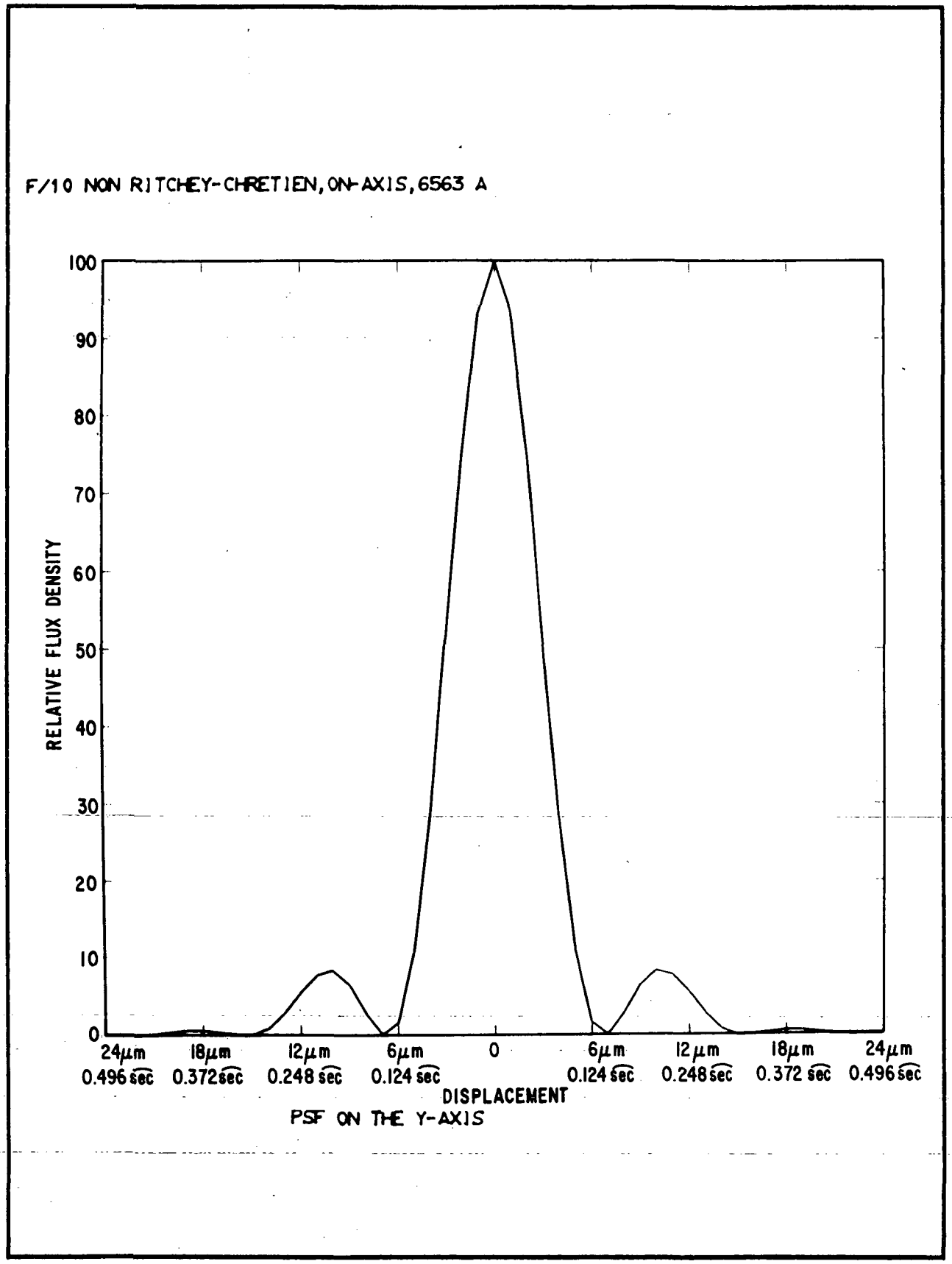

Figure 3-27 PSF, f/10, On-Axis, 6563 Å, Y-Axis

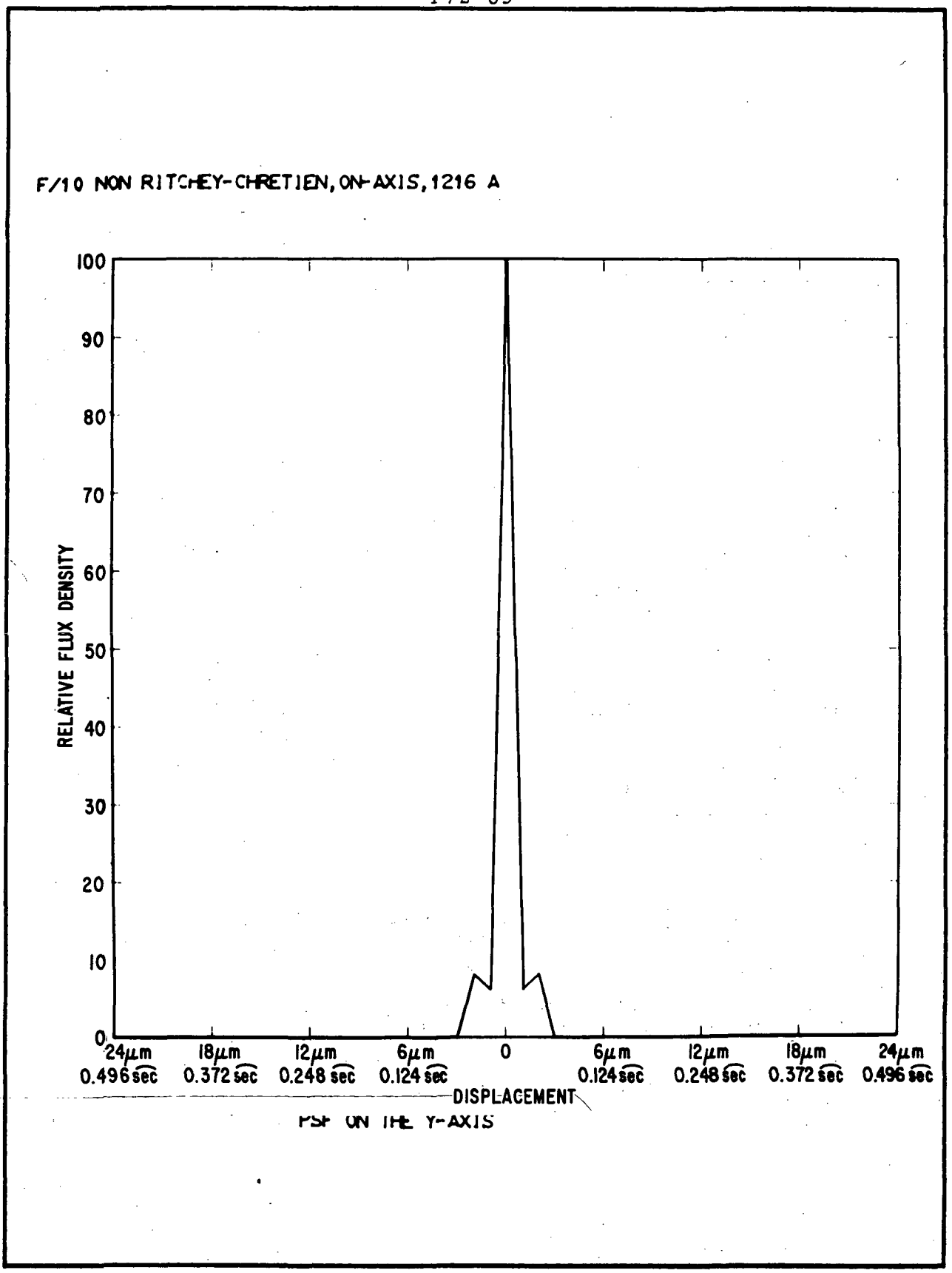

Figure 3-28 PSF, f/10, On-Axis, 1216 Å, Y-Axis

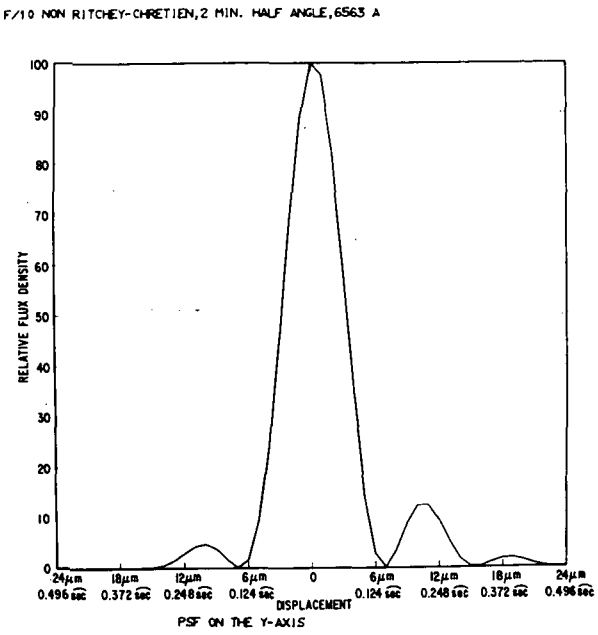

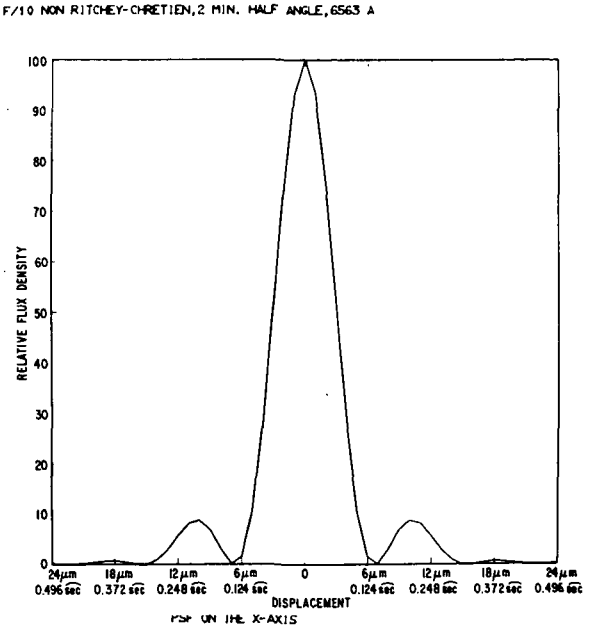

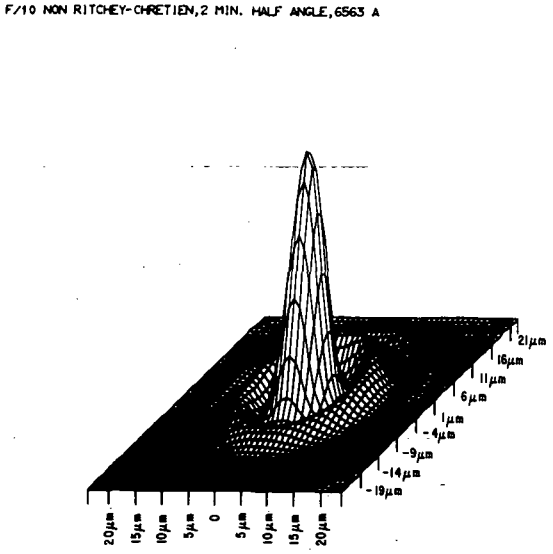

Figure 3-29 PSF, f/10, Off-Axis, 6563 Å, X and Y Slices, and 3-D Plot

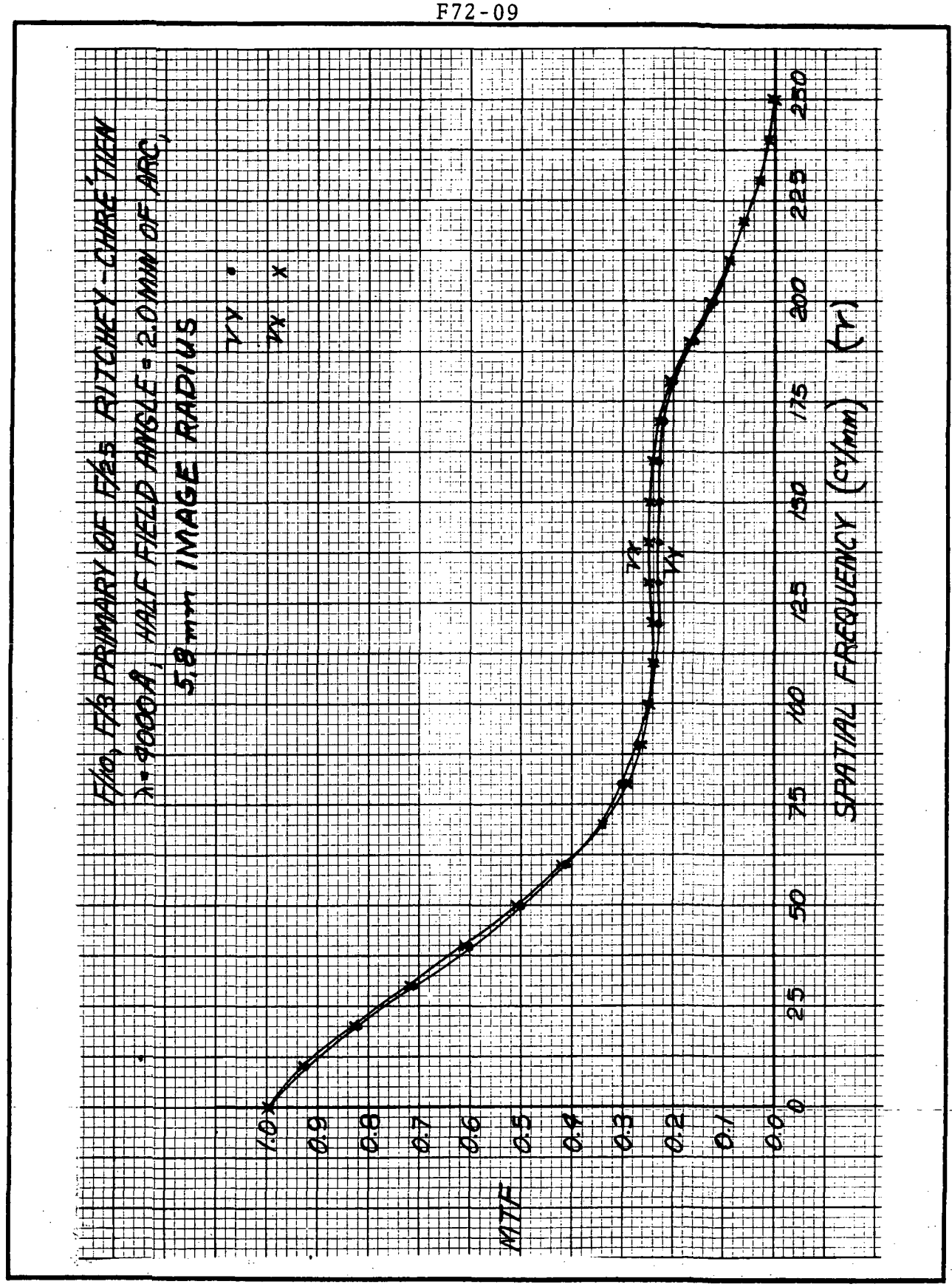

Figure 3-30 MTF Versus Spatial Frequency, f/10, Off-Axis

MTF degradation is minimal. (At the wavelength of this MTF curve, one Rayleigh limit is 4 μm, so the third order coma of 3.3 μm is still less than one Rayleigh limit.)

The plots of Figure 3-31 are PSF's for the f/10 telescope at the edge of a 40 mm diameter science format for λ = 6563 Å. These show coma due to 1.74 Rayleigh limits. For the Y slice the central peak is broadened and the secondary ring is severely modified. The X slice shows a large amount of energy appearing in the secondary ring coming from the central peak, and the diameter of the central peak reduced from the on-axis case. The MTF at 4000 Å (Figure 3-32) shows a drastic reduction (this corresponds to 2.8 Rayleigh limits). In actual practice, the resolution will still be better than 0.25 arc-second by the Rayleigh criteria and the pointing will "wash out" all except the central peak.

Figure 3-33 shows PSF's for the f/10 telescope at 13.75 arc-minute field (80 mm image diameter) at λ = 6563 Å. It shows a larger amount of coma. Resolution is degraded to about 0.37 arc-second.

The plots of Figure 3-34 are for the f/10 telescope at 2 arc-minutes field angle and at λ = 1216 Å. Third order sagittal coma is 3.3 μm and one Rayleigh limit is λF = 1.2 μm so we are not diffraction-limited, which would be 0.03 arc-seconds or 1.5 μm at this wavelength. Resolution is of the order of 0.1 arc-second for the telescope and hence is adequate for this application. System resolution will be determined by pointing errors.

The plots of Figure 3-35 are PSF's at the edge of a 40 mm science field for the f/10 telescope at λ = 1216 Å. Third order sagittal coma is 11.5 μm; hence we have 9.5 Rayleigh limits of coma. The central peak is still reasonably small and although energy appears well away from the central peak, it is small in amplitude and will be "washed out" by tracking errors. Resolution remains on the order of 0.1 arc-seconds for the telescope.

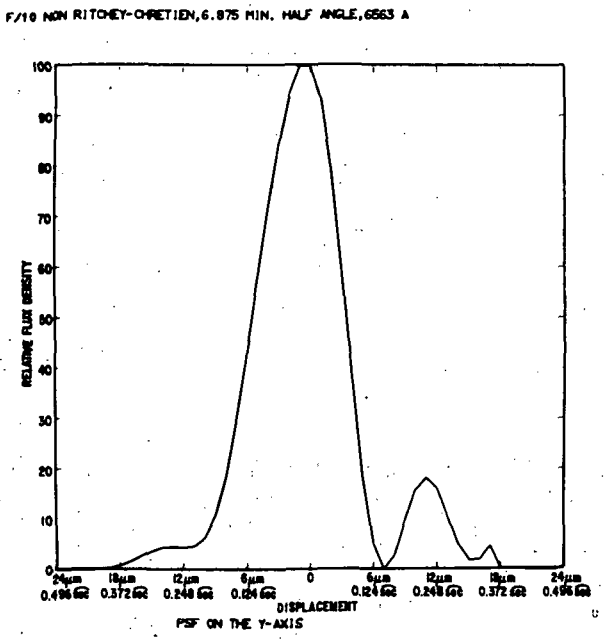

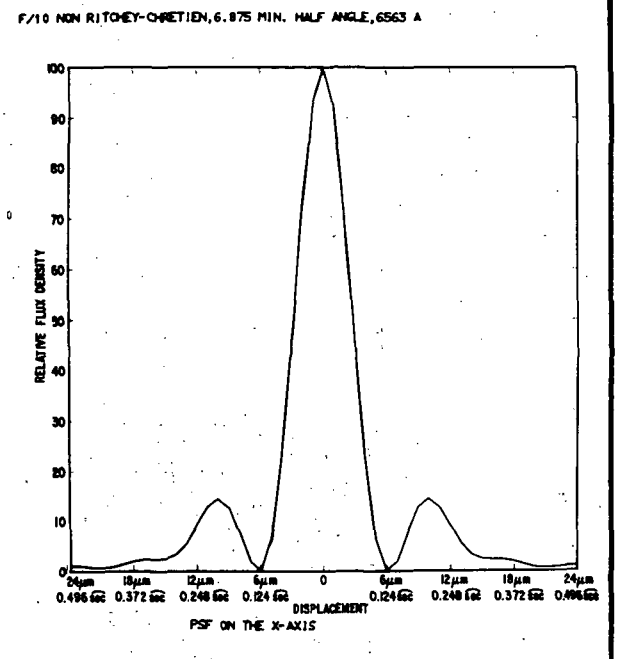

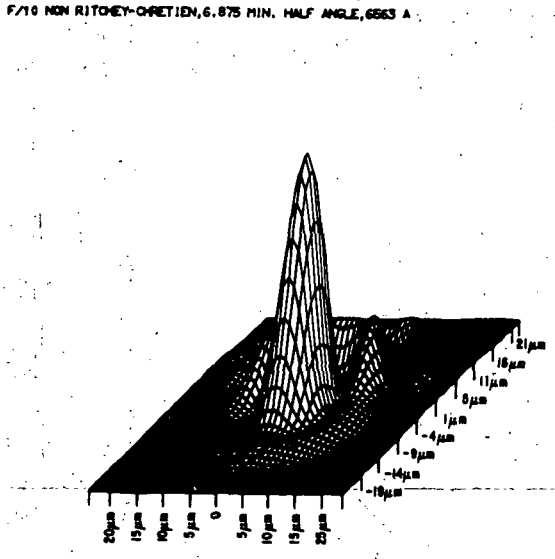

Figure 3-31 PSF, f/10, Off-Axis, 6563 Å, X and Y Slices, 3-D Plot

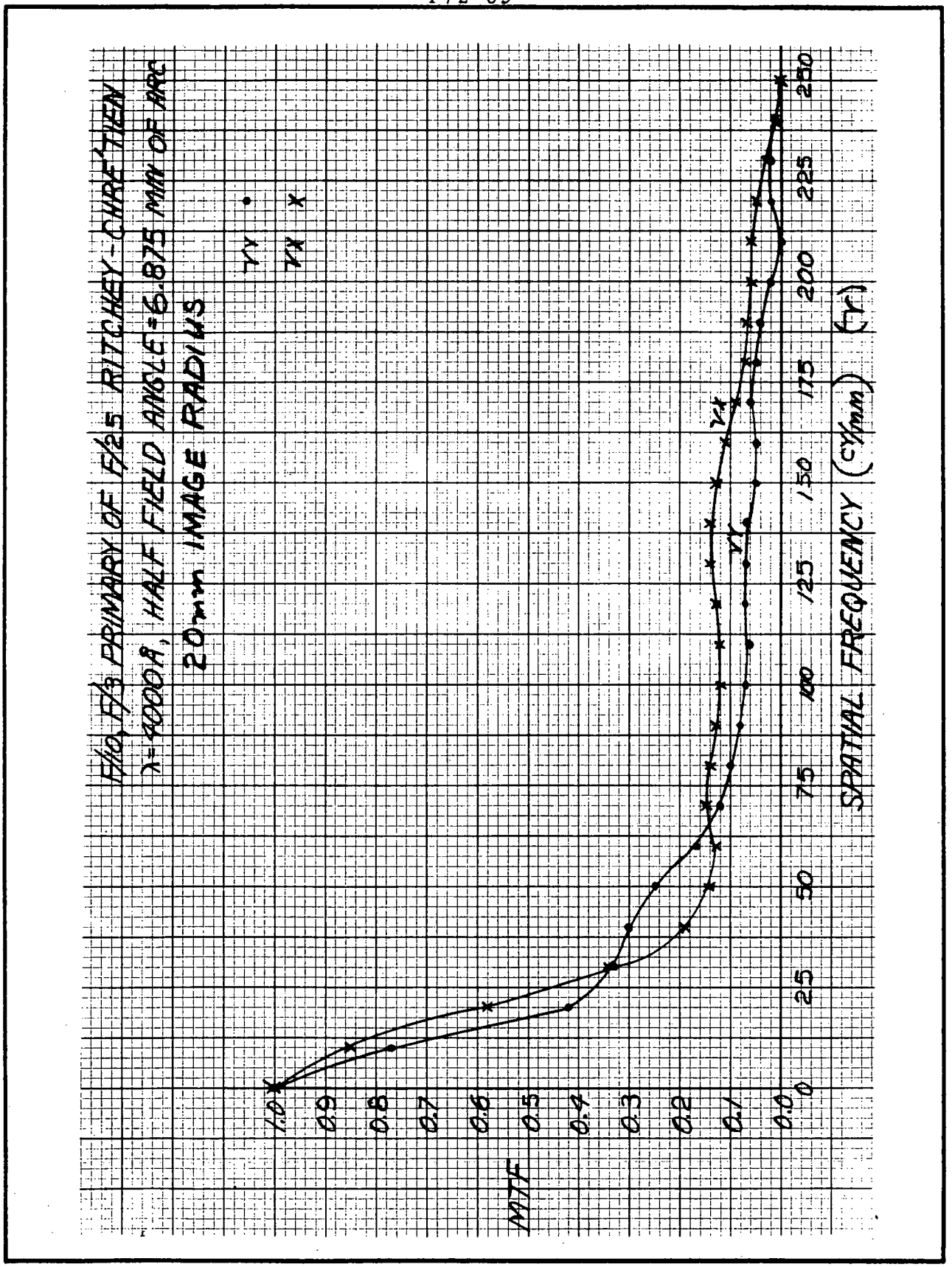

Figure 3-32 MTF Versus Spatial Frequency, f/10, Off-Axis

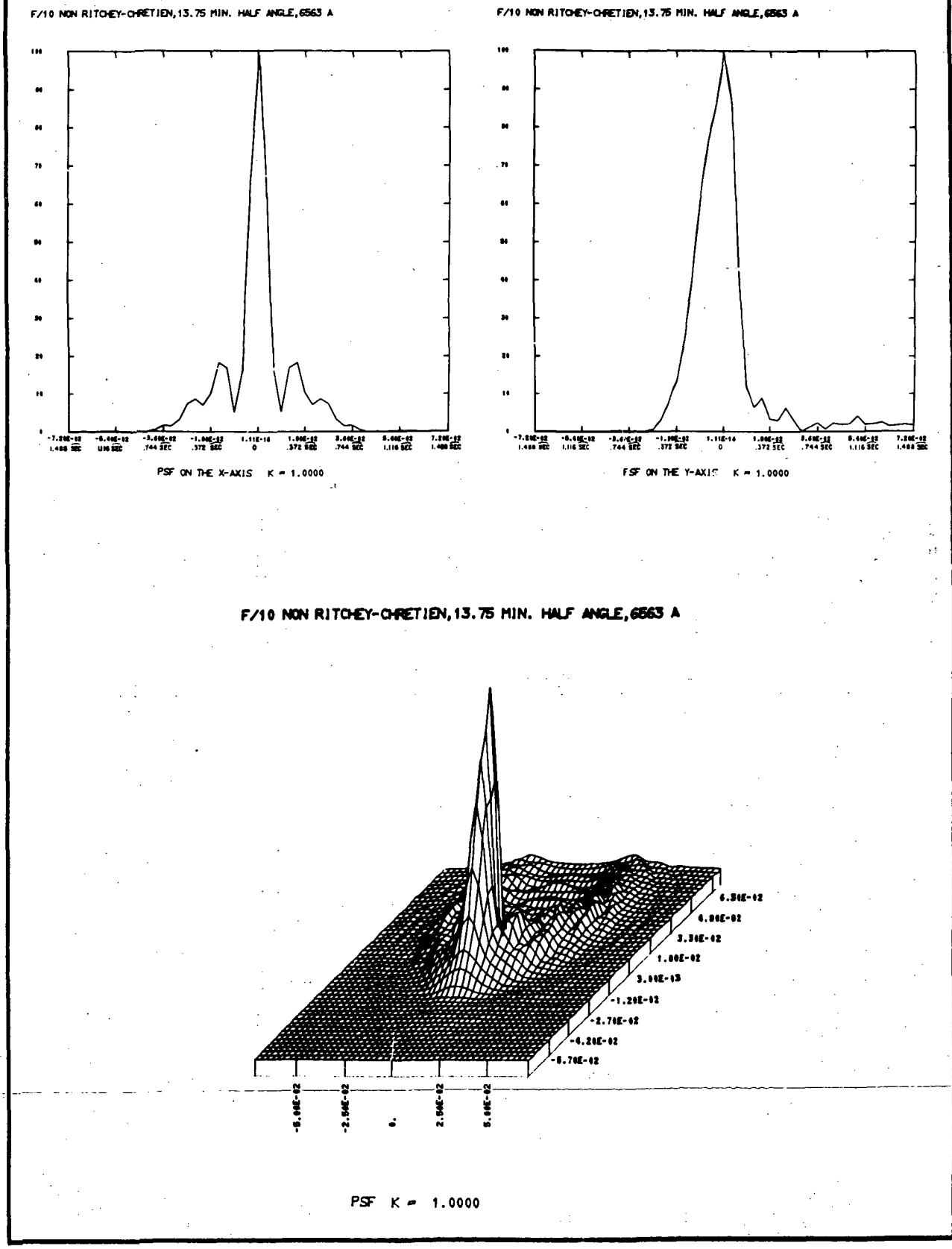

Figure 3-33 PSF, f/10, Off-Axis, X and Y Slices, and 3-D Plot

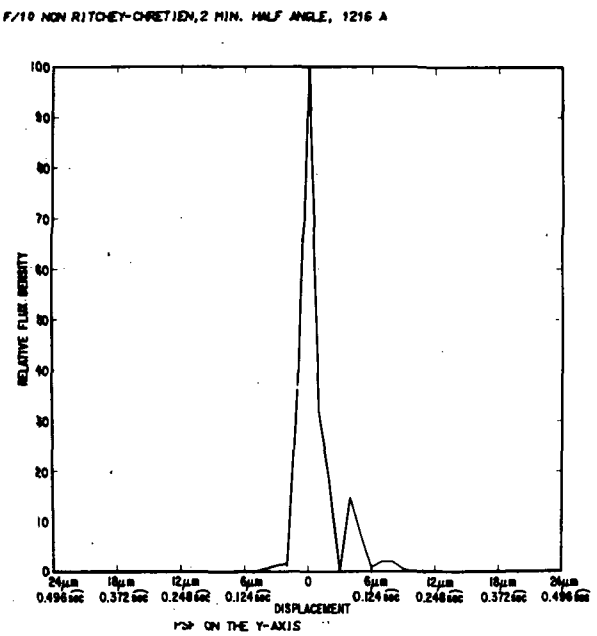

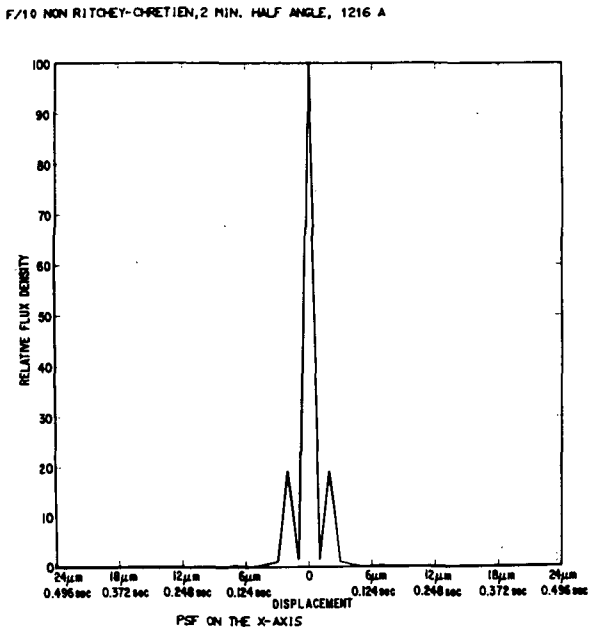

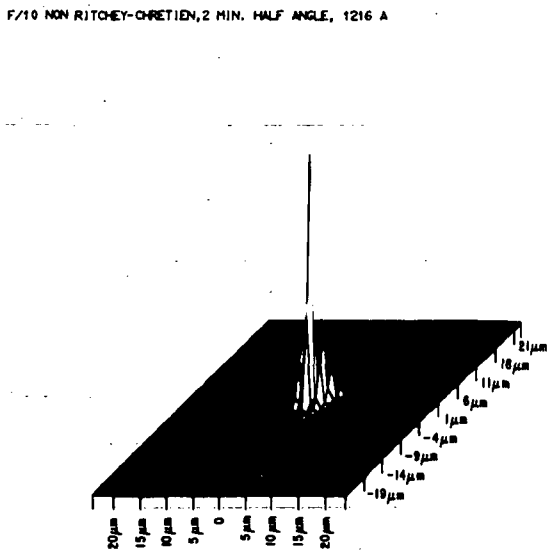

Figure 3-34 PSF, f/10, Off-Axis, 1216 Å, X and Y Slices and 3-D Plot

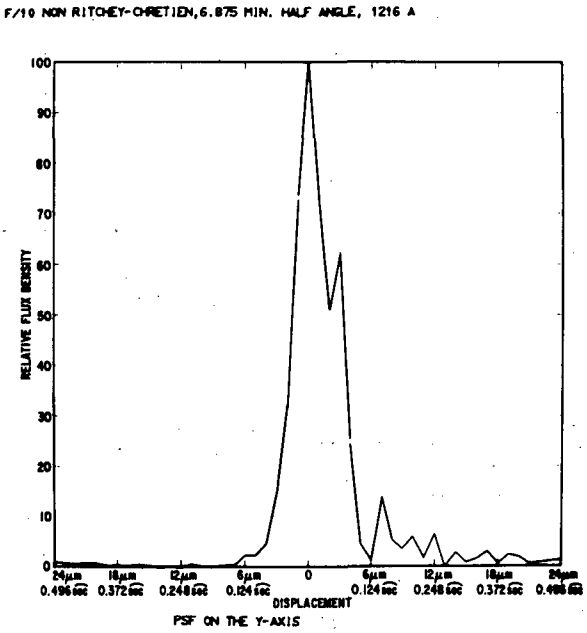

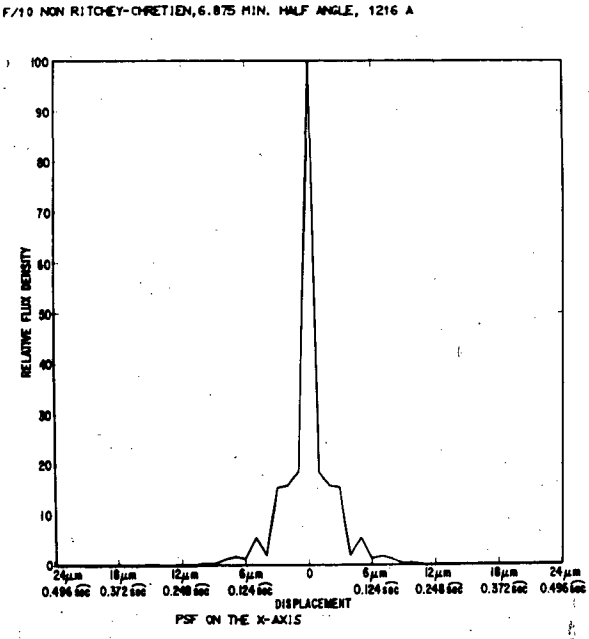

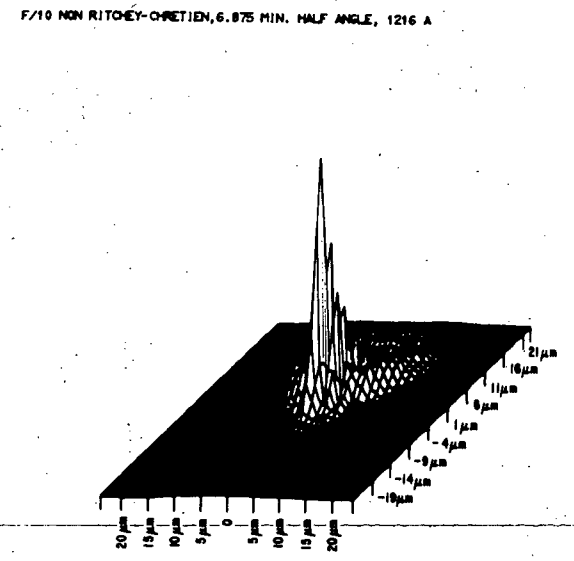

Figure 3-35 PSF, f/10, Off-Axis, 6563 Å, X and Y Slices and 3-D Plot

The f/10 PSF's show that the f/10 telescope will provide spatial resolution of better than 0.25 arc-second over a 40 mm diameter field over the entire wavelength range used. Figure 3-36 is a summary plot showing telescope spatial resolution across the usable fields of both the f/10 and f/25 configurations.

3.7.2 Modulation Transfer Function

The MTF curves in Figures 3-37 through 3-45, including diffraction effects, were calculated with BBRC's diffraction MTF computer program, POLYPAGOS. As shown in Figure 3-37, the f/25 Ritchey-Chretien's on-axis performance is controlled by the obscuration of 0.45. Over a 40 mm diameter field (2.75 arc-minutes half angle), its performance is essentially unchanged (Figure 3-38), but over an 80 mm diameter field, severe loss of resolution occurs near the edge of the field (Figure 3-39). The corresponding f/10 non-Ritchey-Chretien (Figures 3-40 and 3-41) shows no important loss of resolution over an 11.6 mm diameter field (2.0 arc-minutes half angle), but a severe loss at the edge of a 40 mm diameter field (Figure 3-42).

The remaining MTF curves (Figures 3-43 through 3-47) show performance for the f/10 Ritchey-Chretien design telescopes and are included for completeness.

3.7.3 Convolved Point Spread Functions

Figures 3-48 and 3-49 are point spread functions (PSF) that result from the convolution of the PSF of the telescope with the induced pointing error. It can readily be seen that system performance is negligibly affected at the longer wavelengths and that the spreading occurring at the shorter wavelengths is a direct result of pointing dynamics. However, even at the shorter wavelengths the desired spatial resolution is still attained.

Figure 3-48 shows the convolution of the f/25 telescope with pointing error and Figure 3-49 is for the f/10 telescope.

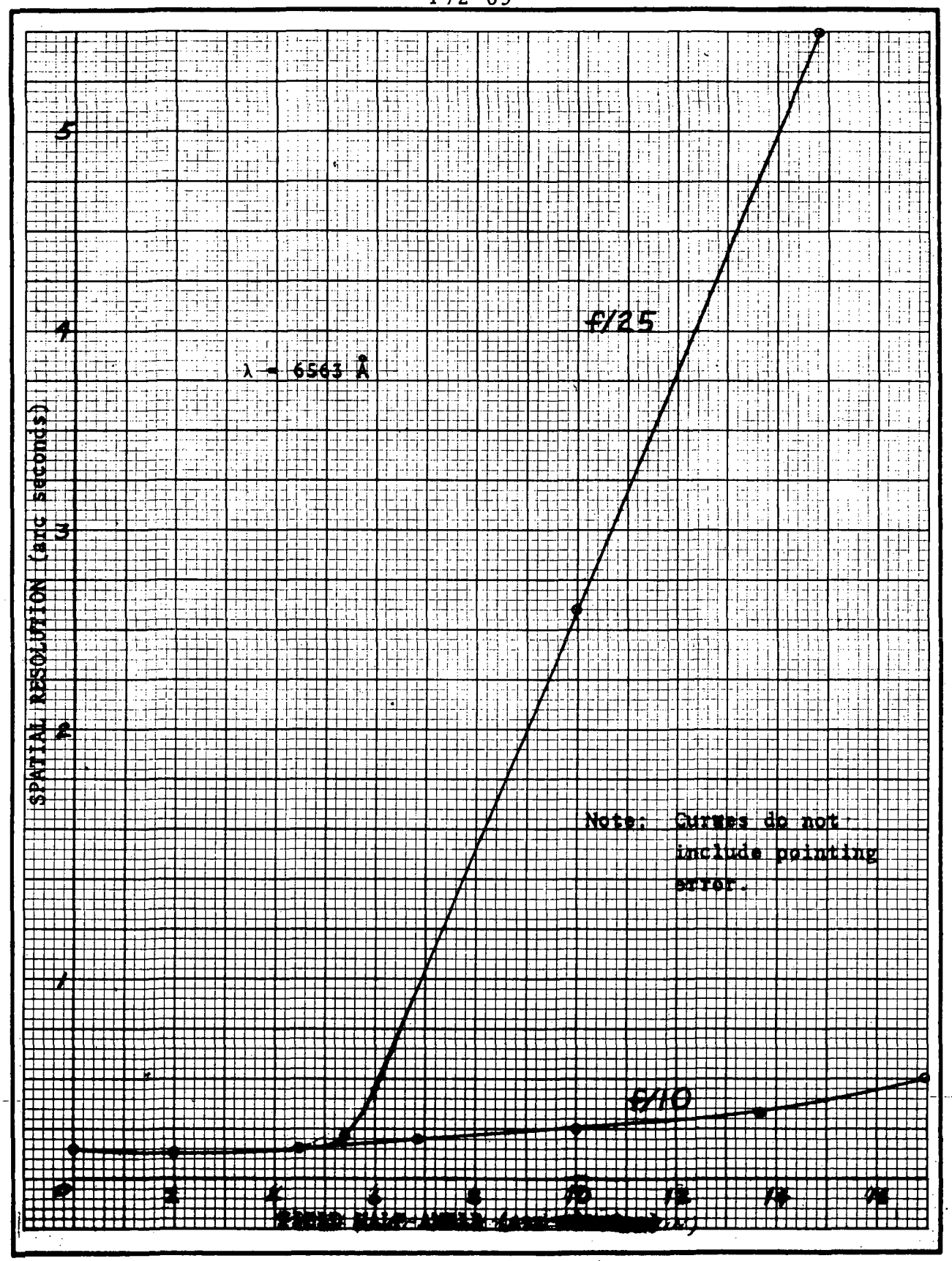

Figure 3-36 Telescope Spatial Resolution

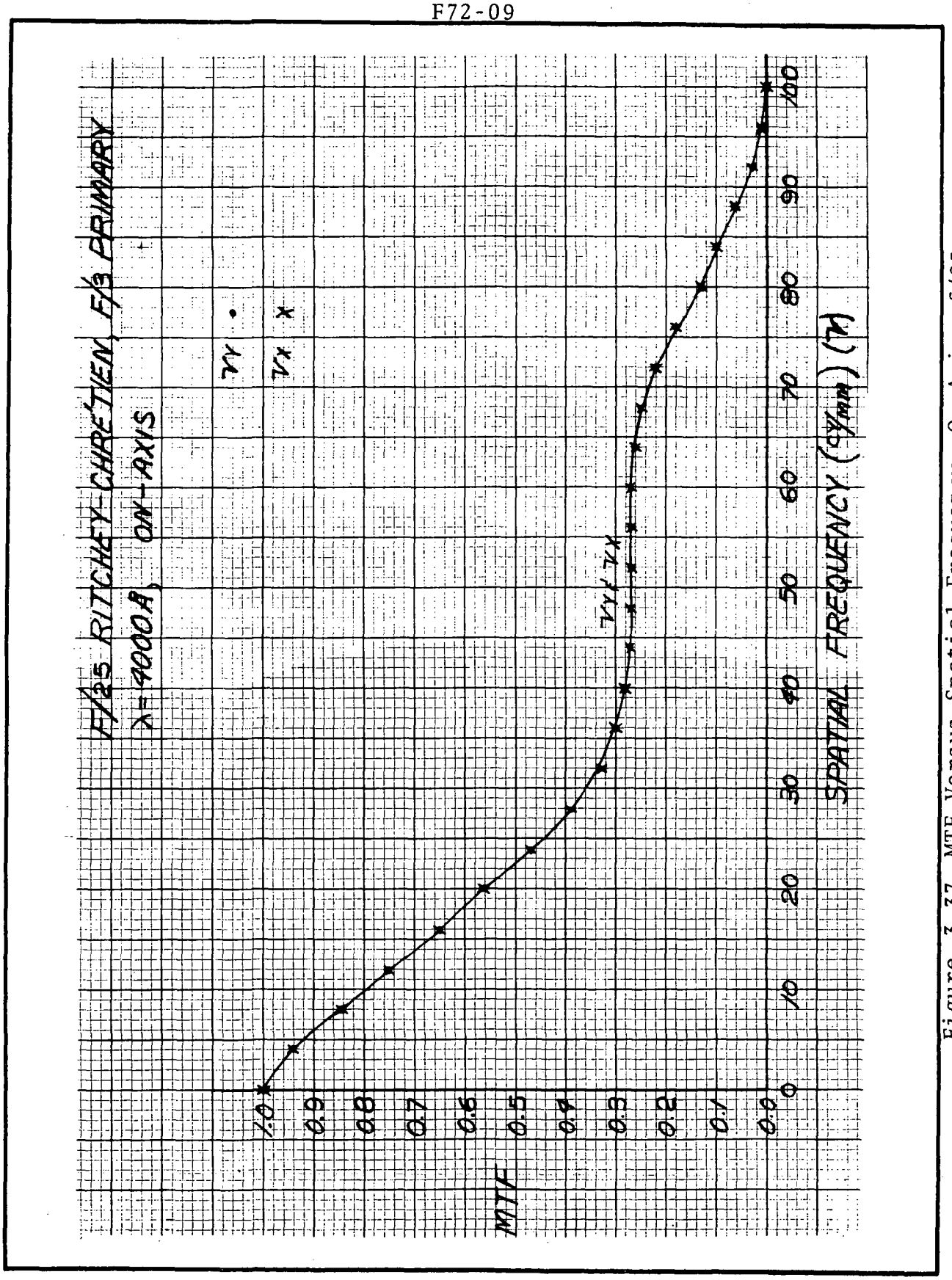

Figure 3-37 MTF Versus Spatial Frequency, On-Axis, f/25

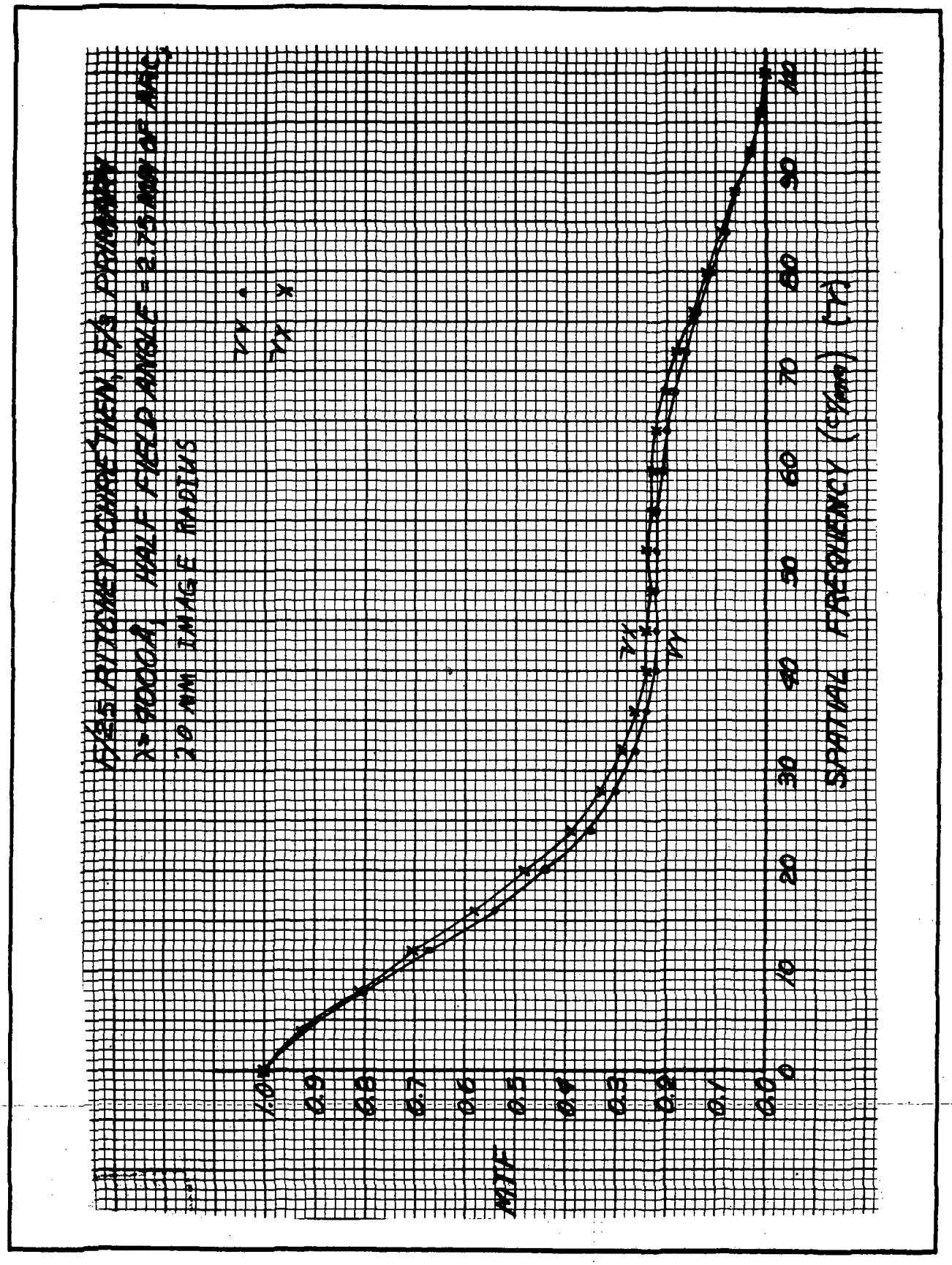

Figure 3-38 MTF Versus Spatial Frequency, Off-Axis, f/25

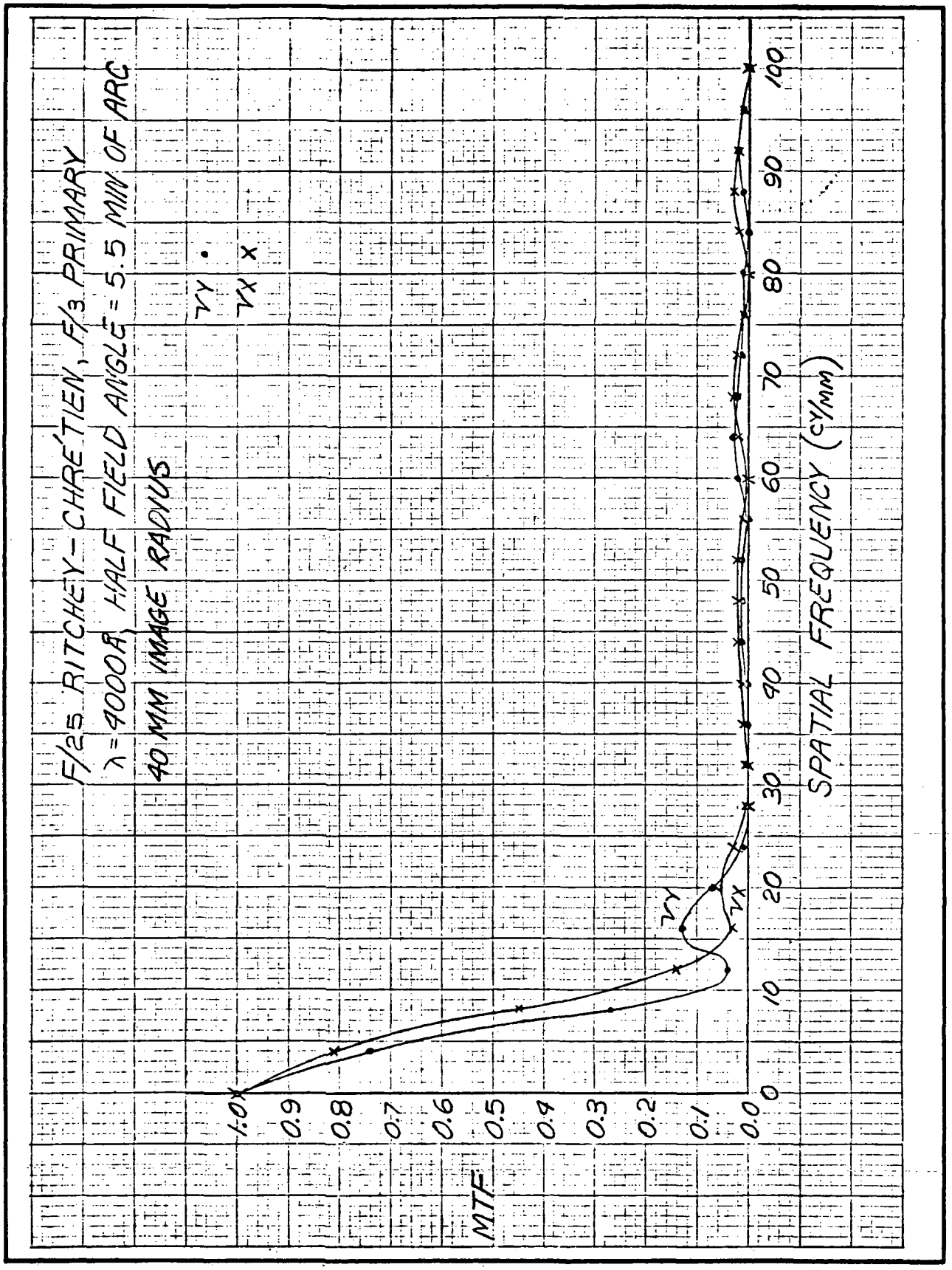

Figure 3-39 MTF Versus Spatial Frequency, Off-Axis, f/25

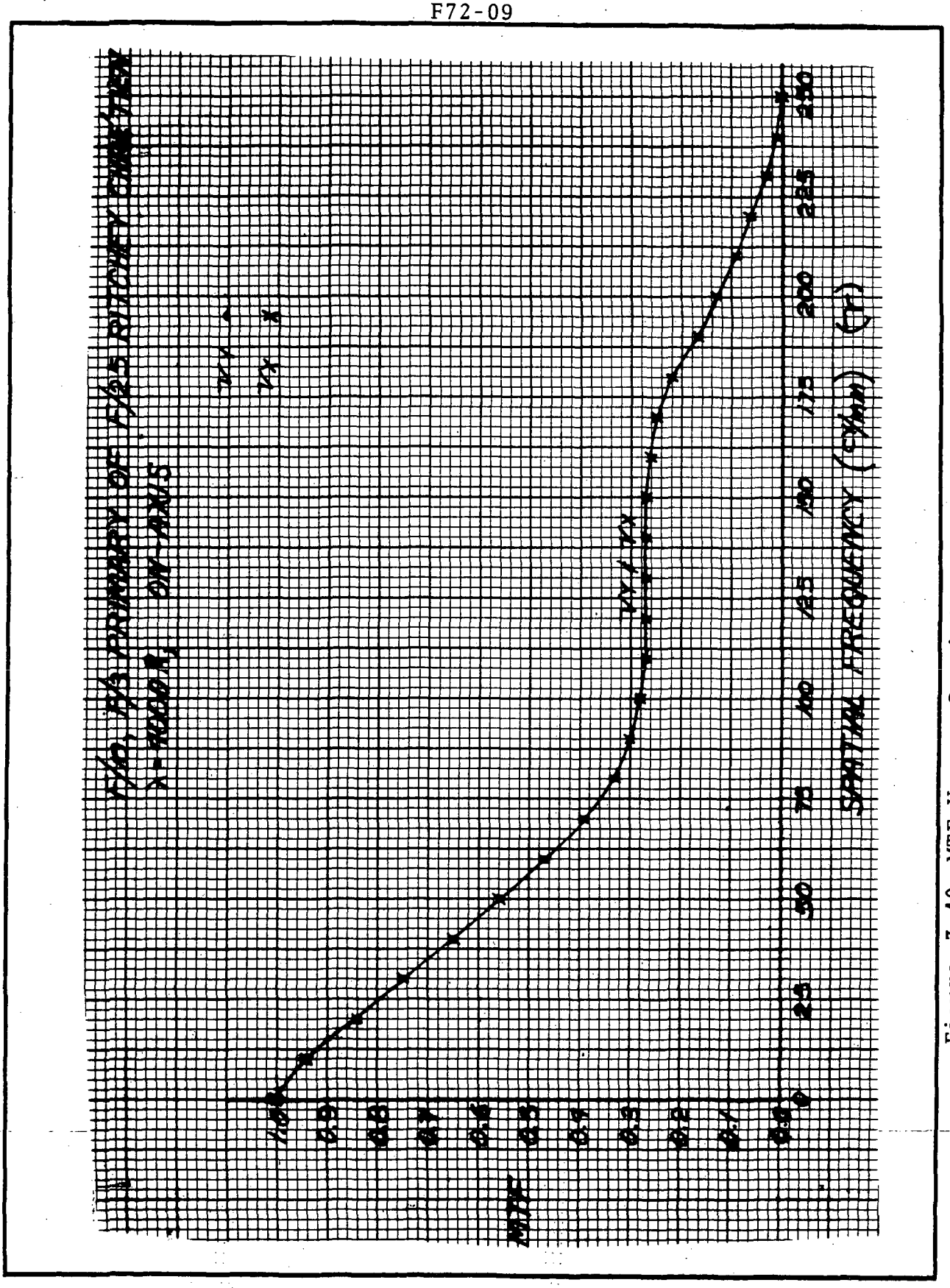

Figure 3-40 MTF Versus Spatial Frequency, On-Axis, f/10

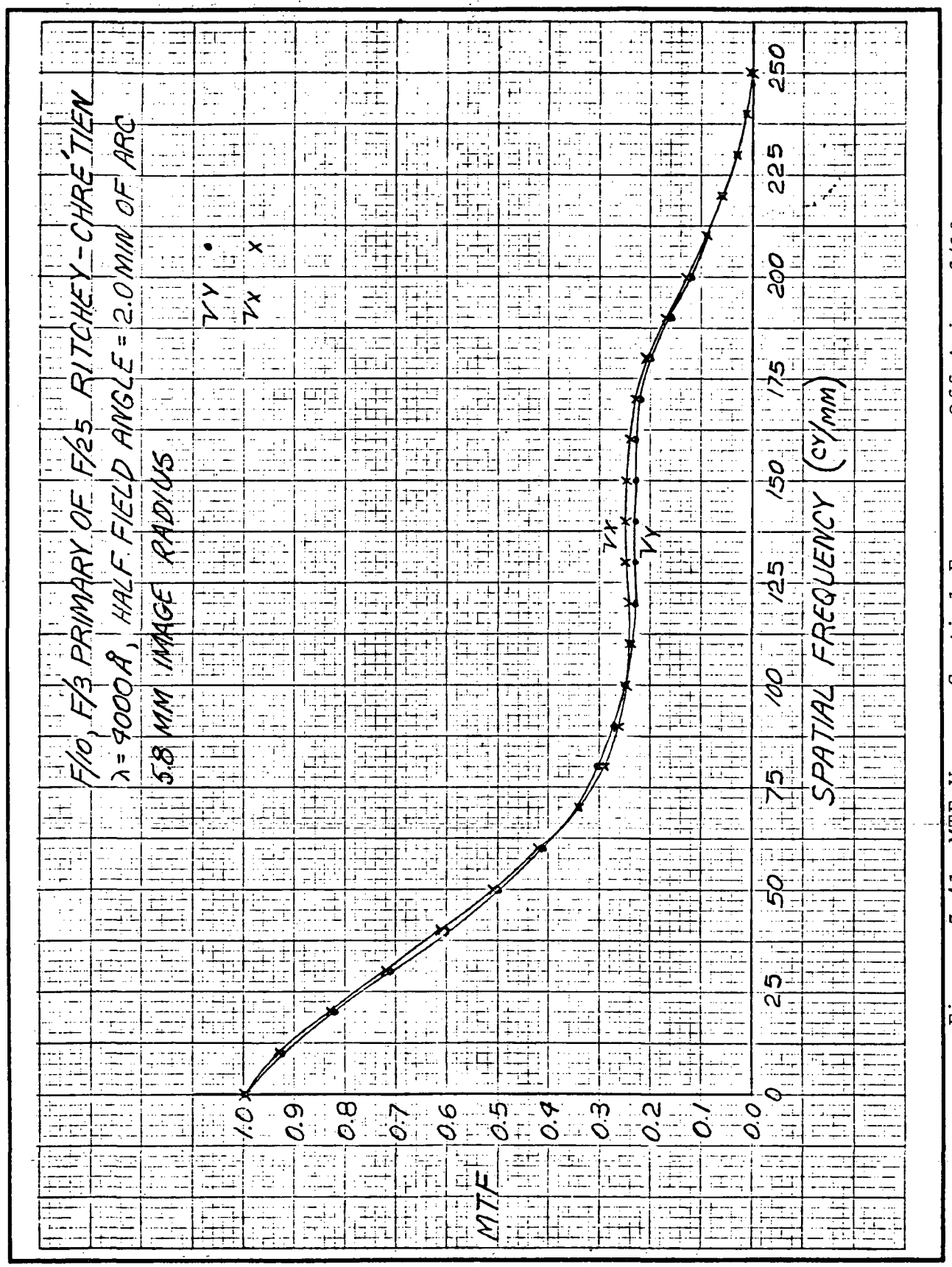

Figure 3-41 MTF Versus Spatial Frequency, Off-Axis, f/10

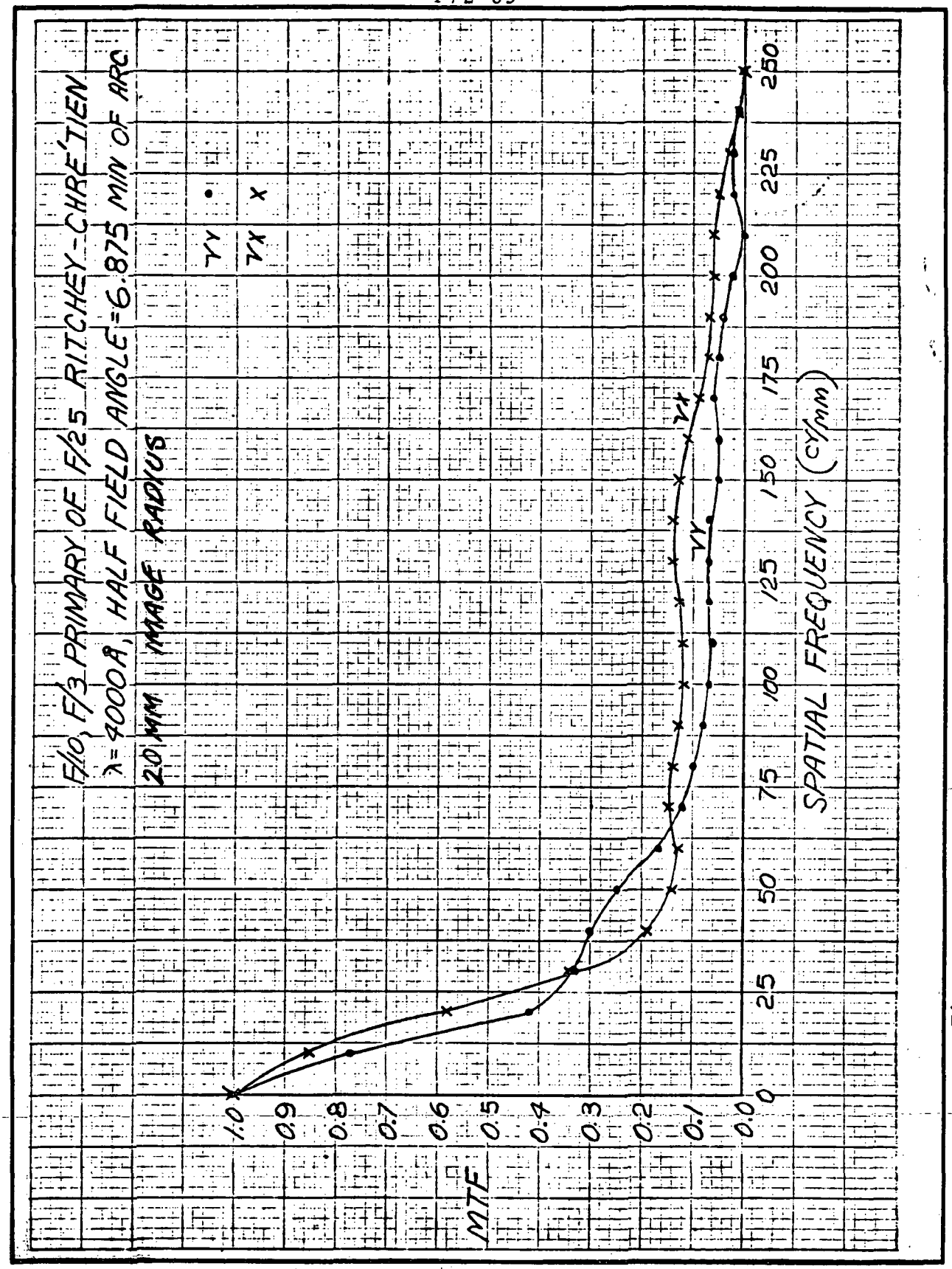

Figure 3-42 MTF Versus Spatial Frequency, Off-Axis, f/10

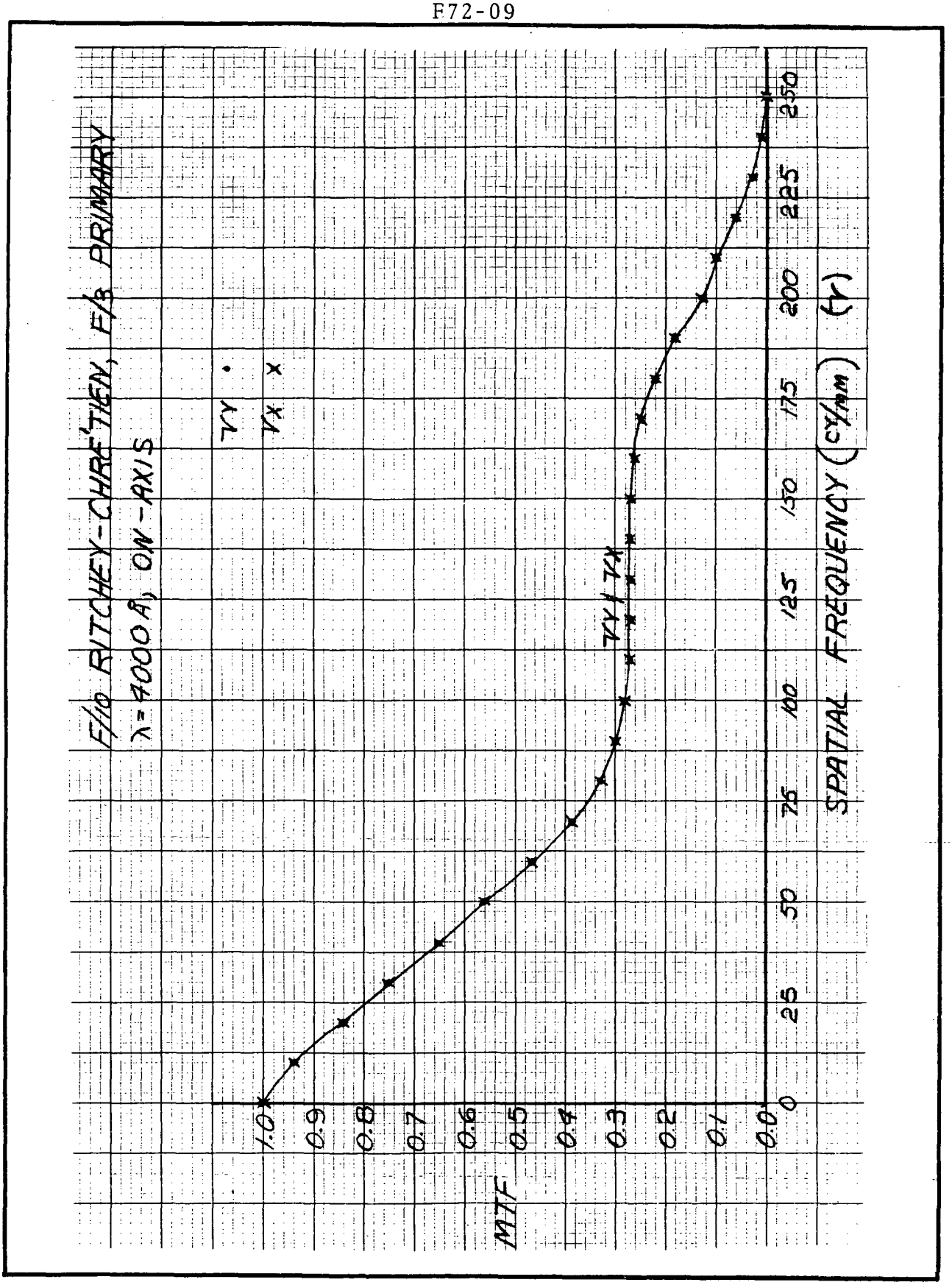

Figure 3-43 MTF Versus Spatial Frequency, On-Axis, f/10 R.C.

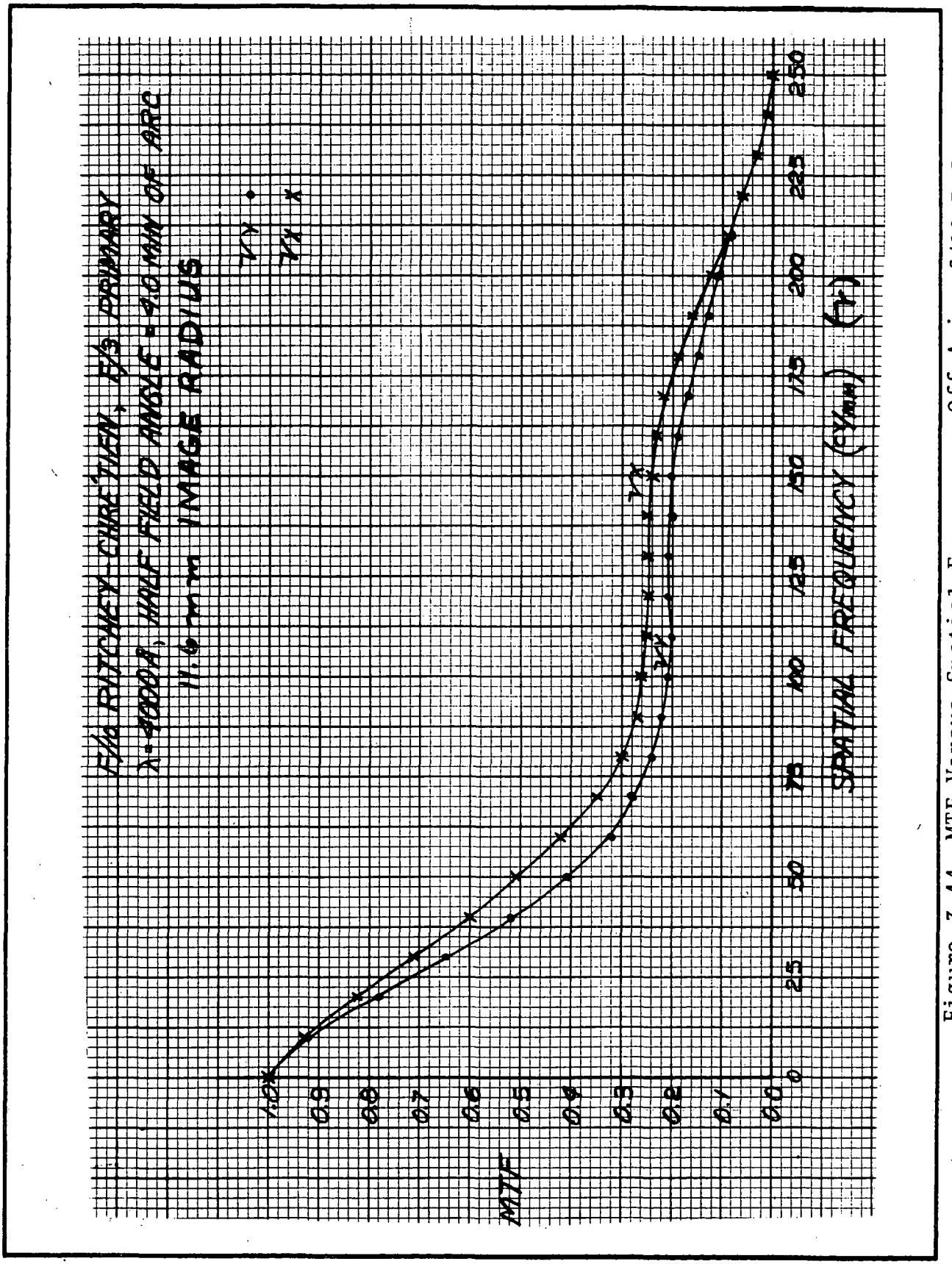

Figure 3-44 MTF Versus Spatial Frequency, Off-Axis, f/10 R.C.

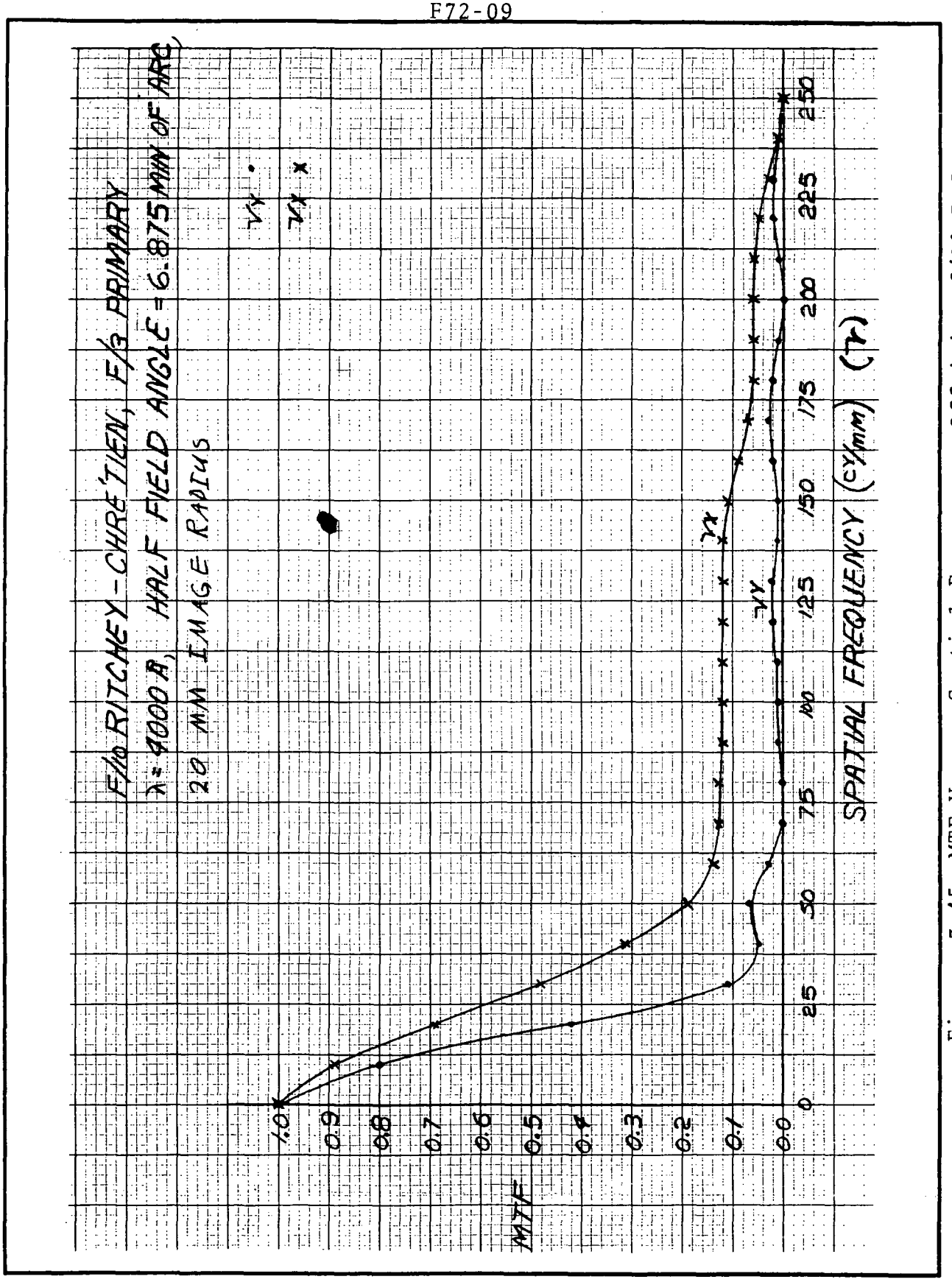

Figure 3-45 MTF Versus Spatial Frequency, Off-Axis, f/10 R.C.

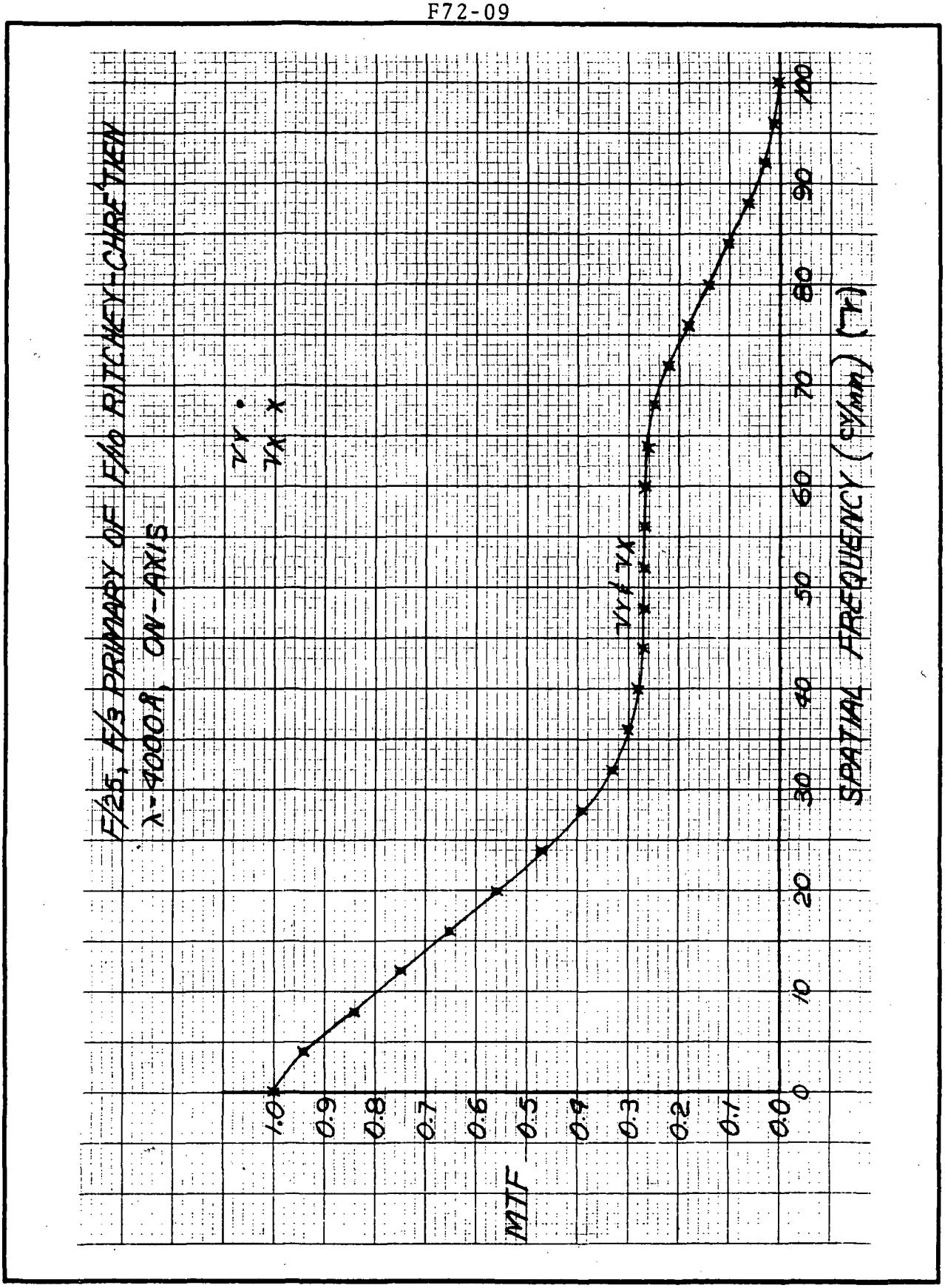

Figure 3-46 MTF Versus Spatial Frequency, On-Axis, f/25, R.C.

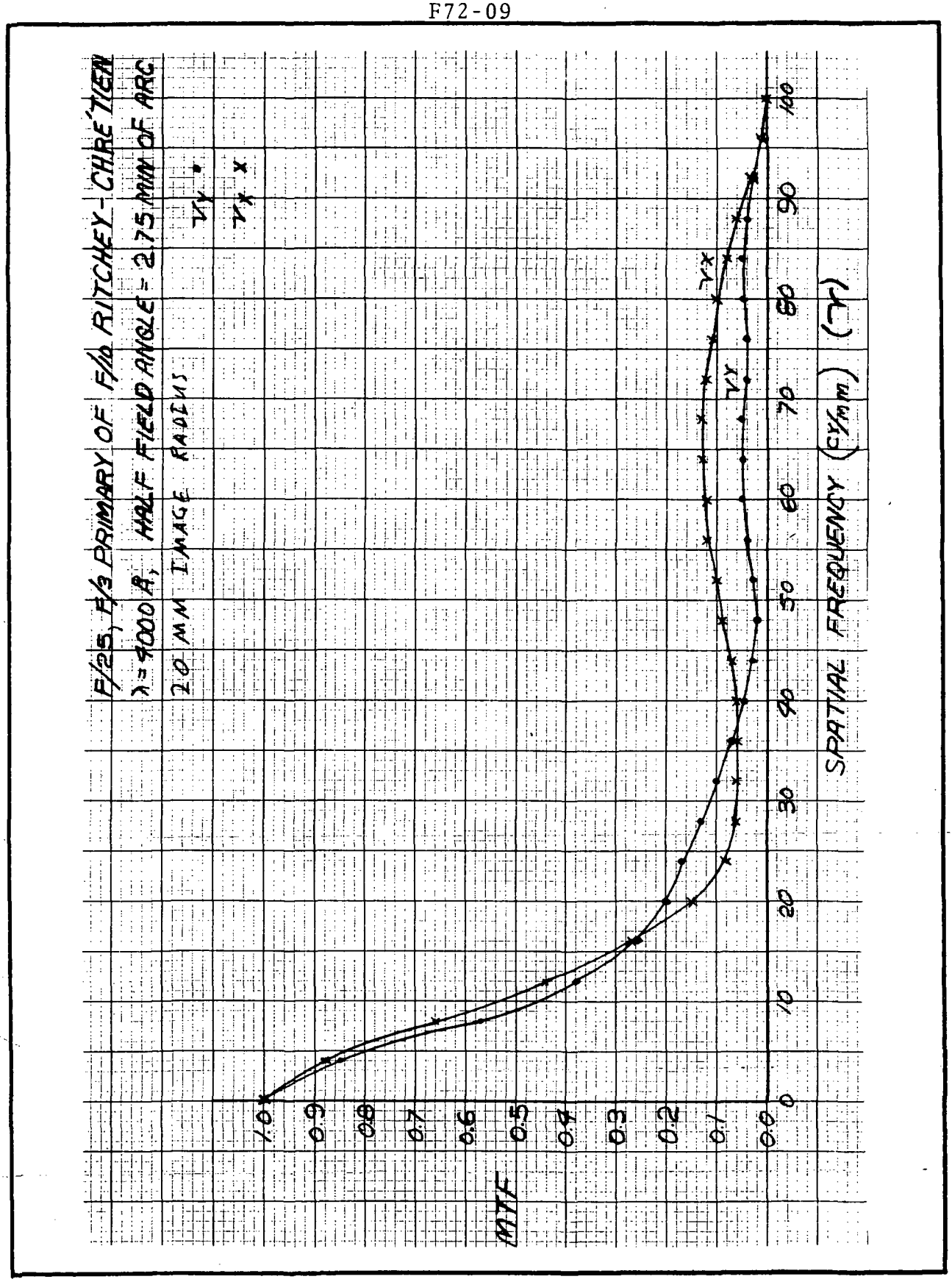

Figure 3-47 MTF Versus Spatial Frequency, Off-Axis, f/25 R.C.

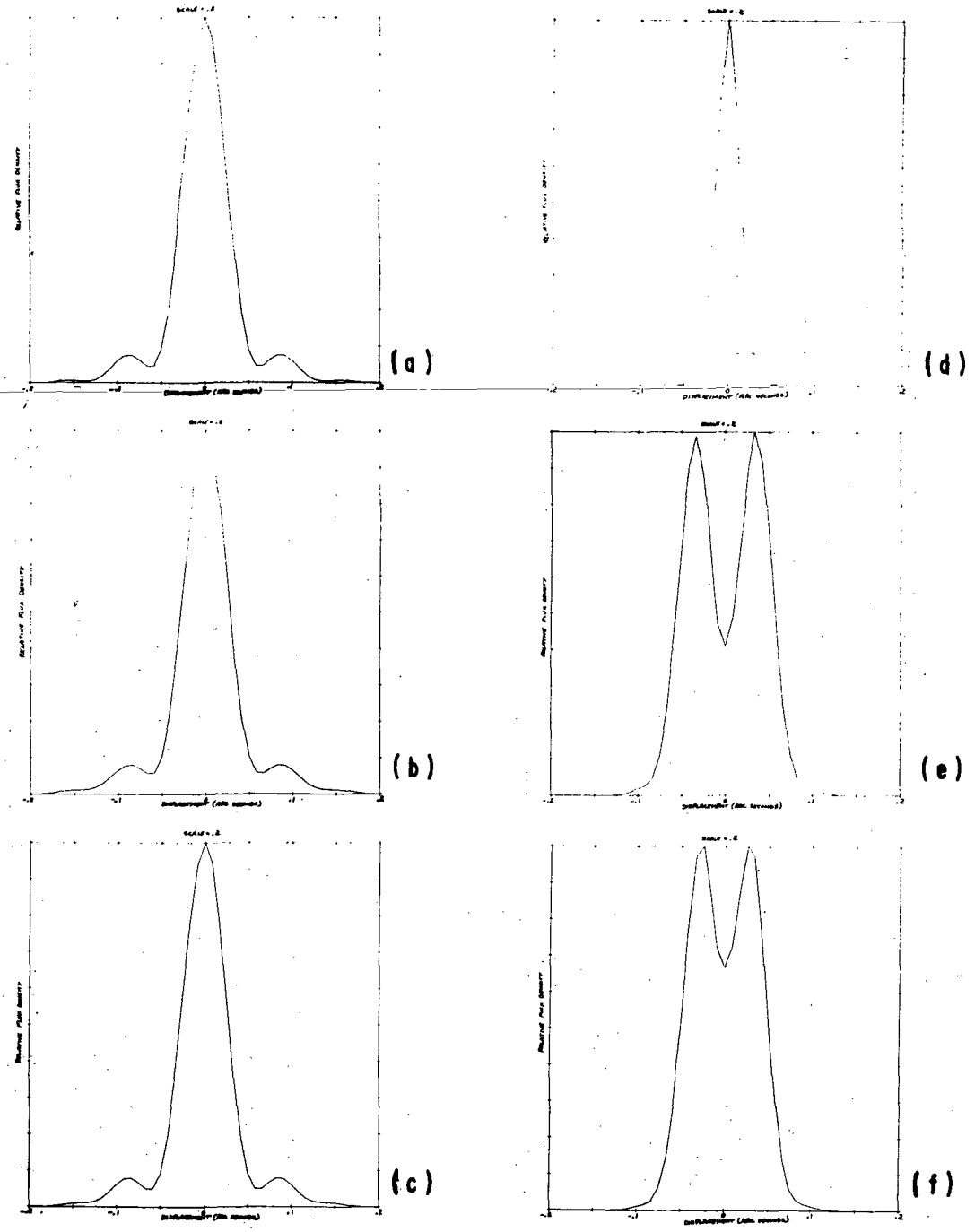

	Wavelength, Å	Field Angle, Arc-Min	Slice
a	6563	0	—
b	6563	2.75	Y
c	6563	2.75	X
d	1216	0	—
e	1216	2.75	Y
f	1216	2.75	X

Figure 3-48 Convolved PSF for f/25 Telescope

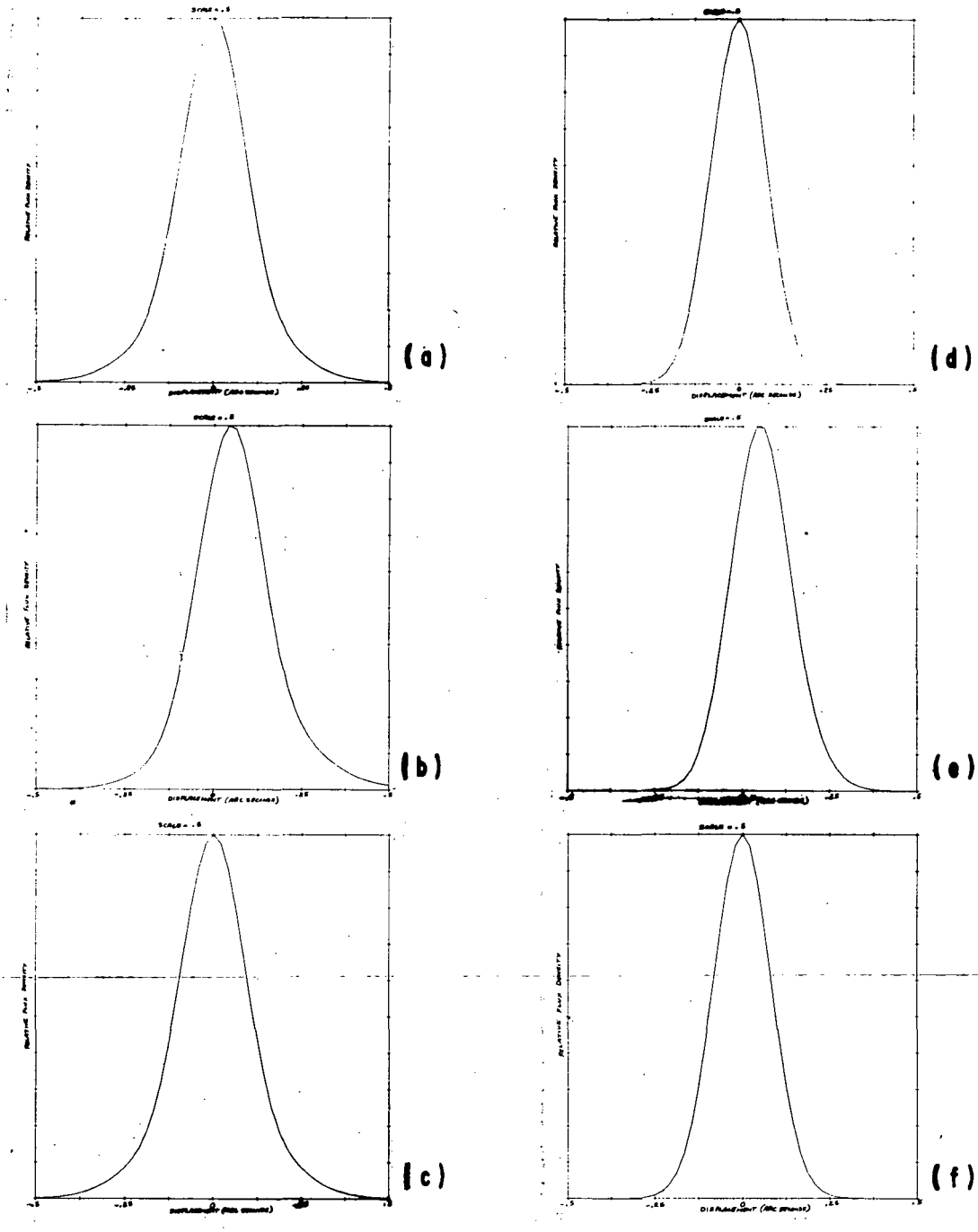

	Wavelength, Å	Field Angle, Arc-Min	Slice
a	6563	0	—
b	6563	2.0	Y
c	6563	2.0	X
d	1216	0	—
e	1216	2.0	Y
f	1216	2.0	X

Figure 3-49 Convolved PSF for f/10 Telescope (1 of 2)

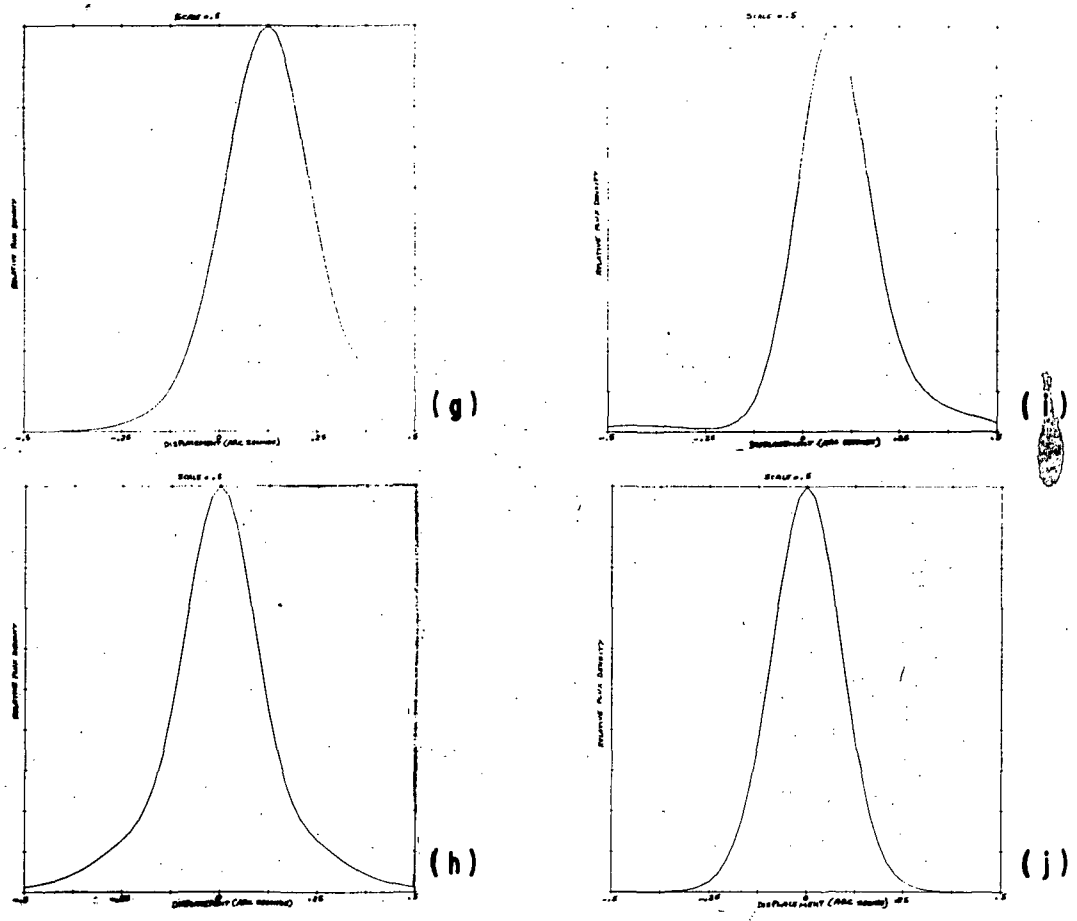

	Wavelength, Å	Field Angle, Arc-Min	Slice
g	6563	6.875	Y
h	6563	6.875	X
i	1216	6.875	Y
j	1216	6.875	X

Figure 3-49 Convolved PSF for f/10 Telescope (2 of 2)

3.7.4 Environmental Effects

3.7.4.1 Thermal Tolerancing

Thermal Defocus At Telescope Image Plane. The following table summarizes the temperature system required to maintain focus, and the conclusions reached in this section.

Telescope Component	Material	Maximum Temperature Deviation During Data Acquisition
Primary Mirror	Fused Silica	±1°K relative to structure
Structure	Invar	±7°K
Secondary Mirror	Cer-Vit C-101 or ULE 7971	±10°K relative to structure

Use the following notation:

linear expansion coefficient of primary = α_1, temperature change ΔT_1

linear expansion coefficient of secondary = α_2, temperature change ΔT_2

linear expansion coefficient of intermediate structure = α_3, temperature change ΔT_3

linear expansion coefficient of back focal distance (between primary and Cassegrain focus), β_1, = α_4, temperature change ΔT_4.

For a Cassegrain type telescope it can be shown that the defocus, ΔZ, relative to the image plane is

$$\frac{\Delta Z}{f} = m\alpha_1\Delta T_1 - \alpha_2\gamma(m-1)\Delta T_2 - \alpha_3\frac{(m^2+1)}{m}(1-\gamma)\Delta T_3 - \frac{\alpha_4\beta}{f}\Delta T$$

where the ΔT_i's represent temperature change from the alignment temperature.

To estimate the required temperature control values, assume

$$\Delta T_1 = \Delta T_3 = \Delta T_4 \equiv \Delta T$$

$$\Delta T_2 = \Delta T - \delta, \ \delta > 0$$

These assumptions are valid since the secondary mirror will be colder than the primary and the structure which will be more or less or equal temperature.

$$\frac{\Delta Z}{f} = \Delta T\left[m\alpha_1 - \alpha_2\gamma(m-1) - \alpha_3\frac{(m^2+1)}{m}(1-\gamma) - \frac{\alpha_4\beta}{f}\right] + \delta\ \alpha_2\gamma(m-1)$$

At f/25: $m = 8.333$, $\gamma = 0.115$, $\beta = 230$ mm, $f = 25 \times 10^3$ mm

$$\frac{\Delta Z}{f} = \Delta T\left[8.33\alpha_1 - 0.84\alpha_2 - 7.48\alpha_3 - 0.009\alpha_4\right] + \delta[0.84\alpha_2]$$

Over an exposure it is desired to remain within the diffraction limit which for focus is given by[12] $\Delta Z = \pm 2\lambda(F)^2$. At $\lambda = 0.4\ \mu$ and $F = 25$,

$$\frac{\Delta Z}{f} \leq \frac{2\lambda(F)^2}{f} = \pm 200 \times 10^{-7} \text{ allowable.}$$

This must be error budgeted with the accuracy the payload specialist can focus the telescope, so for this analysis use

$\frac{\Delta Z}{f} \approx \pm 100 \times 10^{-7}$, yielding a depth of focus $\Delta Z \approx \pm 0.250$ mm.

If $\alpha_3 = 25 \times 10^{-6}/°K$ (aluminum), $7.48\alpha_3 = 1870 \times 10^{-7}$ so that $\Delta T \approx 0.02°K$ would be required. This is impractical. Using $\alpha_3 = 8 \times 10^{-7}/°K$ (Invar) more reasonable tolerances are obtained. To avoid bimetallic thermal bending problems, $\alpha_4 = \alpha_3$ is chosen.

The system is very insensitive to secondary mirror temperature if $\alpha_2 = 1 \times 10^{-7}/°K$ (Cer-Vit C-101 or ULE 7971).

Hence

$$\frac{\Delta Z}{f} = 8.33\alpha_1\Delta T - [60.8 \times 10^{-7}]\Delta T + \delta[0.84 \times 10^{-7}]$$

Case A: $\alpha_1 = 1 \times 10^{-7}/°K$ (Cer-Vit C-101 primary)

$$\frac{\Delta Z}{f} = -52.4 \times 10^{-7}\ \Delta T + \delta[0.84 \times 10^{-7}]$$

Hence $\Delta T \leq 2°K$ and $\delta \leq 10°K$ is allowed, yielding $\frac{\Delta Z}{f} \leq -104 \times 10^{-7}$.

If the primary mirror is colder than the structure by a temperature δ_1, $\frac{\Delta Z}{f} = -52.4 \times 10^{-7}\ \Delta T - 8.33 \times 10^{-7}\ \delta_1 + \delta[0.84 \times 10^{-7}]$. If $\delta_1 = 1°K$, and $\Delta T = 2°K$, $\frac{\Delta Z}{f} \leq -113 \times 10^{-7}$ and $\delta \leq 10°K$ is allowed. Hence for a Cer-Vit primary, the system is relatively immune to primary mirror temperature.

Case B: ~~$\alpha_1 = 5.6 \times 10^{-7}/°K$ (fused silica primary)~~

$$\frac{\Delta Z}{f} = -14.2 \times 10^{-7}\ \Delta T + \delta[0.84 \times 10^{-7}]$$

Hence if $\Delta T \leq 7°K$ and $\delta \leq 10°K$, $\frac{\Delta Z}{f} \leq 99 \times 10^{-7}$

which is allowable.

If, in addition, the primary mirror is δ_1 colder than the structure, then $\frac{\Delta Z}{f} = -14.2 \times 10^{-7}\ \Delta T - 46.6 \times 10^{-7}\ \delta_1 + 0.84\ \delta \times 10^{-7}$. If $\delta_1 = 1°K$, $\Delta T = 4°K$, and $\delta \leq 10°K$, $\frac{\Delta Z}{f} \leq -103 \times 10^{-7}$ which is allowable. Hence a fused silica primary causes a tighter temperature

uniformity tolerance to be placed on the primary mirror thermal control system. But since $\Delta T \leq 2°K$ is required for Case A, a fused silica primary is necessary. This is the preferred case.

Case C: If $\alpha_3 = 0$ (thermal compensating structure),

$$\frac{\Delta Z}{f} = 8.33\alpha_1 \Delta T - 0.9 \times 10^{-7} \Delta T + \delta(0.84 \times 10^{-7})$$

Now if $\alpha_1 = 1 \times 10^{-7}$ (Cer-Vit C-101 primary)

$$\frac{\Delta Z}{f} = 7.4 \times 10^{-7} \Delta T + \delta(0.84 \times 10^{-7})$$

Also if the primary is δ_1, colder than the structure,

$$\frac{\Delta Z}{f} = 7.4 \times 10^{-7} \Delta T - 8.33\delta_1 \times 10^{-7} + \delta(0.84 \times 10^{-7})$$

It should be noted now that large values of temperature (like $\delta_1 = 5°K$ and $\Delta T = 10°K$) do not have a large impact on the error budget.

At f/10: $m = 3.333$, $\alpha = 0.248$, $\beta = 230$ mm, $f = 10 \times 10^3$ mm

If

$$\alpha_3 = \alpha_4 = 8 \times 10^{-7}/°K, \ \alpha_2 = 1 \times 10^{-7}/°K, \ \alpha_1 = 5.6 \times 10^{-7}/°K$$

$$\frac{\Delta Z}{f} = \Delta T[-3.9 \times 10^{-7}] + 0.58\,\delta \times 10^{-7}$$

Over the center of the field diffraction-limited performance or

$$\left|\frac{\Delta Z}{f}\right| \leq \frac{2(0.4\mu)(10)^2}{10 \times 10^3 \text{ mm}} = \pm 80 \times 10^{-7}$$ should be obtained.

Allowing thermal defocus corresponding to half this amount, then

$$\left|\frac{\Delta Z}{f}\right| \leq 40 \times 10^{-7}$$

If, as in Case B above, $\Delta T < 7°K$, $\delta = 10°K$

$$\frac{\Delta z}{f} = -27.3 \times 10^{-7} + 5.8 \times 10^{-7} < 40 \times 10^{-7}$$

In addition, if the primary is $\delta_1 = 1°K$ colder than the structure,

$$\frac{\Delta z}{f} = -27.3 \times 10^{-7} -18.7 \times 10^{-7} + 5.8 \times 10^{-7} \simeq 40 \times 10^{-7}$$

Thus the f/25 case sets the system temperature tolerances.

3.7.4.2 Alignment Tolerances

The secondary mirror parameters are chosen to balance the third order spherical aberration introduced by the primary mirror. The compensation is exact only when the distance between the primary and secondary mirrors is perfect and the optical axes of the mirrors coincide. In the following sections limits on the allowed misalignments are derived.

Tilt of Secondary Relative to Primary. If the secondary is tilted an angle $\delta = \frac{\kappa}{2\gamma}$, the imaged field angle goes from α to $\alpha + \kappa$. For small tilts, only a third order coma is introduced and it becomes

$$\eta = c\left(\frac{r}{f}\right)^2 (2 + \cos 2\theta)$$

$$\xi = c\left(\frac{r}{f}\right)^2 \sin 2\theta$$

$$c = \left(-\frac{1}{4} m^2 - ta_1 - a_2\right)\left(\alpha + \frac{\kappa}{2}\right) - \left(\frac{1}{4} m^2 + ta_1\right) \frac{\kappa}{2},$$

For a Ritchey-Chretien,

$$a_1 = -\frac{1}{4}(m + s), \qquad t = \frac{1}{m + s}$$

and

$$\eta = -\frac{1}{8}(m^2 - 1)\kappa\left(\frac{r}{f}\right)^2(2 + \cos 2\theta)$$

$$\xi = -\frac{1}{8}(m^2 - 1)\kappa\left(\frac{r}{f}\right)^2 \sin 2\theta \ .$$

The maximum tangential coma introduced is

$$|\eta_{max}| = \frac{3}{32}\frac{(m^2-1)\kappa}{(F)^2}$$

where

$$F = f/D \ .$$

Now

$$F = -mF_p$$

so

$$|\eta_{max}| = \frac{3}{32}\frac{\kappa}{(F_p)^2}\frac{(m^2-1)}{m^2} \simeq \frac{3}{32}\frac{\kappa}{(F_p)^2} \ .$$

Using

$$F_p = 3 , \qquad |\eta_{max}| \leq 0.63\kappa$$

where

η_{max} is in arc-seconds and κ is in arc-minutes

Taking

$$|\eta_{max}| \leq 0.1 \text{ second},$$

we obtain

$$\kappa \leq 0.16 \text{ minute}$$

or

$$\varepsilon \leq 19.2 \text{ arc-second for } \gamma = 0.25.$$

This total error must be budgeted between initial alignment, launch-induced misalignment, and thermal bending. A preliminary allocation is as follows:

Thermal bending:	1 arc-second
Launch-induced:	8 arc-seconds
Initial alignment:	10 arc-seconds

The 1 arc-second thermal bending corresponds to a lateral temperature differential of 2.3°K. The thermal control system will do better than this.

Axial Tolerance of Primary Mirror Relative to Secondary Mirror. Spherical aberration is introduced when the secondary mirror is not used at its designed conjugates. The diameter of the aberration is given by:[2]

$$SA = 1/8\ A_1\left(\frac{1}{F^3}\right)$$

where $$A_1 = -1/8\ m^3\ e_1 - \frac{p}{f_p}\ a_1$$

and $$a_1 = 1/8\ (m-1)\{4m + (m-1)^2\ e_2\},$$

assuming the ability to refocus in the image plane.

If $|SA| \leq 0.1$ arc-second, one finds that the tolerance on p becomes ±0.6 mm for the f/25 case and ±0.7 mm for the f/10 case. The f/25 tolerance given above requires the ability to vary B by ±40 mm so it may be necessary to tolerance and align the mirrors to a tighter tolerance on p than ±0.6 mm. The exact tolerance must await more detailed design.

In orbit temperature variations will cause a separation of conjugates, the defocus being

$$df = -\alpha_1 f_1 \Delta T_1 + \alpha_3 d \Delta T_3 - \alpha_2 p \Delta T_2 .$$

Assume that

$$\Delta T_3 = \Delta T$$
$$\Delta T_1 = \Delta T - \delta_1 , \quad \delta_1 > 0$$
$$\Delta T_2 = \Delta T - \delta , \quad \delta > 0$$

Then

$$df = \Delta T[-\alpha_1 f_1 + \alpha_3 d - d_2 p] + \alpha_1 f_1 \delta_1 + \alpha_2 p \delta$$

or

$$f/25: \quad |df| \leq 5.4 \times 10^{-3} \text{ mm}$$

$$f/10: \quad |df| \leq 3.8 \times 10^{-3} \text{ mm}$$

In each case df is negligible compared to the allowed defocus set by aberration, so the thermal defocus will not affect the telescope's ability to correct aberration.

Lateral Alignment Tolerance of Primary Mirror and Secondary Mirror. To estimate this tolerance consider the coma introduced to the on axis field point if the secondary mirror is shifted perpendicular to its axis a distance Δ.

The total tangential coma is

$$C_t = \frac{3}{16} m (m^2-1) \frac{1}{F^2}(\Delta/f).$$

Allowing $C_t = 0.2$ arc-second, one finds

$$f/25: \quad |\Delta| < 0.14 \text{ mm}$$

$$f/10: \quad |\Delta| < 0.15 \text{ mm}.$$

Thermal warp of the telescope structure can introduce up to 6 μm deflection thus introducing negligible aberration.

The requirement of $|C_t| \leq 0.2$ arc-second may be overly stringent. A more realistic requirement may be for sagittal coma to be less than 0.2 arc-second, yielding $|\Delta| < 0.4$ mm. In any event, a complete and detailed error analysis must be performed during the detail design phase.

The tolerance of 0.14 mm is tight enough to require further consideration for it must be maintained through initial alignment, handling, and launch induced misalignment. One method of minimizing the effect of induced misalignment is to mount the primary and secondary mirrors with solid mounting plates on their figured surface so that any lateral movement pivots the mirror roughly about its center of curvature. This technique approximately halves the effect of lateral mirror movement. Ideally the secondary mirror should be mounted to move about its near focus. Further analyses may want to consider a man-operated secondary mirror drive in which man performs a knife-edge test on a star image to check image quality. Such a mechanism must maintain secondary mirror tilt alignment to be useful.

3.8 OTHER DESIGNS EVALUATED

3.8.1 Baker Three-Mirror Telescope

One telescope configuration which will provide a large usable field of view is a Baker three-mirror telescope configuration.[13] D. H. Schulte has the following comments about Baker's scheme:[14]

"Recently, Baker proposed what he called a 'two-mirror corrector' to use with existing parabolic mirrors. Figure 3-50 shows a representative three-mirror Baker system. The converging beam from the parabola is recollimated by a parabolic convex mirror. A spherical concave mirror with its center of curvature at the vertex of the convex mirror then reimages the parallel bundle. If the convex mirror is made slightly nonparabolic to cancel the spherical aberration of the concave mirror, the final image is, to a high degree, free from spherical aberration, coma, and astigmatism.

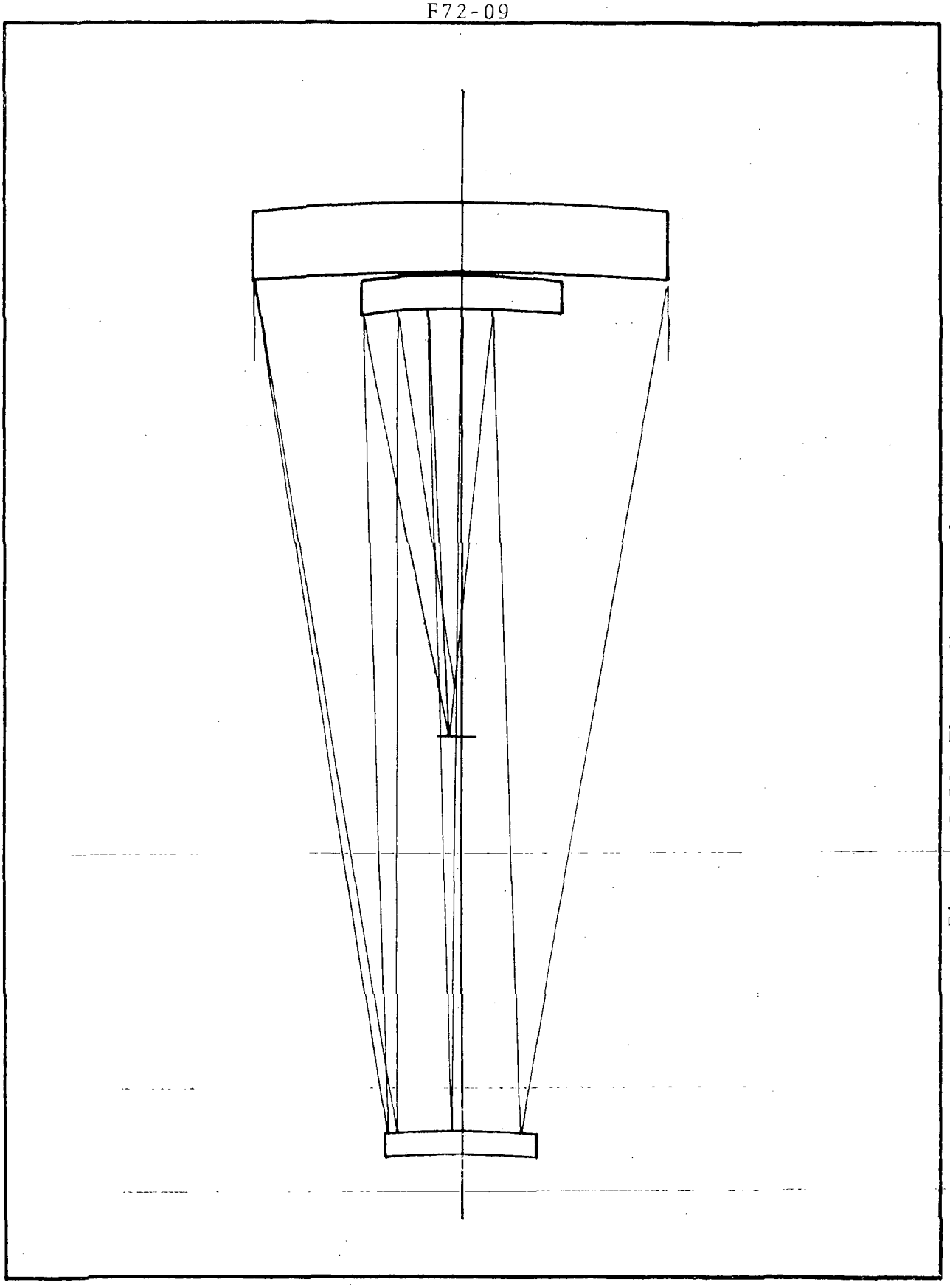

Figure 3-50 Three-Mirror Baker Telescope

In addition, the curvature of the three mirrors can be distributed in a way to yield a flat field. Slight additional aspheric touchup on all three mirrors, plus small departures from the exact spacing relationships implied above, brings about the balancing of the higher-order aberrations so that fields of 2 degrees or more in diameter can be realized with exceedingly fine resolution. For the design shown in Figure 3-50, the image size is less than 1/100-second-of-arc diameter at 33 minutes off-axis."

The three-mirror Baker provides the desired field correction without limiting the spectral bandpass as refracting correctors do. It suffers from having a larger central obscuration than a two-mirror configuration and the image plane is not accessible. Also, to our knowledge, none have been built so we are hesitant to recommend its use at this time.

3.8.2 All-Reflecting Schmidt

A folded all-reflecting Schmidt telescope has been constructed.[15] It is a six-inch aperture, f/4.0 using a spherical primary mirror and an aluminum, Invar thermal differential focus compensation. The deviation of the corrector plate from a flat is equivalent to 4.7 fringes at the sodium D line. The corrector is initially tested against a flat and finally in the telescope.

During the study we ray traced an all reflective Schmidt and found all the third order aberrations to be small on the curved focal plane which is inherent in the Schmidt configuration. But the fifth and seventh order spherical aberration was quite large, all of it originating on the corrector. The form of the corrector can be selected differently from what was used, and would perhaps, yield better results.

For completeness, a conceptual layout of an f/5 Schmidt has been included and is illustrated in Figure 3-51. The corrector plate, being a second order aspheric, would be very difficult to make. The primary is spherical and hence would be rather easy to make. The concept requires the use of four mirrors, three of them 1 meter or larger in diameter. Also, there are large distances between the elements, giving rise to serious mechanical and thermal problems. The additional reflection (versus the two-mirror telescope plus tertiary mirror approach) would reduce throughput. In addition, the second f-number requirement would be very difficult to implement. All things considered, the Schmidt is thought too developmental to be included on the AOS.

3.8.3 Schiefspiegler Configuration

A Schiefspiegler configuration avoids the diffraction effects associated with spiders and secondary mirrors, by operating decentered. It is fundamentally a Cassegrain with $F_p/12$ and a magnification m = 1.667. For apertures >230 mm, an elliptical primary is used with a spherical secondary, similar to a Dall-Kirkham. The curvature of the primary and secondary are approximately equal; i.e., the Petzval condition is accomplished, guaranteeing a flat field. If $F_p \approx 13\text{-}14$, correction of field errors is easier but the system is considerably longer.

There are three different basic devices:

- Anastigmatic device, free from astigmatism but not from coma. Astigmatism is eliminated by tilting the secondary. Kutter[16] reports that a residual coma of 4.8 arc-seconds remains for a 200 mm, f/20 telescope.

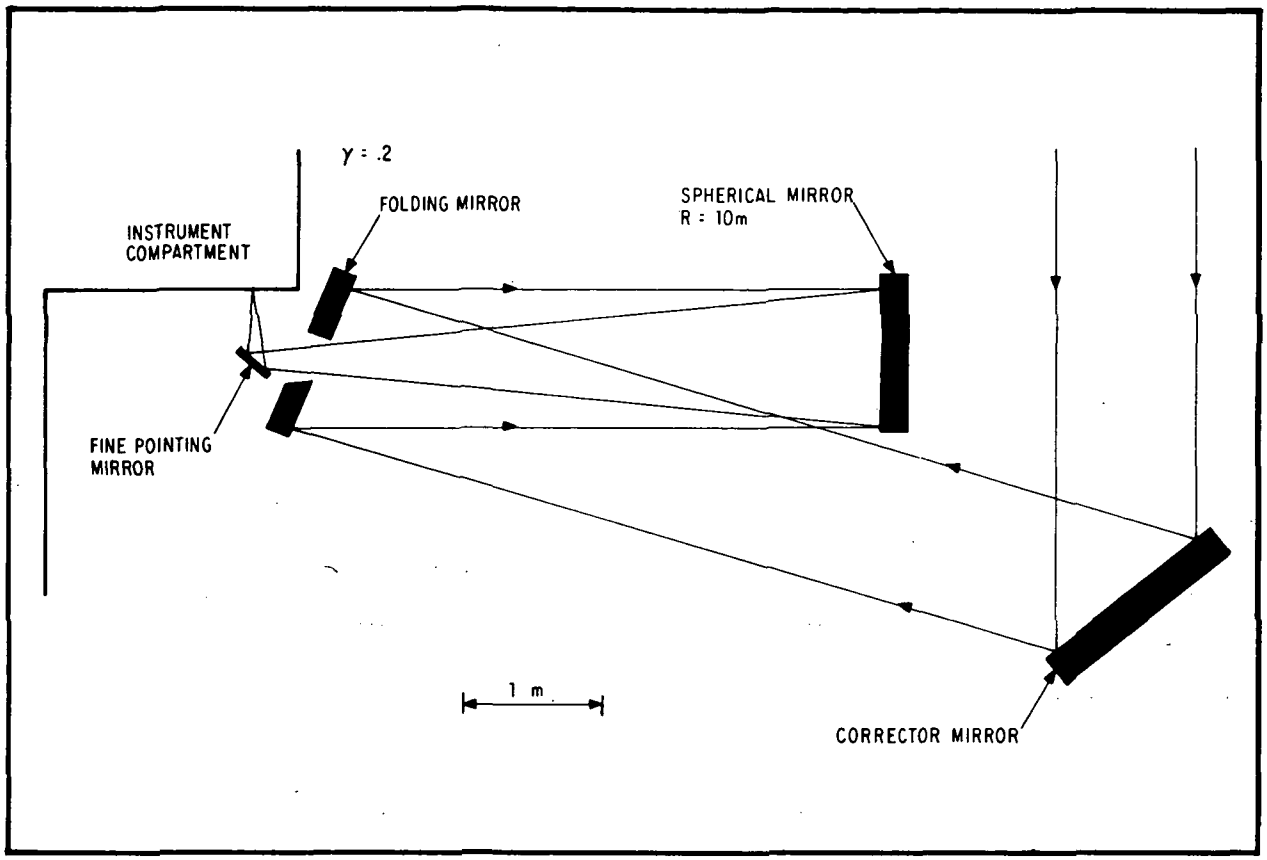

Figure 3-51 All-Reflective Schmidt Telescope

- Coma-free device, where coma is eliminated by tilting the secondary, which overcorrects astigmatism. Kutter finds 30 arc-seconds of residual astigmatism. Astigmatism is eliminated by cylindrical deformation of the secondary.

- Catadioptic device, of which at least three variations are available: First, a plano-convex cylindrical lens is used between the secondary mirror and the focus to eliminate the astigmatism of the coma-free device. Second, a basic configuration is used which lies between coma-free and anastigmatic and also uses a spherical corrector lens. Third, a two-lens corrector (cylindrical)

can be used in place of the single plano-convex lens to correct chromatic aberration also. All the catadioptic devices use refractive elements which absorb ultraviolet radiation.

The Schiefspiegler configuration suffers from two deficiencies which eliminate it from consideration for the AOS: The f/number is too slow and the image quality is inadequate. The catadioptic device also severely limits wavelength coverage.

3.8.4 Reflective Relays

As an alternative to the use of multiple secondary mirrors in the AOS Telescope, some effort was devoted to achieving a variety of focal lengths through the use of relay optics. We were encouraged in this effort by reports that there are reflective relay devices that contribute virtually nothing to MTF loss.[17]

If this approach should prove feasible, it would provide important advantages. First, it would make available a variety of focal lengths at a modest expenditure. Second, the one telescope system that is required could be made Ritchey-Chretien and all image planes could be made free of coma and spherical aberration.

Before making an analysis that would be specific enough to have any meaning, it was necessary to arrive at a nominal magnification. Three values were chosen, because it is sufficiently different from unity to be meaningful, yet not quite beyond the bounds of usefulness in terms of real detectors and telescope performance. The prescription was drawn from a table prepared by S. Rosen.[18] This table includes in its makeup the Schwartzschild condition of concentric elements so as to assure simultaneous correction for spherical

aberration, coma and astigmatism. Figure 3-52 is a scaled drawing of the prescription which points up two potential sources of trouble. First, the image plane is buried between the elements so that a diagonal mirror must be added to bring it out. Second, even without the diagonal mirror, clearances around the secondary mirror of the relay are so tight that vignetting surely will become severe. In fact, the LST report warned of the vignetting.

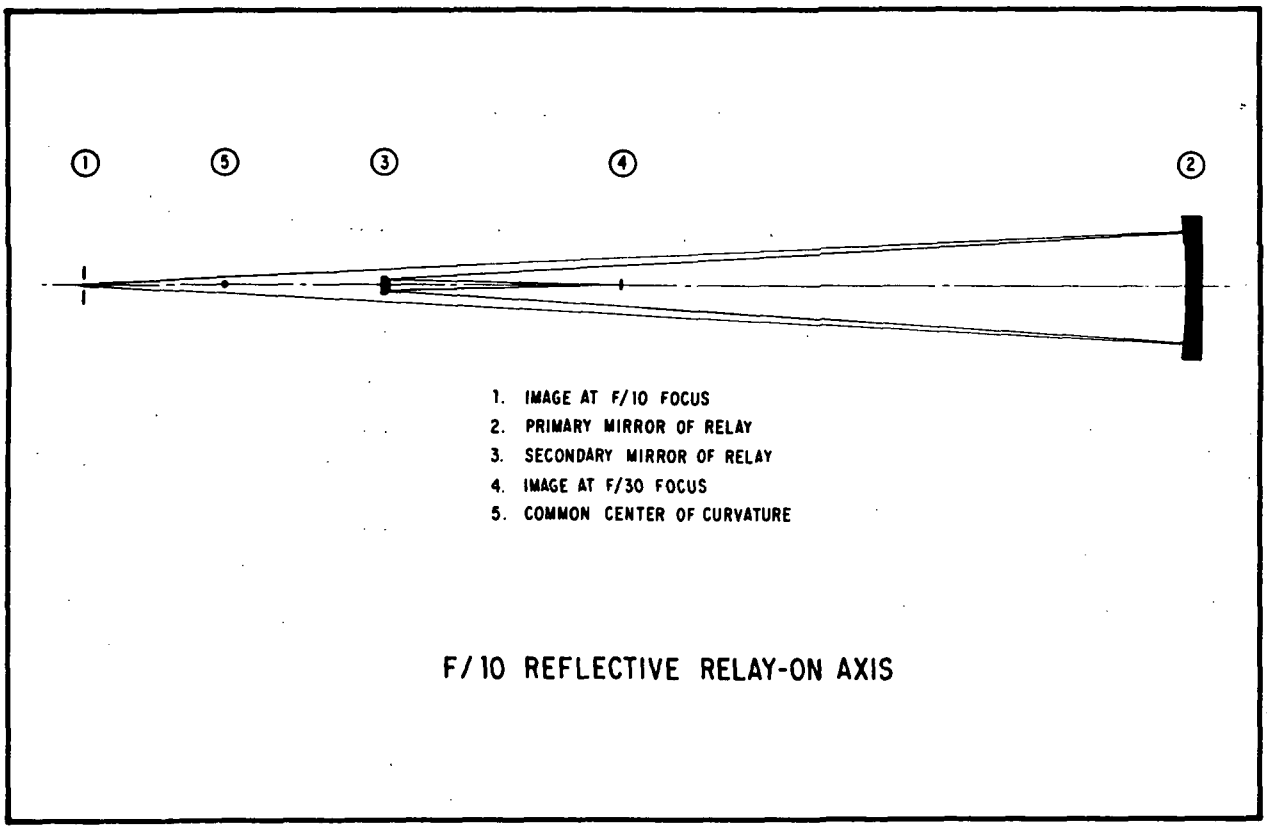

Figure 3-52 f/10 Reflective Relay, On-Axis

A solution is suggested by Rosen, who states that the Schwartzschild prescription is good up to speeds of f/1.0. This suggestion is borne out by the use of these prescriptions in fast ultraviolet microscope objectives. Figure 3-53 exemplifies the concept.

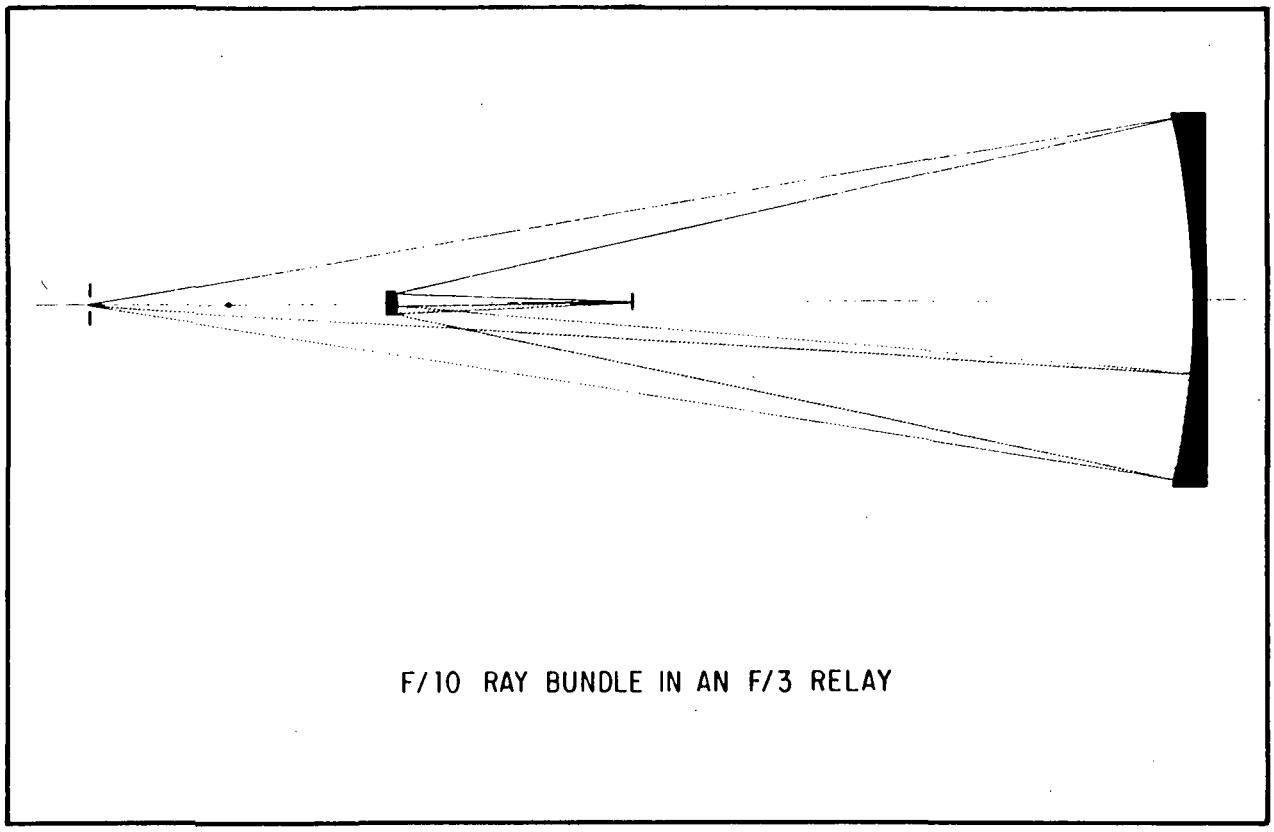

Figure 3-53 f/13 Reflective Relay with f/10 Ray Bundle

The prescription of Figure 3-52 was broadened to accept an f/3 cone and the f/10 cone was bent at the first image to strike the primary mirror near the edge rather than at the center. The shaded area shows the path of the rays to the image. It points out clearly that both the secondary mirror and the image are well separated from the incoming cone of rays, thus doing away with both the vignetting problem and the awkward position of the image. Figure 3-54 shows the off-axis version swung around into position.

The prescription was analyzed using the General Automation 1830 Computer and SCIP software. The results indicate a combination of a tilted image and severe field curvature. Because of the off-axis arrangement, the unmagnified image is apparently tilted about 6.5° to the relay axis. The longitudinal magnification, being related to the lateral magnification as its square, exaggerates the image

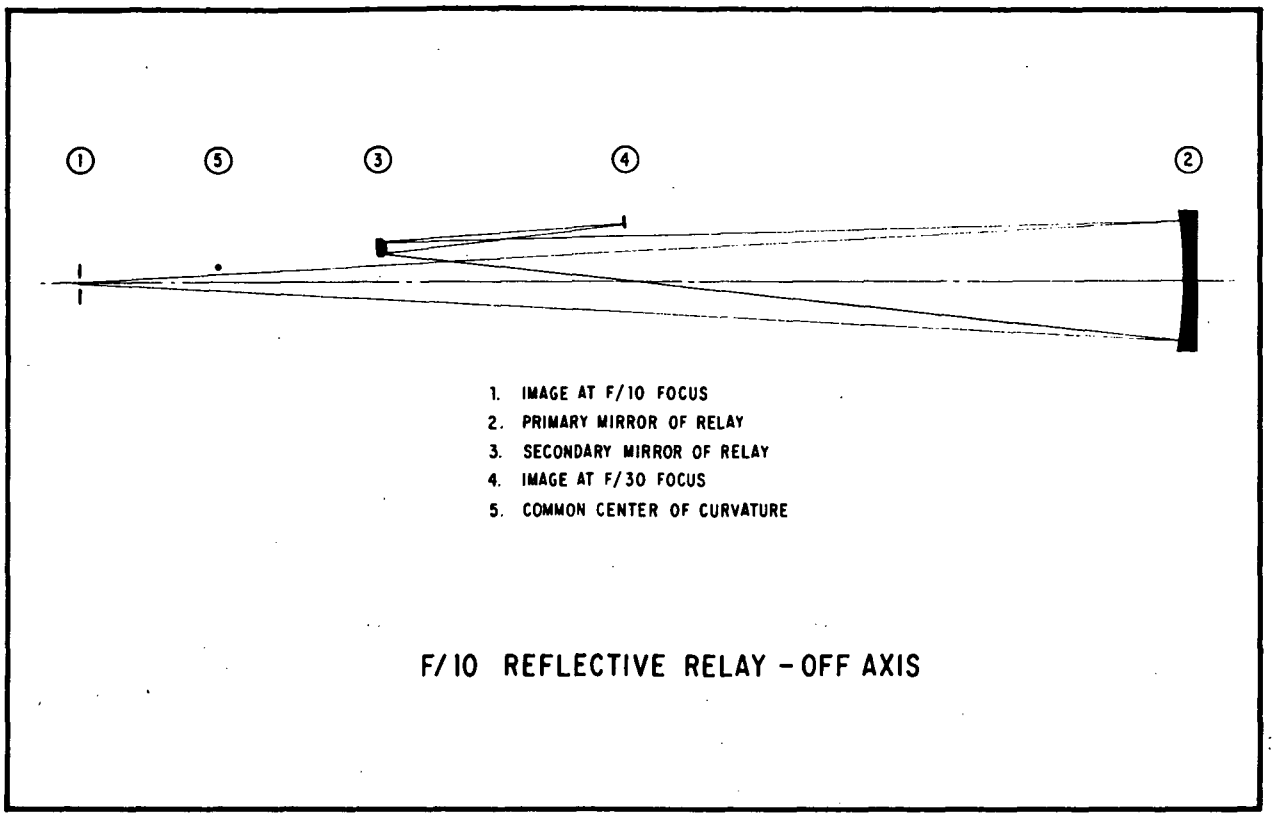

Figure 3-54 f/10 Reflective Relay, Off-Axis

tilt to about 20°. This effect could be handled by tilting the detector an appropriate amount, and the resulting keystoning could be rectified as part of the data reduction.

However, after the tilt was isolated, the field curvature showed itself to be 4.5 mm in a field of 20 mm radius. A field flattener of such drastic proportions is not possible and a fiber optic corrector severely limits the spectral response.

After these results were verified, further study of the literature revealed that the Schwartzschild version of the reflective relay promises to be corrected for spherical aberration, coma and astigmatism, but not for Petzval curvature. If there is some way that the astigmatism of the Ritchey-Chretien telescope could be made to compensate

for the Petzval curvature of the relay, a suitable system could be found. But as it is, except for very small fields of approximately 10 mm diameter or less (about 1 arc-minute), the inverse Cassegrain relay is not a solution.

REFERENCES

1. Wetherell, William B., "The Use of Image Quality Criteria in Designing a Diffraction-Limited Large Space Telescope", S.P.I.E. Conference on Instrumentation in Astronomy, Tucson, Ariz., March 13-15, 1972. Proceedings S.P.I.E., 28, (1972), page 45.

2. Bottema, M. and R. A. Woodruff, "Third-Order Aberrations in Cassegrain-Type Telescopes and Coma Correction in Servo-Stabilized Images", Applied Optics, Vol. 10, No. 2, 1971 (p 300) and Vol. 11, page 2965 (1972).

3. Hass, G., and R. Tousey, J. Opt. Soc. Amer. 49, 593 (1959).

4. Canfield, L. R., G. Hass, and J. E. Waylonis, Appl. Opt. 5, 45 (1966).

5. Angel, D. W., W. R. Hunter, R. Tousey, and G. Hass, J. Opt. Soc. Amer. 51, 913 (1961).

6. Cox, J. T., G. Hass, and J. E. Waylonis, Appl. Opt. 7, 1535 (1968).

7. Madden, R. P., L. R. Canfield, and G. Hass, J. Opt. Soc. Amer. 53, 692 (1963).

8. Hunter, W. R., J. F. Osantowski, and G. Hass, Appl. Opt. V10, 540 (1971).

9. Hutcheson, E. T., G. Hass, and J. T. Cox, Appl. Opt. 11, 2245 (1972).

10. Wilson, R. N., "Corrector Systems for Cassegrain Telescopes", Appl. Opt. 7, p 253.

11. Smith, W. J., Modern Optical Engineering, McGraw-Hill Book Co., New York (1966) p 298.

12. Born and Wolf, Principles of Optics 3rd Revision, Pergamon Press, London, 1965, p 441.

13. Baker, J., "On Improving the Effectiveness of Large Telescopes," presentation at meeting of National Academy of Science, Seattle, 1966.

14. Schulte, D. H., "Field Correctors for Reflecting Telescopes," Optical Telescope Technology Workshop, Huntsville, Alabama, 1969.

15. Wray, J. D., and O'Callaghan, F. G., "A Folded All-Reflecting Schmidt Camera and Ultraviolet Image Converter for Space Astronomy Applications."

16. "Gleanings for ATM's", Auton Kutter, Sky and Telescope Bulletin A.

17. "Instrumentation Package for a Large Space Telescope (LST)" Goddard Space Flight Center, November 1970, p 6-3ff.

18. Rosen, S., "Inverse Cassegrain System", Appl. Opt. 7 (August 1968) p 1483.

Page Intentionally Left Blank

Section 4
INSTRUMENTS

4.1 INTRODUCTION

Since the Astronomical Observatory for Shuttle is intended to operate as a national facility, it is appropriate both that some general-purpose or highly integrated instrument be supplied by the Laboratory sponsors, and that provisions also be made to easily accommodate special purpose instrumentation. General purpose instruments selected for inclusion as facility sponsored instruments are the echelle and imaging spectrographs and imaging cameras. These capabilities probably will be required by a number of experimenters, and the most cost-effective way of fulfilling these requirements is to supply the instruments as a core set.

The SEC vidicon and electronographic detectors are examples of highly integrated subsystems with a substantial impact on the design of the peripheral equipment in the laboratory. They are included as sponsored systems for this reason. Also in this category are the filter, polarizer and field stop mechanisms, which impact the volume required of the airlock design.

Special purpose instruments are those whose nature is such that it is most cost-effective for individual experimenters to build them and supply them to the AOS for specific missions. Examples are interference filters, polarizers, cameras, special emulsions, and spectrographic instruments with unique requirements.

4.2 HIGH RESOLUTION SPECTROGRAPH (0.01Å)

The high resolution spectrograph is used for studies of line profiles, for high-accuracy doppler velocity measurements, magnetic field determinations, etc. Three instruments are considered for AOS:

- An echelle spectrograph of the LST design
- A High Resolution Ultraviolet Spectrometer of the OSO-I design
- An echelle spectrograph designed especially for this application.

The various characteristics of these instruments are compared in Table 4-1.

The LST echelle spectrograph is designed to operate at f/12 and use a 35 x 35 mm detector format. To achieve the ultimate in resolution, parabolic collimator and camera mirrors are used. The cross disperser is ruled on an aspheric blank which acts as a corrector in the Wright-Schmidt configuration. The dispersion of the LST echelle spectrograph is appropriate for a 60 line pairs per millimeter detector. A layout of this instrument is given as Figure 4-1. Ray tracing shows that the instrument is capable of 0.01 Å resolution.[1]

For use in the AOS, the LST echelle spectrograph could be modified in two ways: The focal ratio would be increased to f/10, and the dispersion decreased to a 40 millimeter diameter format with a 100 line pairs per millimeter detector.

Table 4-1
INSTRUMENT CHARACTERISTICS

	LST Echelle Spectrograph	OSO-I High Resolution Ultraviolet Spectrometer	Echelle Spectrograph
Configuration	Wright-Schmidt	Ebert-Fastie Monochromator	Modified Wright-Schmidt
Wavelength Range, Å	1200-2400	1050-2300	1200-3000 3000-6000
Resolving Power	$\gtrsim 10^5$	$\sim 2 \times 10^5$	1.2×10^5
Focal Ratio	f/12	f/15	f/10
Focal Length	1.83 meters 72 inches	1.0 meters	0.95 meters
Image Format	35 x 35 mm	Single Slit 8μm x 8mm	40 mm dia.
Number of Reflections(1)	4	3	4
Number of Aspheric Surfaces	3	0	0
Grating Ruling Size	160 g/mm(2) 25 x 25 cm	3600 g/mm 65 x 76 mm 2500 A Blaze	333 or 133g/mm(3) 128 x 254 mm
Echelle Ruling Size	67.5 g/mm 25 x 35 cm	----------	79 or 31.6 g/mm 128 x 154 mm

NOTES: (1) Counts dispersive elements, does not count telescope.
(2) Ruled on an aspheric blank.
(3) 50 mm diameter central hole.

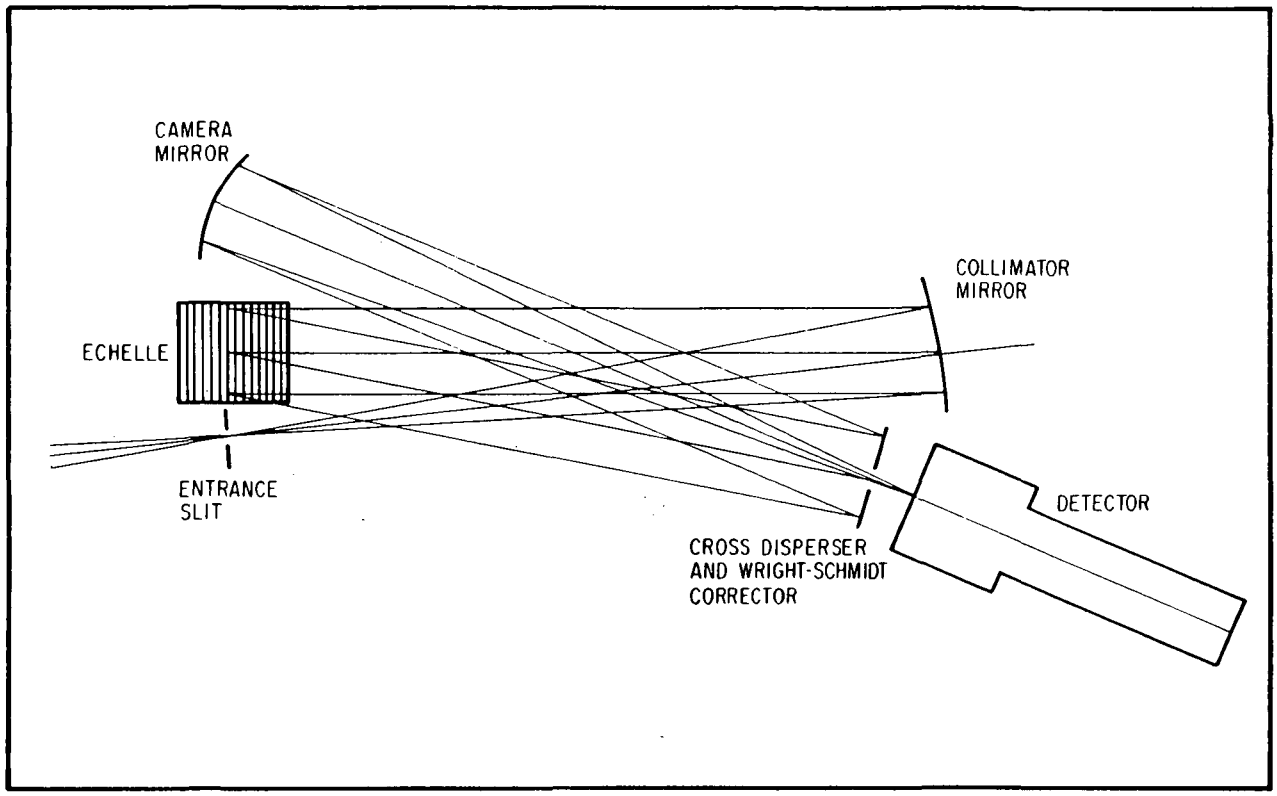

Figure 4-1 LST Echelle Spectrograph Layout

The OSO-I High Resolution Ultraviolet Spectrometer (Figure 4-2) is designed both to measure accurate solar line profiles as a spectrometer and as a monochromator for use in a raster scanning mode. The instrument is unique in that high resolution is obtained in a normal incidence mode using a diffraction grating in first and second orders. A resolving power of ~2 x 10^5 is achieved with an Ebert-Fastie mount at f/15. Although the instrument is configured with a single exit slit for the OSO-I application, it is possible to modify the design for use as a spectrograph, or a multiple-exit slit spectrometer. The dispersion, as presently used, is appropriate to a 125 line pair per millimeter detector or an 8 μm exit slit. Care has been taken in the design to insure that wavelengths can be determined to within ± 0.01 Å in the severe thermal environment caused by the frequent occurrence of solar eclipses.

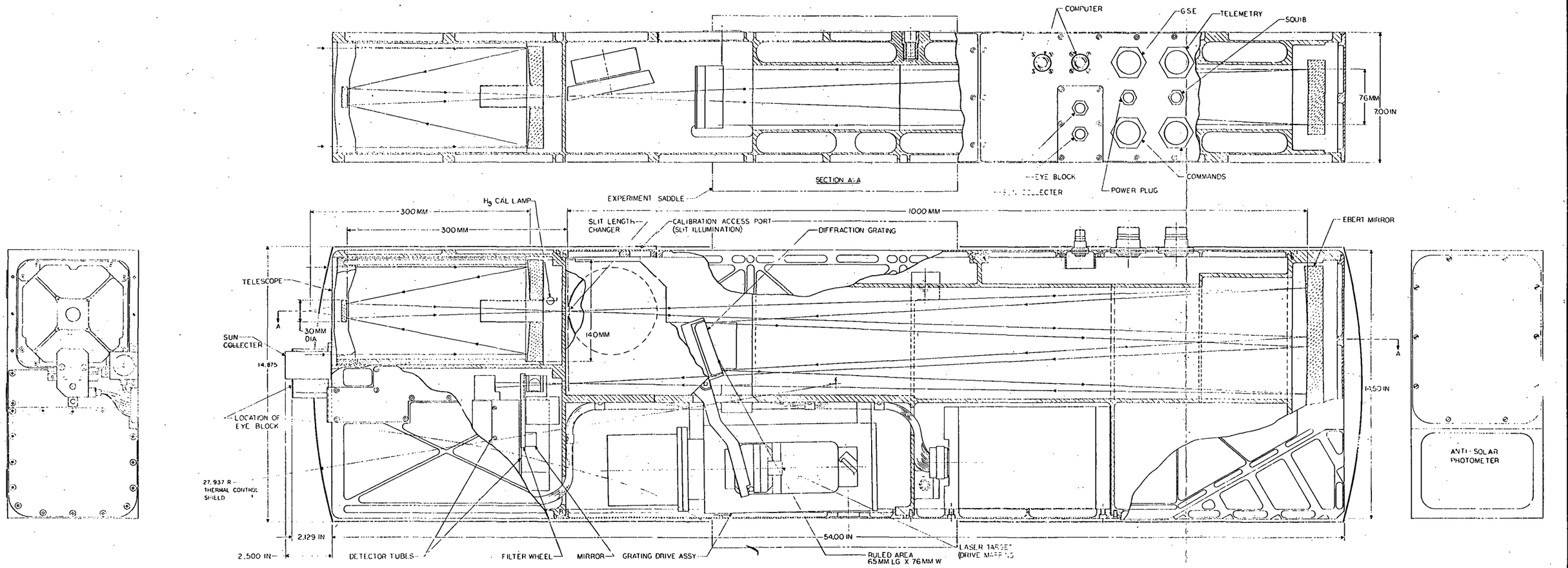

Figure 4-2 OSO-I High Resolution Ultraviolet Spectrometer

Both of the above instruments could be modified for use in the AOS. The principal source of concern with the LST echelle spectrograph is the manufacturability of the cross disperser. This requires an aspheric blank with a hole in it. A grating must then either be ruled or replicated onto it. At best, this will be an expensive, long lead item. An f/10 spectrographic version of the OSO-I High Resolution Ultraviolet Spectrometer could be easily built using off-the-shelf components, but since it is a single-dispersion instrument, only a relatively small spectrum interval is available to the detector for a given grating setting (about 40 Å for 40 mm detector format). This may or may not be a significant disadvantage.

For these reasons, an optimized echelle instrument has been designed for the AOS.

4.2.1 Design Goals for Echelle Spectrograph

The principal requirement for the spectrograph is to record the spectra of stars in great detail and over a wide range of wavelengths. By making use of the two-dimensional properties of a recording format, the echelle spectrograph is ideally suited to the task. In the present application, it is desired to record with a resolution of 0.01 Å over the range from about 1200 Å to about 7000 Å.

For several reasons, including detector wavelength limits, excessive dynamic range requirements, and the peculiarities of energy distribution in the echelle spectrogram format; and because of the intra- and inter-order modulation in an echelle spectrogram, it was decided to limit the range of an exposure to as close as possible to one octave of spectrum.

There is, however, only a limited selection of grating frequencies available; namely, 31.6, 79 and 316 grooves per millimeter. The ratio between 31.6 and 79 is 1 to 2.5, so the wavelength range covered by the 31.6-groove grating will be 2.5 times as long as the range covered by the 79-groove grating.

The approach taken is based on the LST design, but with the aspheric corrections removed from both the grating and the camera mirror. This approach provides the required resolution, and could even be used with an improved SEC vidicon should one become available. A layout of this arrangement is shown in Figure 4-3.

4.2.2 Echelle Spectrograph Specifications

The component specifications for the echelle spectrograph that was ray-traced are included in Table 4-2.

Table 4-2
ECHELLE SPECTROGRAPH COMPONENT SPECIFICATIONS

Slit:	20 x 20 μm parallel to grooves in echelle grating	
Collimator:	Off-center parabola	
	Effective focal length	948 mm
	Clear Aperture	100 mm
	(portion of parabola of 300 mm clear aperture)	
Echelle grating:	79 grooves/mm	31.6 grooves/mm
	63°26' blaze	63°26' blaze
	94-234 order	or 94-187 order
	128 x 254 mm	128 x 254mm
	1200 - 3000 Å	3000 - 6000 Å

Table 4-2 (Cont.)

Cross disperser:	333 grooves/mm 1°37' blaze 128 x 154 mm Central hole, 50 mm diameter	133 grooves/mm 1°37' blaze 128 x 154 mm Central hole, 50 mm diameter
Camera Mirror:	Spherical mirror Effective focal length 948 mm Clear Aperture 130 x 160 mm ellipse	
Detector:	SEC Vidicon	

4.2.3 Results

The spectrograph described above was ray traced, and the resulting spot diagrams are given in Figure 4-4. A pair of spots was plotted in a corner of the format at each end of the spectrum as well as in the middle. The resolving capabilities of the spectrograph are readily seen. The appearance of the central spots is due to a focus compromise which sacrificed some of the central resolution for the benefit of the corners. The spots reflect no contribution from the telescope. When allowances for pointing precision and diffraction are included, the spots will increase to about 30 μm in size, a fair match for the SEC vidicon and permits resolution of 0.01 Å at 1200 Å with proportionate increases elsewhere in the spectrum.

Vignetting by the central hole in the cross disperser was calculated. Nineteen percent of the energy coming from the telescope is lost due to the size of the grating hole, and an additional 5 percent loss is suffered at the corners of the format.

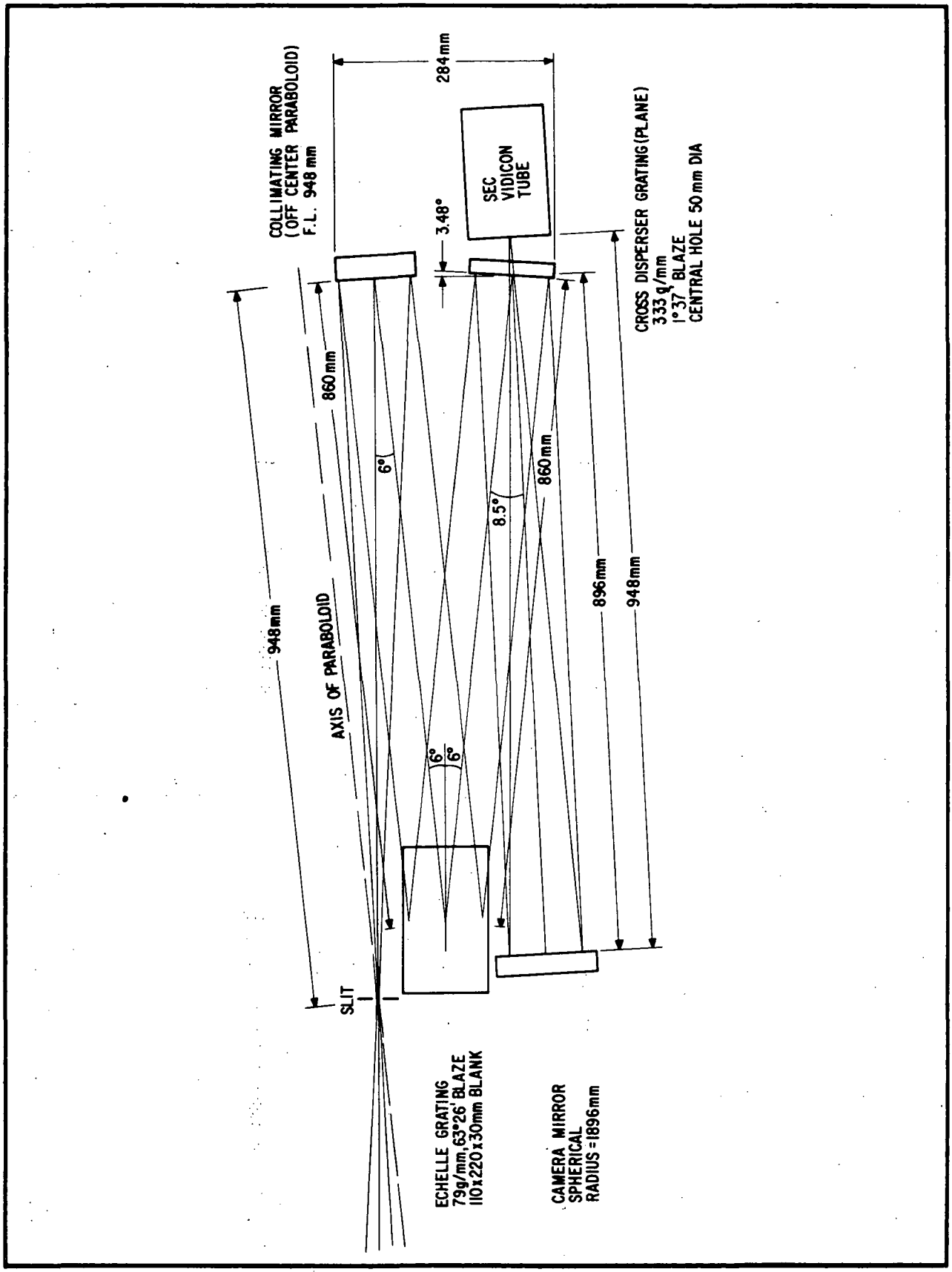

Figure 4-3 Echelle Spectrograph with SEC

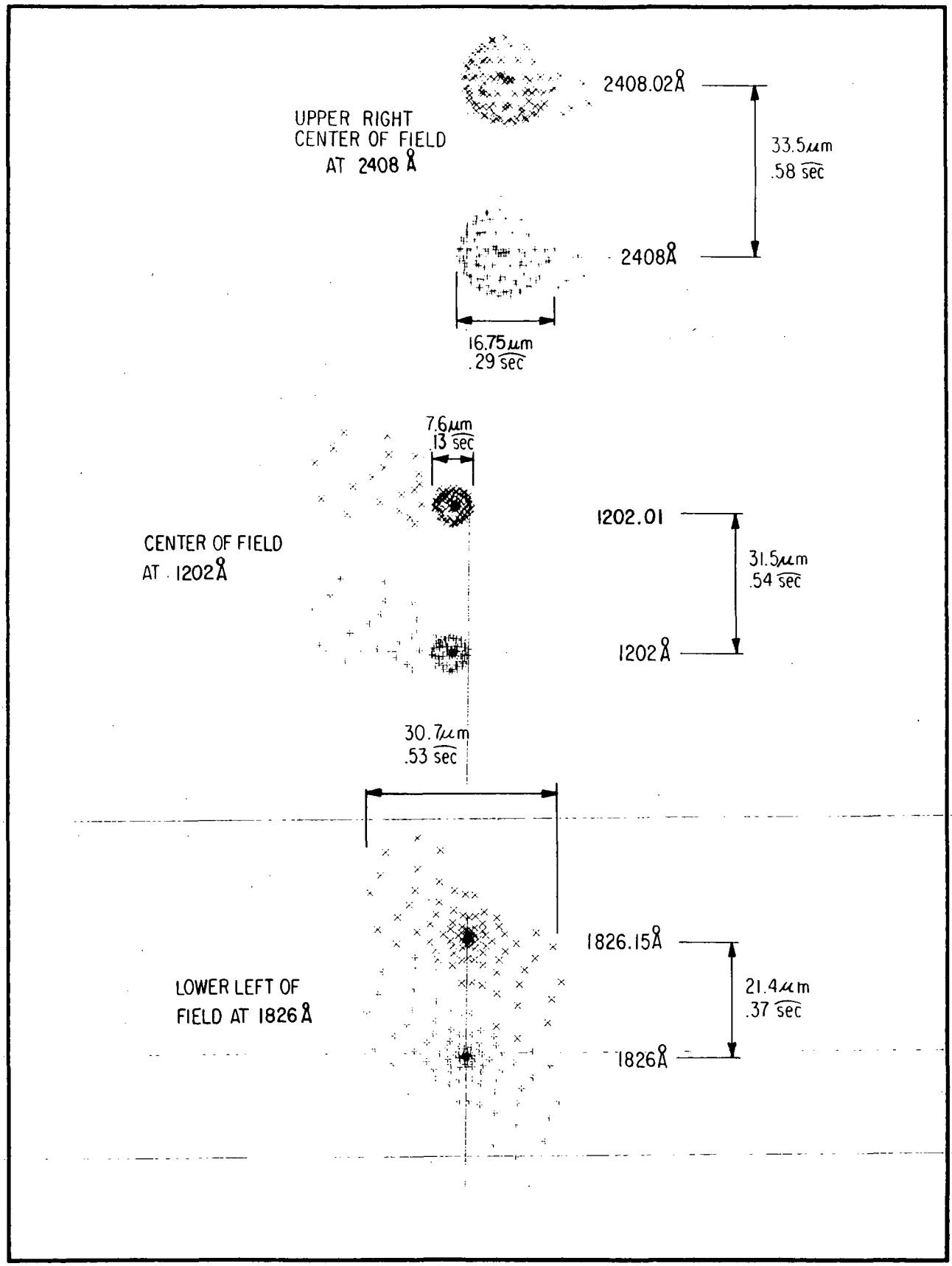

Figure 4-4 Echelle Spectrograph Spot Diagrams

4.2.4 Echelle Spectrograph Variations

F/25 Echelle Spectrograph. The spectrograph design described in the foregoing paragraphs is specifically an f/10 design. The alternative is to use an off-center parabola for the camera as well as for the collimator for use in an f/25 configuration. The mirrors need not be parabolized (the difference in performance is not detectable). The f/25 spectrograph has the advantage of smaller optical parts, gentler angles, and more compact construction.

F/2 Electronographic Camera. The feasibility of incorporating a high-speed camera into the echelle spectrograph for the purpose of recording spectra of faint sources at reduced resolution has been explored. The chief problem with this approach is that the echelle spectrograph is confined to a narrow field of view, whereas the electronographic camera is a wide-angle instrument.

Fortunately, the f/2 electronographic Schmidt camera has a field of view of 10°, the echelle spectrograph has a field of 2-1/2° in the grating space, and the two can be reconciled by replacing the echelle grating of the f/10 instrument by one ruled with 316 grooves per millimeter. This will have the effect of quadrupling the free spectral range and increasing the angular spread to 10°. A 1200 groove per millimeter objective grating can be used as a cross disperser. The arrangement is illustrated in layout form in Figure 4-5.

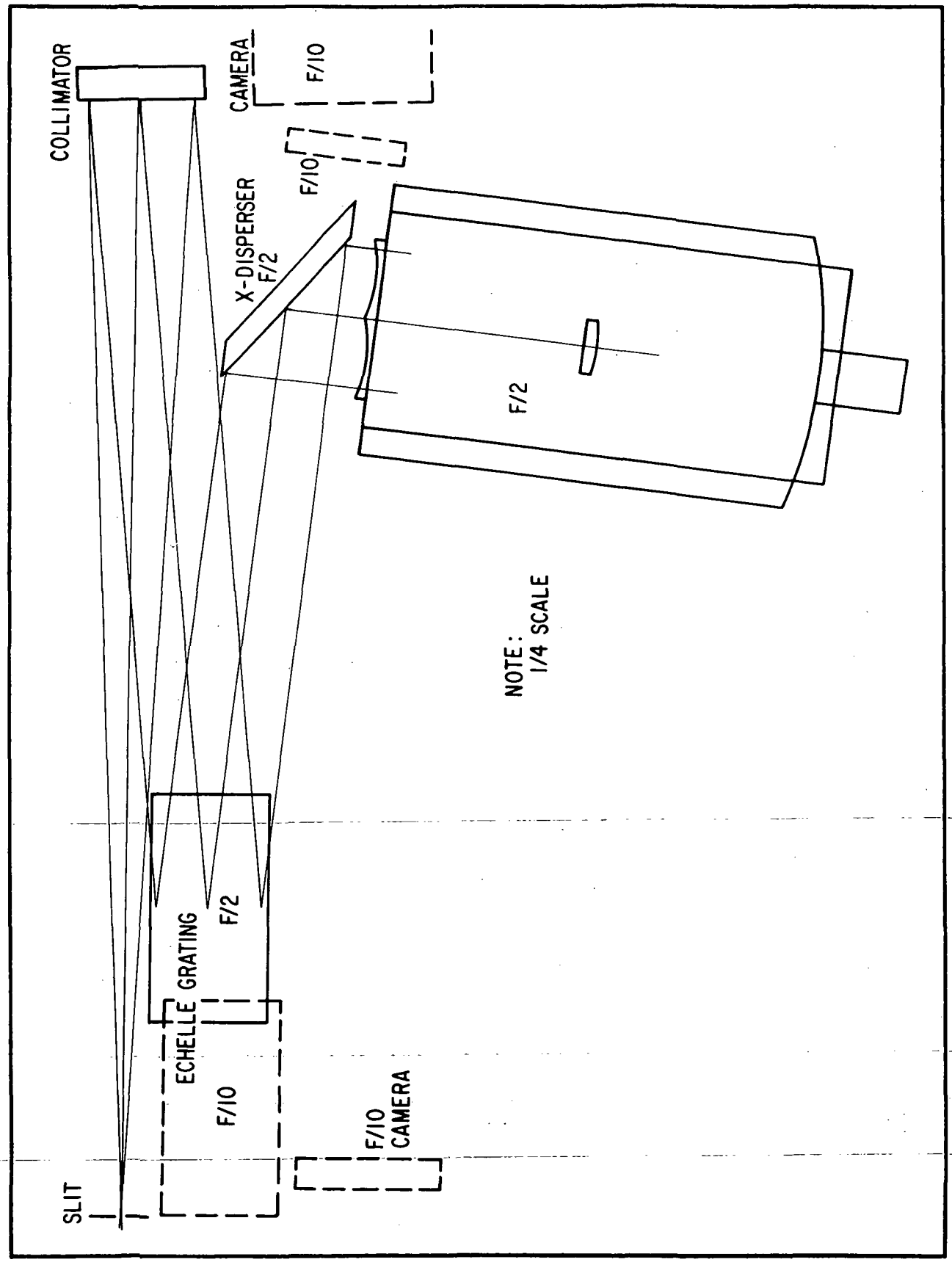

Figure 4-5 Echelle Spectrograph Layout with Schmidt Electronographic Camera

4.3 IMAGING SPECTROGRAPH

4.3.1 Design Goals

A general purpose spectrograph usable either in the slit mode or slitless for investigating spectra of extended sources is required. It is to have a spectral resolution of 0.1 Å and cover the spectrum from the LiF transmission limit at 1050 Å to the red end of the visible spectrum at about 7000 Å. It should be compatible with an SEC vidicon image tube, and a high speed mode should be possible for recording faint objects at reduced resolution.

Initial study using conventional spectrograph forms, such as the Ebert-Fastie and Czerny-Turner, produced excessive astigmatism which reduced the energy density on the detector and therefore demanded longer exposures with decreased resolution in the direction normal to that of dispersion. The LST design, while it could guarantee the spectral and spatial resolution, appeared excessively complex in terms of aspheric corrections on grating and mirror surfaces and required oblate spherical curvatures for the collimator and camera optics.

4.3.2 Imaging Spectrograph Specifications

The LST imaging spectrograph uses aspheric elements, but the departure from sphericity is slight. A modification was formulated using flat surfaces on the mirror and grating and spherical figures for the camera and collimator mirrors. The ray trace verified that a spectrograph can be made that will have the necessary resolution capability. The spectrograph is shown schematically in Figure 4-6.

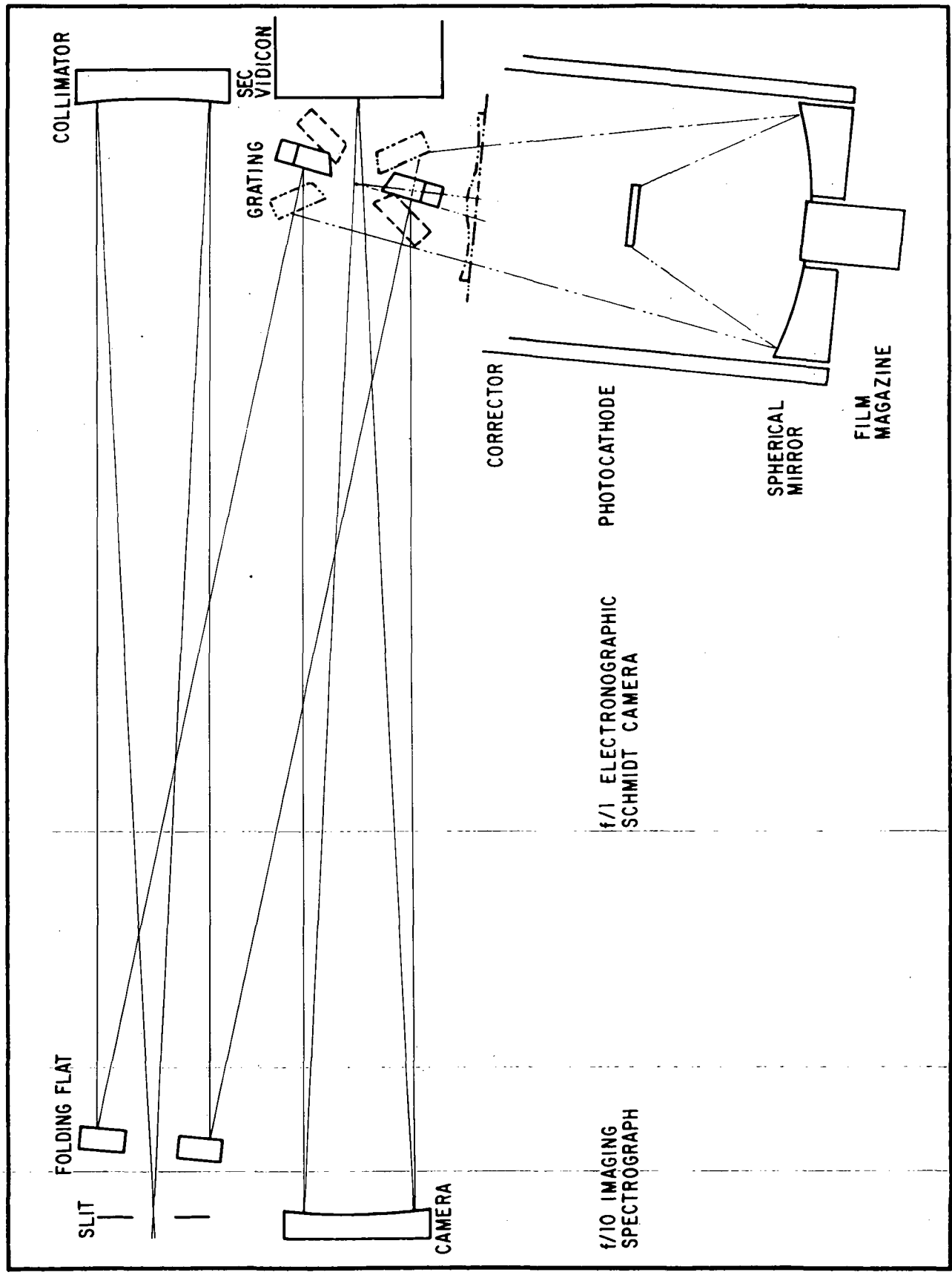

Figure 4-6 Imaging Spectrograph Layout

Since the format of the SEC vidicon covers only a small fraction of an octave of spectrum, the grating is tilted about an axis parallel to its rulings in order to tune the spectrograph to the desired wavelength band. A tilt range of 22 degrees is required. Further, to cover the several octaves, a selection of three detector tubes and two gratings is needed. The photocathode and a characteristic grating for each wavelength are listed in Tables 4-3 and 4-4. Lower spectral resolutions (corresponding to 50-100 Å/mm dispersions) will be desirable for recording spectra of faint extended objects. This may be achieved by using coarser gratings.

Table 4-3
DETECTOR COMBINATIONS FOR VARIOUS WAVELENGTHS

Wavelength Range, Å	Photocathode	Window
3400 - 7000	s-20	Quartz
1800 - 3400	Cesium Telluride	Quartz
1050 - 1800	Cesium Iodide	Lithium Fluoride

Table 4-4
GRATING AND ORDER USED FOR VARIOUS WAVELENGTHS

Grating Frequency	Order	Wavelength, Å	Dispersion	Resolution, Å
1800 g/mm	1	3400-7000	5.27 Å/mm	0.21
	2	1800-3400	2.64 Å/mm	0.10
2160 g/mm	1	1800-3400	4.63 Å/mm	0.18
	2	1050-1800	2.31 Å/mm	0.09

Table 4-5
IMAGING SPECTROGRAPH ELEMENTS

Slit:	40 mm square or 40 mm x 20 μm or 20 μm square		
Collimator:	Spherical mirror 980 mm effective focal length 140 mm clear aperture		
Folding mirror:	Flat 105 mm clear aperture 50 mm central hole		
Grating:	1800 grooves/mm 5000 Å blaze 102 x 206 mm 50 mm central hole	or	2160 grooves/mm 2000 Å blaze 102 x 104 mm 50 mm central hole
Camera mirror:	Spherical mirror 980 mm effective focal length 175 mm clear aperture		
Detector:	SEC vidicon		

4.3.3 Performance

The spot diagrams shown in Figure 4-7 demonstrate that the imaging spectrograph has the capability to produce an adequately resolved image over the entire format. Because of the limitations of the SEC vidicon, the resolution of the system is limited to 0.2 Å in the first order and 0.1 Å in the second order spectrum. If the detector were capable of it, the spectrograph could easily provide a resolution that is at least a factor of two better. The spots were calculated with point sources in the entrance plane. When allowances for diffraction and pointing errors are made, the spot sizes increase to about 17 μm.

Ray traces which include the effects of the central holes indicate an additional loss of about 15 percent of the energy because the holes are oversized with respect to the secondary mirror of the telescope. In addition, a vignetting modulation of 25 percent at the corners with respect to the centers is encountered.

4.3.4 Imaging Spectrograph High Speed Variation

For recording spectra from faint sources, an electronographic Schmidt camera of the type described by Carruthers is suggested. To record an octave of spectrum, a 20 degree field of view is needed. This in turn dictates an f/1 camera. To accept the entire bundle of rays coming off the grating, an aperture of 15 cm is required. To date, the largest f/1 camera in the literature is 10 cm. However, other cameras have been built with 15 cm apertures, so it should be feasible to engineer the proper combination. The location of such a camera is shown in the layout of Figure 4-6.

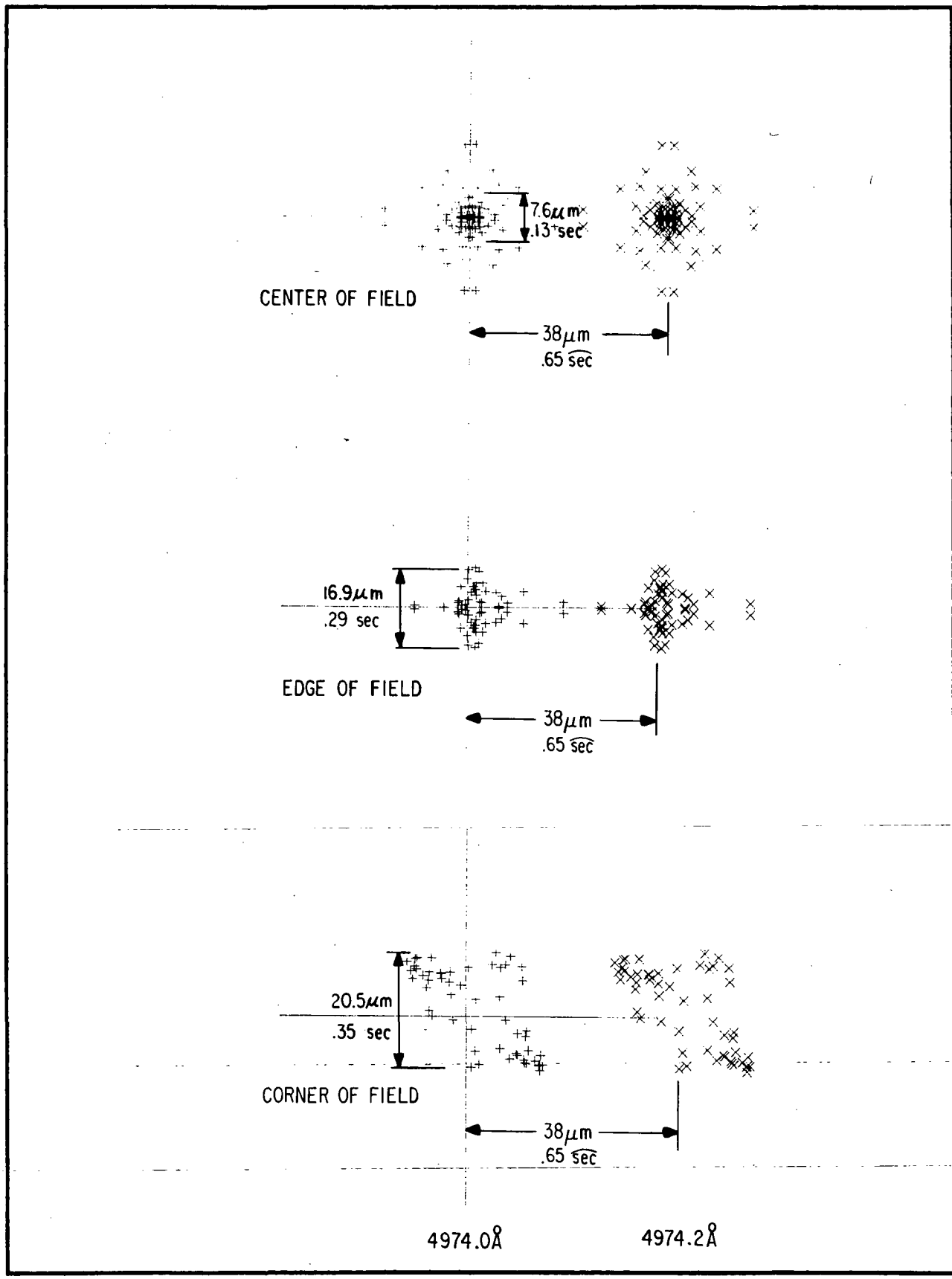

Figure 4-7 Imaging Spectrograph Performance

4.4 LIMITING MAGNITUDES

As a guide for comparison of the performance of the AOS and other astronomical observatories, the minimum useful apparent visual magnitude is calculated for representative stellar classes and AOS configurations. Stellar classes considered are O5, A0, and G2 dwarfs. The O5 V fluxes are taken from Hickok and Morton[1], and the G2 V (solar) fluxes from Brinkmann, et al and the A0 V fluxes are from Mihalas[2]. All limiting magnitudes are uncorrected for interstellar absorption. An observing period of 30 minutes was assumed. For the configurations using the SEC vidicon as a detector, a signal to noise ratio of 5:1 is used. Limiting magnitudes in electronographic camera configurations correspond to an Ilford L4 emulsion density of 0.1 over a 25 μm square. For both detectors, it is assumed that the optimum photocathode materials are used -- a single photocathode is not appropriate at all wavelengths. The results are presented in Table 4-6.

4.5 OTHER DESIGNS EVALUATED

Several other designs were evaluated among which were prism and concave grating instruments and the Ebert-Fastie Spectrograph. These are discussed below.

4.5.1 Prism Instruments

Prism instruments, while highly useful for some applications, such as cross-dispersers in echelle applications, find limited use in single-dispersion ultraviolet instruments because:

- They provide non-linear dispersion.

Table 4-6

AOS LIMITING MAGNITUDES

Wavelength (Angstroms)	Telescope Efficiency	SEC Quantum Efficiency	SEC-Echelle** (0.01 Å resolution)			SEC Imaging** (0.1 Å resolution)			Film*** D=.6 (500 Å band)		
			O5V	A0V	G2V	O5V	A0V	G2V	O5V	A0V	G2V
1200	.55	.09	13.3	9.1	-4.5	17.7	13.5	-0.1	---	---	---
2500	.64	.20	14.9	12.1	8.2	17.9	15.2	11.3	22.6	22.4	16.0
4000	.70	.20	14.0	13.7	11.2	17.0	16.7	14.2	21.0	20.8	18.3
6000	.66	.07	11.4	11.6	10.1	14.4	14.6	13.1	18.9	19.1	17.6

* The O5V fluxes are taken from Hickok and Morton, Ap.J. 152, 203, 1968.
The A0V fluxes are taken from Mihalas, Ap.J. Suppl. 114, 1966.
The G2V (solar) fluxes are taken from Brinkman, et al., JPL Technical Report No. 32-951.

** For the SEC a signal to noise ratio of 5:1 is used. Also, the table does not take into account the effect of pre-amplifier noise. It is assumed that optimum photocathode materials are used at each wavelength. A single photocathode is not appropriate at all wavelengths.

*** The table is for exposure times of 30 minutes on un-reddened stars.
103a-J is used at 2500 Å and 4000 Å. 103a-E is used at 6000 Å.

Note: Electronographic echelle and imaging spectrographs with 0.05 Å and 1.0 Å spectral resolutions, respectively, attain effectively the same limiting magnitudes as those given above for the SEC spectrographs.

- The dispersive power of most useful materials is highest near their short wavelength transmission cutoffs. In practice, this means that several prism materials would have to be prepared. In addition, the instrument can never work shorter than ~1050 Å, - the LiF cutoff.

Prisms do possess significant advantages over diffraction gratings, namely:

- Only a single dispersion mode operates for optically inactive materials; thus, no order overlap problems occur.

- The polarization properties of prisms are well understood, in contrast to the situation with gratings.

- The efficiency of prisms is often a factor of two greater than that of gratings.

4.5.2 Concave Grating Instruments

Concave gratings, in high incidence angle mounts, are appropriate where high efficiency is desired at the price of astigmatism. This configuration was rejected since no significant advantage is obtained above ~1200 Å; but it is recommended for work in the 900 to 1200 Å region. One such instrument evaluated is the LST Lyman spectrometer.

The Lyman spectrometer, a name given to the high incidence concave grating instrument specified in section 6.2.4 of the Kollsman LST report (GSFC X-670-70-480), will fulfill the 900-1200 Å spectrographic requirements for the AOS. The high incidence angle combined with the addition of only one reflection beyond the telescope are the features which make this instrument desirable. It is not that this is the only possible design for use in this region, but rather that all other high incidence designs are variations of this one; and normal incidence work is possible with the 0.1 or 1.0 Å instruments if it is desirable to trade-off throughput for astigmatism. Detectors for this instrument, since they must be windowless, are limited to either the channel or channel arrays mentioned in the Kollsman report, or to film.

Performance. Analysis of the Kollsman instrument shows that the only desirable change for the AOS is a decrease in the focal length of a factor of two to match the AOS telescope plate scale. With a 375 mm radius of curvature grating, the entrance slit is ~27 μm wide and the images are ~14 mm high at f/10. A 40 mm format will cover ~140 Å. The grating must be 25 mm high by 40 mm wide and is used in third order; 2400 grooves/mm is appropriate with ~25° blaze angle.

Layout and Performance. The layout is given as Figure 4-8. It is expected that the instrument can easily attain 0.1 Å resolution and will have a transmission (grating only) of ~40 percent.

4.5.3 Ebert-Fastie Spectrograph

The specifications for the 0.1 Å Ebert-Fastie spectrograph are given in Table 4-7. Figure 4-9 is a layout of the instrument. Figure 4-10 shows spot diagrams for this design. This design was rejected because of excessive astigmatism, limited wavelength coverage per exposure, and difficulty in mounting the detector without introducing an additional reflection.

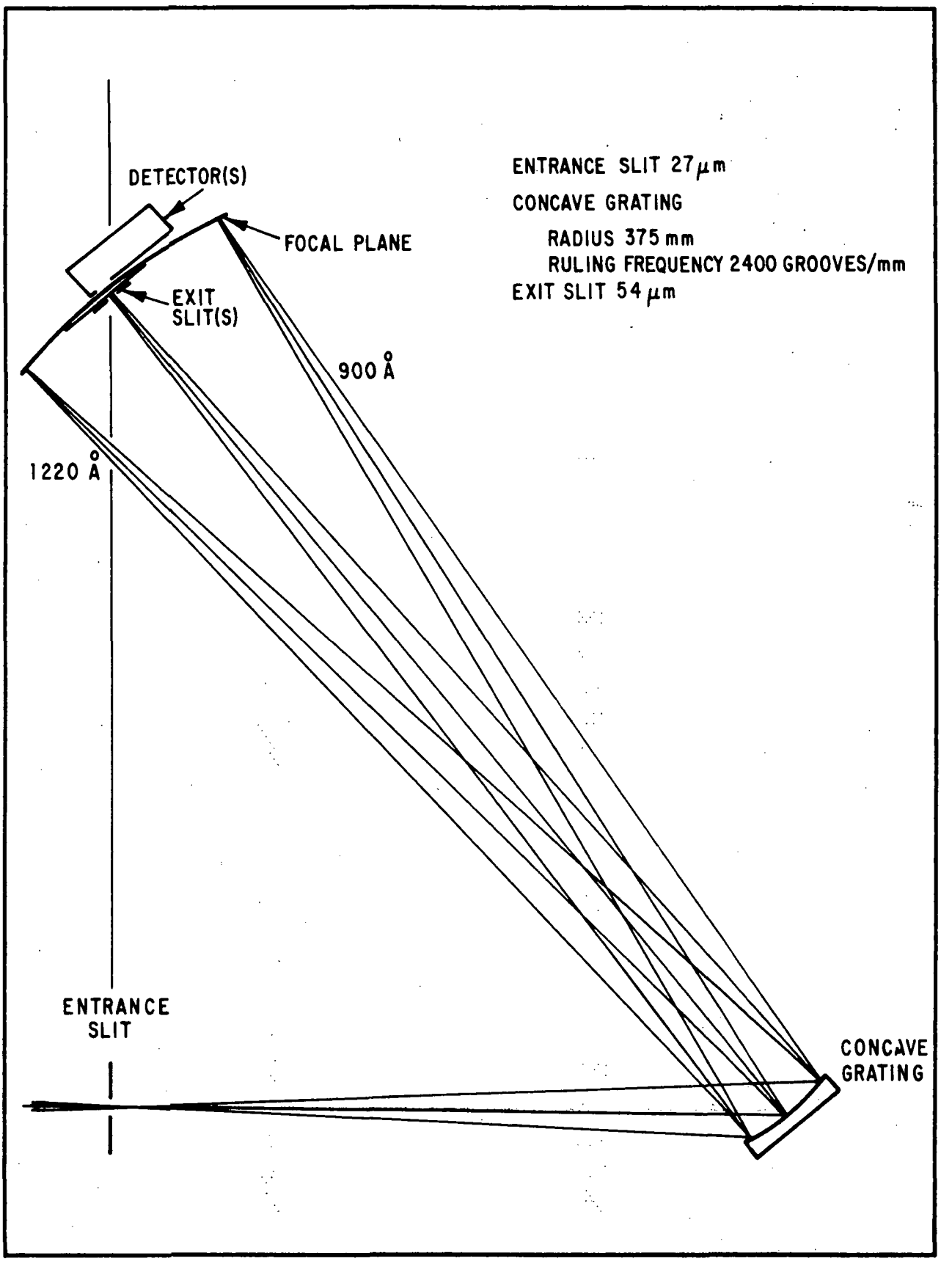

Figure 4-8 Lyman Spectrometer (After Kollsman LST Report)

Table 4-7

0.1 Å EBERT - FASTIE SPECTROGRAPH SPECIFICATIONS

Configuration	Ebert-Fastie
Spectral Resolution	0.1 Å nominal
Mirror Focal Length	1 meter
Mirror Size	14 x 28 cm
Grating--Bausch & Lomb	
Size	10 x 10 cm to 10 x 20 cm depending on wavelength region
Ruling	2400 lines/mm
Blaze	Selected according to wavelength coverage
Required Angular Dispersion (22mm aperture)	2.2×10^{-5} radians/Å
Resulting Inverse Linear Dispersion	4 Å/mm
Required Detector Resolution	40 cycles/mm
Wavelength Coverage (40 mm format)	160 Å
Mirror Off Axis Angle (Max)	10.5°
Grating β Angle (Max)	10.5°
Astigmatic Image Height	
f/10	1 mm
f/25	0.4 mm

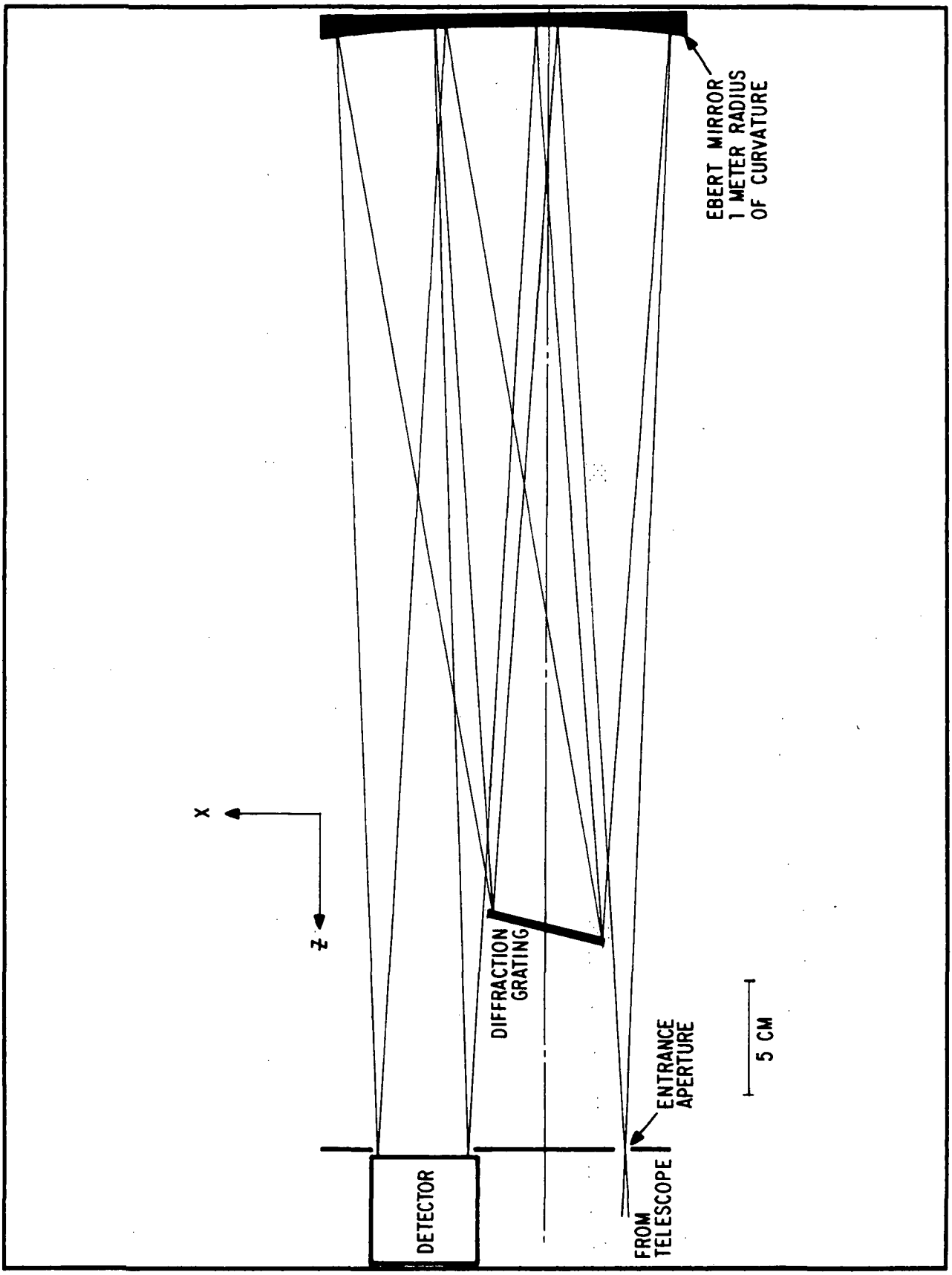

Figure 4-9 0.1 Å Ebert-Fastie Spectrograph Layout

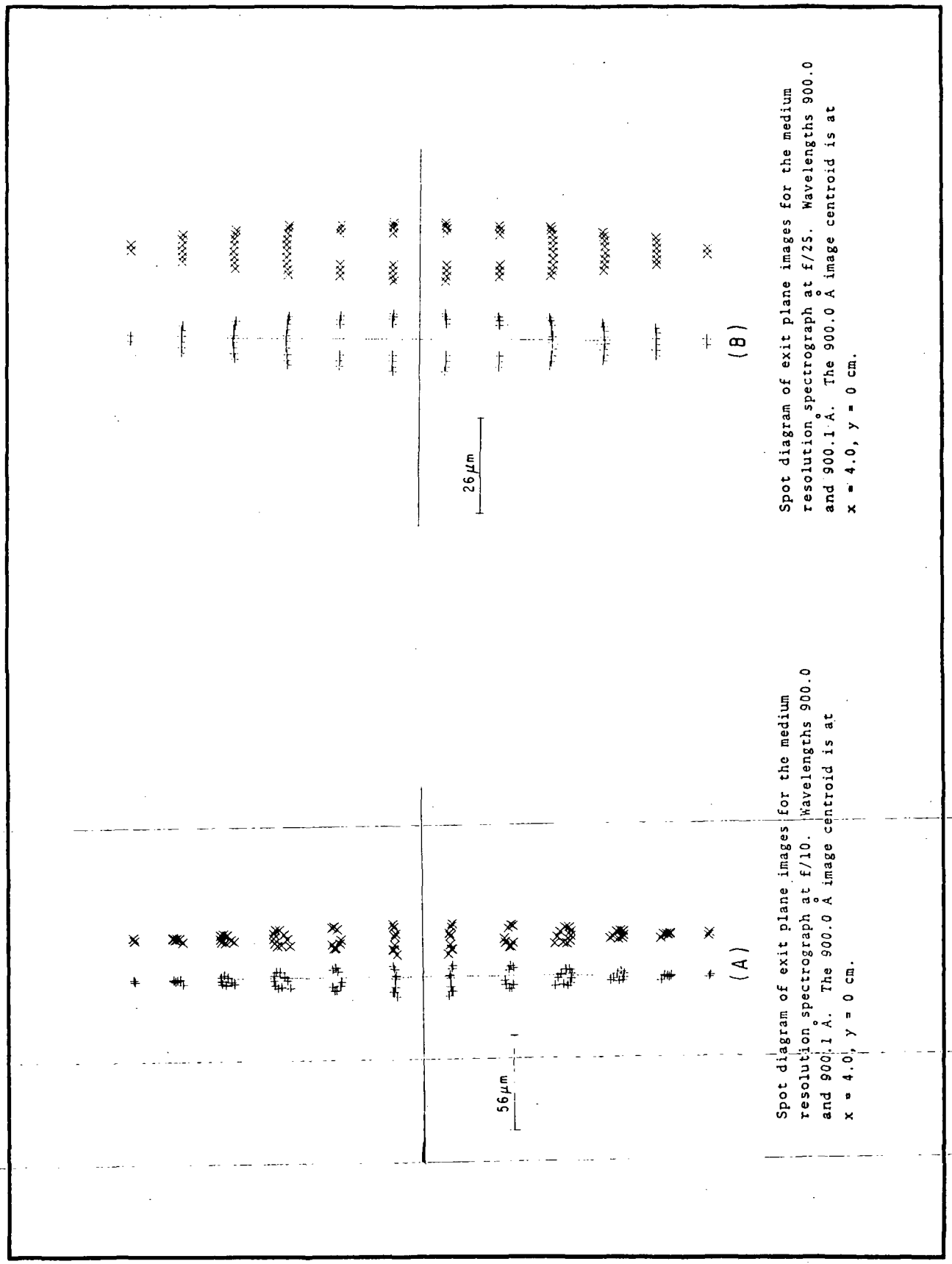

Figure 4-10 Ebert-Fastie Spectrograph Spot Diagram (1 of 3)

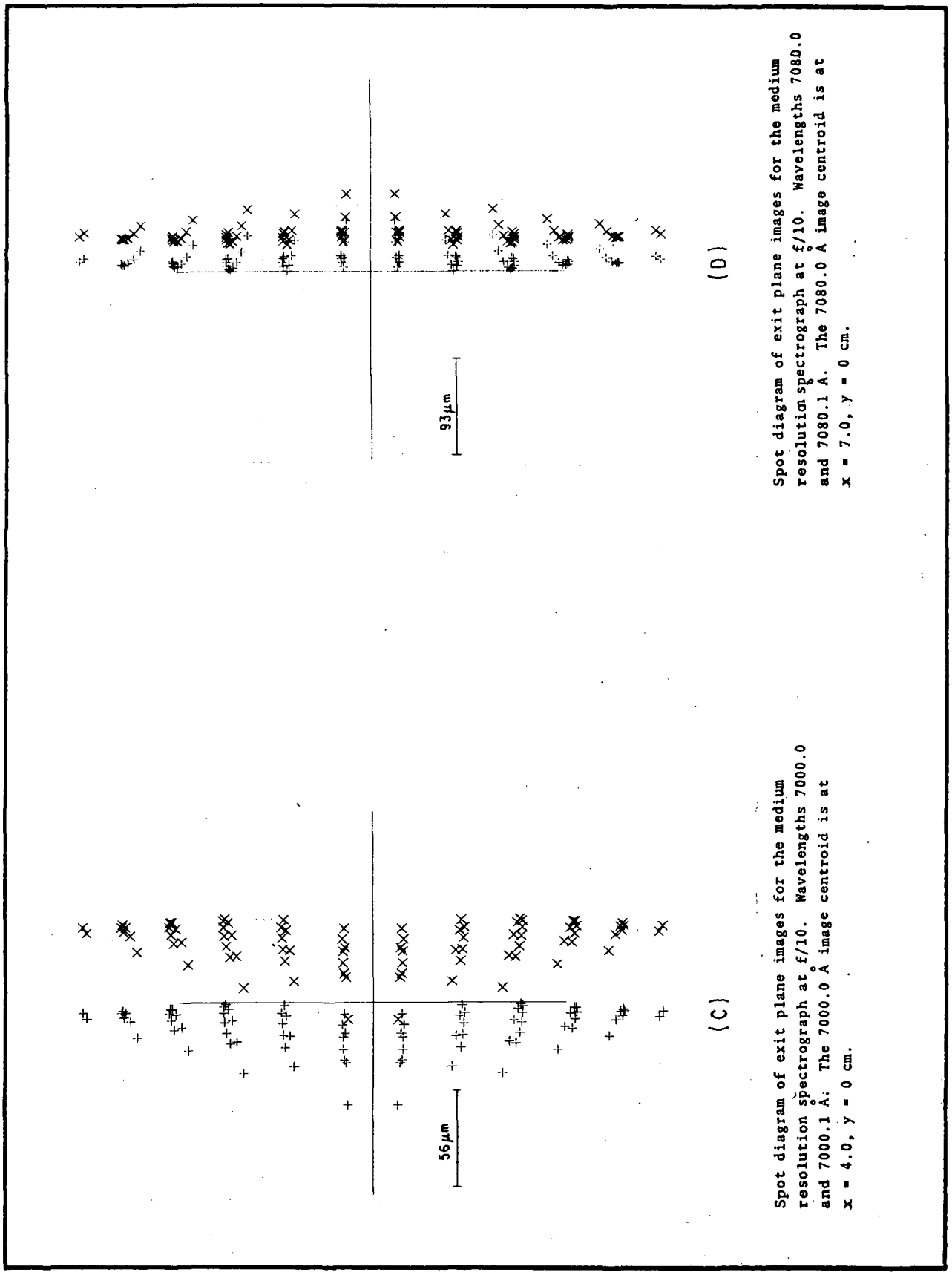

Figure 4-10 Ebert-Fastie Spectrograph Spot Diagram (2 of 3)

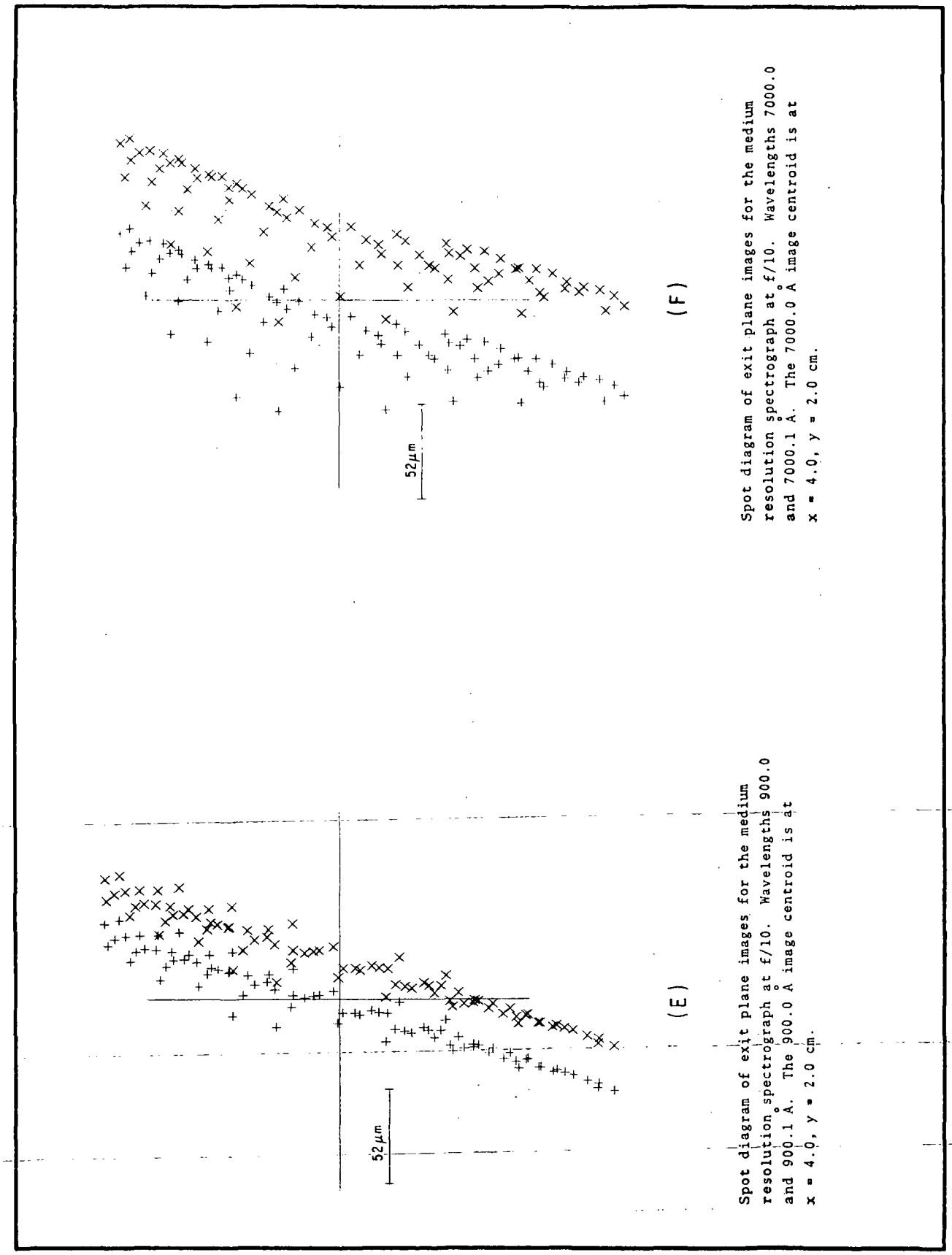

Figure 4-10 Ebert-Fastie Spectrograph Spot Diagram (3 of 3)

4.6 BROADBAND FILTERING

It is necessary to introduce various filters into the beam of the AOS telescope for a variety of purposes. Spectral filters will be used to limit and define the effective wavelength region incident on both the SEC vidicon and the electronographic camera, thus becoming a key element in both spectral imagery and filter photometry. In these cases, the efficiency of the filter at various wavelengths enters into the interpretation of the observations in a critical way. Filters will also be used in ways less critical to the data; for example, to block interfering wavelengths from the entrance slit of a spectrograph or reflect heat from a cryogenically cooled detector.

A number of manufacturers make bandpass and blocking filters for a variety of purposes. Usually, when an astronomer uses a filter for photometry or imaging he chooses one specially designed for his specific purpose. Thus, with a few exceptions, there are no standard filters. For this reason, the follow-on detail design of the AOS will provide:

- The means of manipulating such filters in the beam
- A set of specifications for such filters giving their necessary mechanical, thermal, and environmental properties.

Transmission filters, the ones most commonly available, are most suitable for photometric measurements. Unfortunately, they do degrade image quality. A plane parallel flat, a reasonable model for an etalon-type filter, introduces a small amount of both spherical and chromatic aberrations into the system.

The image size for the f/10 system due to this effect is given by Smith [4]

$$d = 2 \frac{10^{-2} t}{10} \frac{(n^2-1)}{n^3}$$

where: t is the filter thickness
d is the spot diameter
n is the index of refraction.

If n = 1.33 and t = 5 mm, then d = 3.3×10^{-3} mm, or 3.3 μm. Thus, only very thick or high index of refraction filters can impact image quality.

For this reason, fairly thin filters or reflective filters are necessary for broadband imagery at high resolution. If narrow band filters are used, correction of the spherical aberrations should be relatively easy.

A means to insert and manipulate one or more filters in the telescope beam is required. The position, and in the case of polarizers, the orientation of the elements must be controllable to fairly precise tolerances. Plane filters should be locatable axially to within 0.1 mm and laterally to within 1 mm. Once they have been located, they must be held to tolerances comparable to the image dimensions. The orientation of critical elements must be settable to within 0.5 milliradians (~1 arc-minute). If convenient, such a mechanism might also be used in the focal plane for spatial filters (field stops) for photometric work.

One possible mechanism is the filter wheel. The advantage of a filter wheel is that it can be very accurately and stably aligned, and this alignment can be accomplished simultaneously for all elements in the wheel. Disadvantages include difficulty in controlling the orientation of polarizers, a rather large size, and difficulty in making translational adjustments.

Other possibilities include the use of a slide or a manipulator to select and plane individual items in the beam. While capable of any of the necessary motions, manipulators tend to be complex. If a manipulator cannot be provided for each filter required in the beam at a given time, some method of capture must be devised.

The support system for the mechanisms must be capable of both manual and automatic operation ($\lesssim$ 15 seconds per operation) and to indicate to the data handling system its status at all times.

4.7 POLARIZERS

A number of techniques are available for polarization analysis in the 2200 - 4000 Å region. Calcite prism polarizers of the Glan-Thompson and Glan-Taylor design are available commercially as standard items in a range of aperture sizes up to 20 mm. Extinction ratios of up to 1×10^6 can be obtained. Likewise a variety of sheet polarizing materials, with lower extinction ratios are available very inexpensively but their vacuum exposure properties are suspect.

Below 2000 Å, alkali-halide plate piles or Brewster angle polarizers may be necessary. As with all dielectric materials, the properties of these polarizers change drastically as the wavelength of the incident light nears an absorption feature. Therefore, this method is limited to relatively narrow spectral bandwidths.

REFERENCES

1. Hickok, F.R., and D.C. Morton, Astrophysical Journal, No. 152, 1968, p.203.

2. Mihalas, D., Astrophysical Journal Supplement No. 114, 1966.

3. Brinkmann, R.T., A.E.S. Green, and C.A. Barth, JPL Technical Report, No. 32, p. 1966, p.951.

4. Smith, Warren J., Modern Optical Engineering, New York: McGraw -Hill Book Co., 1966.

Section 5
DETECTORS FOR THE AOS

5.1 GENERAL DISCUSSION

The versatility inherent in the AOS concept provides unprecedented freedom in the choice of detectors for capturing astronomical data in a space environment. The ready accessibility of the instrument compartment and the telescope image plane, adequate storage space, and the ability to use expendable materials are major contributors to this flexibility.

Table 5-1 lists some examples of detectors which could be used on AOS. In actual practice, it is desirable to narrow down the list to a few of the sensors most effective for astronomy, but it is significant that the choice is primarily one involving relative scientific merits of available detectors with very little limitation by spacecraft constraints. Therefore, each astronomer can select one or more detectors as dictated by the science involved along with his own personal experience and preference. He can choose from available photographic plates and emulsions much as he does at a ground-based observatory. He can choose single element detectors such as multiplier phototubes or silicon diodes for photoelectric radiometry in either dc or photon counting modes. He can use a conventional approach such as photographic film or a linear array of photosensors to measure stellar spectra. Or, he can take advantage of more recently proved techniques such as use of the "smoothing dissector." (This is a combination of an image dissector tube with image intensifiers which under proper conditions can function as a near-ideal 2000 or 4000 channel photon counter for faint spectra.)

Table 5-1

CANDIDATE IMAGING SYSTEMS

Single-Element Detectors

(Require X-Y scan to record 2-D image. Integration may be performed point-by-point in external circuitry.)

Examples:

Multiplier Phototube
Optical/Mechanical Scan

Silicon PIN Photodiode
Optical/Mechanical Scan

Image Dissector
Electronic Scan

One-Dimensional Detectors

(Particularly suitable for spectrophotometry. Require orthogonal scan to record 2-D imagery.)

Examples:

Spectracon
Electronographic tube with rectangular Lenard window, nuclear emulsion.

Digicon
A linear array of silicon diodes acting as photon counters. Integration and scanning in external electronic circuits.

Reticon
A linear array of silicon diodes in charge-storage mode, providing time integration of flux. Internally self-scanned by integral shift register.

Image Dissector Plus Intensifier
Short-term integration provided by phosphor on intensifier. Functions as near-perfect multi-channel photon counter in spectrophotometric applications.

Two-Dimensional Detectors

(Provide time-integration over entire 2-D flux distribution while preserving spatial relationships within the field.)

Examples:

Photographic Emulsion
Many types and spectral sensitizations.

Nuclear Emulsion
Used to record photoelectrons in electronographic cameras. Provides excellent 2-D proton counting and integration.

Image Intensifier Plus Photographic Film
Enables ordinary photographic film to be used in a photon-counting mode.

Integrating Photoelectronic Camera Tubes with Electronic Readout
Includes vidicon, orthicon, isocon, SEC, SIT, silicon diode matrix etc. Some can also be used in discrete photon counting mode with an external multi-channel memory for integration.

At the primary focal plane for imagery of starfields, clusters, and galaxies, the astronomer can decide to use photographic plates either alone or in conjunction with a high-gain image intensifier (such as a channel electron multiplier array) in order to obtain increased sensitivity (photographic speed) at the cost of resolution and granularity. More likely, however, if he is intent on achieving the ultimate in dynamic range along with high spatial resolution and precise radiometry of all objects in the field-of-view simultaneously, he will take advantage of this opportunity to use an electronographic camera in space.

On the other hand, if the ability to transmit the data to ground for immediate scrutiny and analysis is desired, or if the payload specialist would like a quick-look display of the focal plane image to assist in focusing or in guiding to stars beyond the visual limit, a detector with electrical readout would be called for. Although the spatial resolution and total information storage capacity may be inferior to that of the electronographic emulsion, certain electrical readout camera tubes do achieve true photon-limited performance while maintaining sufficiently high spatial resolution and radiometric precision for many astronomical applications. The output may be stored on tape in the SAL or transmitted immediately to ground for computer processing and display. In this way, the astronomer on the ground can get a first-hand look at the image plane of his spaceborne telescope or see the output of his spectrophotometer. Using a voice link he could, if desired, work directly with the payload specialist in selecting objects for study, choosing exposure times for the electronographic camera, etc.

5.1.1 Candidate Detectors

The most elemental technique of photoelectronic imaging probably would be the use of a simple phototube or photodiode that by either mechanical or optical means is caused to scan or "dissect" a two-dimensional image in some ordered sequence until every part of the field has been observed. The gathering of data or "exposure" is applicable to only a single picture element at any time, and a very large portion of the total energy available is necessarily lost. Very high quality results can be obtained in this way provided sufficient energy and/or time is available to accumulate the required data. The image dissector tube falls in this category. It can be scanned electrically, eliminating the need for any optical-mechanical scan mechanism.

The inefficiency of this approach can be alleviated somewhat by using, for example, a linear array of detectors with a mechanical scan orthogonal to the array. This reduces the fraction of wasted energy at the expense of considerable complication in the readout electronics, requiring a separate data gathering chain for each detector in the array. If the sensor elements can integrate and store the flux signal over the period of a line scan, however, then a single set of data gathering electronics may still be sufficient. The Reticon and the image dissector plus intensifier are devices which can be used in this manner. The latter must be scanned at a sufficiently high rate to maximize the effectiveness of the intensifier phosphor as a storage medium. The data from each scan is injected into an external circulating memory. This allows data integration to continue for as many scans as needed to achieve the desired precision. At the end of the integration period, the data in the circulating memory are read by computer and stored on magnetic tape.

The most efficient detectors for images are those now-numerous types of two-dimensional image integrating sensors. One way or another, all these detectors have the ability to collect and store energy from an entire two-dimensional field while preserving the information on its spatial distribution. Photographic emulsion is, of course, the oldest and most widely used image integrating detector but it has now been joined by a considerable variety of photoelectronic imaging devices. These include electronographic tubes such as those devised by Lallemand, Carruthers, Kron, and McGee, and hybrid approaches using image intensifiers with photographic film output (Carnegie tube, microchannel plate intensifier, etc.) and a variety of electrical read-out camera tubes.

The electronographic cameras employ a nuclear emulsion exposed to a photoelectron replica of the incident photon image while the Carnegie and other hybrid arrangements use photographic film sensitive to the luminescent phosphor output of the intensifier tube. There is no scanning process and no electrical readout is available. All the other photoelectronic image integrating tubes have one common characteristic; the information stored on the integrating medium is retrieved by sequential scanning of the entire image area, point-by-point, with an electron beam. The scanning beam restores the original (pre-exposure) charge and in the process the two-dimensional spatial distribution is converted to a one-dimensional function of time, that is an electrical output signal. With this form of a time varying voltage or current waveform the image information is readily recorded on tape or transmitted by conventional radio-telemetry techniques to distant recording stations. There the data is received in serial form and is used to reconstruct the spatial energy distribution characterizing the original optical image. The precision possible in reconstructing the image depends therefore not only on the camera tube

but also on the care and attention to engineering detail on each link in the chain of signal processing, transmitting and reprocessing to a final picture. Table 5-1 gives a few examples of the many possible detector types which could be used on the AOS.

Basic Vidicon. The basic vidicon has a photoconductive film in its image plane which plays a dual role as a photosensing element and a storage medium. As a photosensor, the film can exhibit fairly high quantum efficiency over a limited spectral range. It can also be made thin enough to have high spatial resolution. As a storage medium, however, unless cryogenically cooled, it is generally limited to short retention times of a few seconds at most, by leakage current and lateral charge spreading. (Special slow-scan targets can push the time up to a minute or so.) Thus the vidicon should be used where the available flux is large enough to build up a charge-image rapidly and the stored picture can be read out without delay at a reasonably high rate. Under these conditions, a high level of performance can be achieved.

The vidicon output signal as shown in Figure 5-1, is obtained directly from the excursions of the storage target as it is traversed by the scanning electron beam. The sensitivity of the vidicon is low since there is neither prestorage gain nor readout gain. As a result, the output signal/noise ratio is generally limited by the noise in the first amplifier stages, preventing quantum-limited performance from being reached. The silicon target vidicon has the highest sensitivity in this group due to its high quantum efficiency. The silicon target exhibits a gamma of unity and can be used to integrate for periods as long as an hour when cooled to -65°C. It has served well in astronomical photometry.[1]

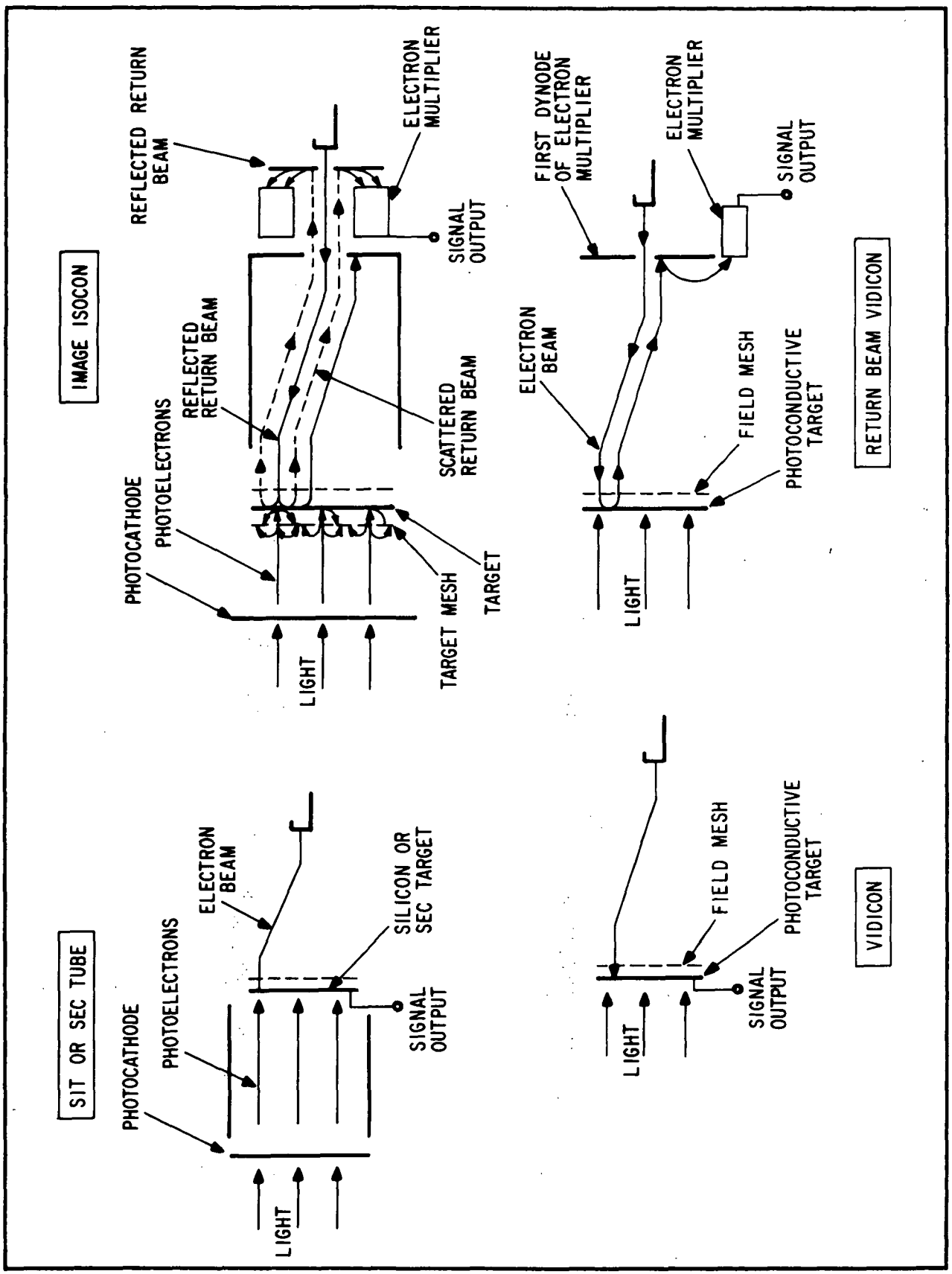

Figure 5-1 Types of Image Integration Sensors Having Electrical Readout

Sensors Incorporating Gain Mechanisms. Figure 5-1 also shows that the other common types of photoelectronic camera tubes separate the functions of sensing layer and storage medium. A photoemissive cathode surface at the image plane is used as the light sensor. The photoelectrons emitted from this cathode are directed by an electron lens to the storage surface or target, building up an electron image corresponding to the photon image at the photocathode. This approach is used in image orthicons and isocons, SEC tubes, EBS or SIT tubes and electronographic camera tubes. The storage target in these classes of imaging sensors can integrate and store a charge image for much longer periods without degradation than is possible with the photoconductive target of the common vidicon. Most of these tubes also include internal amplification processes which result in considerably increased sensitivity over the basic vidicon.

Image Orthicon/Isocon. This type of sensor falls in the category of return-beam readout tubes. Instead of taking its output directly from the target, the read beam electrons reflected (or scattered) back from the target are directed into a multi-stage electron multiplier where a large amount of signal amplification is obtained. The signal output is taken from the anode of the electron multiplier. A small amount of prestorage gain is also realized as the photoelectrons from the input photocathode impinge on the insulating material comprising the storage target. The total gain achieved in these sensors is considerable and the output signal is great enough to render negligible the noise generated in any external amplifiers. The image orthicon does have a significant noise factor introduced by the reflected electron beam which acts as a carrier for the image information from the target. The shot noise in this beam presents the problem.

The image isocon is a much improved version of the orthicon, where the signal to beam-noise ratio is enhanced by using the electrons scattered from the target rather than reflected by it. Both of

these types of tubes require a target mesh between the photocathode and the storage target. The mesh reduces the effective quantum efficiency of the sensor by a factor equal to the mesh transmission, generally one-half to two-thirds. The use of the target mesh also degrades the spatial resolution somewhat.

SEC and EBS Camera Tubes. These sensors are similar to the basic vidicon insofar as the readout signal is taken directly from the target. The difference arises from the use of a separate photocathode like the isocon and orthicon. Unlike the latter types, however, a very substantial amount of prestorage gain is obtained. The gain is developed by imparting energy to the photoelectrons by means of a high accelerating voltage. Then a target material is used which greatly multiplies the effect of the high energy incident photoelectrons. Potassium chloride is used in the SEC tube and a silicon diode matrix is used in the EBS (or SIT) tube.

These types have no target mesh to impair the effective quantum efficiency. The target in the SEC tube generates and stores about 100 secondary electrons for each incident photoelectron in the image. The silicon target can produce two to three thousand stored electrons per incident photoelectron. Prestorage gain acts to reduce the preamplifier noise relative to the fundamental quantum noise in the original photoelectron image by a factor equal to the gain.

The effective thickness of the storage layer in the SEC and EBS tubes can be made smaller than in the orthicon/isocon tubes and this allows higher spatial resolution to be achieved. The resolution of broadcast-type SEC tubes is limited by the suppressor mesh placed on the reading beam side of the target to prevent self-destruction from crossover when the target is being simultaneously exposed and scanned with the electron gun. In scientific and

astronomical applications, where a controlled sequence of exposure-readout-erase is employed, the suppressor mesh is not needed and the spatial resolution is significantly improved, depending primarily on the thickness of the target itself.

Broadcast and night-vision type SEC tubes rely on an electrostatic lens to focus the photoelectron image on the KCP target. The inherently more demanding nature of astronomical applications requires that a magnetic lens be used which results in improved overall spatial resolution and MTF of the sensor. The same applies to the tubes with silicon matrix targets.

Return Beam Vidicon. This is a hybrid type which uses a photoconductive target like the basic vidicon but derives its readout signal from the return electron beam like the image orthicon. Like the vidicon it has no prestorage gain but does gain some sensitivity with its output electron multiplier. The output signal can be large compared to preamplifier noise but the absence of prestorage gain makes it impossible to achieve a quantum noise-limited signal due to beam shot noise.

Extremely high spatial resolution has been obtained with the return beam vidicon by considerable study and refinement of the electron optics involved in focusing the read beam. This sensor seems well suited to high resolution-low sensitivity applications such as daytime imagery of the Earth's surface from the ERTS satellite.

Future Expectation. The best hope for the future appears to be the charge-coupled (bucket-brigade) silicon diode matrix. For astronomical applications, it should be made in a large format and used in an intensified mode similar to the EBS or SIT tubes but with a magnetically focused electron image. The absence of an electron beam and associated deflection paraphernalia eventually should permit very high quality photon-limited astronomical imagery with a very simple and reliable detector.

5.2 SELECTED DETECTORS

5.2.1 Basis for Choice

Any of the detector types studied, as summarized briefly above, could be put to use on the AOS. The overall results of the study become much more manageable and meaningful, however, if further analysis and numerical computations are restricted to the one or two presently available detectors which most effectively utilize the full potential of the AOS concept. The choice was finally narrowed down to two detectors: an electronographic camera for maximum information capacity and a meshless SEC vidicon as the most effective astronomical sensor providing electrical readout and the opportunity for quick-look use in AOS and at the ground station.

Both detectors have excellent long term integration ability and are capable of photon-limited performance. They have linear stable transfer characteristics and no reciprocity failure, highly desirable qualities for precise radiometry over a two-dimensional field.

The electronographic camera is a near-ideal 2-D photon detector in that all photons are recorded with equal weight, background noise is negligible, and storage capacity is extremely large. The latter is the result of a very large dynamic range combined with excellent spatial frequency response. The electronographic camera with certain emulsions can store 100 to 200 times more information in one picture than is possible with a IIa-O photograph. This opens the door to exciting future possibilities for the recovery of spatial information by deconvolution of the observed image with the instrumental profile function. Other advantages over conventional photography are better uniformity of sensitivity over the plate, reduced proximity and diffusion effects and total lack of halation.

The electronographic camera appears to be the camera of the future for the extraction of maximum astronomical data in a given time. Its exemplary properties are not only theoretical but have been experimentally proved. It remains only to do additional engineering and detail design to minimize the operational problems which exist when using photocathodes in the visible and near infrared. In the ultraviolet these problems are absent and the existing designs of Carruthers have proved simple to use and entirely reliable in the field on sounding rockets. The use of such a detector in space, even with a telescope of only one meter aperture, should give access to a whole new universe insofar as spatial resolution and accessible limiting magnitude are concerned.

The salient shortcoming of the electronographic camera is the lack of electrical readout for instant or quick-look analysis and/or display of the recorded data. The existing electrical readout sensor which has properties which most closely approach those of the electronographic camera is the meshless SEC camera tube. Thus this sensor has been selected as the second detector for use on AOS. The storage medium in this device can accommodate at maximum exposure roughly the same photoelectron density as Ilford L4 nuclear emulsion at a density of one. (The information content of the nuclear emulsion is much greater, however, due to its high spatial resolution and because of its ability to respond linearly to well above a density of one [as high as 4 or 5].) It has a linear transfer characteristic and can integrate for several hours with excellent reciprocity and can store for much longer periods without cooling. The internal tube background is sufficiently low so that the signal-to-noise ratio is quantum noise-limited. It has a flat image plane needing no fiber optics and can therefore be used with photocathode-window combinations which are efficient in the ultra-

violet, according to the scientific requirements. It has a 50 mm x 50 mm image format. It does limit the spatial resolving power attainable with the AOS telescope but no more so than many photographic emulsions such as IIa-O. At the image plane of the f/25 telescope, the system MTF degradation by the meshless SEC sensor is less than that due to an 0.1 arc-second rms pointing error.

The isocon and image orthicon must be ruled out due to poor quantum efficiency and inadequate single frame MTF (both due to the target-mesh arrangement). Also, beam noise degrades the available signal-to-noise ratios to values well below that inherent in the stored photoelectron image. These tubes have many critical potentials and can be more difficult to adjust and operate than less complex sensors.

Ordinary vidicons, including the return beam vidicon, are also incapable of quantum noise limited operation. Since these tubes have no prestorage gain, preamplifier noise limits the performance of the simple vidicon and beam noise prevents quantum-limited operation with the return beam vidicon. Cryogenic cooling is required for long exposures with these tubes. The addition of an external image intensifier to the vidicon via phosphor-fiber optics coupling results (at present state of the art) in degraded spatial resolution and introduces an intolerable amount of multiplicative, fixed-pattern noise.

The EBS or silicon intensified vidicon would be a good choice for the AOS if it was available with the 50 mm square format and with a magnetically focused image section similar to the chosen SEC sensor. This presumably will be available in the future when the larger silicon target can be successfully fabricated. In any event, cryogenic cooling would be required to use the silicon target for the typical exposure times on the AOS. Without cooling, the silicon intensified tube is still a good candidate as a quick-look sensor.

5.2.2 Electronographic Cameras

The concept of the electronographic camera originated in 1936 by A. Lallemand at the Paris Observatory.[2] His first experimental models were very awkward to use, but they verified the soundness of the concept and provided sufficient data to reveal the great potential of this method for recording astronomical phenomena. Since then, improved versions of the device have been made by Lallemand and by other workers in France, England and the U.S.[3-9]

Increased use was held back by the operational difficulties inherent in these devices. A major step forward several years ago was the introduction by Kron[3,4] of a high-vacuum valve to prevent contamination of the photocathode by volatile emulsion components. Lallemand and most others in the field[6] now use magnetic focusing to escape the limitations on resolution, uniformity and format size which characterized earlier designs. Liquid helium cooling is also proving to be a boon, making it much easier to work with the more delicate photocathodes. This allows a drastic reduction in preparation time and the vacuum is maintained for long periods of time by cryogenic pumping. Residual oxygen is completely suppressed by cryogenic pumping. Liquid helium cooling brings with it the capability of using a superconducting solenoid to provide the focus field. A more intense magnetic field can be obtained with much less weight than when a conventional solenoid is used. The magnetic electron lens itself can have a resolving power of several hundred line pairs per millimeter. The obtainable resolution is then determined by the nuclear emulsion itself in most cases. (Some extremely fine-grained holographic emulsions can resolve several thousand line pairs per millimeter, however.)

The ultimate in operational simplicity is achieved when the electronographic concept is applied in the ultraviolet region from 1000-2000 Å where alkali halide photocathodes such as CsI and KBr can be used. Along with extremely good rejection of visible wavelength flux, the materials can be exposed to dry air without damage. Therefore, neither vacuum operation nor cooling is required in an electronographic camera using these photoemitters. Carruthers at NRL has taken advantage of these qualities and has developed electronic cameras for far-ultraviolet imagery and spectrography. By combining the photon and electron optics into one integral design, he has made it possible to use front-surface (opaque) photocathodes. Figure 5-2 illustrates the resultant substantial gain in quantum efficiency over the semi-transparent layers more commonly used in photoelectronic imaging devices. Figure 5-3 is a sketch of an electronographic Schmidt camera which illustrates Carruther's design approach.

The spherical mirror is integral with the electron-optics and serves as an electrode. The photon image is formed on the opaque photocathode. The photoelectrons are focused by an external magnet and converge on the electron-sensitive emulsion located slightly behind the mirror. Since the photocathode requires no window, the only transmission loss is that due to the corrector plate. The material used for the corrector is chosen to provide the desired lower limit on the effective bandpass of the system. The upper wavelength limit is set by the choice of photocathode material. Figure 5-4 illustrates the variety of spectral characteristics Carruthers achieves. The ordinate represents the product of quantum yield, corrector-plate transmission and mirror reflectance. (The latter is assumed to be a constant at 70 percent above 1050 Å.)

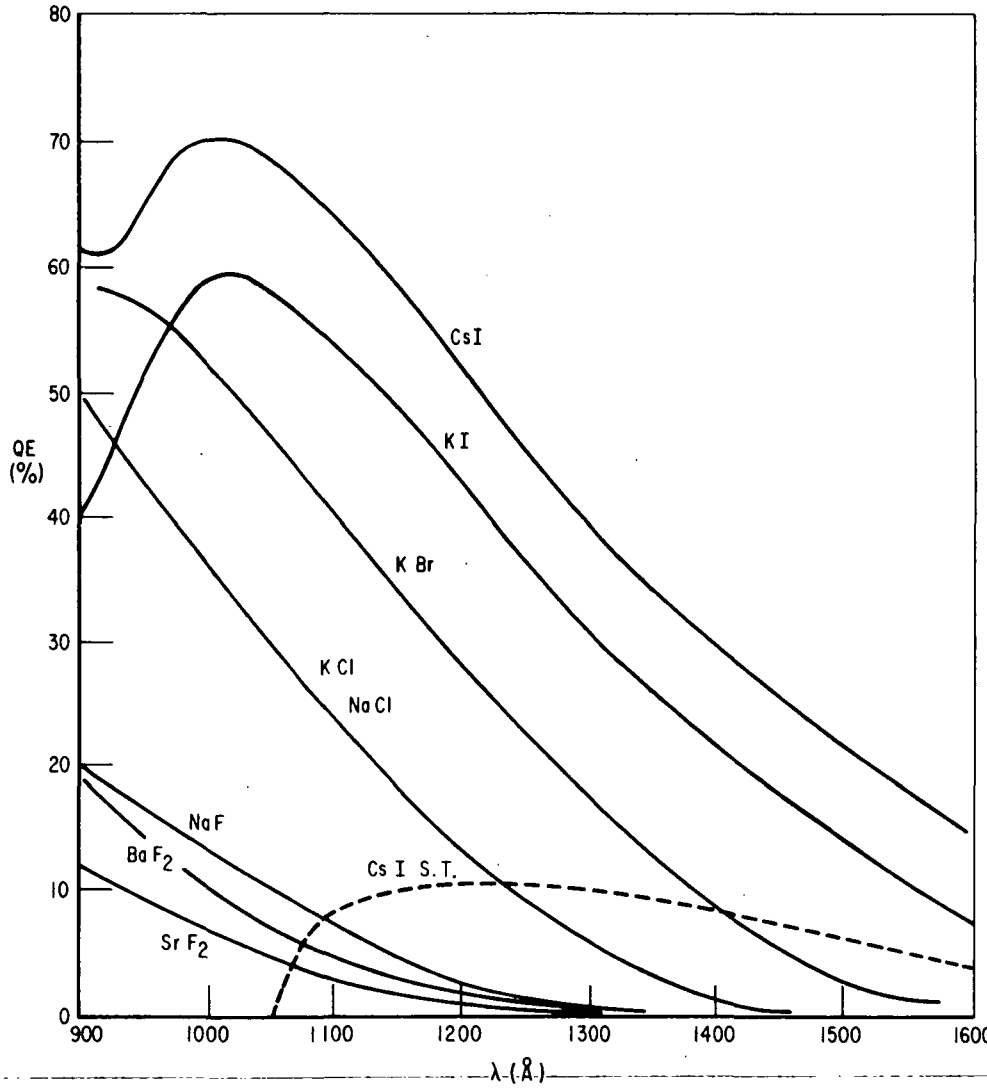

Figure 5-2 Efficiency Gain of Front-Surface Over Semi-Transparent Photocathodes

The barrier membrane shown in Figure 5-3 is an optional feature to prevent fogging of the emulsion when the camera is used under conditions of high incident flux in the visible part of the spectrum, such as daylight operation. It consists of thin aluminum films on plastic and is essentially transparent to 25 kV electrons.

The overall resolution obtainable is limited by the Schmidt optics rather than the electron optics, but the curved photocathode does introduce a noticeable center-to-edge fall-off in resolution.

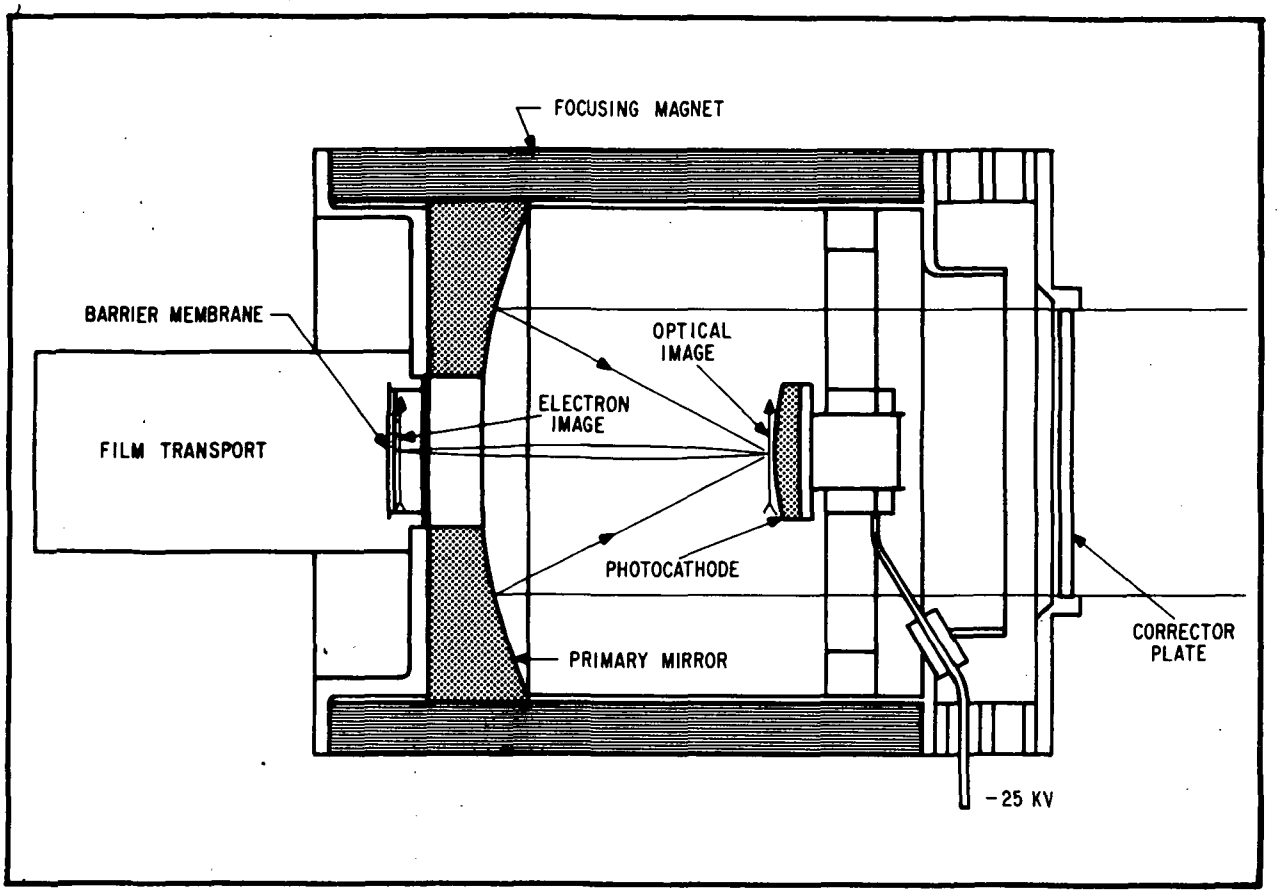

Figure 5-3 Schmidt Electronographic Camera

5.2.3 Electronographic Camera Performance

The performance which can be achieved with electronographic cameras in general has been well documented, by both laboratory testing and actual observatory use.[4-16] The references contain all the details; therefore, only some of the results are given briefly here.

Grain counts made at Lick Observatory[4] shown in Figure 5-5, illustrate one of the advantages of electronography over conventional photography. Ilford nuclear emulsions L4 and G5 are compared to baked Kodak IIa-O. It is seen that for any picture element size, the L4 emulsion contains a great deal (10X) more information than IIa-O on the basis of grain count alone. An example

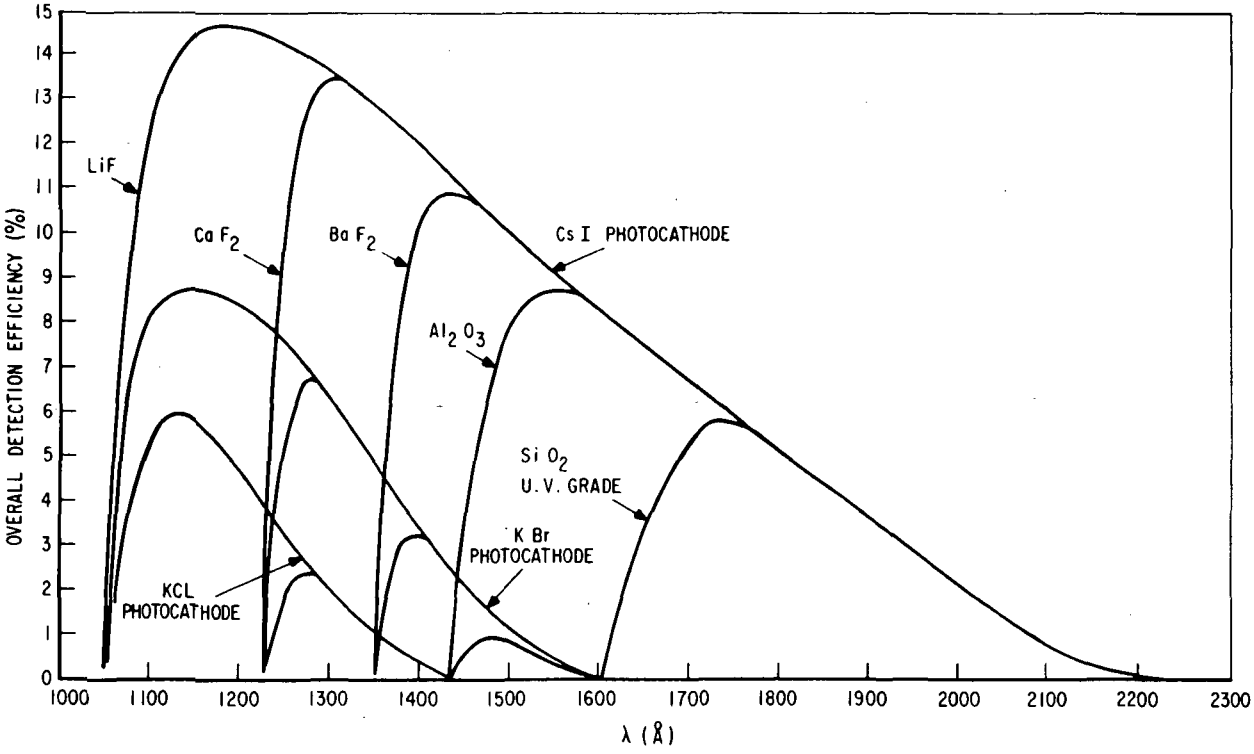

Figure 5-4 Spectral Characteristics of Various Photocathodes

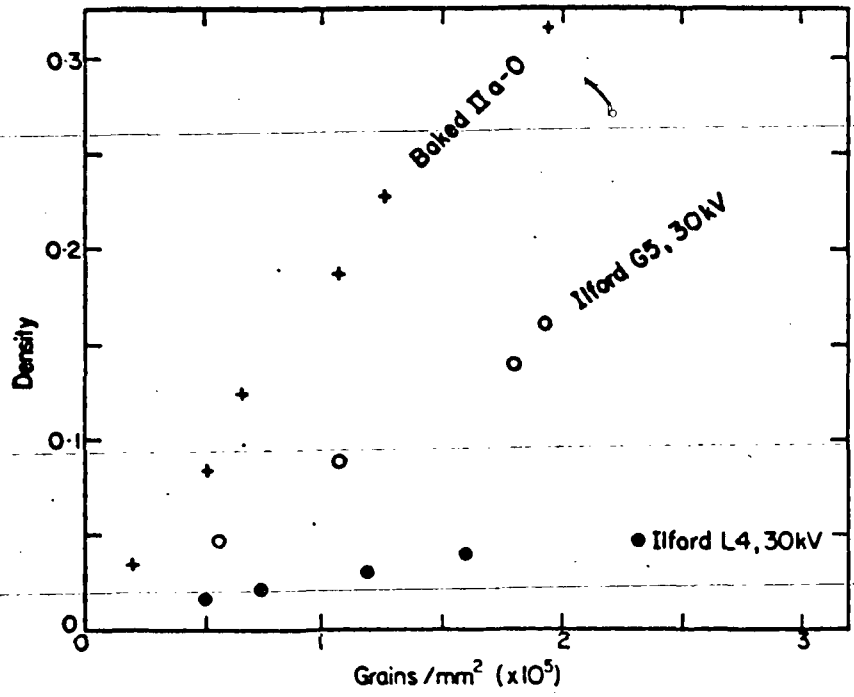

Figure 5-5 Grain Counts for Photography and Electronography

of the linearity of the density versus exposure transfer characteristics is given in Figure 5-6, from Kron. It is seen that the linear density range for L4 is several times greater than that of the photographic emulsion. Taking the data from Figures 5-5 and 5-6 together shows that the total storage capacity under linear conditions is 30 to 40 times greater for L4 than for IIa-0 emulsions.

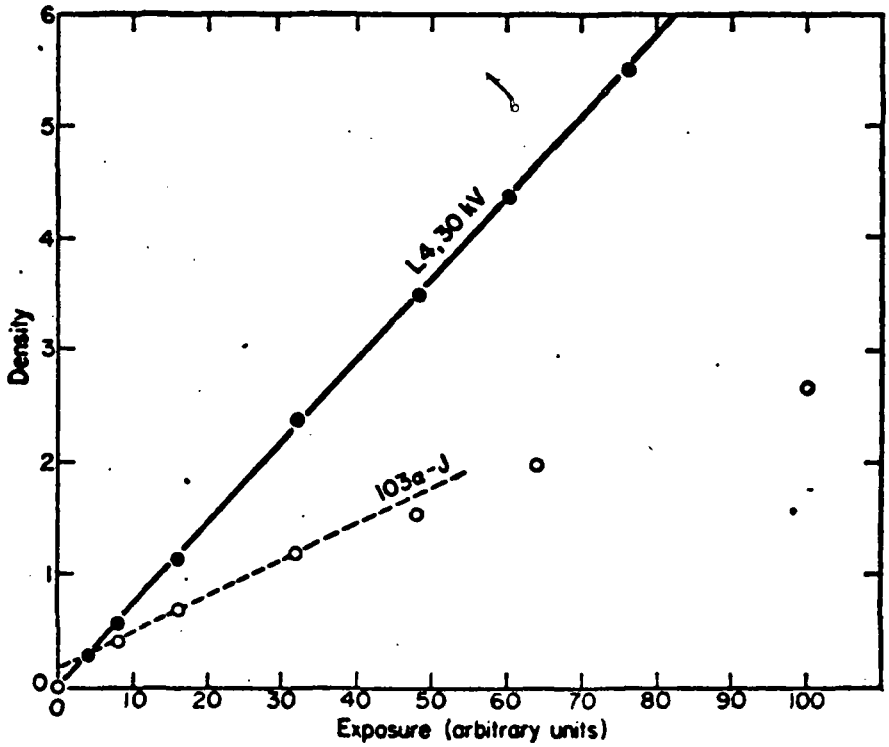

Figure 5-6 Plot of Density Versus Exposure for Photography (103a-J) and Electronography (L4, 30 kV)

Additional measurements of information gain over photography were made using the 61-inch Navy astrometric reflector and the 200-inch Hale telescope. Figure 5-7 shows the resultant information gain which takes into account both the signal and the noise of the density-image on photographic and electronographic plates. These and many other measurements all tend to indicate information gains from 30 to 100 over photography.

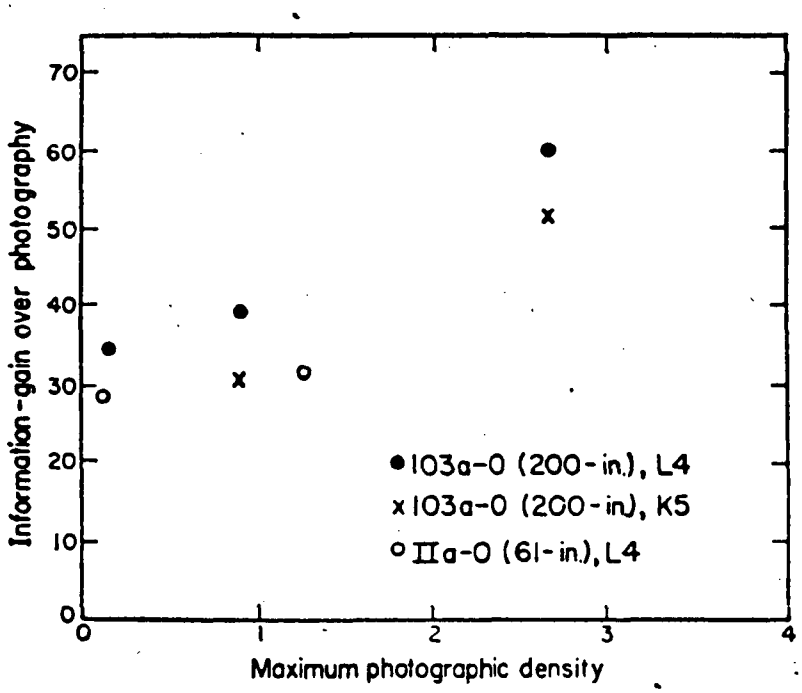

Figure 5-7 Measurements of Information-Gain in Blue Light of the Electronic Camera Over the Photographic Camera

Figure 5-8 is a rough qualitative illustration by Kron[11] of the effect of emulsion storage capacity. The IIa-O recording is a photograph while the L4 and E56 are electrographs. Much is lost in the reproductions, but it is obvious that both electronographic emulsions are far superior to the photograph, even though the latter actually has the widest spacing in the sky. Of the two electrographs, the one on Agfa 8E56 is clearly superior, as would be expected from its superior storage capacity over the Ilford L4.

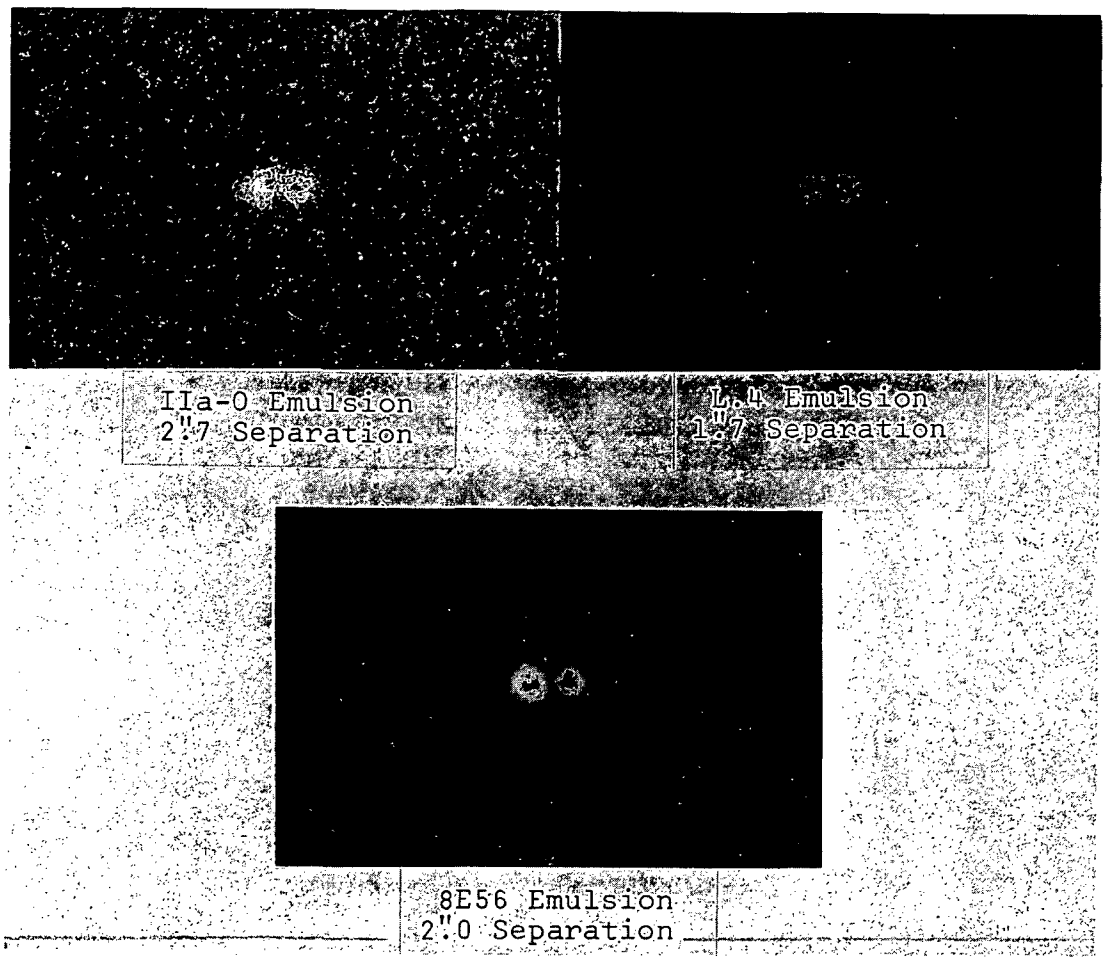

The recording on IIa-O emulsion is a photograph; the others are electrographs. The separations quoted are the actual separations in the sky in seconds of arc. The apparent separations have been rendered equal by scaling with the enlarger.

Figure 5-8 Recordings of Double-Star Images Slowing Effect of Using Larger and Larger Storage of Information

The table below gives the results of measurements made at the Flagstaff Station.

Emulsion	Grains/sq mm at Unit Density
Kodak IIa-O	0.6×10^6
Ilford G.5	1.3×10^6
Ilford L.4	5.4×10^6
Agfa 10 E 56	50×10^6
Kodak Q-166-10	50×10^6
Agfa 8E56	135×10^6
Kodak 649-O	500 (nonlinear)

The very large information gathering capability of the electronographic camera with emulsions like Agfa 8E56 (a holographic emulsion) suggests that spatial information may be gleaned by deconvolution of a recorded image with the telescope point spread function. The latter can be obtained by recording a star image. The deconvolution should make it possible to obtain much improved recordings of planetary detail, galactic nuclei, planetary nebulae, distant star clusters, and other difficult astronomical objects. A simple one-dimensional example of this, as accomplished by Kron[11], is shown in Figure 5-9.

The large linear range and low noise (fine grain) of electron sensitive emulsions make them highly desirable for stellar photometry and radiometry. The radiometric precision available has proved equal to that obtainable from careful photoelectric photometry of a single star. The electronographic camera can gather such data simultaneously on all stars in its field of view, however, resulting in a great saving in telescope time over photoelectric photometry. This has been shown by numerous measurements and comparisons. Figure 5-10 shows a plot made by Kron[4] using data extracted both ways. The average errors of both methods are about the same. The large linear dynamic range provides a capability for precise photometry of faint stars even when only a few arc-seconds away from a star 1000 times brighter[12].

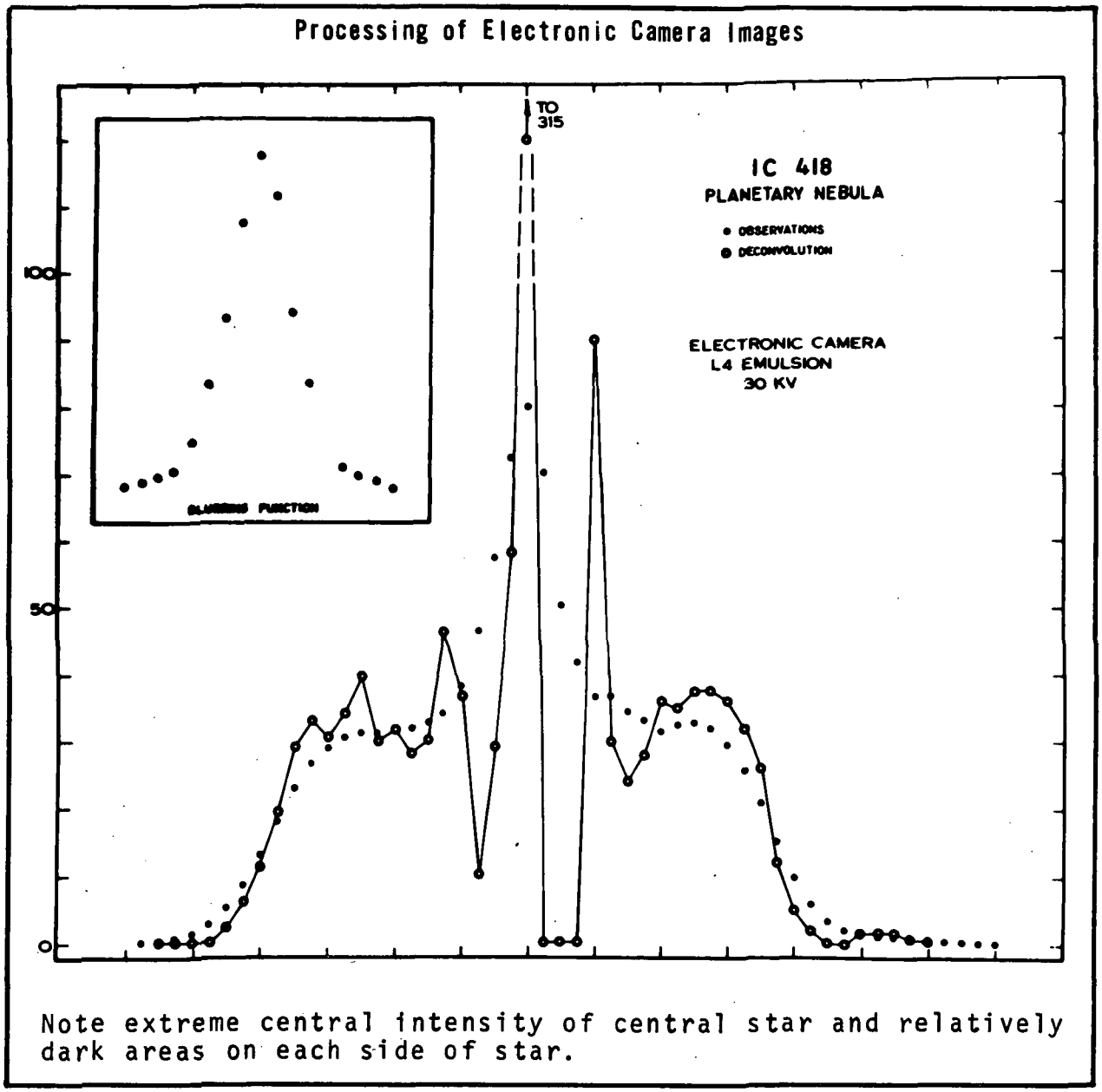

Figure 5-9 Deconvolution of an Electronic Camera Image of a Planetary Nebula

The increase in telescope time required by the photoelectric method would be by a factor roughly equal to the number of stars measured in the field of view. Figure 5-11 shows the results of another set of measurements comparing the two methods of making stellar measurements[11]. The photoelectric photometry was done with high precision by Kinman while the electronographic measurements were made by Ables.

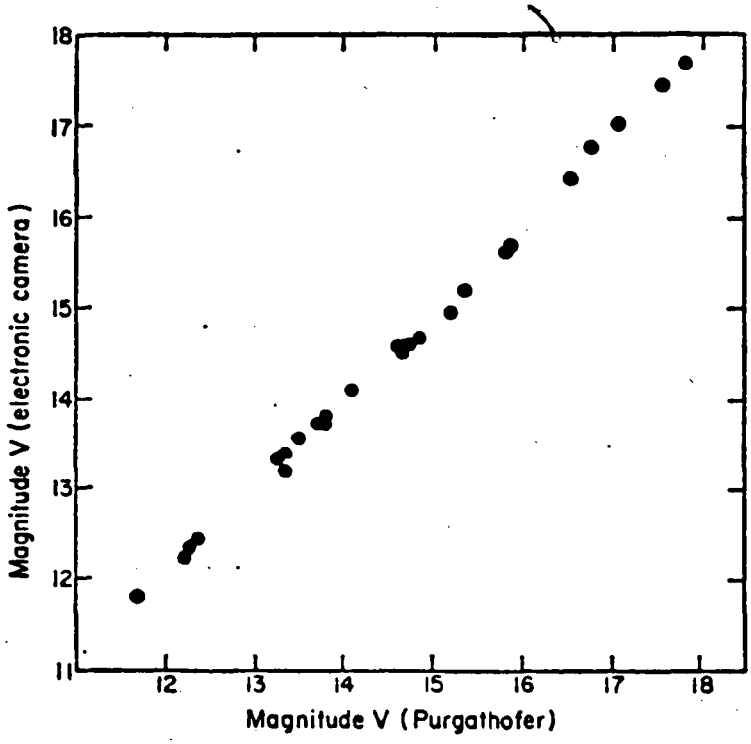

Figure 5-10 Electronic Camera Stellar Magnitudes (Selected Area 51) Plotted Against Photoelectric Stellar Magnitudes Measured by Purgathofer

The conclusion reached was that electronographic camera plates, when measured by an integrating densitometer, yield stellar magnitudes on the Pogson scale with the assumption of linear response, and that the experimental errors are comparable to those that accompany presently accepted methods of photometry. It was found easy to extend a magnitude sequence to a B magnitude of 23 on the basis of reasonable exposure times with the electronic camera and a 61-inch telescope. Other comparisons were made with limiting photoelectric stellar photometry by W. A. Baum on stars in the globular cluster M13. Baum carried photoelectric photometry to

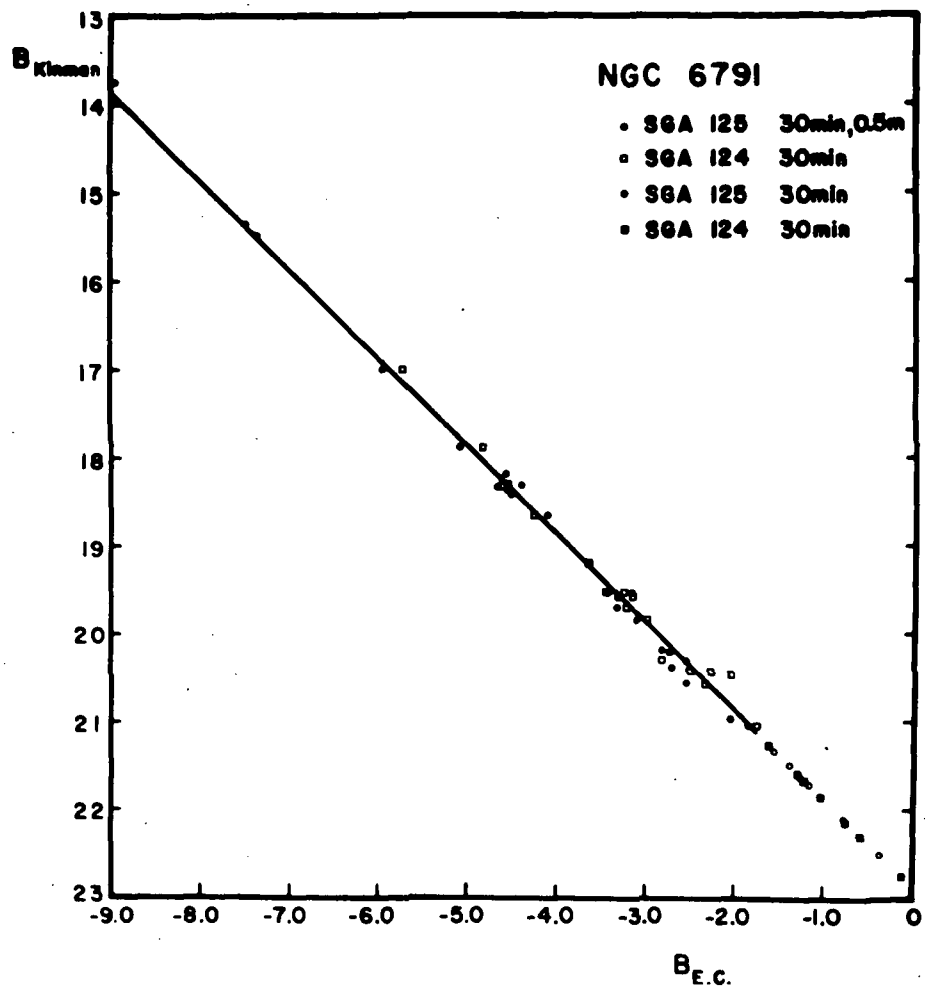

Figure 5-11 Stellar Magnitudes Determined with the Electronic Camera and Integrating Isodensitometer Compared With Photoelectric Magnitudes by Kinman

the faintest magnitudes that appeared to be at all practical with the 200-inch Hale reflector. Kron obtained an electronic camera plate of one-hour exposure with the 61-inch telescope of Baum's star field and found he could identify and measure all of the stars in Baum's sequence and extend it by another half magnitude. He was convinced that with excellent "seeing" conditions, he could extend the sequence to B = 24m.

5.2.4 The Meshless SEC Integrating Camera Tube

The sensor chosen for the AOS second detector is the newer, large format version of the SEC integrating camera tube which has been used and improved for several years by Lowrance and Zucchino[17,18] at Princeton, working with Westinghouse. In contrast with broadcast and night-vision types of SEC tubes, the astronomical version is all-magnetic. Both the image section and the readout section enjoy the advantages of magnetic focus and the deflection is also magnetic. The KCl targets for this application are thinner and exhibit a higher storage capacitance than ordinary SEC tubes. This results in better spatial frequency response and higher information capacity, comparing favorably with many fast photographic films. The removal of the suppressor mesh also improves spatial resolution and helps reduce preamplifier noise by reduction of the shunt capacitance at the target lead. The overall result is a capability of giving essentially photon-limited performance over a good working range. The flat image plane eliminates the need for fiber optics with the attendant resolution loss and the possibility of fixed pattern noise.

A sketch illustrating the simplicity of the tube and coil configuration is shown in Figure 5-12. The glass envelope of the image section has a diameter of 4 1/2 inches.

5.2.5 SEC Performance

A summary of some of the more important characteristics of the sensor is given in Table 5-2. Tables 5-3 and 5-4 list exposure times to just reach full target exposure for extended sources and for stars, both based on visual magnitudes and 1000 Å bandpass, centered at λ = 5500 Å.

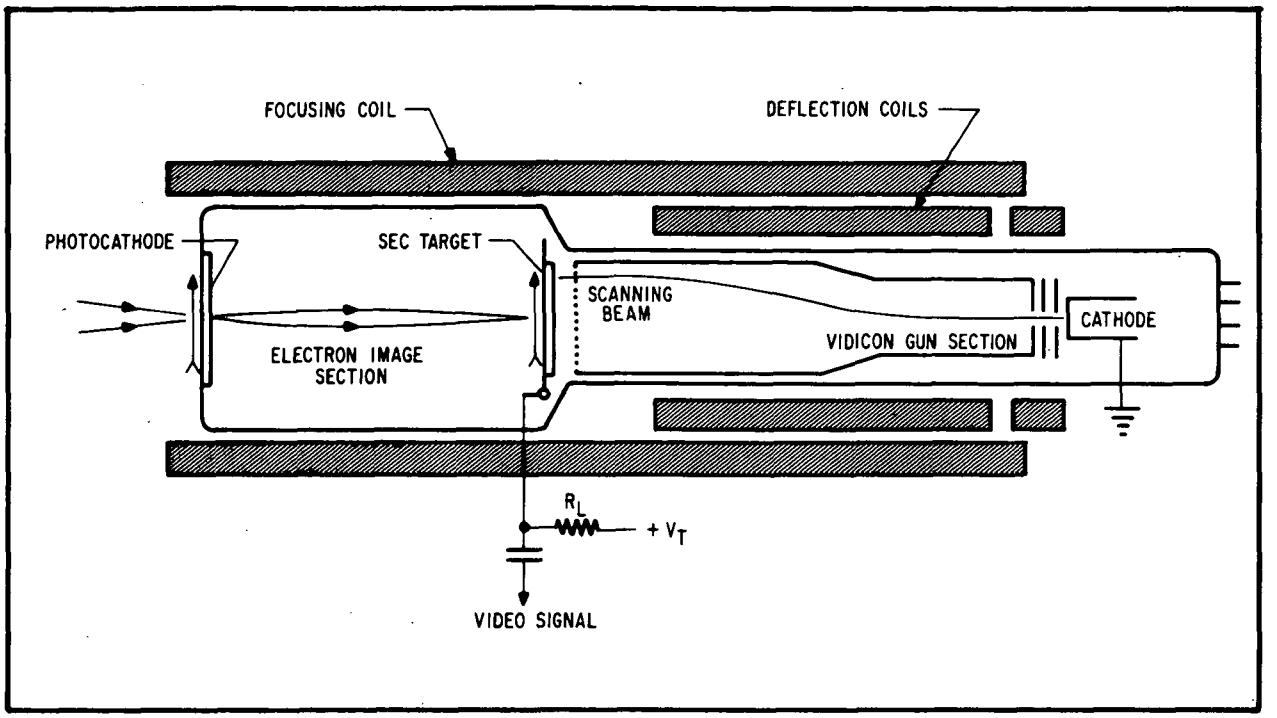

Figure 5-12 Meshless SEC Integrating Camera Tube

The SEC target in the chosen sensor is supported on a rugged frame which provides an active area 50 mm x 50 mm square. The useful image area at the photocathode is slightly larger than this. An MTF of 50 percent is achieved at 25 line pairs per millimeter. At this frequency, the 50 mm square target can accommodate 2500 x 2500 picture elements (half-cycles) or a total of 6.25×10^6 elements per frame.

The storage capacity is such that when operated with a target gain of 70, the target can store a charge equivalent to about 2.56×10^6 photoelectrons per square millimeter. (At higher values of charge density, the transfer characteristic saturates as shown in Figure 5-13. This amounts to 1025 photoelectrons for each 20 μm picture element (ν = 25 cycles/mm). The rms uncertainty in a single element is thus given by a σ of 3 percent. Computer summation of four adjacent picture elements would reduce the rms deviation to 1.5 percent, a trade-off of spatial resolution for radiometric precision.

Table 5-2

MESHLESS SEC INTEGRATING CAMERA TUBE SPECIFICATION

Spectral Sensitivity: Determined by photocathode quantum efficiency and window chosen

Image Diameter: ϕ = 70 mm (flat faceplate)

Useful Target Area: 50 mm x 50 mm

Photoelectron Storage Capacity: 2.56×10^6 photoelectrons/mm^2

Picture Element Storage:
- 20μ Pixel: 1025 photoelectrons, σ = 3.1%
- 25μ Pixel: 1600 photoelectrons, σ = 2.5%
- 50μ Pixel: 6400 photoelectrons, σ = 1.25%

Signal/Noise Ratio: See Figures 5-13 and 5-16

Dynamic Range:
- Extended Sources $>10^2$
- Point Sources $>10^4$

~~Integration Time: 24 hours~~

MTF:
- 10 line pair/mm (50μ Pixel): 0.90
- 20 line pair/mm (25μ Pixel): 0.60
- 25 line pair/mm (20μ Pixel): 0.50

Image Section - Magnetic Focus

Readout Section - Magnetic Focus and Deflection

Table 5-3

MESHLESS SEC CAMERA TUBE EXPOSURE TIMES FOR EXTENDED SOURCES
(Based on 1.1 x 10^6 photons/sec/cm^2 at m_V = 0)

Visual Magnitude per arc-sec^2	Exposure Time f/10, $\Delta\lambda$=1000Å λ=5500Å	Exposure Time f/25, $\Delta\lambda$=1000Å λ=5500Å
0	8 x 10^{-6} sec	5 x 10^{-5} sec
5	8 x 10^{-4} sec	5 x 10^{-3} sec
10	8 x 10^{-2} sec	0.5 sec
15	8 sec	50 sec
20	13 min	1.4 hr
25	22.2 hr	140 hr

ASSUMPTIONS: Diffraction Limited Telescope
Optical Transmission = 50%
Photocathode Quantum Efficiency = 20%

Table 5-4

MESHLESS SEC CAMERA TUBE EXPOSURE TIMES FOR STARS
(Based on 1.1 x 10^6 photons/sec/cm^2 at m_V = 0)

Visual Magnitude	Exposure Time f/10, $\Delta\lambda$=1000Å λ=5500Å	Exposure Time f/25, $\Delta\lambda$=1000Å λ=5500Å
0	1.8 x 10^{-7} sec	1.13 x 10^{-6} sec
5	1.8 x 10^{-5} sec	1.13 x 10^{-4} sec
10	1.8 x 10^{-3} sec	1.13 x 10^{-2} sec
15	1.8 x 10^{-1} sec	1.13 sec
20	1.8 x 10 sec	2 min
25	30 min	3.1 hr

ASSUMPTIONS: Diffraction Limited Telescope
Diameter = 1 Meter
Optical Transmission = 50%
Strehl Ratio = 0.6
Photocathode Quantum Efficiency = 20%

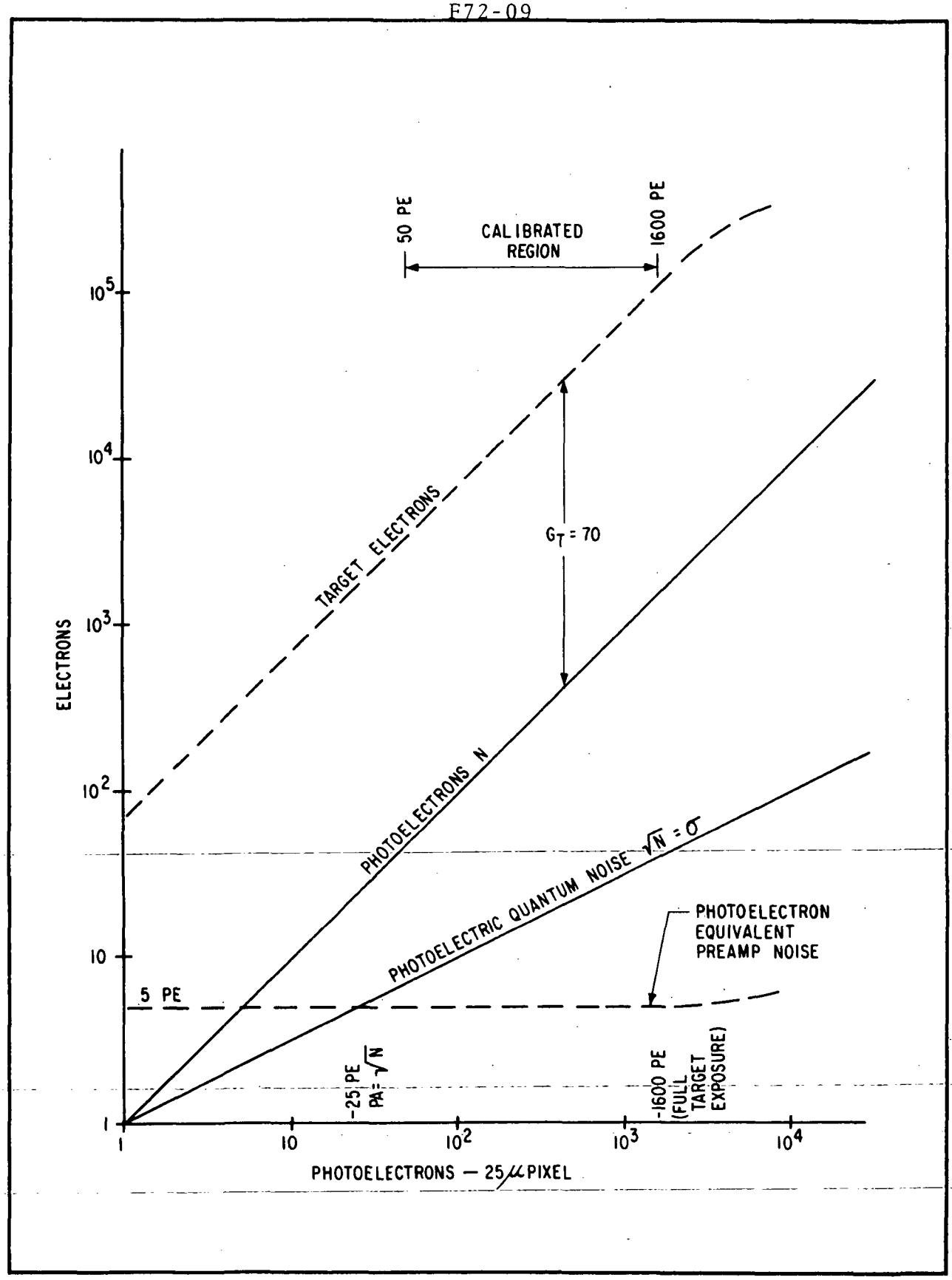

Figure 5-13 Meshless SEC Transfer Characteristic

The same improvement in precision can be achieved without sacrificing spatial resolution by computer summation of the individual 20 μm elements after four successive full exposures, a trade-off of time for accuracy.

The above numbers are based on "photon noise" alone, assuming that other sources of noise such as that due to the preamplifier, beam-switching, tube background, signal processing, interference, etc. are held well below the quantum noise. Figure 5-14 from Lowrance and Zucchino illustrates the validity of this assumption as far as sources in the sensor itself and the preamplifier are concerned. Very careful system design is of course necessary to preserve this precision in the final output data. Since the presentation in Figure 5-14 is given in terms of primary photoelectrons, the equivalent preamplifier noise is seen to effectively increase as the sensor MTF falls off above 10 cycles per mm.

The above data are used in Figure 5-15 to compute the resultant sensor signal/noise ratio at full exposure as a function of spatial frequency. Figure 5-15 also shows the degradation of signal-to-noise ratio resulting from object contrasts of 20 percent, 10 percent and five percent (where $C = (N_{max}-N_{min})/N_{max}$). Stars would have essentially 100 percent contrast but distributed sources such as nebulae and weak absorption lines in a background continuum from a spectrophotometer can exhibit much lower contrast. The dashed lines illustrate the performance expectation for an ideal quantum noise-limited detector. The curves show that for any object contrast the meshless SEC at full exposure performs like an ideal detector below 20-25 cycles per mm. Above that frequency, preamplifier noise, etc. begin to intrude on the ideal result. Figure 5-16 shows the performance degradation resulting from the target receiving only 10 percent and 1 percent of full exposure, assuming 100 percent object contrast. It is clear that departure

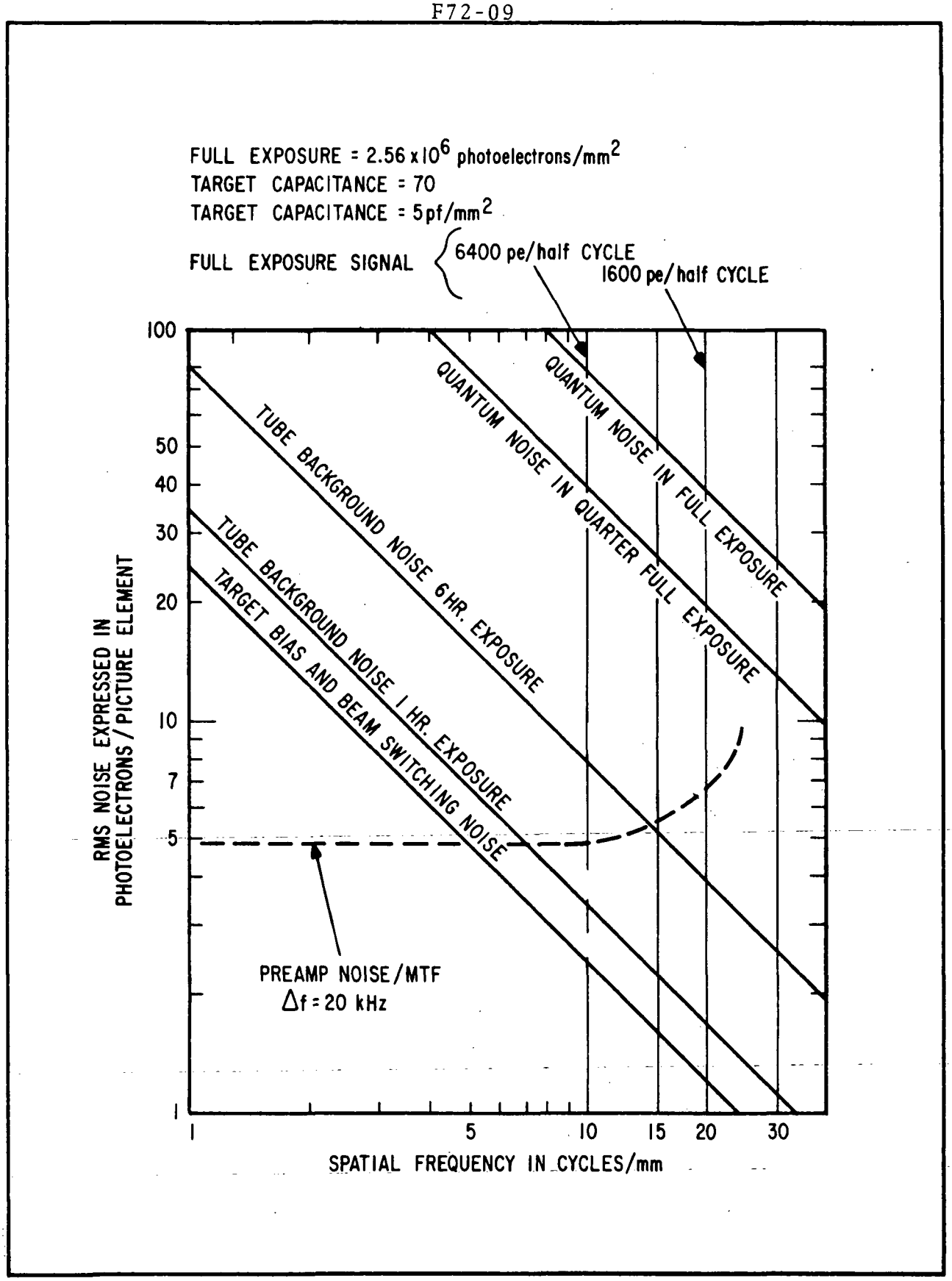

Figure 5-14 RMS Noise Versus Spatial Frequency, Meshless SEC

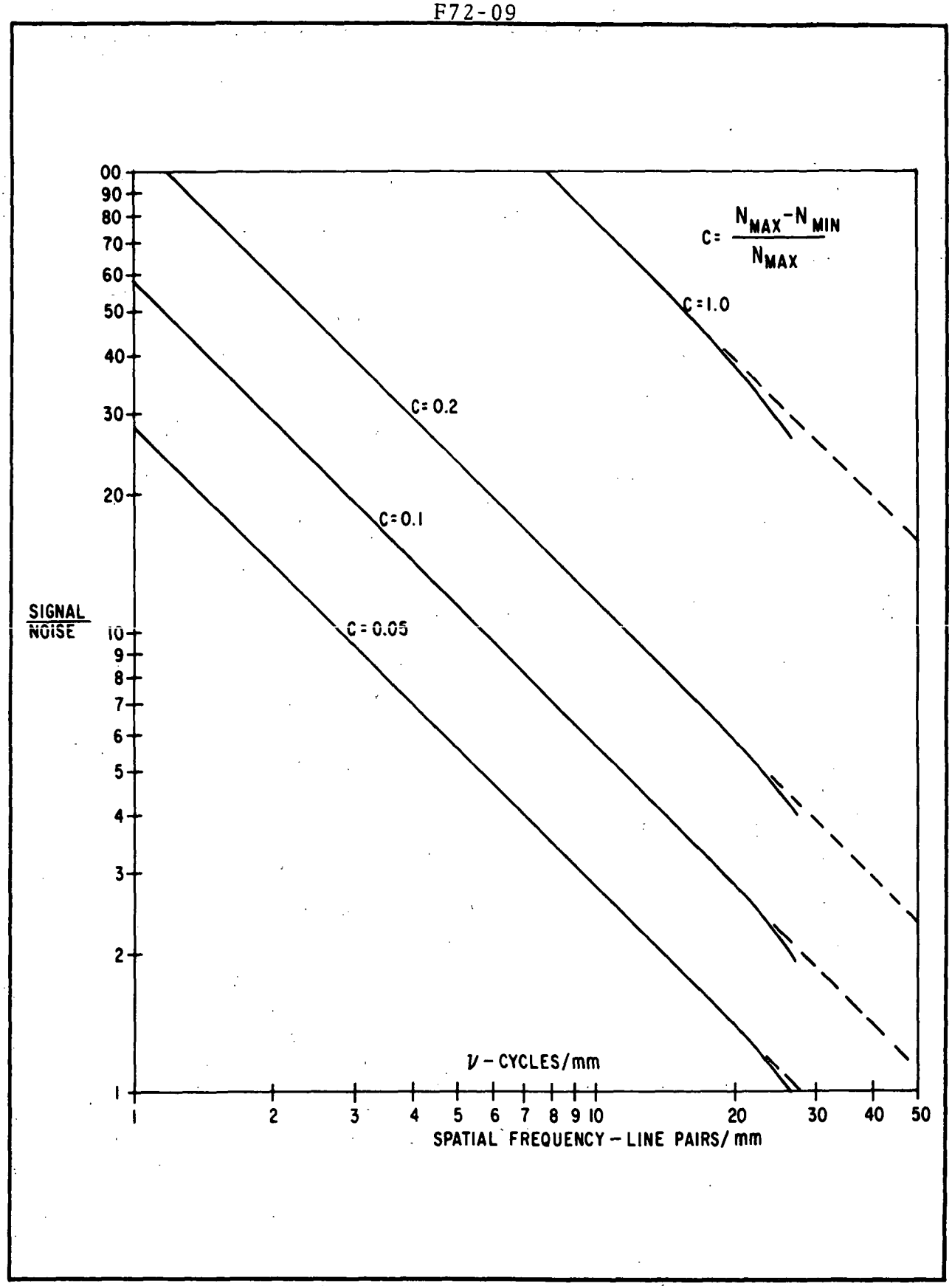

Figure 5-15 Signal-to-Noise Ratio at Full Exposure-Meshless SEC

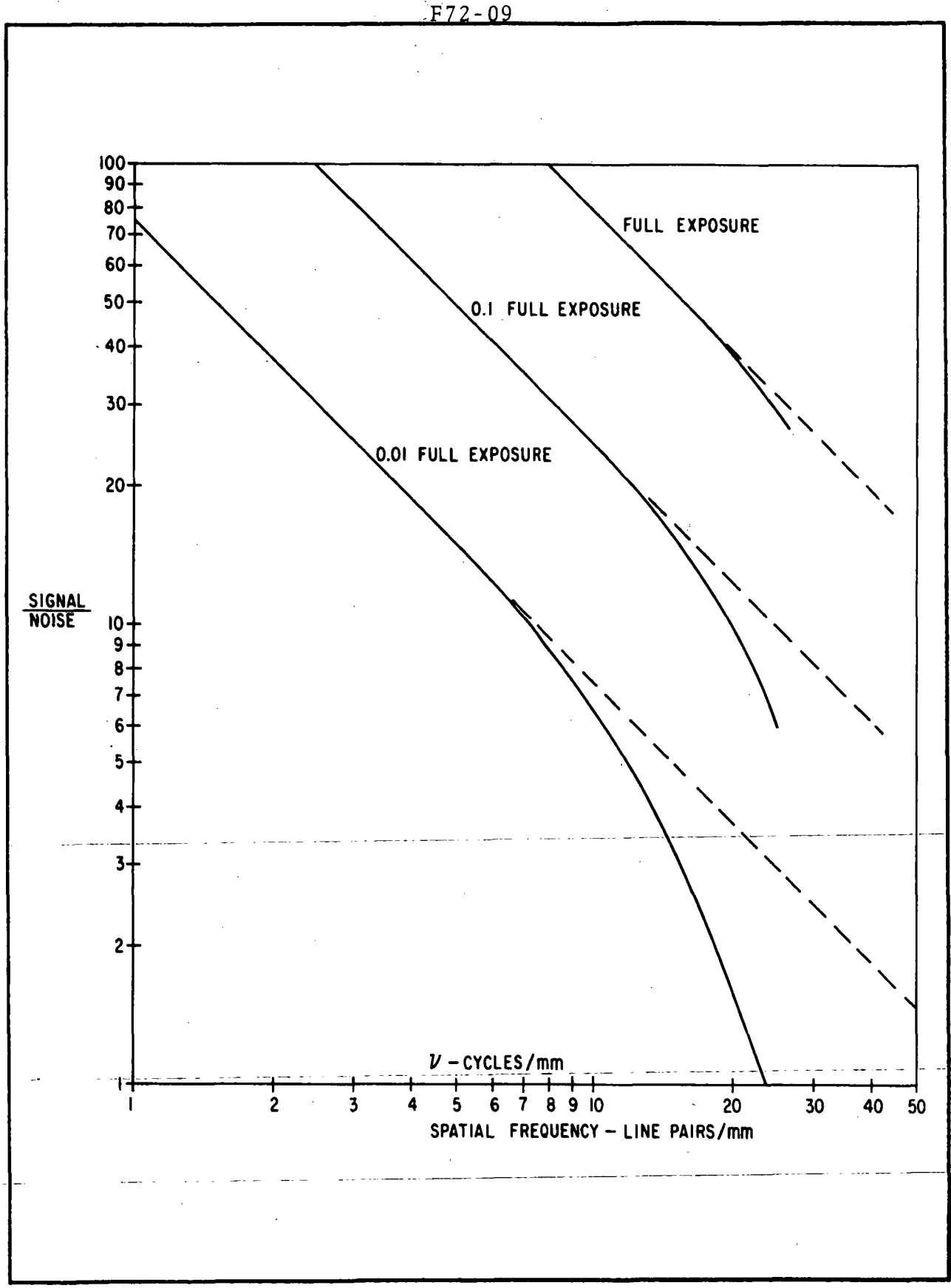

Figure 5-16 Signal-to-Noise Ratio at 10 Percent and 1 Percent Exposure, Meshless SEC

from ideal response becomes more and more marked as exposure is reduced. For example, at 1/10 of full exposure, preamplifier noise becomes about equal to the quantum noise in the signal at 25 line pairs per mm.

For quick-look usage, a reasonable loss in quality is not necessarily harmful and probably would be more than offset by the time saved. When primary data is being gathered, however, whether of imagery or spectra, a full exposure should be taken whenever possible.

The data involved in computing the curves of Figures 5-15 and 5-16 can also be used in the computation of a modulation detectability curve. This is the aerial image modulation required (at the sensor focal plane) to yield a specified probability of detection, plotted as a function spatial frequency. A high probability of detection results, for example, by using the criterion that a signal-to-noise ratio of 5 be achieved. The resulting modulation demand functions for the meshless SEC at full exposure are plotted as dashed lines on Figures 5-17 through 5-20. This function is very useful in system analysis as it makes possible simple graphical solutions of the overall performance of sensor plus telescope optics, pointing accuracy, etc. The intersection of the MTF curve of the optical system (including pointing) with the sensor modulation detectability curve indicates the highest spatial frequency at which the entire system can satisfy a particular detectability criterion. This is illustrated in Figures 5-17 through 5-20 for a diffraction-limited telescope having an obscuration $\varepsilon \doteq 0.45$. Figures 5-17 and 5-18 represent the f/25 telescope while Figures 5-19 and 5-20 are for the f/10. Figures 5-17 and 5-19 are computed at λ = 2000 Å while Figures 5-18 and 5-20 are computed at λ = 4000 Å. Curves are also included to illustrate the degradation due to several Gaussian rms pointing errors. A second set of curves is given in each figure to illustrate the effect of a reduced object contrast of 10 percent on system performance.

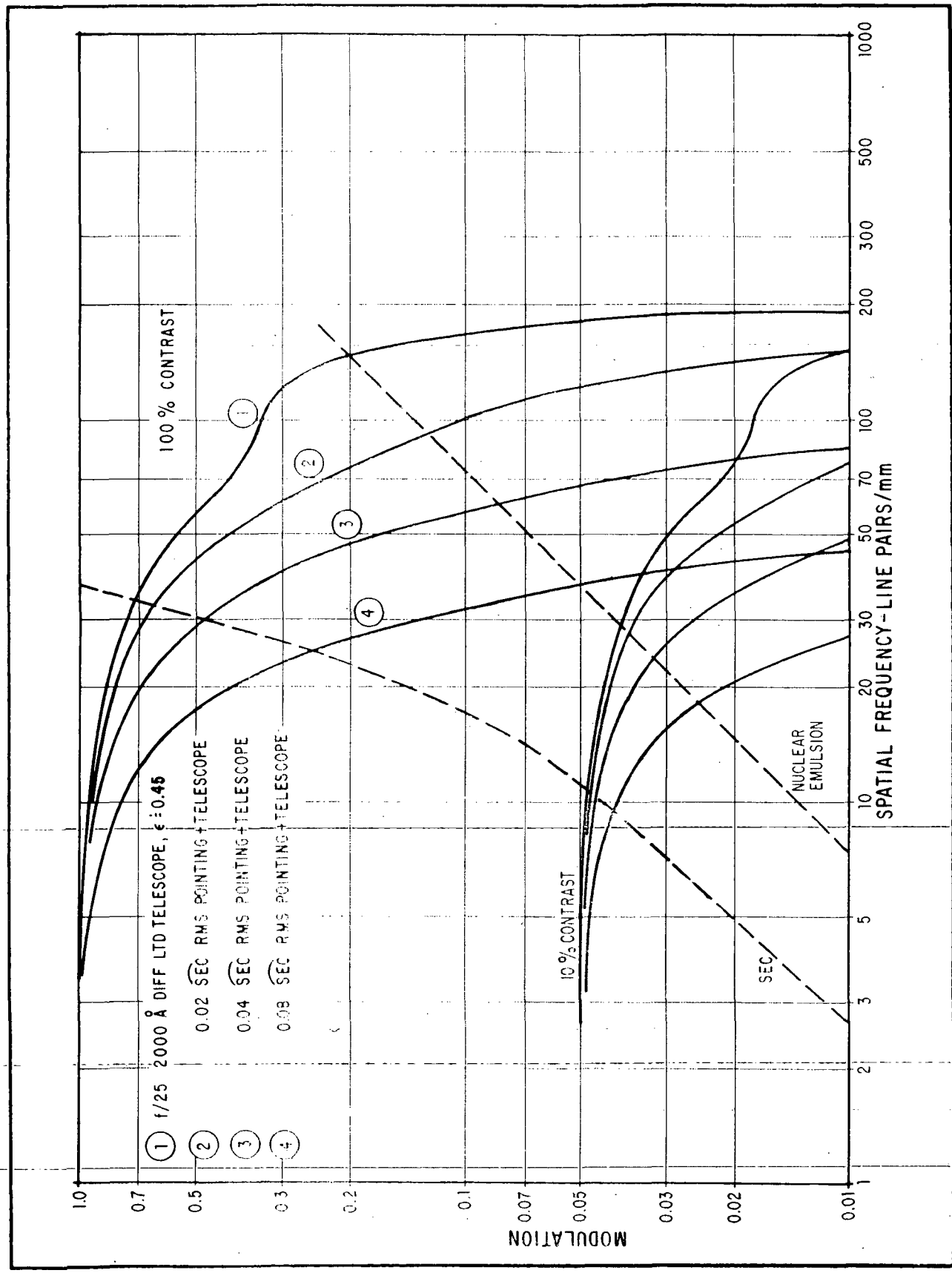

Figure 5-17 Modulation Detectability, λ=2000Å, Meshless SEC with f/25 Telescope

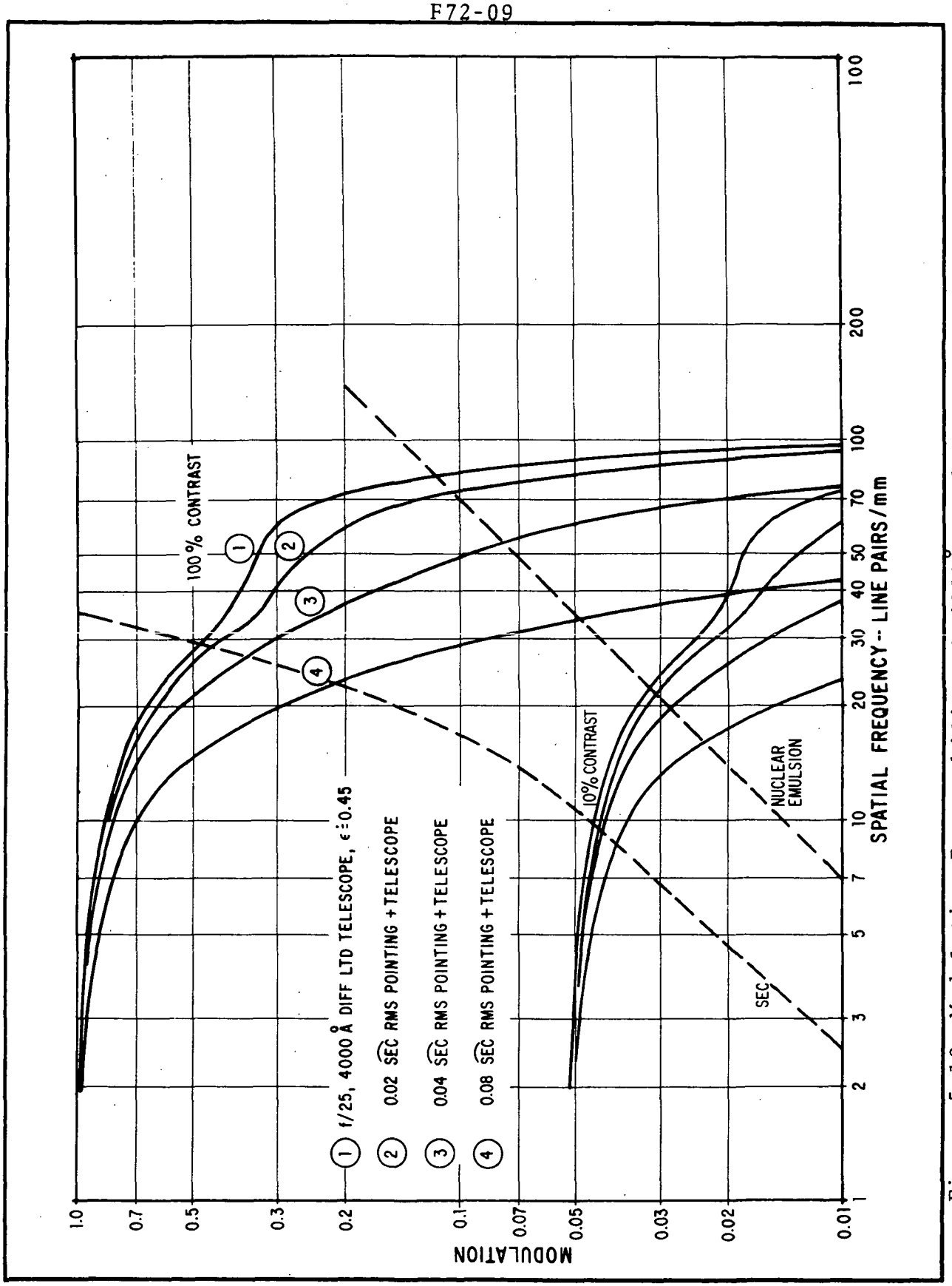

Figure 5-18 Modulation Detectability, λ=4000Å, Meshless SEC with f/25 Telescope

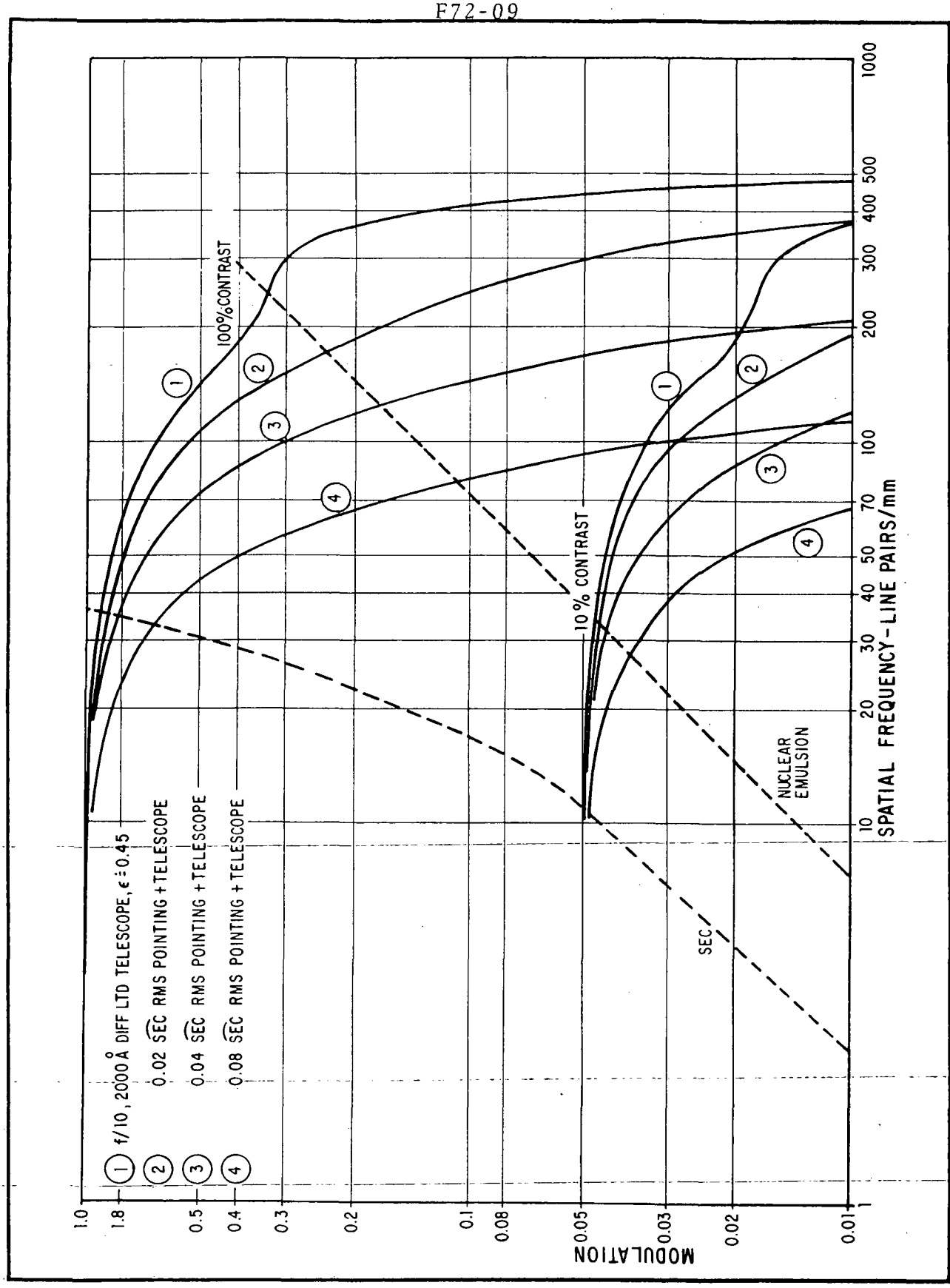

Figure 5-19 Modulation Detectability, λ=2000Å, Meshless SEC with f/10 Telescope

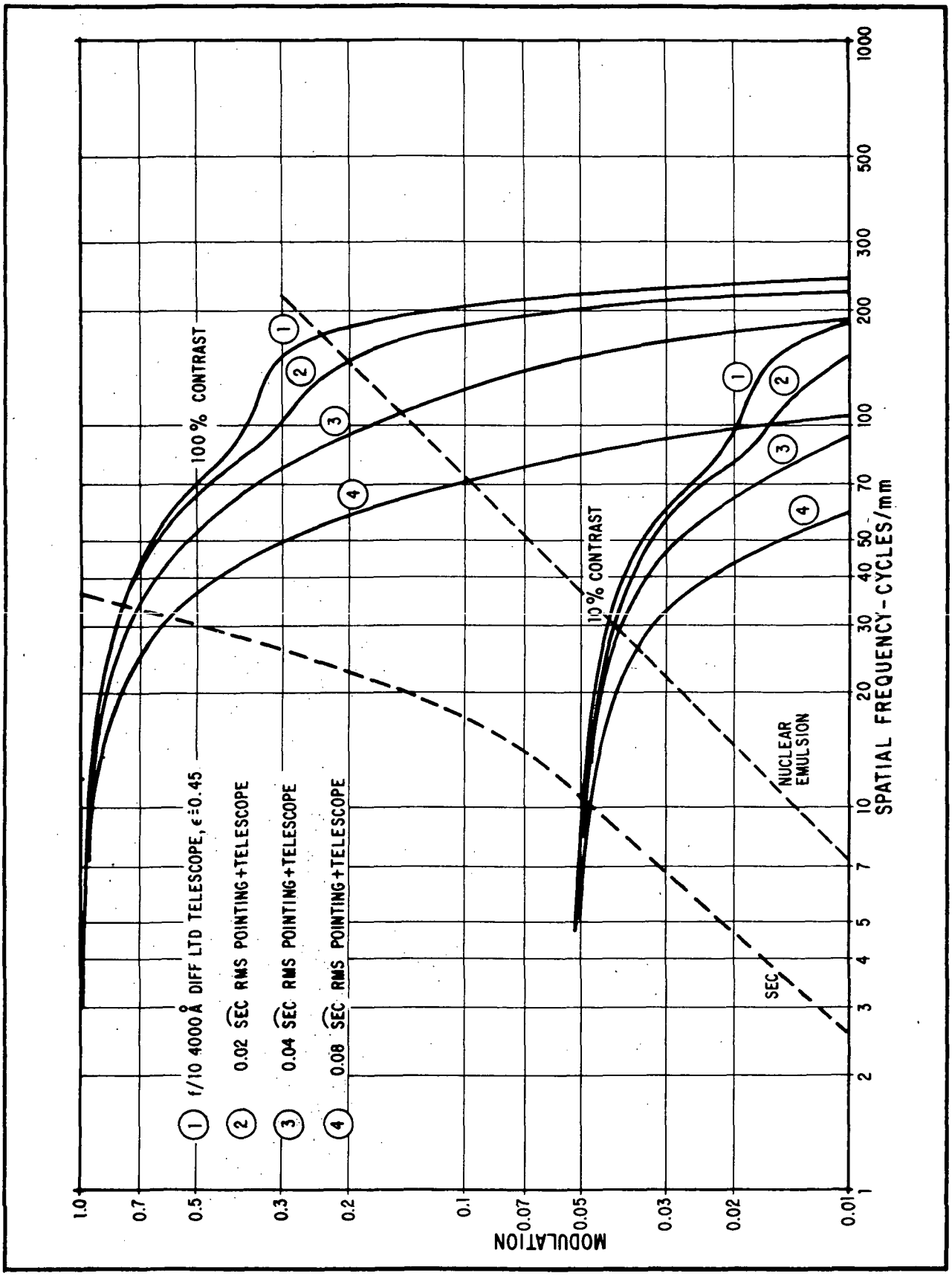

Figure 5-20 Modulation Detectability, λ=4000Å, Meshless SEC with f/10 Telescope

A second modulation detectability function labeled "nuclear emulsion" is drawn to the right of the one for the SEC tube on the above figures. It was placed to represent a high resolution, fine grain emulsion (such as L4 or 8E56) which has been given ten times the exposure required to fill the SEC target. The system performance is obviously improved. The curve for the electronographic emulsion can be translated still further to the right by increasing the exposure even more. For a given available flux, the time required for exposure must be increased as the square of the spatial frequency ratio in translation of the modulation detectability curve (under photon-limited and non-MTF limited conditions).

The sensor development which has been proceeding for some time by Lowrance, Zucchino, et al, at Princeton, has included a continuing program of actual use of these sensors for the collection of scientific data at various observatories around the country. These observations are continuing at the Princeton Observatory as well as those on Mt. Palomar, Mt. Wilson, Kitt Peak and other observatories.[18,19] The experience gained in performing these ground-based observations has led to sensor improvements as well as better insight into data handling methods, etc. Presently, an imaging system using the meshless SEC sensor is being built for a sounding rocket payload by Princeton Observatory. As shown in Figure 5-21, this camera records the spectra from an objective grating echelle spectrograph covering the spectral region from 1150 Å to 1800 Å with $\lambda/\Delta\lambda$ of 10^4.

A few excerpts of ground-based results obtained more than a year ago are shown in the figures. One of the most notable achievements[19] has been the observations of very faint quasi-stellar objects and galaxies at high dispersion on the 200-inch Hale telescope's Coudé spectrograph. Spectra of the radio quiet quasar PHL 957 (V-16.5 mag) were obtained from 4270 to 4495 Å with 0.75 Å resolution in a six hour exposure. Thirty-one absorption lines were recorded and several of the lines were resolved and reached zero central intensity. Figure 5-22 shows the unwidened Coudé spectrum of PHL 957 obtained

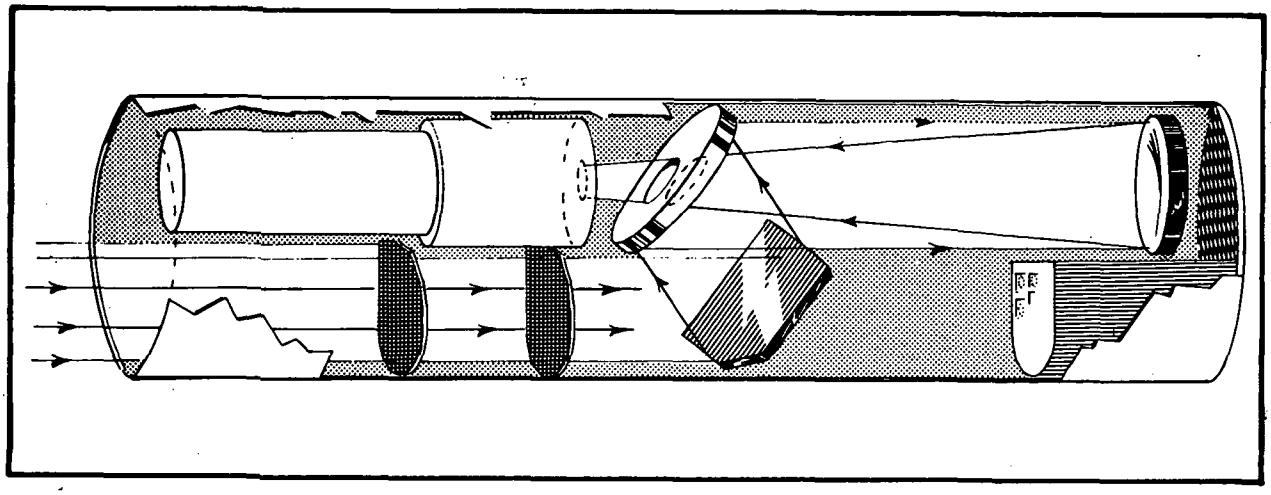

Figure 5-21 UV Echelle Spectrograph-TV Payload for Sounding Rocket

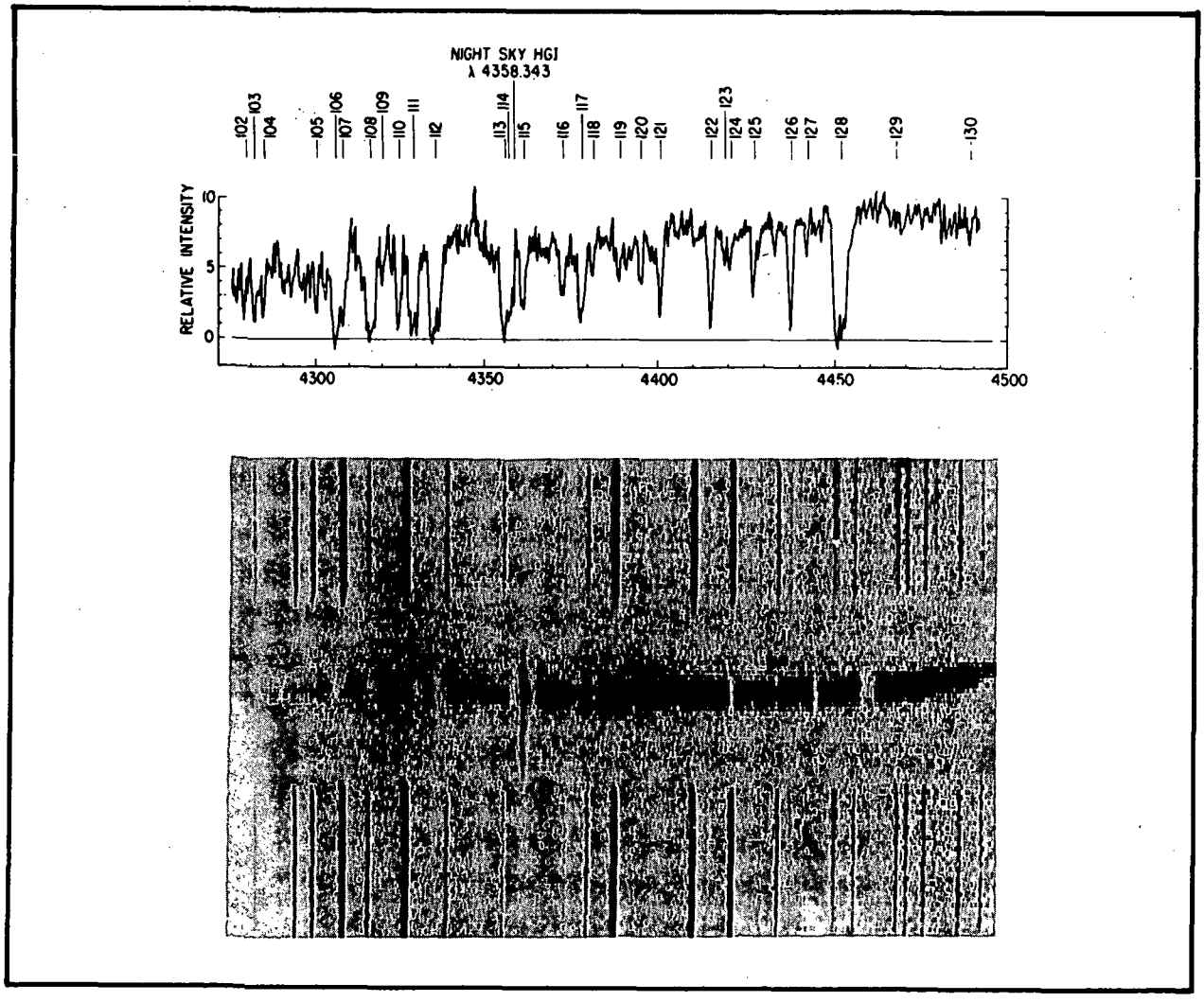

Figure 5-22 Spectrum of the Quasar PHL-957, Obtained with Princeton Integrating TV System on Hale 200" Coude Spectrograph

on October 9, 1970 in a six-hour exposure with the integrating television camera using the SEC-vidicon, WX-31718. The horizontal lines are the television scan lines, and the smallest rectangles on each line are the digital picture elements whose width corresponds to one-third the net resolution of 0.75 Å. The vertical scale has been magnified 4.5 times relative to the horizontal scale. The comparison spectrum is an iron arc and the emission line crossing the spectrum left of center is 4358.3 Å line of HgI in the night sky. The intensity trace of the same spectrum is also shown in Figure 5-22.

The imaging system has been used with a half-meter Ebert-Fastie spectrograph for high dispersion spectrographic observations. The output is magnified by 2.25:1 resulting in a dispersion of 3.5 Å/mm at the photocathode. Figure 5-23 shows the spectrum of two stars, λ Hya (M_V = 3.62) and γ Tau (M_V = 3.66) taken in 15 minute exposures on the Princeton 36-inch reflector during the winter. The Mt. Wilson 60-inch has also been used for high dispersion spectroscopy.

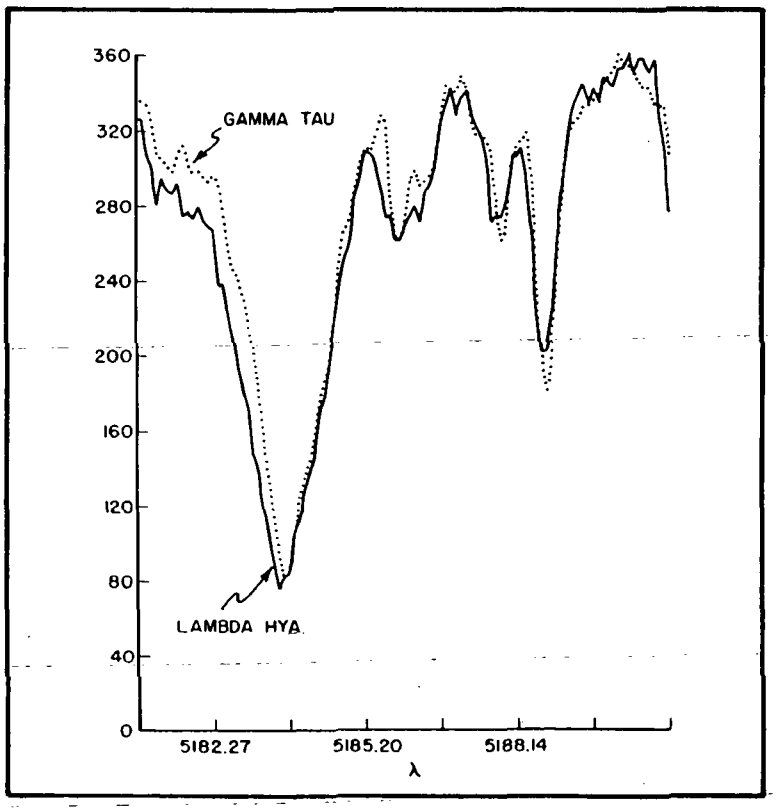

Figure 5-23 Spectra of Lambda Hya and Gamma Tau, 15-Minute Exposure on 36-Inch Princeton Telescope with TV System

The imaging system has been used at Princeton and Kitt Peak by P. Crane of Princeton to do photometry of galaxies.

Figure 5-24 shows an image of the galaxy NGC 3842 obtained on the Kitt Peak 36-inch reflector. An advantage of the television system for this work is the fact that the data is recorded on magnetic tape and can, therefore, be easily analyzed by computer as shown by the equal brightness contours in Figure 5-25 of the double galaxy, NGC 3845.

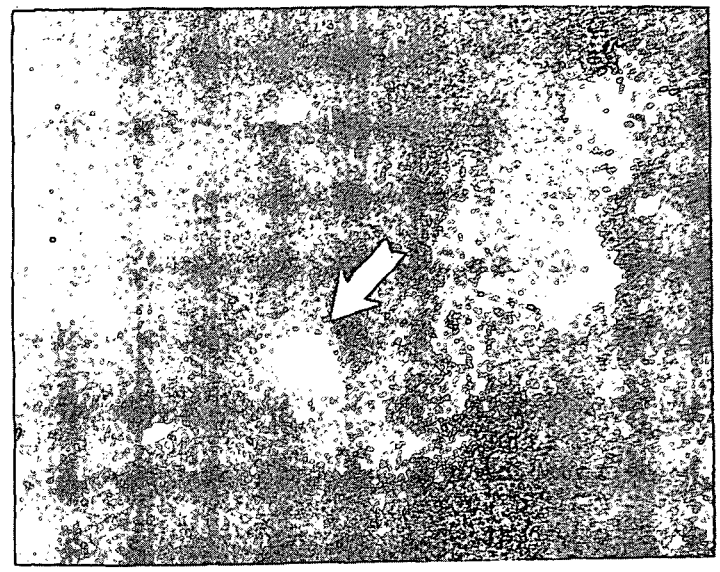

Figure 5-24 Galaxy NGC 3842 Taken with Princeton Integrating TV on Kitt Peak 36-Inch Telescope, 2.5 Minute Exposure at f/13.5

5.3 DETECTOR OUTPUT FORMAT

5.3.1 Electronographic Camera

The output of the electronographic camera is formed on certain silver halide emulsions as chosen from a trade-off considering speed, granularity, information capacity, etc. as demanded for each specific scientific requirement. The electron image is developed by chemical processing of the film as in ordinary photographic astronomy. Meaningful radiometry requires that the processing be carried out under carefully controlled conditions. Thus, it is presumed that all plates or film containing primary data will be returned to the ground for optimum processing.

Quick-look type exposures with fast, coarse film for test purposes could, of course, be developed on board, but this would require only minimal darkroom facility.

Full retrieval of all scientific data from the ground-processed electrographs will require careful scanning of the finished negatives by a precision microdensitometer or integrating isodensitometer followed by computer analysis such as described by Kron. This yields the volume under each three-dimensional density solid representing a star image on the electrograph (after subtraction of the background level). If desired, this can be followed by one or two-dimensional deconvolution using the telescope point spread function (a trade-off of radiometric information for spatial information). In any case, the image analyzing and restoration techniques are applied only after the exposed plates have been returned from the AOS and processed at a ground-based laboratory.

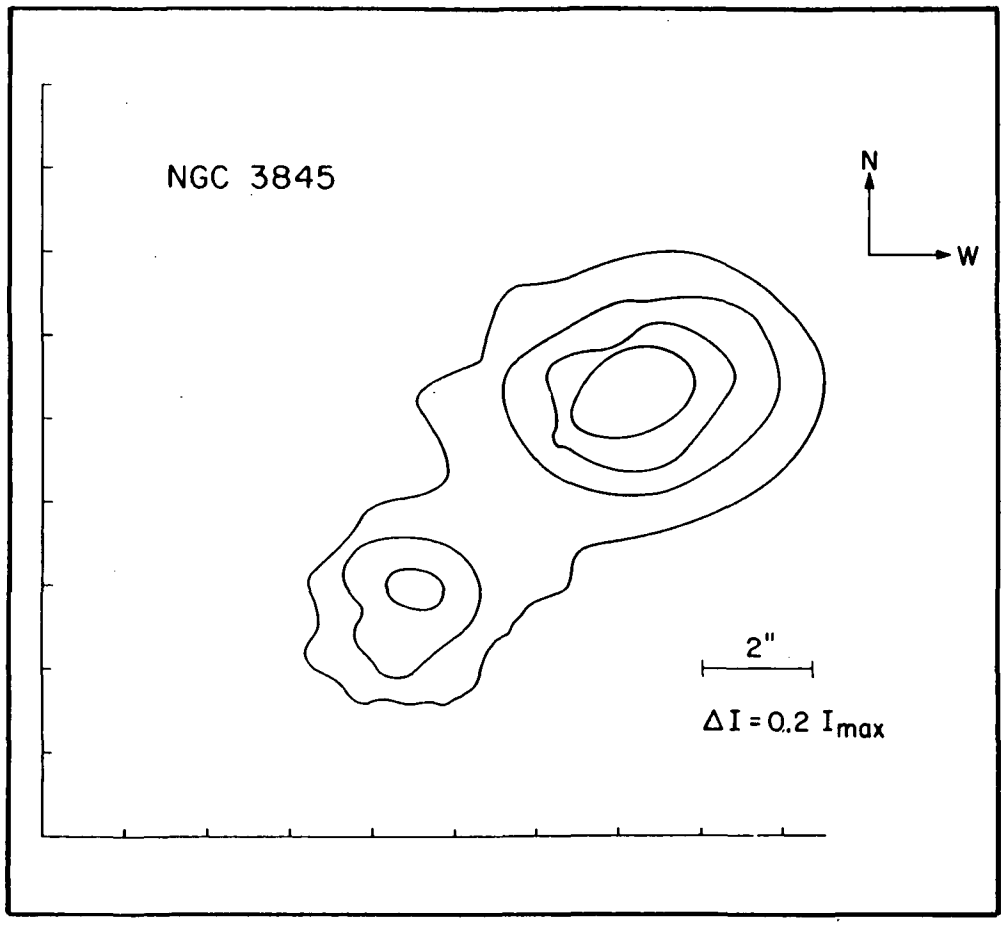

Figure 5-25 Equal Brightness Contours of NGC 3845

5.3.2 SEC Camera

As described earlier, the electron image stored on an exposed SEC target must be read out point-by-point by an ordered sequence of linear scans, resulting in an analog output signal which varies with time according to the electron density variations across the image and the scanning rate employed. This analog signal is continuous except for the brief intervals between each line scan. The "raw" output can be used as-is for quick-look scan conversion and visual display. However, in most cases, the image information will be converted to digital form by periodic sampling and analog-to-digital conversion of the output signal as the image is scanned. Since the data samples are equally spaced in time and the scan is linear, the data represent the incident radiant flux density over an equally spaced array of points or picture elements in the scanned image. The sampling density must be high enough to assure retrieval of all useful information from the recorded picture. An upper limit on useful sampling density is imposed by the telescope MTF or point spread function (including the loss due to pointing errors) and the sensor MTF.

The output format for each complete image or "frame" is then basically a sequence of digital words. The total number of words is equal to the number of picture elements in the image plus line and frame identification words inserted in the appropriate intervals between each scan line and at the beginning and end of each complete frame. The number of bits in the digital word describing each picture element is determined by the dynamic range expected, the noise present in the signal, and the precision required of the output data.

Typically, the meshless SEC on the AOS would be set up to have an array of 2000 by 2000 picture elements over a 40 x 40 mm square image format. If the flux in each element can be adequately measured by an eight-bit word (256 levels), then the total number of bits per picture is $8(2000)^2 = 3.2 \times 10^7$ bits. (This does not include line and frame identification.) This figure is a lower limit, however. To reduce the possibility of extraneous data introduction by the aliasing type of phenomena, it is often desirable to increase the sampling density relative to the highest spatial frequencies actually being measured. Thus, if three samples rather than two per cycle are taken in both x and y directions, the total number of bits is roughly doubled. Therefore, the total number of bits per picture should be taken as 7×10^7.

Thus, the on-board tape recorder needs a capacity of at least 7×10^7 bits for each picture recorded. If the data are to be transmitted to ground, the bandwidth required by the communications link will be established by the number of pictures to be transmitted and the time available to dump the data to the ground station. In those cases where the useful data does not fill the entire square format, such as is notably the case at spectrophotometer outputs, considerable conservation of data capacity can be achieved by selective readout of narrow rectangular areas corresponding to the geometry of the desired spectrum.

The above discussion pertains especially to prime data where a permanent, maximum quality image is to be stored on tape on board and either transmitted to ground over a high quality downlink or returned physically at the end of the mission.

As pointed out earlier, the SEC camera can also serve a very useful purpose as a near real-time finder scope or guide scope, especially when looking for faint stars at and beyond the visual limit. In

this mode, a scan conversion memory and a high resolution display are needed as part of the peripheral equipment on AOS. This equipment is required to take the serial bit stream representing a single exposure readout and translate it electro-optically into what the human eye sees as a constant (flicker free) picture of reasonably high quality for as long as desired or until updated by the data sequence following the next exposure, etc. The displayed replica of the focal plane image can be updated as often as once every second when the objects of interest are bright enough; hence the phrase "near real time" display. There is still a dependence on the available photons, however, so faint objects may be updated only once every 20 or 30 seconds or once per minute. This should make it possible, however, to locate and track stars having visual magnitudes between 15 and 20 at 1000 Å bandpass. When the star or other objects of interest have been located and placed in the center of the field, the star tracker can be locked onto nearby reference stars. Then the focal plane image can be integrated by the electronographic camera, if desired, and exposures up to 30 minutes taken on fine grained film for maximum information capture.

The SEC camera can also be used as a quick-look scope to verify proper operation of a spectrophotometer. In this case, a small on-board storage oscilloscope would be used to display one or more line scans normal to the dispersion of the exit image. The oscilloscope display would be a graph of spectral irradiance as a function of wavelength. An exposure of the order of a minute or so should be sufficient in many cases to verify the presence of expected absorption or emission lines.

5.4 ENVIRONMENTAL CONSIDERATIONS

5.4.1 Radiation Environment

Sensor damage is always a potential problem in the presence of higher than normal radiation environment. One of the very sensitive components is the class of photographic emulsions that must be used to obtain reasonable sensitivity to flux in the far ultraviolet part of the spectrum. The choice of an electronographic camera over direct photography alleviates this problem by making it possible to use emulsions which are much less sensitive to radiation fogging in those situations when an unfavorable radiation environment is expected.

Of course, if the radiation becomes sufficiently intense, all films can suffer and performance of the camera tube target and other components may be degraded. Certainly, the mission should be designed to mitigate such possibilities, thereby avoiding the need for excessive shielding. As a matter of principle, however, it seems advisable to store all film in a practical shielded vault to minimize the risk of losing valuable data during unexpected radiation peaks.

5.4.2 High Voltage

Proper handling of the high voltages (10-25kV) needed to operate the selected sensors is extremely important. All phases of design in any way connected with the high voltage source must involve safety engineering.

The space in and around a vehicle in space is far from being an ideal vacuum, and the ionizing effect of ultraviolet and X-rays encountered in space is very complicated compared to a safe vacuum chamber in a ground laboratory. Outgassing and other characteristics

of all the materials used on the AOS as well as the contaminants which will inevitably be present from attitude control and propulsion systems, leakage, etc. should be considered. At the very least, all high voltage systems must be designed so that they can withstand corona and other forms of high voltage breakdown without damage. Far better would be the elimination of such effects.

In addition, Carruthers[10] found it necessary with some emulsions to add a grounded grid a few centimeters in front of the film plane to permit any gas given off to expand to a low density before reaching the intense electric field region. Otherwise, breakdown could occur.

Carruthers also found that the presence of the high (20-25kV) accelerating potential at the photocathode of his camera made it essential to include ion-repeller grids and baffles to prevent positive ions from being drawn into the instrument (with resultant fogging). He used two or more independently supplied grids (at ≈12 V) in all his flight instruments. It also may be a wise precaution with the SEC camera in view of the 8-10kV present.

REFERENCES

1. McCord, T. B., and Westphal, J. A., "Two Dimensional Silicon Vidicon Astronomical Photometer," Applied Optics Vol. 11, No. 3, 1932, p.522.

2. Lallemand, A., C. R. Acad. Sci. 203, 243, 1936.

3. Kron, G. E., Advances in Electronics and Electron Physics, Vol. 16, Ed. by J. D. McGee, W. L. Wilcock, and L. Mandel Academic Press, New York, 1962, p. 25.

4. Kron, G. E., Ables, H. D., and Hewitt, A. V., Advances in Electronics and Electron Physics, Vol. 28A, Academic Press, London, 1969, p. 1.

5. Combes, M., Felenbok, P., Guerin, J., and Picat, J. P., Advances in Electronics and Electron Physics, Vol. 28A, Academic Press, London, 1969, p. 39.

6. Combes, M., Applications Spatiales des Tubes de Prises de Vues, Centre National d'Etudes Spatiales, Paris, 1971, p. 163.

7. Decker, R. W., and Mestwerdt, H., Advances in Electronics and Electron Physics, Vol. 28A, Academic Press, London, 1969, p. 19.

8. McGee, J. D., McMullan, D., Bacik, H., and Oliver, M., Advances in Electronics and Electron Physics, Vol. 28A, Academic Press, London, 1969, p. 61.

9. Carruthers, G. R., Address Presented at 139th Meeting, AAAS, December 28, 1971.

10. Carruthers, G. R., Applied Optics, Vol. 8, 1969, p. 633.

11. Kron, G. E., Astronomical Use of Television Type Sensors, Symposium/Princeton Observatory, May 1970, NASA SP-256, 1971, p. 27.

12. Lelièvre, G., and Wlérick, G., Applications Spatiales des Tubes de Prises de Vues, Centre National d'Etudes Spatiales, Paris, 1971, p. 153.

13. Walker, M. F., Sky and Telescope, September 1970, p. 132.

14. Walker, M. F., and Kron, G. E., Publications of the Astronomical Society of the Pacific, 79, 551, 1967.

15. Walker, M. F., Astrophysical Journal, 161, 3(1), September 1970, p. 835.

16. Kahan, E., and Cohen, M., Advances in Electronics and Electron Physics, Vol. 28B, Academic Press, London, 1969, p. 725.

17. Zucchino, P., and Lowrance, J. L., Astronomical Use of Television Type Sensors, Symposium/Princeton Observatory, May 1970, NASA SP-256, 1971, p. 27.

18. Lowrance, J. L., and Zucchino, P., Applications Spatiales des Tubes de Prises de Vues, Centre National d'Etudes Spatiales, Paris, 1971, p. 43.

19. Lowrance, J. L., Morton, D. C., Zucchino, P., Oke, J. B., and Schmidt, Maarten., Astrophysical Journal, Vol. 171, 2(1), January 15, 1972, p. 233.

Section 6
CALIBRATION

A calibration may be defined as that body of information necessary to allow a determination of the stimulus in an experiment from the response of the sensor. In the case of astronomical observations, the stimuli may be characterized by the spectral, polarization and temporal characteristic of light coming from various directions. The responses consist of photographic images or electronic signals. Diffraction, aberrations, reflection losses and scattering all contribute to the nonideal characteristics of such a system. If the transfer function is known the stimuli can still be determined, though with some uncertainty. The data on reflectivities, aberrations, etc., comprising the calibration, will be used to infer the system transfer function.

6.1 DESIGN GOALS

The AOS is intended to extend our knowledge of the absolute intensities of celestial sources into the ultraviolet. An important goal of the AOS is to measure absolutely the flux of the many "standard" stars, used as comparison standards in sounding rocket and OAO photometric work, with an accuracy of a few percent throughout the 1100 to 3000 Å range. This accuracy is to be maintained primarily in the wide band imagery mode, with the capability to transfer these measurements to the spectrographic instruments. In addition, wavelengths are to be determined to less than one resolution element for the spectrographic instruments.

6.2 IMPLEMENTATION

The precise method for absolute calibration of flux levels is yet to be chosen. The National Bureau of Standards is actively pursuing two methods for *in situ* vacuum ultraviolet calibrations. The methods involve either an emission or a detection standard.

The emission standard is a well stabilized hydrogen arc-source. Current test results indicate that 5 to 10 percent accuracies are obtainable in the 1650 to 3600 Å region and 10 to 30 percent in the 1100 to 1650 Å region. The accuracy in the latter region is expected to be increased to 10 to 15 percent when an adequate comparison standard is developed.

The output of this standard is an f/150 to f/200 beam of Lyman continuum radiation with an effective temperature of about 20,000°K. A 100 amp, 1 kV (100 kW) power supply is required during operation.

The usual problem encountered in using a continuum source for calibration at these wavelengths is severe scattered light contamination in spectrographs. It is to some extent mollified in this case by the high temperature of the source with its peak in the region of interest. In fact, the source has, in the first approximation, the spectrum of a BO star.

Potential problems using the emission standard are its relatively immature state of development and the focal ratio mismatch. The focal ratio mismatch can be handled in two ways:

1. Ignore it. The measurements can be made at a specific point on the primary mirror at a fixed angle and the energy of the beam passed by a field stop calculated from the geometry of the situation. An absolute calibration can then be obtained by assuming that the detailed vignetting function remains constant in shape throughout a given mission.

2. Introduce auxiliary optics and map the system. A collimating system can be used to form parallel light

and this collimator articulated to map the system vignetting function. In this way the assumption regarding the shape constancy of the vignetting function can be removed at the price of introducing additional optics (whose efficiency must be independently determined) and considerably increasing procedural complexity.

Experience shows that the latter method can increase the overall system accuracy and confidence but at a considerable price. A quantitative comparison of these methods should be made as the program continues.

The detection standard is a highly passivated photodiode having a CsTe photocathode and a MgF_2 window. This detector is actually a comparison standard deriving its calibration ultimately from electron synchrotron radiation at the National Bureau of Standards. Current results indicate ~2 percent repeatability for these diodes in the 1100 to 2200 Å region. Thus far no detectable long term variations have been found since the start of the program in 1970. These diodes possess the advantage that they are simple, light and relatively inexpensive. For operation in the AOS, however, they require considerable additional instrumentation. Most complex is the necessary transfer source. The transfer source is, in essence, calibrated by the diode for the short time necessary to excite the AOS instruments. Thus, the transfer source need not have the extreme stability necessary of an emission standard.

However, two different geometries are required. The diode is calibrated only on a 1 cm x 1 cm area in a relatively slow focal ratio beam. The telescope would ideally use a 1 meter diameter beam of perfectly collimated light. Thus the transfer source must have auxiliary optics. The two approaches mentioned above the emission

standard are again appropriate. When the errors introduced into the system by the transfer source and its auxiliary optics are considered, it may be that the initially superior accuracy of the diode will be degraded to levels equal to that of the emission based system.

The development of both systems by the National Bureau of Standards should be carefully monitored during the next few years. The detailed design and performance estimates for the auxiliary support systems should be studied during the next AOS phase so that cost and performance estimates can be reliably obtained.

Wavelength calibration can be provided through use of discharge sources. The system described for a discharge lamp in Section 4.12.2 of the SAS-D report (GSFC, March 1971) seems appropriate.

Section 7
ACQUISITION AND TRACKING

7.1 GENERAL DISCUSSION

The purpose of the pointing control system is to precisely point the telescope at a selected celestial body while performing field photography or spectrography. The system consists of the telescope and tertiary mirror support structures, and the sensors and drive systems required to acquire and track guide stars. The telescope structure is gimbaled in azimuth and elevation for coarse pointing. Fine guidance pointing is accomplished by controlling the two-axis gimbaled tertiary mirror. In addition, the optical bench inside the airlock is gimbaled in the roll axis to control the slit aperture orientation and correct for image smearing due to shuttle vehicle motion.

Direction error sensing for the various tracking loops is provided by star sensors. A two-axis wide field of view star sensor mounted on the telescope assembly is used in controlling the coarse guidance telescope acquisition and tracking. The fine guide error sensor is mounted on the roll stabilized optical bench, and the roll star sensor is on the telescope assembly, mounted orthogonal to the coarse guidance star sensor. The star sensor operation is described in detail in Section 7.2.1.

Offset guide stars are used for both coarse and fine guidance tracking. An electrical offset (equal to the angle between the coarse pointing guide star and the target star) is added to the coarse sensor error signal to point the telescope toward the target star. Relative motion between the fine guide star image, reflected from the tertiary mirror, and the guide (photo) sensor is required to achieve full coverage of the telescope field of view. To accomplish this, the sensor is translated in the focal plane an amount determined by the angle between the target star and the fine guide star,

and the geometry of the optical path. The resulting offset added to the fine guide sensor error signal is used to point the tertiary mirror toward the target star.

Since the guide stars are fixed in inertial space, the tracking system controllers need not possess the ability to track a moving target. Instead, they must have the ability to keep the telescope fixed in inertial space in spite of the disturbances which tend to move it. The fine pointing axes (tertiary mirror) of the telescope must be supported in such a manner that the telescope is effectively isolated from high frequency torque disturbances. The flex pivot mount accomplishes this, whereas a roller or ball bearing does not. To further reduce frictional disturbance torques, brushless DC torque motors are used to drive the tertiary mirror gimbals.

7.2 COMPONENTS AND FUNCTIONS

7.2.1 Fine Guide Error Sensor

The fine guide error sensor is used to detect angular deviations in line of sight of the telescope and provide error signals for the control system to rotate the tertiary mirror in the manner necessary to minimize the target motion in the telescope focal plane.

The most significant parameters affecting sensor design considerations are output signal accuracy and bandwidth. The rms angular noise of the sensor output signals should contribute negligible target position error. This ideal may not be consistent with all other system considerations; however, the upper limit of acceptable sensor noise is reached when it contributes approximately as much target blur as the resolution of the optical system. For the f/25 telescope this limit is approximated by the range 0.02 to 0.10 arc-second, and for the f/10 telescope by the range 0.10 to 0.50 arc-second.

A preliminary estimate of the bandwidth required of the output position signals to allow proper operation of the tertiary mirror control system in the shuttle environment is 50 Hertz.

Initial Considerations. At the outset of the study, the decision was made to employ an offset guiding technique in which only stars outside a designated target area are used by the fine guiding sensor for control. This conclusion was reached for the following reasons:

- It is undesirable to use target energy potentially useful to the experimenter.
- The target may not always have sufficient irradiance to provide acceptable guide signals.
- The object of interest may not always be a point source.
- If offset guiding is required for any target condition, it must be made available and it may as well be used for all conditions.

Guide Star Availability. Data on the distribution of stars over the celestial sphere as a function of star magnitude and galactic latitude is provided by Allen.[1] Figure 7-1 provides a plot of the number of stars per square degree at the galactic poles. As the galactic equator is approached this density increases several times.

Figure 7-2 shows the probability of having at least one star in the field of view as a function of the average number of stars in the field of view. It indicates that with an average of three stars

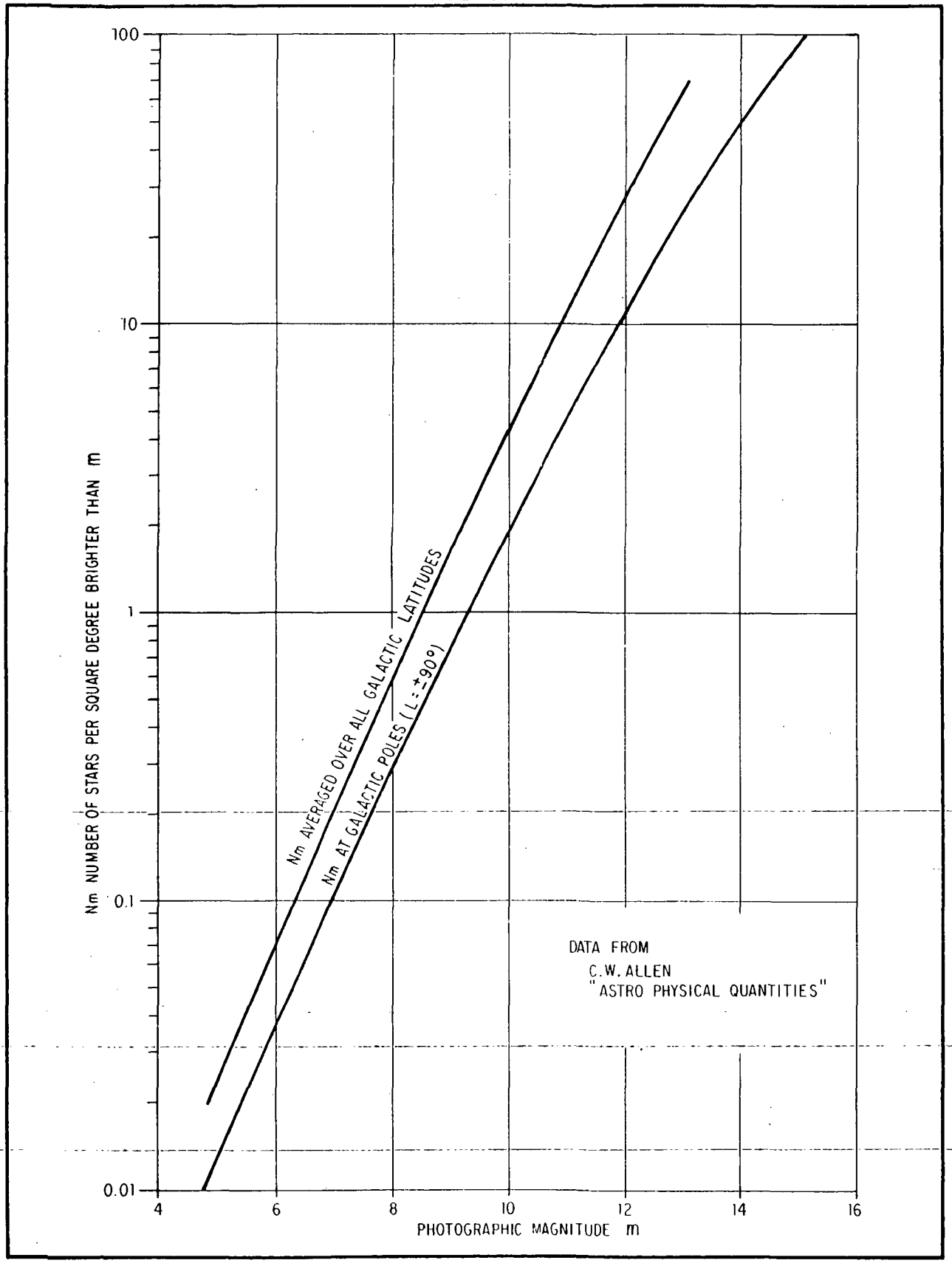

Figure 7-1 Number of Stars per Square Degree at Galactic Poles

in the field of view the probability of having at least one star is 0.9. Since the density increases for angles away from the galactic poles, an acceptable overall probability of having trackable guide stars will result if the magnitude corresponding to this stellar density is selected as the minimum trackable star. The galactic latitude corresponding to the stellar density averaged over the full celestial sphere is about 30°. The star magnitude corresponding to an average of one star in the field of view at this latitude corresponds to the brightness of the average star which the system will be required to track. Figure 7-3 provides the field of view area versus star magnitude for the minimum and average star just discussed.

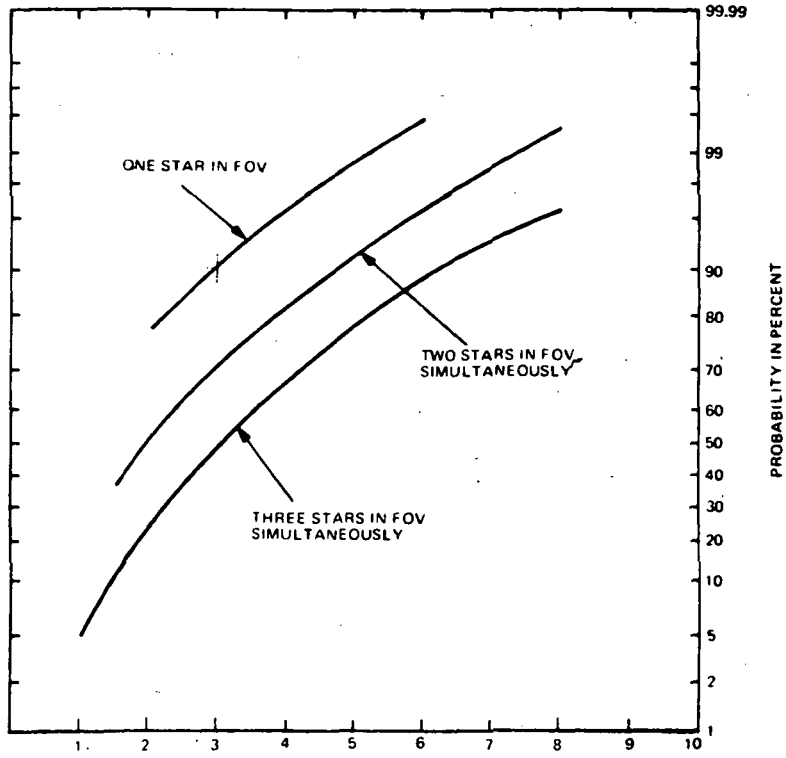

Figure 7-2 Guide Star Probability Versus Average Number of Stars in Field of View

The telescope field of view at the beginning of the sensor study was 30 arc-minutes diameter. This field of view provides an average of three 12.5 magnitude or brighter stars.

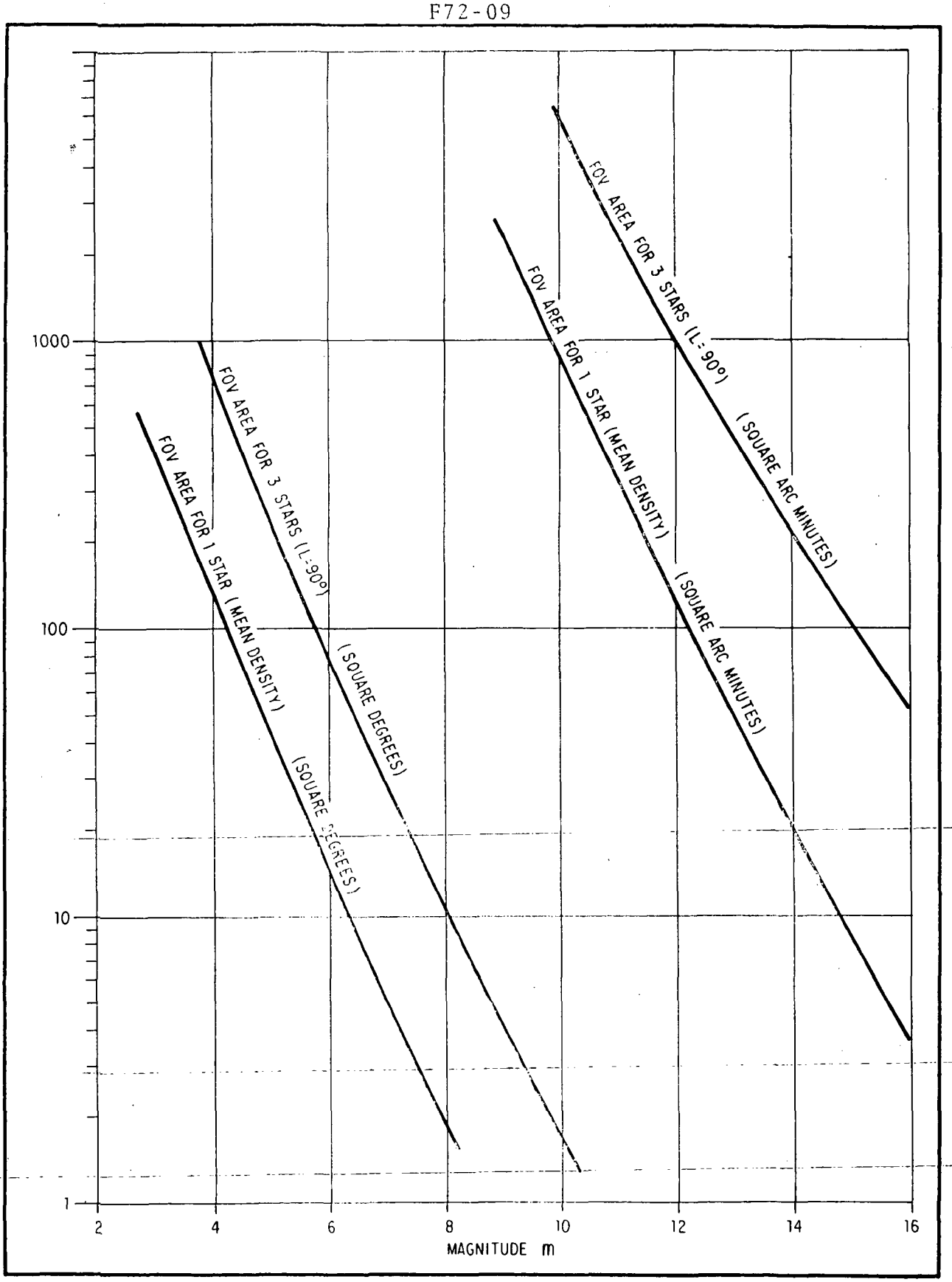

Figure 7-3 Field of View Area Versus Star Magnitude

Mechanization Concepts. The physical dimensions of the image in the focal plane have a dominant influence on the design of the sensor. The diameter of a 30-minute field in the f/25 configuration is nearly 22 cm (8.6 inches) in diameter. No suitable image tube has a photocathode anywhere near that large. Therefore, some means of producing relative motion between the guide star image and the photo sensor is required to achieve full coverage of the available field of view.

The first concept considered was a system of relay optics with a pointing mirror between the collimating and imaging lens. This system is shown schematically in Figure 7-4. When it was realized that for optics of reasonable speed (like f/2) the optical path would be greater than a meter and that the diameter of these elements were on the order of 25 cm in diameter, the decision was made to look for a more reasonably-sized system.

The next scheme placed a perforated pointing mirror in front of the focal plane. This is shown in Figure 7-5. This simple system is attractive because it requires only the pointing mirror to focus the guide star onto the guide sensor. Two principal drawbacks led to its being rejected. The first occurs because the folding mirror is located away from the focal plane. The cone formed by the rays from all positions of the collecting area converging to a target image in the focal plane must not be occulted by the folding mirror. As the folding mirror is moved away from the focal plane to make the pointing geometry reasonable, the size of the mirror perforation required to prevent occultation of the images in the science field of view increases as well. This is especially true with the f/10 telescope where the angle of convergence is much larger than with the f/25 case. This large occultation means that the outer radius of the guide star field of view must increase to retain the required field of view area. The telescope optical design could

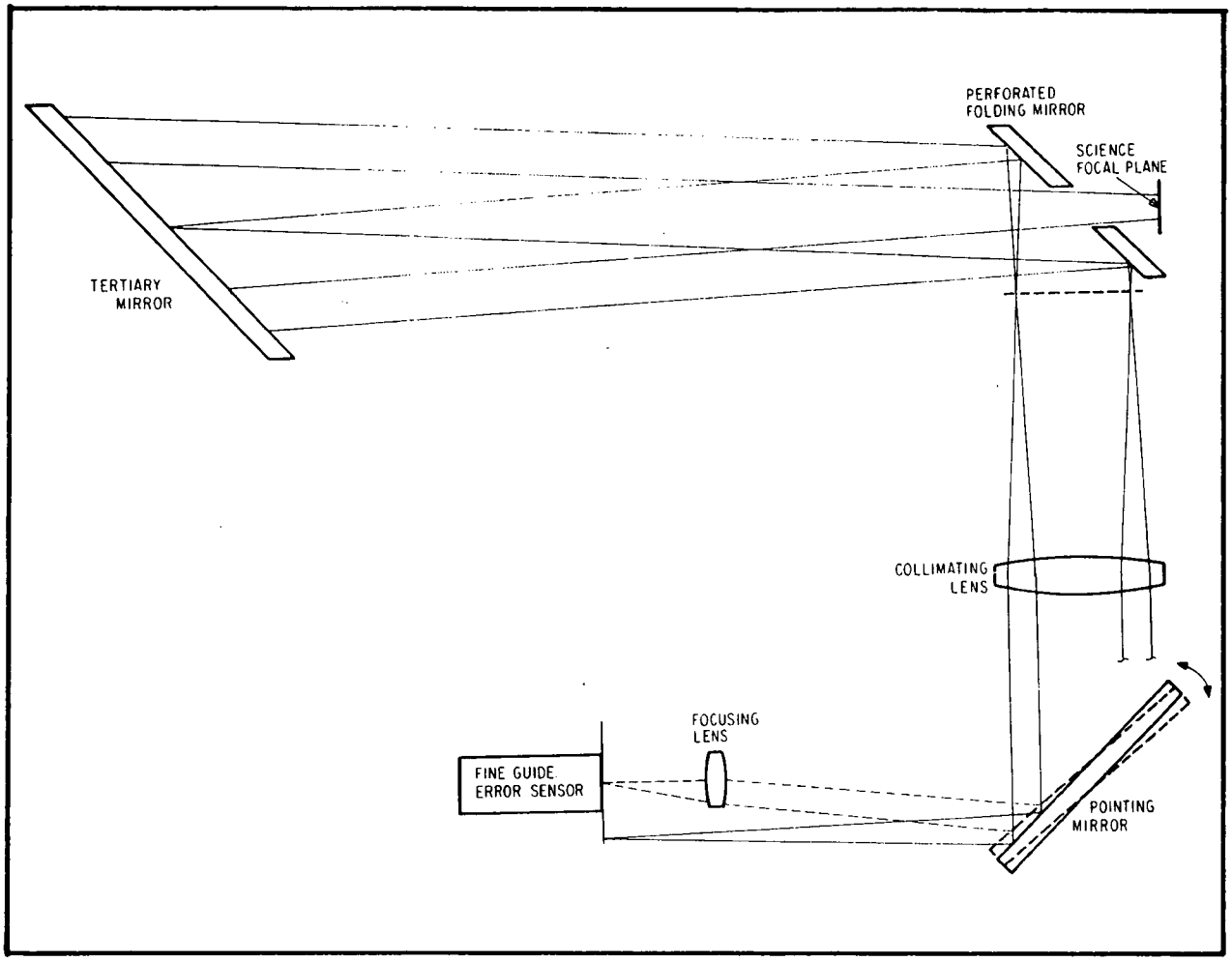

Figure 7-4 Schematic Representation, Relay Optic Method of Imaging Field of View on Fine Guide Error Sensor

not provide the added field without significantly compromising the performance in the target field of view. The second problem with the perforated pointing mirror system is that the image translation accomplished by the mirror produces an accompanying focus change. This is a troublesome but not insurmountable problem.

Selected Mechanization. To avoid the previously mentioned problems it was decided to use a movable folding mirror that could be positioned anywhere in the field and to move the sensor tube in the focal plane. This makes most of the telescope field available to the science removing only that energy reflected by the movable folding mirror.

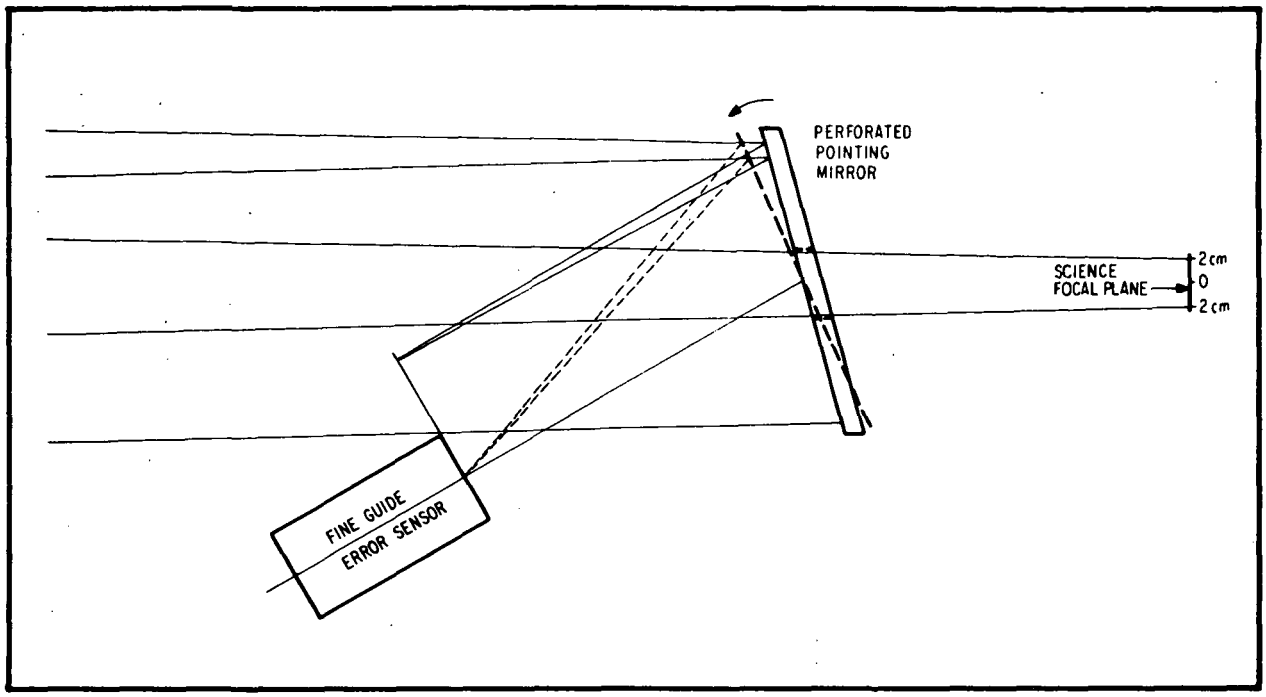

Figure 7-5 Schematic Representation, Pointed Folding Mirror Method of Imaging Field of View on Fine Guide Error Sensor

With this system, the folding mirror can be located very close to the actual focal plane, making the entire system more compact and avoiding the large loss of usable field of view resulting from the large folding mirror perforation necessary when the mirror is located farther from the focal plane. The focal plane geometry for the f/10 and f/25 systems is shown in Figures 7-6 and 7-7, respectively.

The mechanism for translating the sensor in the focal plane and for moving the folding mirror has not been considered in detail during this study. The resolution need only be great enough to place the sensor on the star image within a few millimeters to stay within the highest resolution portion of the image tube. The system must be stable within about 2.5 microns over the observing period to maintain image stability of 0.02 arc-second. This should not be too difficult for observing periods of an hour or less with reasonable thermal stability in the vicinity of the sensor.

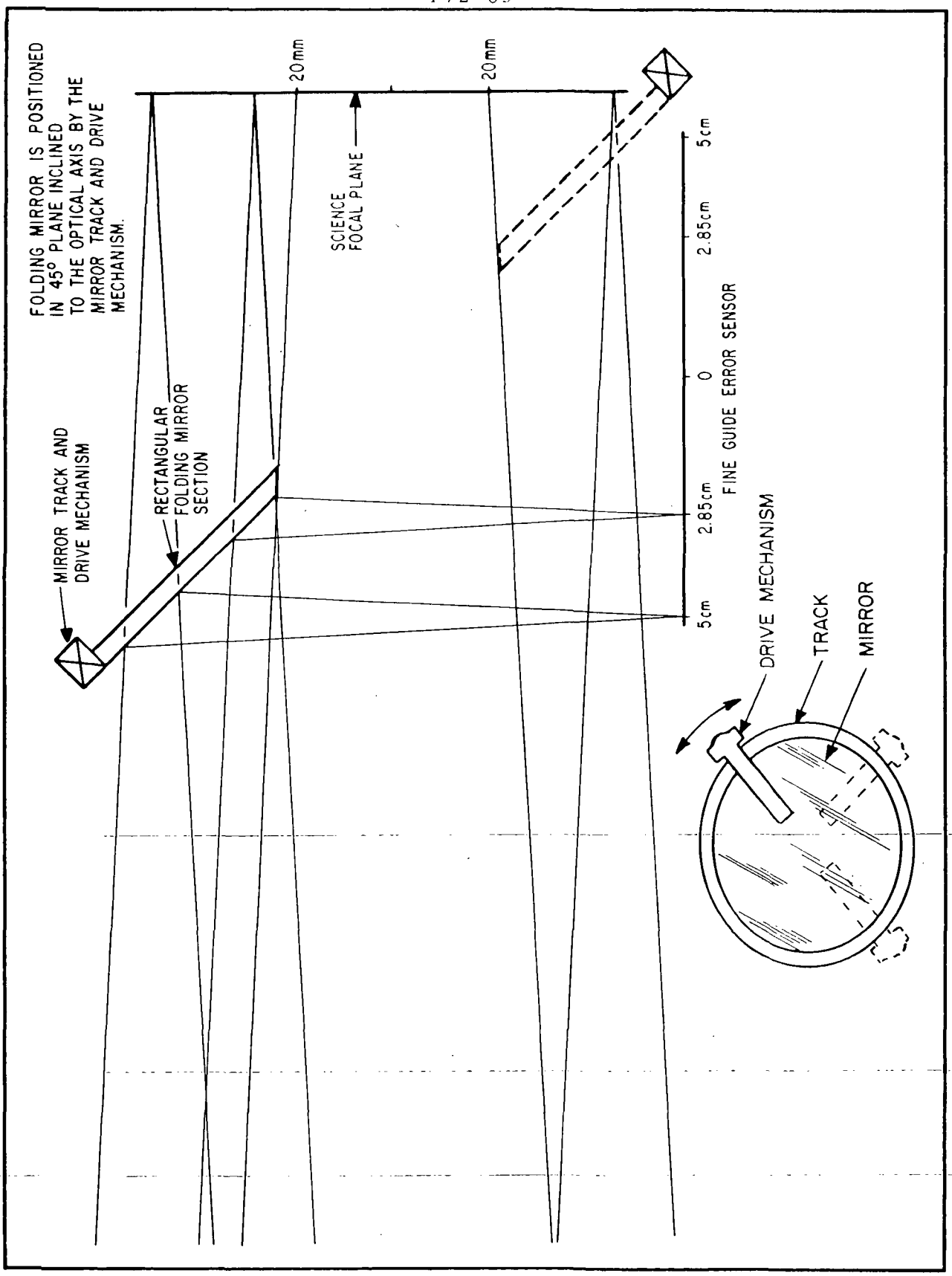

Figure 7-6 Focal Plane Geometry, f/10 Telescope

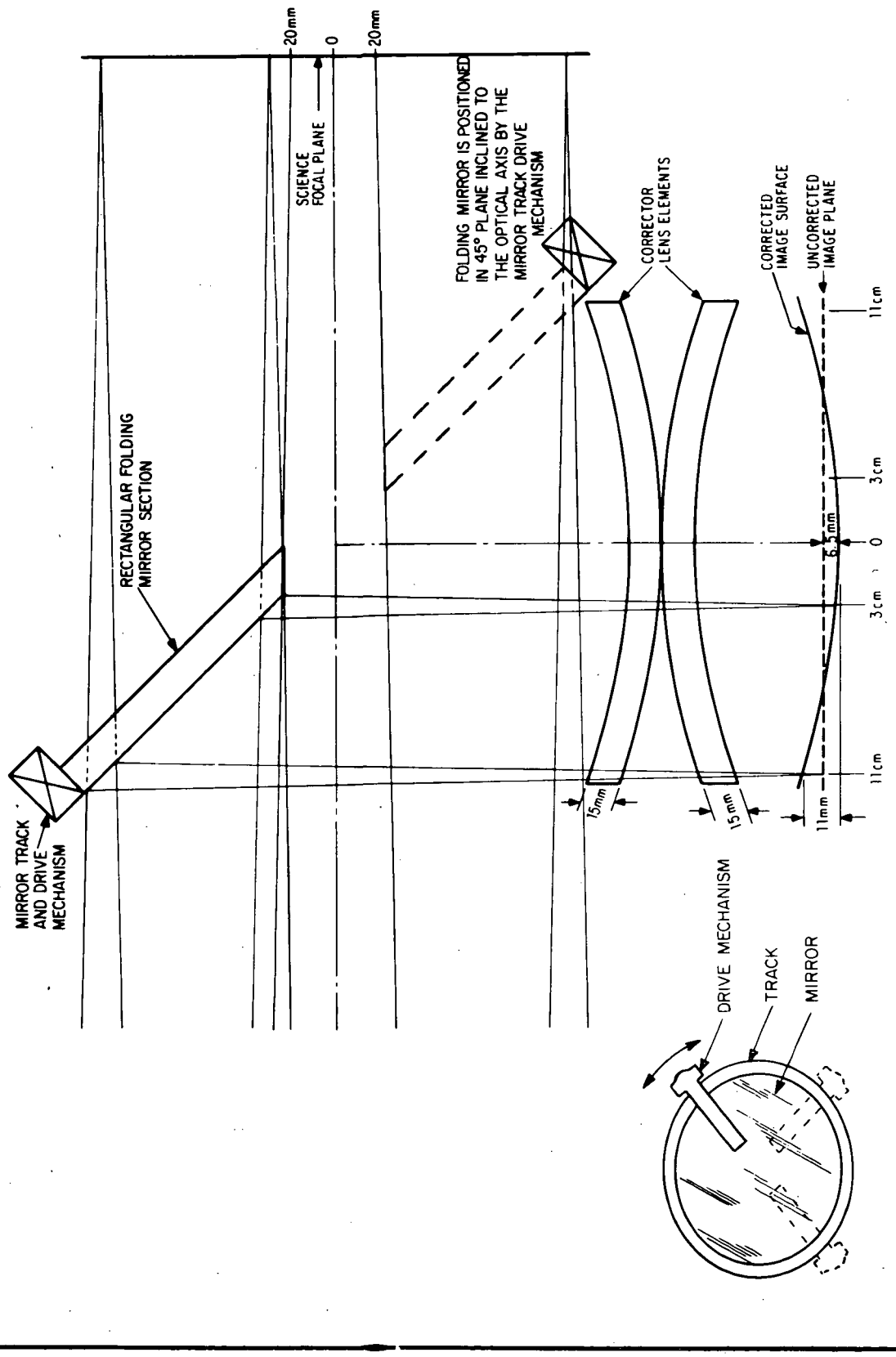

Figure 7-7 Focal Plane Geometry, f/25 Telescope

Sensor Considerations. The fine guide error sensor uses an image dissector tube as the image position sensor. This tube type is selected over the presently available integrating camera tubes primarily because of its low noise, good linearity and its freedom from position errors associated with the scanning electron beam.

An image dissector tube operates by forming a deflectable electron image of the optical image incident on the photocathode. The electron image is focused on a plane containing a small aperture. Those photoelectrons passing through the aperture are amplified by an electron multiplier and become the signal current at the anode. The aperture therefore defines a small portion of the photocathode called the Instantaneous Effective Photocathode Dimension or IEPD, which will produce signal current with incident photons.

In conventional star sensor operation the IEPD is scanned in a symmetrical cross pattern across a star image focused on the tube cathode. A signal pulse is obtained at the image tube anode. The deflection signal is sampled at the leading and trailing edges of this signal pulse. The average of these two samples is a measure of the star image position on the tube cathode. The two-directional scan pattern deflection is sampled in each direction, providing a two-axis output error signal.

During the early phases of the study a pulse-counting tracking scheme was considered because of the small number of photons in the signal pulse when tracking minimum stars. It was found that, because of the relatively high scan rates required of the fine guide error sensor, the analog and pulse counting techniques are nearly equal in performance. The analog technique was chosen because it is less costly.

The tertiary mirror control system requires a comparatively wide bandwidth signal from the fine guide error sensor to follow telescope motions and overcome disturbances in the system. The estimate of required bandwidth used for this study is 50 Hz. This very wide bandwidth is a major constraint on sensor performance and if it is found in later phases of this program that sensor output bandwidth can be reduced, significant reductions in output random error or relaxations on other sensor constraints may result.

For computation purposes it was assumed that the f/10 uncorrected image size would be about 3.3 arc-seconds and that the f/25 corrected image (by refractive correction) size would be about 0.5 arc-seconds. The linear dimension of the image size is 0.16 mm and 0.06 mm for the f/10 and f/25 systems, respectively. In the design of the fine guide error sensor, the image dissector IEPD must be selected as close to the image size as possible for optimum performance. Since there is a significant disparity in the size of resolution element with the f/10 and f/25 systems, it is recommended that different fine guiding sensors with IEPD optimized for the two resolutions be used with the f/10 and f/25 telescope configurations.

In the following analysis, the sensor output angular error is computed at the signal levels corresponding to the magnitude of the average guide star and a guide star availability of 95 percent.

			f/10	f/25
The field of view (FOV) determines the star magnitude which must be tracked.				
Inner radius of FOV	arc-min	=	10	3
Outer radius of FOV	arc-min	=	17	15
Area of FOV	$arc\text{-}min^2$	=	595	675
About 50% of the time there should be stars brighter than $m_{0.50}$ (that magnitude for which there is an average of one star in the FOV at a galactic latitude of 30°).	$m_{0.50}$	=	10.6	10.5
About 95% of the time there should be stars brighter than $m_{0.95}$ (that magnitude for which there is an average of 3 stars in the FOV at the galactic poles).	$m_{0.95}$	=	12.7	12.5
Signal Current				
Effective collecting area (A_e) of optical system (assumes 4% loss in refractive corrector)	$A_e(cm^2)$	=	6170	5930
Useful spectrum of Optical System	(microns)		0.2 to 0.8	0.4 to 0.8

		f/10	f/25
Signal current density (ρ_s) is the signal current per cm^2 of collecting area. It is a function of star color class sensor and optical system spectral response. The ρ_s given here assumes GOV stars, S-20 tube response, and optical system spectral transmission given above.	ρ_s(amp/cm^2) =	6.7×10^{-15}	4.45×10^{-15}
Signal current (i_c) is found from the expression: $i_c = 2.51^{-m} \rho_s A_e$			
for average stars ($m_{0.5}$)	i_c(amp) =	23.5×10^{-15}	16.7×10^{-15}
for minimum stars ($m_{0.95}$)	i_c(amp) =	3.4×10^{-15}	2.6×10^{-15}
The resolution of the optical system (ϕ) (Image tube resolution contribution is negligible.)	ϕ(arc-sec) =	3.3	0.5
Selected Image Tube Aperture (α)	α(arc-sec) =	5.0	0.8
Sensor scan angle (θ) Selected such that $\theta \simeq \alpha + 2\phi$	θ(arc-sec) =	12.0	1.9

		f/10	f/25
Sensor scan time (t_s) Selected to meet the output bandwidth requirement.	t_s(m sec) =	3.2	3.2

let:

$$n_c = \frac{i_c t_s}{q}$$

	n_c for		
	$m_{(0.5)}$ =	470	334
	$m_{(0.95)}$ =	68	53

The average number of photo events between the beginning of the scan and the centroid of the star ($\bar{n}$) is:

$$\bar{n} = 1/2\ \alpha/\theta\ n_c$$

The rms variation in $\bar{n}$ is $(\bar{n})^{1/2}$

Then the rms angular variation (ε) in samples of $\bar{n}$ is:

$$\varepsilon = \frac{\theta}{n_c}(\bar{n})^{1/2}$$

but

$$\varepsilon^2 = \frac{\theta^2}{n_c^2}(\bar{n}) = \frac{\theta^2}{n_c^2}\left(\frac{n_c}{2}\frac{\alpha}{\theta}\right)$$

then

$$\varepsilon = \left(\frac{\alpha\ \theta}{2\ n_c}\right)^{1/2}$$

	ε(arc-sec) for		
	$m_{(0.5)}$ =	0.25	0.048
	$m_{(0.95)}$ =	0.66	0.120

ε is the rms angular noise on the fine guide error sensor output signal resulting from photon arrival and signal processing noise. This is the primary source of signal instability or fine guide sensor error.

It should be noted that if the f/10 non-Ritchey-Chretien image were corrected from the assumed 3.3 arc-seconds to 1.25 arc-seconds or less resolution element size, the linear resolution of the f/10 and f/25 systems would be the same, allowing identical image tube apertures. Preliminary telescope data indicates that this is possible.

The fine guide error sensor will then be common to both telescope configurations. The ultraviolet spectral energy lost to the refractive corrector elements would be more than offset by the improved resolution. Output angular noise on the average star would improve as follows:

$$\sigma = 0.25 \text{ arc-sec} \times \frac{1.25}{3.3}\left(\frac{1.5}{1}\right)^{1/2} = 0.13 \text{ arc-sec}$$

7.2.2 Coarse Star Sensor

The telescope control sensor or outer loop sensor is hard-mounted to the telescope, with its pointing axis nominally parallel with the telescope optical axis. This sensor clearly cannot have enough collecting area to track the same guide stars used by the fine guide error sensor. It must, therefore, have sufficient field of view and sensitivity to ensure the availability of its own trackable stars.

A preliminary configuration for a coarse sensor was developed around a 40 mm format image dissector tube (either the ITT F4077 or the EMR 575E). The optical system was assumed to be a 410 mm focal length, f/2.0 catadioptric objective system. This system provides a 5 degree diameter field of view and has an average of 3 stars in the field of view when the star magnitude is 7.5. The output rms noise for this system was projected to be 2.2 arc-seconds with an output bandwidth of 5 Hertz.

The telescope control system may have disturbance inputs which prevent it from taking advantage of sensor output control signals with noise levels below about 15 arc-seconds. It appears, therefore, that the preliminary version of the coarse star sensor has significantly more capability than is required by the control system.

An adaptation of the star tracker which BBRC is making for attitude determination on the SAS-C mission now seems quite appropriate as the coarse star sensor for the SAL telescope.

The BBRC SAS star tracker is a strapped down scanning and tracking device using an image dissector tube as the sensing element. The tracker can search and acquire stars within an 8-degree square field-of-view with energy equivalent to GO V stars in the magnitude range +6.0 to +2.0.

Commandable thresholds determine the minimum star signal to be tracked. These threshold levels correspond approximately to stars of magnitude 6, 5, 4, and 3.

The search pattern is a left to right, right to left horizontal (X) sweep with a staircase signal applied to the vertical (Y) axis. The pattern is shown in Figure 7-8. The track pattern is generated by gating the ascending ramp of a triangle waveform to the X axis

and the descending ramp to the Y axis, producing the deflection patterns shown in Figure 7-9. The resultant unidirectional cross-scan track deflection pattern is shown at the bottom of Figure 7-9. The track signal is the sum of the deflection signals shown in Figure 7-9 and a dc level representing the location of the star being tracked. This dc signal centers the track pattern over the star image.

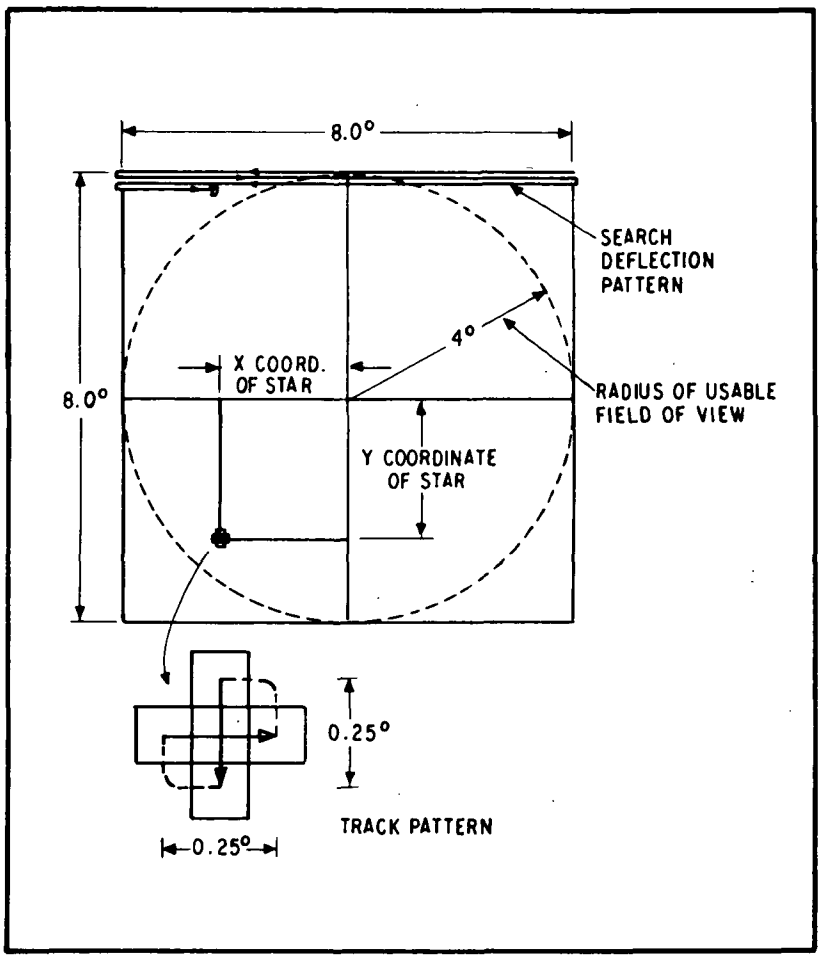

Figure 7-8 Search Pattern

Measures of star position are obtained by sampling the deflection signal during multiplier anode pulse leading and trailing edges. The average of the two samples represents the deflection signal corresponding to the centroid of the pulse and is, therefore, a measure of the star position in the field of view.

This sampled star position is fed back to the deflection amplifier as the dc bias for the track pattern signal and effectively centers the pattern on the star image. The sampled star position is provided at the sensor output as the signal representing star position in the field of view.

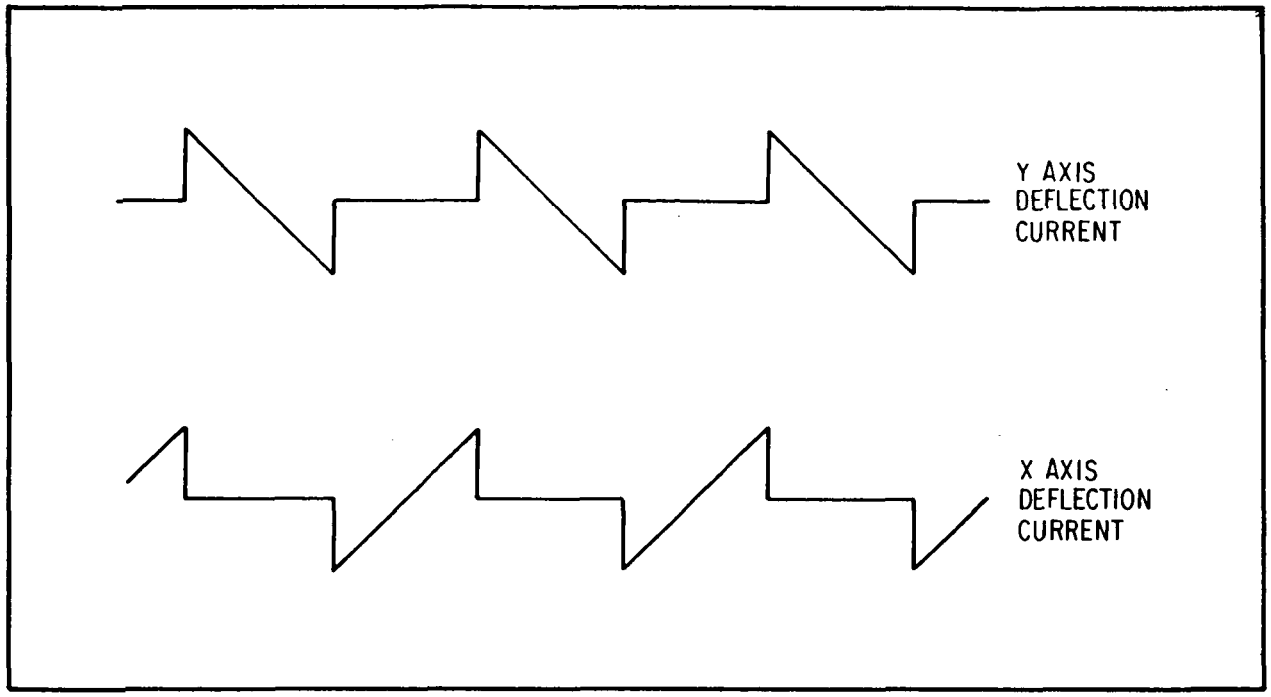

Figure 7-9 Deflection Pattern

The AOS application requires somewhat better noise/bandwidth performance than the SAS tracker presently delivers. The 6th magnitude minimum star does not quite meet the criterion of a three-star average at the galactic pole. In addition, when this system response is increased to 5 Hertz the output noise equivalent angle increases from 3 to about 17 arc-seconds.

A much more conservative design will result if the objective lens focal length is increased from 76 to 100 mm. This increase in focal length while keeping the same 0.87 f/number and lens design will provide an 8 degree diameter circular field of view. The required minimum star is 6.4 magnitude instead of 6.0 but the increased collecting area provides a net increase of 30 percent in signal current over the SAS tracker. The noise equivalent angle with a 5 Hertz bandwidth is about 11 arc-seconds with the 100 mm lens.

7.2.3 Roll Star Sensor

Rotations of the vehicle about the telescope line of sight produce target error motion proportional to the angle of the guide star from the center of the field of view. Assuming that the allowable target motion resulting from roll error is 0.02 arc-second, the roll attitude must be controlled within 4.6 arc-seconds.

The coarse star sensor design can be used for this roll function as well. The estimated bandwidth required by the roll control loop is 0.5 Hertz. If the coarse star sensor output noise is filtered to 0.5 Hertz the output noise is reduced to about 3.4 arc-seconds. This is clearly an acceptable performance level.

7.2.4 Guide Sensor Summary

Table 7-1 provides a summary of the more pertinent design and performance parameters of the sensors described in this section.

7.2.5 Gimbal Drive Mechanisms

Several different telescope gimbaling systems were considered. The one selected was briefly described in Section 7.1. The coarse pointing of the telescope is performed using bearings as gimbal supports. The tertiary mirror within the telescope assembly is supported by gimbaled flexure pivots which permit limited rotation about two axes. The fine guidance sensing is accomplished by slaving the tertiary mirror to the two-axis output error signals of the fine guide error sensor. Thus only the small mass of the mirror, within the telescope, must be precision pointed.

Due to the telescope optical configuration, the tertiary mirror elevation axis moves half the angle between the telescope and the shuttle vehicle. Hence, when the telescope points 10° off the shuttle vehicle axis, the tertiary mirror changes its position 5°.

Table 7-1

GUIDE SENSOR PARAMETER SUMMARY

	Focal Length (m)	Effective Collecting Area (cm^2)	Resolution ($\widehat{sec}$)	Output Time Constant (ms)	Average Star (Visual Magnitude)	Output Error On $m_{0.5}$ ($\widehat{sec}$)	Minimum Star (Visual Magnitude)	Output Error On $m_{0.95}$ ($\widehat{sec}$)
Fine Guide Error Sensor								
f/25	25	5930	0.5	4.8	10.5	0.048	12.5	0.120
f/10	10	6170	3.3	4.8	10.6	0.25	12.7	0.66
Telescope Control (Coarse Star Sensor)								
f/0.87	0.1	70	206	48	4.8	5.1	6.4	10.6
Roll Control (Roll Star Sensor)								
f/0.87	0.1	70	206	480	4.8	1.6	6.4	3.3

Since precision flex pivot rotation is limited to less than a degree, this type of support cannot be used directly for controlling the elevation axis of the tertiary mirror. The problem is solved by mounting the elevation axis flex pivot on a gimbal which is slaved to one-half the elevation angle between the telescope and the shuttle vehicle. The flex pivot then is always operating near its null position. The additional gimbal can be either mechanically driven or electrically servoed.

Gears cannot be used because of their backlash. The auxiliary, or intermediate gimbal could be band-driven from the telescope elevation gimbal. Several other types of mechanical linkages might be considered in the hardware design phase. However, for the purposes of this study, it was decided to servo drive the intermediate gimbal electrically. The servoed gimbal is easy to mechanize, and requires no specially developed mechanical linkages.

The electromechanical block diagram of the elevation axis mechanization is given in Figure 7-10. The configuration of the azimuth axes is similar, except the mirror flex pivot support is mounted directly to the telescope. The telescope gimbal, intermediate elevation gimbal, and tertiary mirror are all driven with brushless dc torque motors. The mirror flex pivot servo and the intermediate gimbal utilize tachometers for rate damping, whereas the rate damping on the telescope is furnished by an angular accelerometer and an electrical integration. The angular accelerometer also improves the pointing accuracy, as will be described in Section 7.4. A double electrical integration (Type II servo) is used in the mirror drive compensation. This allows the tertiary mirror to follow shuttle vehicle rates with theoretically zero error. Other possible servo drive configurations are discussed in Section 7.3.

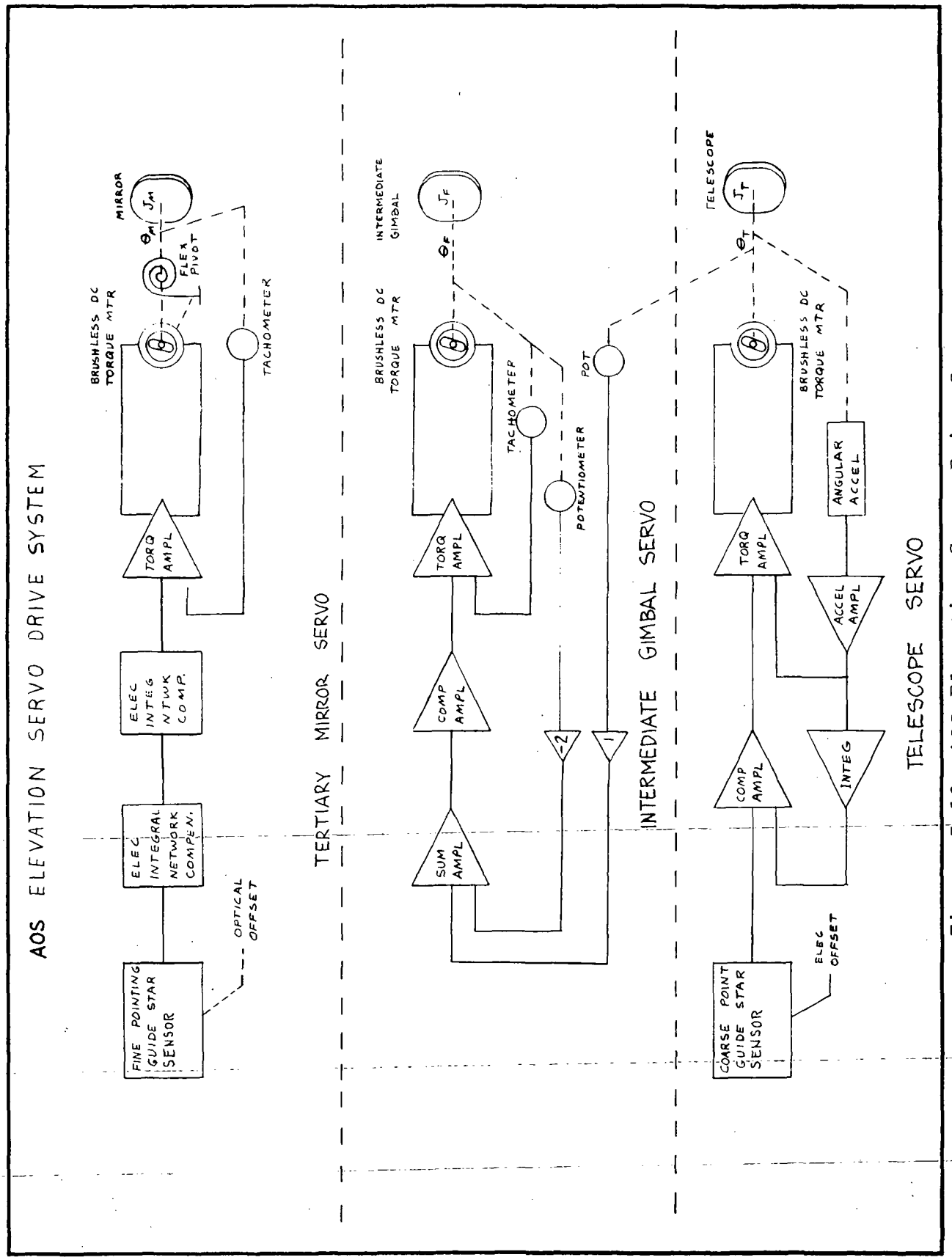

Figure 7-10 AOS Elevation Servo Drive System

7.3 CONTROL SYSTEM PRELIMINARY DESIGN AND SPECIFICATION

The elevation axes were modeled using the IBM 1130 Continuous System Modeling Program (1130 CSMP) in which the functional blocks at the input language represent the elements and organization of an analog computer. This program was used since it allows easy experimentation with various system configurations and parameters. The telescope, intermediate elevation gimbal, and tertiary mirror loops were studied simultaneously, considering all interconnections and cross-coupling between the loops. The effects of vehicle motion and sensor noise on pointing accuracy were studied.

The conventions and assumed parameters used in the detailed study of the elevation axes are given in Figure 7-11. All angles are measured with respect to the target star. For example, Θ_T is the angle between the telescope elevation pointing axis and the target star. The assumed vehicle motion is also given in Figure 7-11. The ±0.1 degree per second vehicle rate and ±0.5 degree vehicle deadband are values furnished early in the AOS study. Other parameters such as moment of inertia values, are estimates based on system size and configuration. Values pertaining to components, such as flex pivot spring constants, are taken from manufacturer's catalog data. All assumed models of devices are derived from existing hardware.

7.3.1 Positive Feedback Control of Flexure Pivots

The block diagram of the elevation axes using positive feedback damping control of the flex pivots is given in Figure 7-12. This damping technique is used on the Skylab S055A primary mirror, and has been quite successful.[1,2] The tertiary mirror is mounted in a two-gimbal frame which uses spring flex pivots for gimbal supports. The gimbals are driven by brushless dc torque motors.

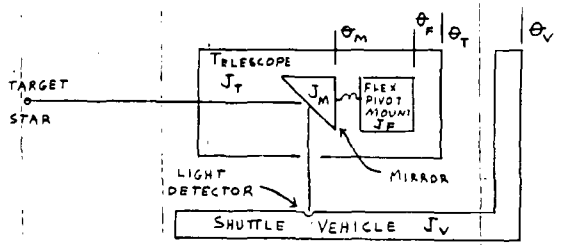

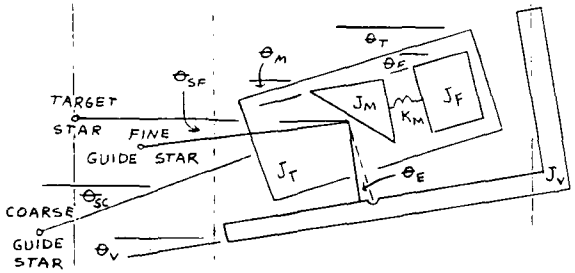

ERROR DETECTOR CONVENTION

CCW ⇒ + ROTATION

CW ⇒ − ROTATION

$\theta_M^+ \Rightarrow \theta_E \rightarrow +2\theta_M$

$\theta_V^+ \Rightarrow \theta_E \rightarrow -\theta_V$

$\Rightarrow \theta_E = 2\theta_M - \theta_V$

SHUTTLE VEHICLE MOTION

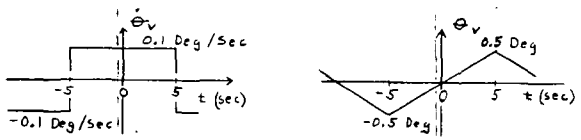

ASSUMED CONSTANTS

MIRROR DRIVE:

$J_M = 0.05$ Slug-Ft^2

$K_M = 107.5$ Lb-Ft/Rad (0.1 Oz-In/Rad)

$\omega_M = \sqrt{K_M/J_M} = 46.4$ Rad/sec (7.4 Hz)

POS FDBK SYS

$S^2 + S\,300 + K_F/J_M$

$= (S+\alpha)(S+\gamma)$

$= (S+7.357)(S+292.6)$

$K_D = 10$

$K_A = \frac{2K_D}{J_M} = 400$ (Accel. Const.)

TACH FDBK SYS

$S^2 + S\frac{K_{MV}}{J_M} + \frac{K_M}{J_M}$

$= (S+21.5)(S+100)$

$K_{MV} = 6.075$

$K_D = 13438$

$K_A = \frac{2K_D}{K_M} = 250$ (Accel. Const.)

INTERMEDIATE GIMBAL DRIVE:

$J_F = 0.06$ Slug-Ft^2 Bearing Friction = 0.01 Lb-Ft = 1.92 Oz-In.

$K_{FV} = 10$ $K_{PM} = 3$ $K_{PE} = 1250$ $K_{VP} = \frac{2K_{PE}}{K_{FV}} = 250$ (Vel Const.)

OPEN LOOP TRANS FUNC $\frac{2K_{PM}/K_{FV}}{S\left[1 + S\frac{J_F}{K_{PM}K_{FV}}\right]} = \frac{250}{S\left[1+\frac{S}{500}\right]} = \frac{125000}{S(S+500)}$

CHARACTERISTIC EQUATION $S^2 + S\frac{K_{PM}K_{FV}}{J_F} + \frac{2K_{PE}K_{PM}}{J_F} = (S+250+j250)(S+250-j250)$

TELESCOPE DRIVE

$J_T = 300$ Slug-Ft^2 Bearing Friction = 0.2 Lb-Ft = 38.4 Oz-In

$K_{TV} = 10$ $K_{TM} = 300$ $K_{TE} = 15$ $K_{VT} = \frac{K_{TE}}{K_T} = 1.5$ (Vel Const.)

OPEN LOOP TRANS FUNC $\frac{K_{TE}/K_{FV}}{S\left(1+\frac{S}{10}\right)\left(1+S\frac{J_T}{K_{TM}K_{TV}}\right)} = \frac{1.5}{S\left(1+\frac{S}{10}\right)^2} = \frac{150}{S(S+10)^2}$

CHARACTERISTIC EQUATION $S^3 + S^2 20 + S\,100 + 150 \approx (S+3.3)^2(S+13.5)$

ANGULAR ACCELEROMETER

$\omega_A = 200$ (33.3 Hz)

$S_A = 0.5$

$\frac{S^2}{S^2 + 2S_A\omega_A S + \omega_A^2} = \frac{S^2}{S^2 + S200 + 40000}$

Figure 7-11 AOS Pointing Systems-Elevation Axis Notation

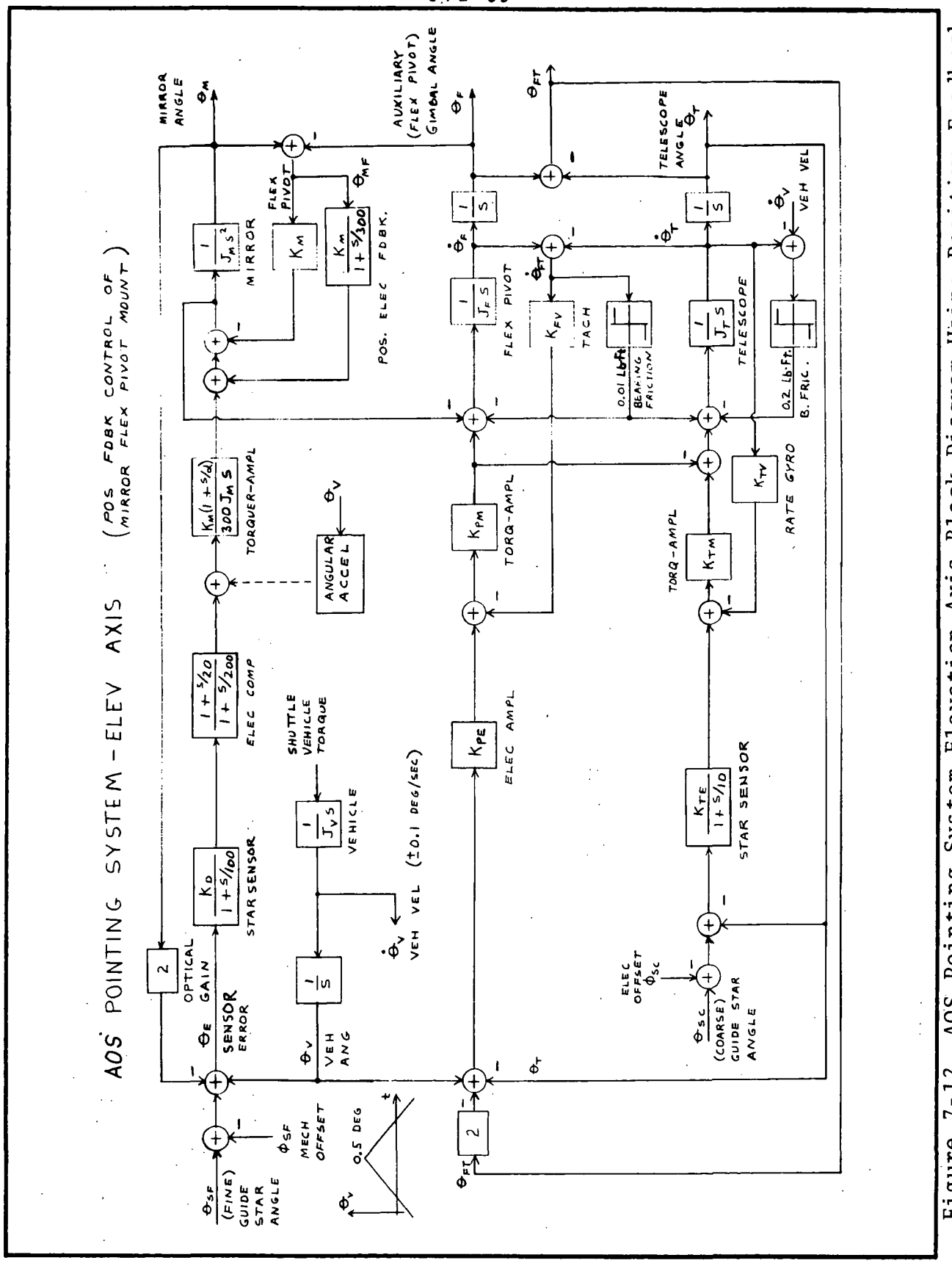

Figure 7-12 AOS Pointing System-Elevation Axis Block Diagram Using Positive Feedback Damping of Flexure Pivots

A linear variable differential transformer (LVDT) is mounted on each gimbal to sense the mirror position in each axis, with a separate servo controlling each axis. The demodulated LVDT output signal is used as the gimbal position indicator. The signal is fed into the torque motor with polarity and gain set to cancel the flexure pivot spring torque. Due to the imperfect cancellation caused by the demodulation filter phase lag, the effective damped spring-mass system appears to the servo loop as a single integration followed by a low pass filter. A second integration is performed electronically to give a Type II servo. Forward loop lead compensation is used to stabilize the mirror servo loop.

Tachometer rate feedback is used for damping the intermediate (flex pivot) elevation gimbal, and a rate gyro provides damping for the telescope gimbal. Other types of compensation or devices could be used, but the results would be similar to those presented below. Exact (high frequency) modeling of the rate gyro is not necessary because of the low bandwidth of the telescope gimbal servo. No additional filtering is used in these loops, other than that in the coarse star sensor. The dc torque motor time constant is neglected, as it is negligible compared to the servo bandwidth for a properly selected motor. The effects of the motor lag can be eliminated by current driving the motor.

The vehicle motion input to the system is given in Figure 7-11. The sample and hold time lag and filtering effect of the star sensors are modeled as first-order simple filters. This approximation is only valid for frequencies that are low compared to the sampling rate[3]. The only nonlinearity considered in the tracking system model is the disturbance torques caused by the friction of the telescope and auxiliary (flex pivot) gimbal bearings. Amplifier saturation is not considered as it can be controlled by judicious choice of gain distribution in the servo loops.

Other effects not considered in the analysis are the random vibration environment of the telescope assembly and structural bending of the telescope optical support elements. These effects, although important, usually cannot be analyzed until more is known about the actual hardware design. As a general rule, the servo bandwidth cannot be greater than 1/5 to 1/3 that of any structural resonances within the loop.

A complete cycle of the vehicle motion requires 20 seconds realtime. The dominant time constants of the elevation axes range from 0.3 second for the telescope loop to approximately 0.03 second for the flex pivot-mirror loop. Hence, the servo errors have essentially reached steady state conditions within a few seconds after spacecraft reaction control system (RCS) actuation (this reverses the rotational direction of the shuttle vehicle and occurs at t = 5 seconds in Figure 7-11). In order to conserve computing time and eliminate excessive readout data, total time for the simulation is 2.5 seconds. This includes 1 second before RCS actuation to allow erroneous initial turn-on transients to die out, and 1 1/2 seconds after RCS actuation to establish steady-state error conditions.

Figure 7-13 is a computer plot of the fine guidance error response to the vehicle motion described above. The transients occurring prior to t = 1 second should be ignored as explained above. The large transient immediately following RCS actuation is as expected, but the "hang-off" error was unexpected. Extensive investigation showed that this error is caused by the telescope gimbal rates coupling into the mirror loop. This error can be reduced somewhat by keeping the telescope bearing friction as small as possible. This possible problem area would not have appeared in the usual single-axis model, where each servo is studied independently.

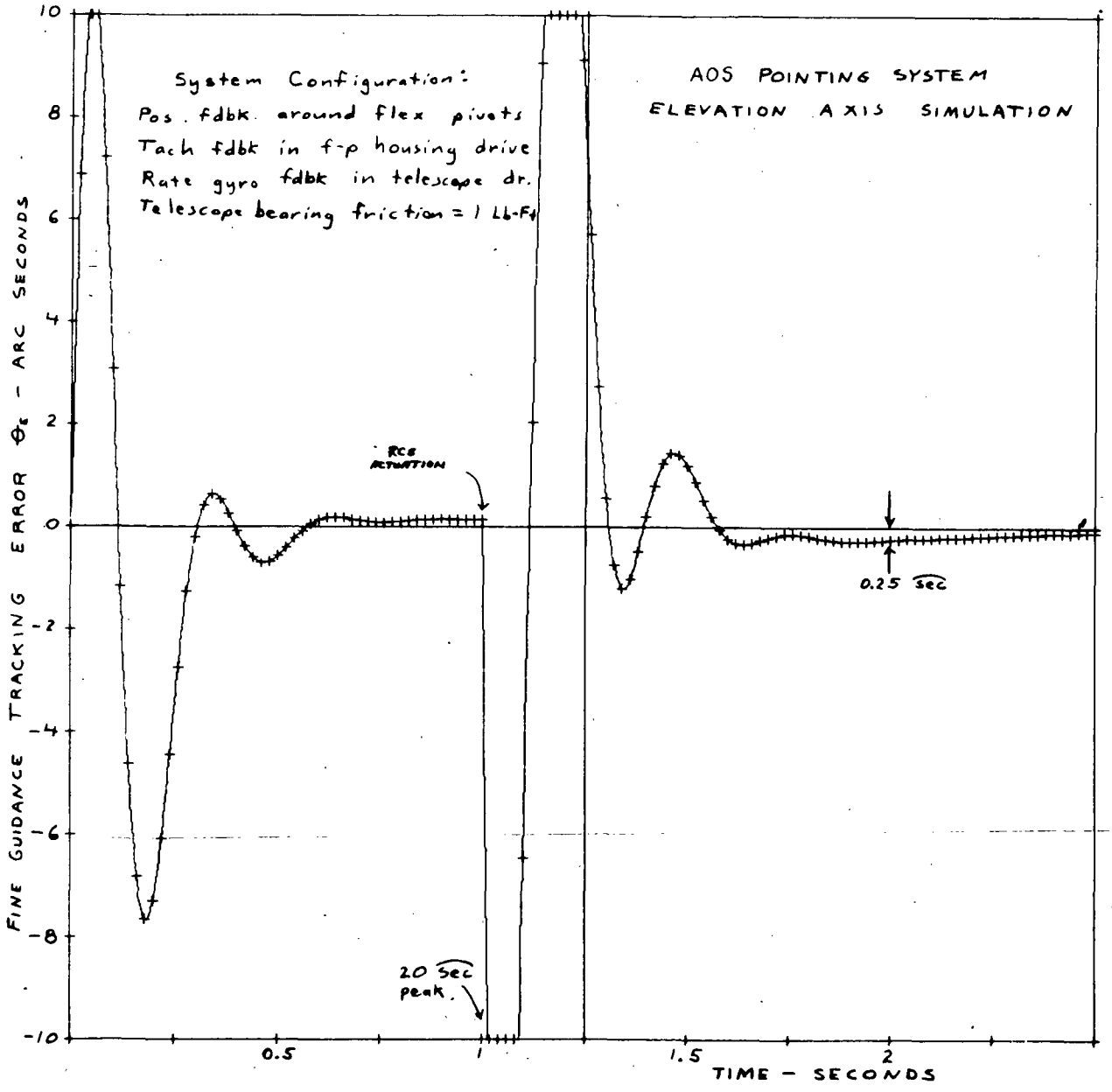

Figure 7-13 Fine Guidance Error Response to Vehicle Motion (Positive Feedback Damping)

Figure 7-14 shows the effect of a small error in the positive feedback gain on the fine guidance error response to vehicle motion.

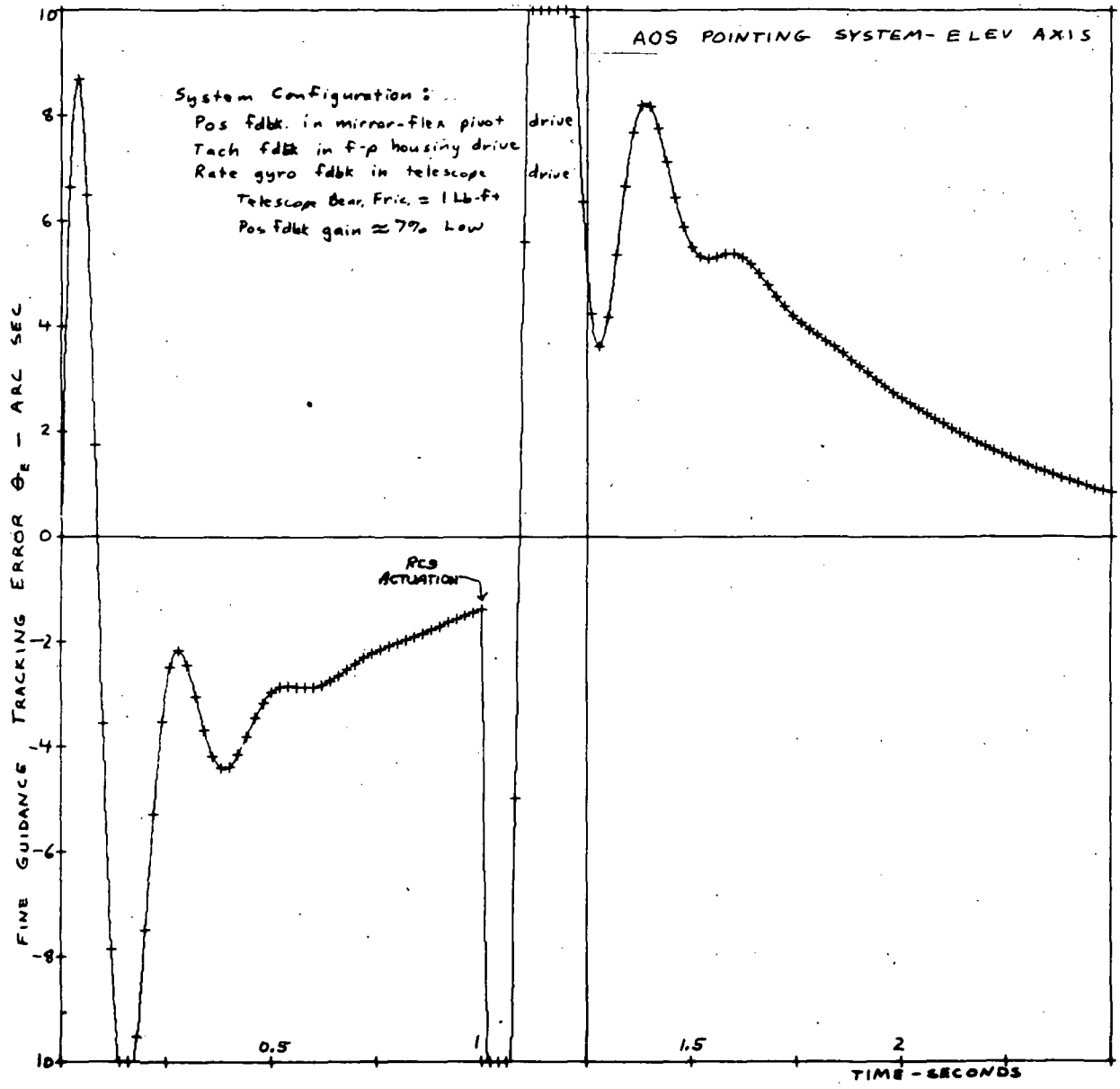

Figure 7-14 Effect of Small Error in Positive Feedback Gain

The long settling time required to reach a reasonable error following firing of the attitude control jets is completely unacceptable.

The positive feedback gain consists of the LVDT gain, the demodulator gain, the power amplifier gain, and the torque constant of the dc torque motor. The gains must be selected to equal the flex pivot spring constant. Since it is unreasonable to assume the gains can be matched better than 7 percent over all environmental conditions, it was concluded that positive feedback damping of the flex pivots cannot give the accuracy required of the fine guidance tracking system.

7.3.2 Tachometer Damping of the Fine Guidance Servo

Figure 7-15 is the block diagram of the elevation axis using tachometer damping of the flex pivots. The tertiary mirror is supported with a two-axis flex pivot gimbal structure, and driven with brushless dc torque motors. A rate sensing device such as a dc tachometer is mounted across the flex pivot. The tachometer signal is fed into the torquer amplifier with negative polarity to electrically damp the flex pivot. Two electrical integrations are used in the mirror loop to give a Type II servo. Forward loop lead compensation is used to stabilize the mirror servo loop.

In the first configuration studied, a rate gyro was used for damping the telescope gimbal instead of the angular accelerometer shown in Figure 7-15. Tachometer rate feedback provided damping for the intermediate (flex pivot) elevation gimbal. Other elements in the system such as vehicle motion and star tracker simulation were modeled as in Section 7.3.1. Rate gyro flex pivot damping was tried but gave much larger transient errors than the tachometer damping. Figure 7-16 is a computer plot of the fine guidance error response to the vehicle motion. The transient peak error immediately following the firing of the attitude control jets is considerably improved over the case using positive feedback

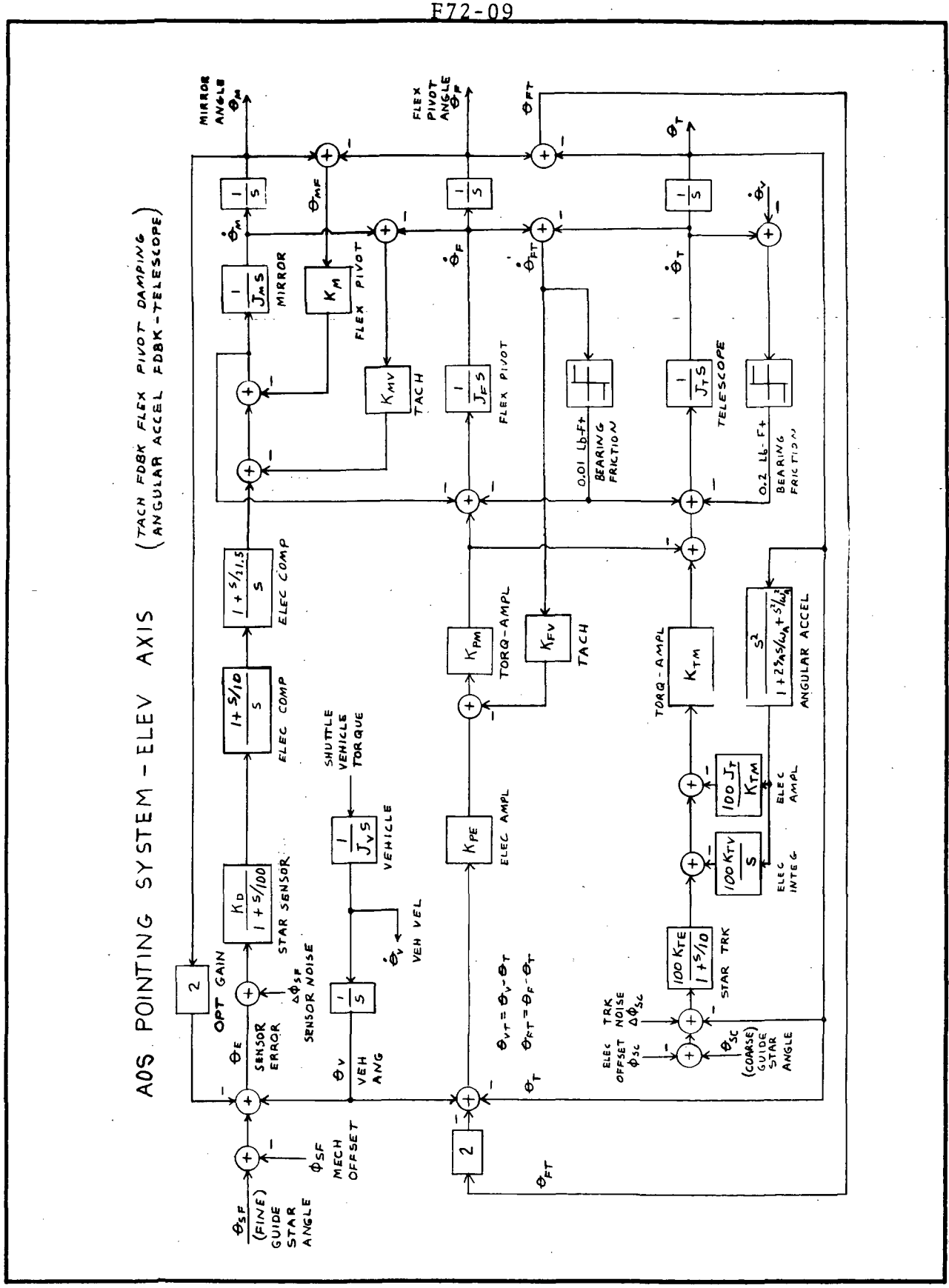

Figure 7-15 AOS Pointing System-Elevation Axis Block Diagram Using Tachometer Damping of Flexure Pivots

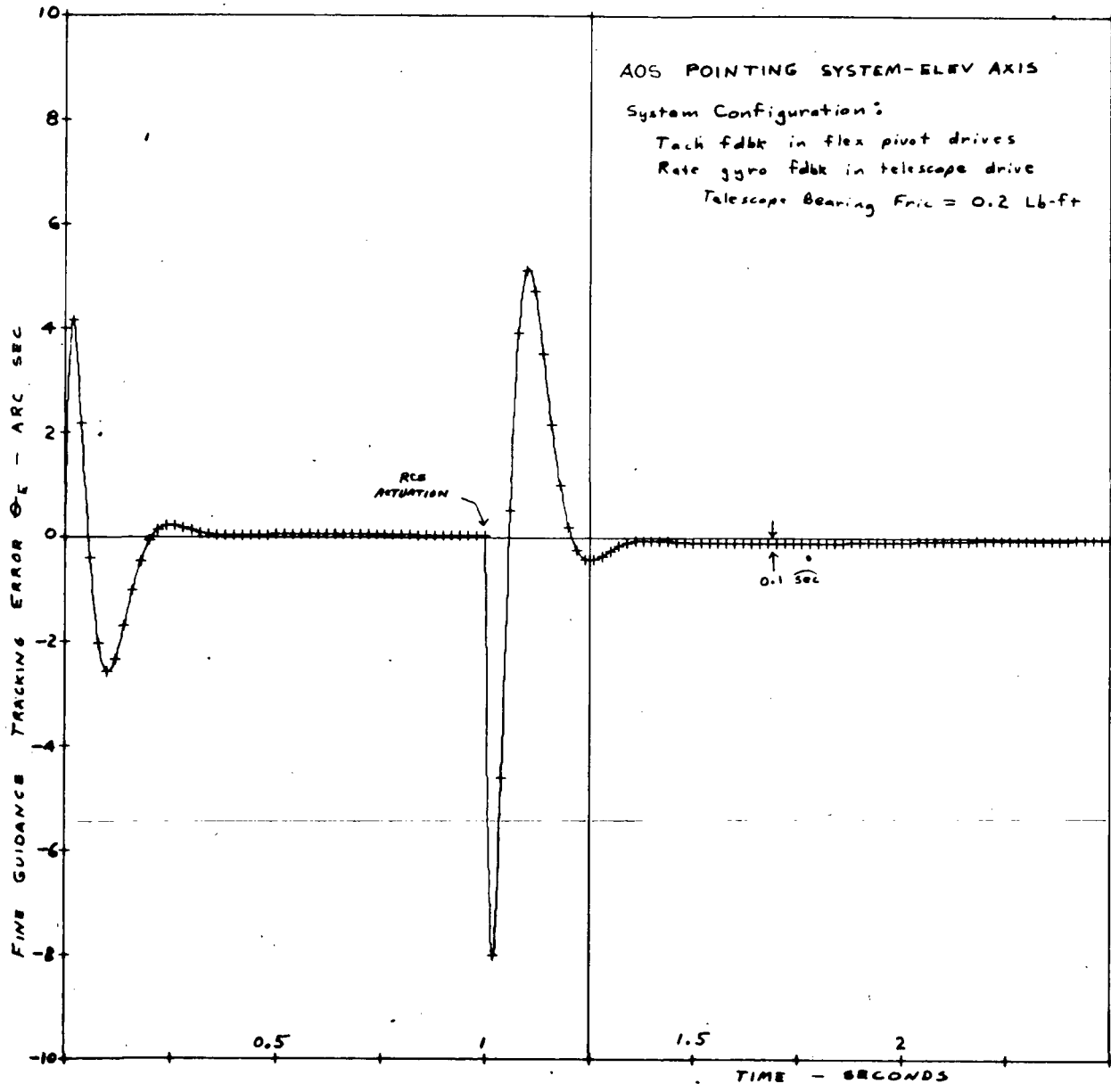

Figure 7-16 Fine Guidance Error Response to Vehicle Motion (Tachometer Damping)

flex pivot damping, but is still quite large (approximately 8 arc-seconds). The error settles to 0.1 arc-second within 0.3 second following the firing of the jets. As explained in Section 7.3.1,

the "hang-off" error is caused by the coupling of the telescope gimbal rate into the mirror loop.

In an effort to improve the tracking error, the effects of both locking the intermediate (flex pivot) elevation axis to the telescope, and of allowing it to "float" uncontrolled, were studied. Both of these system configurations led to degraded performance. Several simulation runs were made to determine the effects of bearing friction on the fine guidance tracking error. The so-called "hang-off" tracking error is negligible when the telescope bearing friction is reduced to zero. This result led to the investigations using an angular accelerometer to decrease the effects of bearing friction.

One of the particularly significant attributes of the angular accelerometer is its ability to sense a variable (acceleration) directly proportional to the torques acting on a body. Also, rate sensing is readily available by electronically integrating the accelerometer output signal. If the accelerometer output is amplified and used as negative feedback to the torque motor, the effect of disturbance torques is reduced by the loop gain. The loss in gain due to the negative feedback loop has to be made up in the external loop servo electronics. This is shown in Figure 7-15, where the amplifier gains have been increased by 100 in the telescope loop. Note that the requirement for a rate gyro has been eliminated.

Use of the angular accelerometer for stabilization and control has become extremely practical and cost-effective due to recent advances in the state-of-the-art in design of the Fluid Rotor Angular Accelerometer (FRAA)[4].

The angular accelerometer as a simple rotation sensor has evolved over the past ten years to a lightweight, highly sensitive, rugged instrument with low power consumption and virtually infinite life.

The device eliminates the rotating elements, run-up time, power consumption and wearout life of gyroscopes. Design at present permits full-scale rate ranges as high as 200 radians per second and as low as 0.1 radian per second. The FRAA has already found numerous applications in the aerospace field, including instrumentation, control, attitude stabilization, and short-term direction reference.

Simulation of the star sensor noise is accomplished by using the jitter (U) block of CSMP. The J block output is a random number, with uniform probability density between ±1, selected at each new integration interval. Suppose the J block is followed by a gain (G) block with gain d. Then, for a small integration interval compared to the system time constants, the G block output may be considered a random process with a zero mean and a variance of

$$\sigma^2 = \int_{-d}^{d} x^2 \, p(x)dx = \frac{1}{2d} \int_{-d}^{d} x^2 \, dx = \frac{d^2}{3}$$

where p(x) = uniform probability density function over ±d.

The coarse and fine guide sensor error is simulated by selecting d such that σ = rms value of the sensor noise. Initial tests were run for the fine guidance star tracker with d = 0.1 arc-second, which is equivalent to an rms noise

$$\sigma = \frac{0.1}{\sqrt{3}} \approx 0.06 \text{ arc-second rms.}$$

and for the coarse guidance star sensor with d = 10 arc-seconds, which is equivalent to an rms noise

$$\sigma = \frac{10}{\sqrt{3\ 1/2}} \approx 6.0 \text{ arc-seconds rms.}$$

Figure 7-17 is a CSMP computer plot of the fine guidance error response to vehicle motion. The transient following the firing of the attitude control jets decays to less than 0.02 arc-second peak

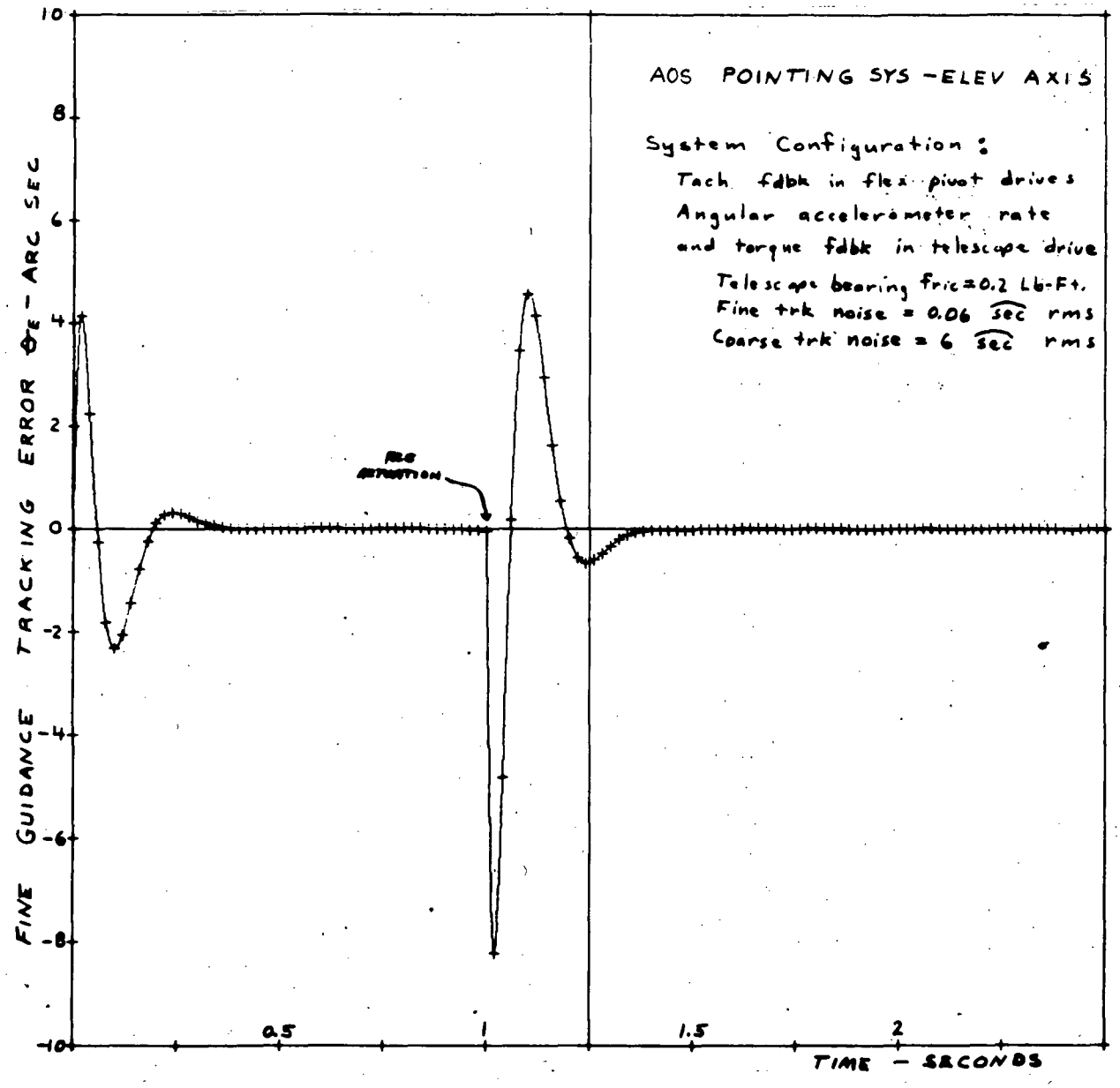

Figure 7-17 Fine Guidance Error Response to Vehicle Motion, Fine Guidance Error Sensor and Coarse Star Noise Applied Simultaneously

error within 0.4 second. The computer simulation also indicated a telescope gimbal tracking error of 0.2 arc second peak. These results must be viewed with certain reservations, since they are an order of magnitude better than any tracking systems known to exist today. Other possible error sources such as shuttle vehicle random vibrations, structural bending, misalignment of the optical elements, and drift in the electronics must be considered in a complete detailed error analysis.

Several CSMP computer runs were made to determine the sensitivity of the pointing system to fine guide error sensor noise. The coarse tracker noise was set at 12 arc-seconds rms for all runs, which is the expected noise level when tracking a minimum brightness star. Figures 7-18 and 7-19 are plots of the fine guidance error response, using f/25 optics, to sensor noise corresponding to average and minimum star brightness, respectively. The peak sensing error after RCS actuation transients have decayed is less than 0.04 arc-second in both cases. The similarity of the two response curves indicates the major error source was from the coarse star sensor noise. Figures 7-20 and 7-21 are plots of the fine guidance error response, using f/10 optics, to sensor noise corresponding to average and minimum star brightness, respectively. The peak sensing error due to noise is approximately 0.05 arc-second for the average star brightness, and less than 0.15 arc-second for a minimum star brightness.

7.3.3 Angular Accelerometer Considerations

The fine guide error sensor results of Section 7.3.2 suggest many areas for possible further study. Of primary importance, it should be remembered that these are only theoretical results. The sensitivity of the fine guidance loop to the telescope gimbal motion should be investigated further in a detailed design study. Also, extrapolation of these results leads to the conclusion that the tertiary

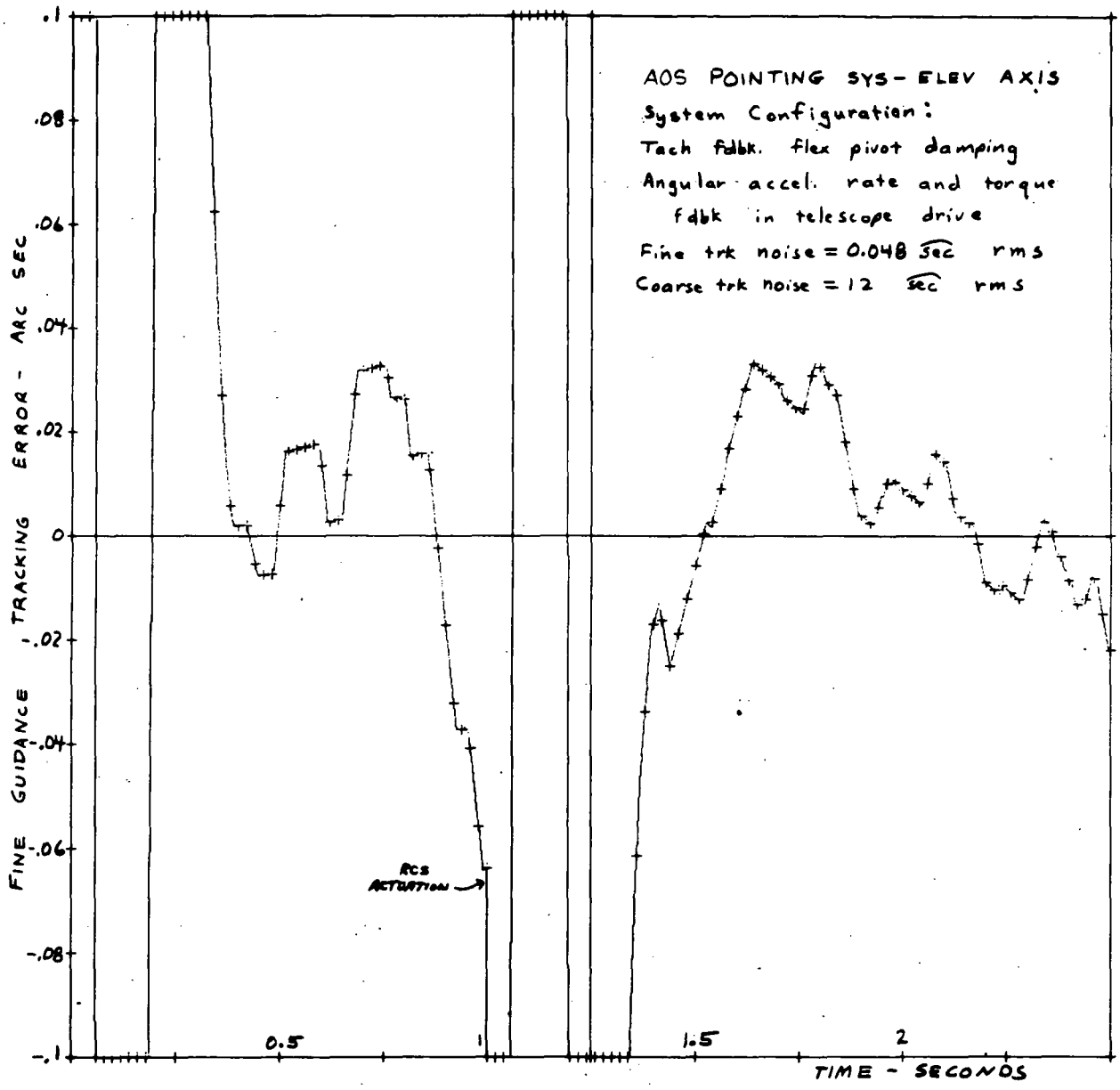

Figure 7-18 Fine Guidance Error Response to Sensor Noise for Average Star Brightness (Using f/25 Optics)

mirror can be bearing-mounted if an angular accelerometer is used in the fine guidance loop also. Such a configuration would simplify the mirror gimbaling problems, but requires actual hardware testing.

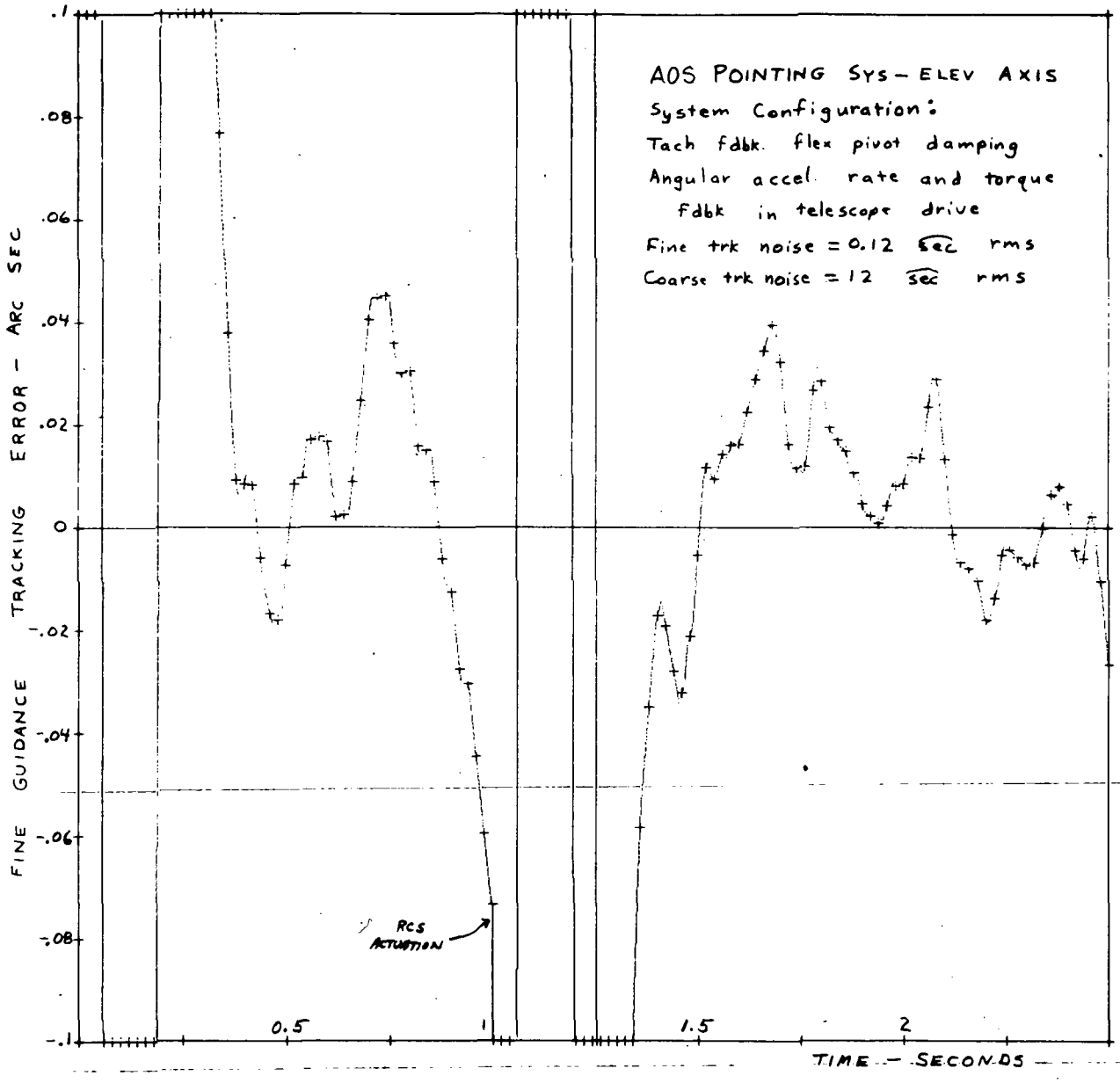

Figure 7-19 Fine Guidance Error Response to Sensor Noise for Minimum Star Brightness (Using f/25 Optics)

The transient errors following the firing of the shuttle RCS pose certain problems. Their magnitude and duration make it impractical to actively utilize the telescope for scientific data gathering

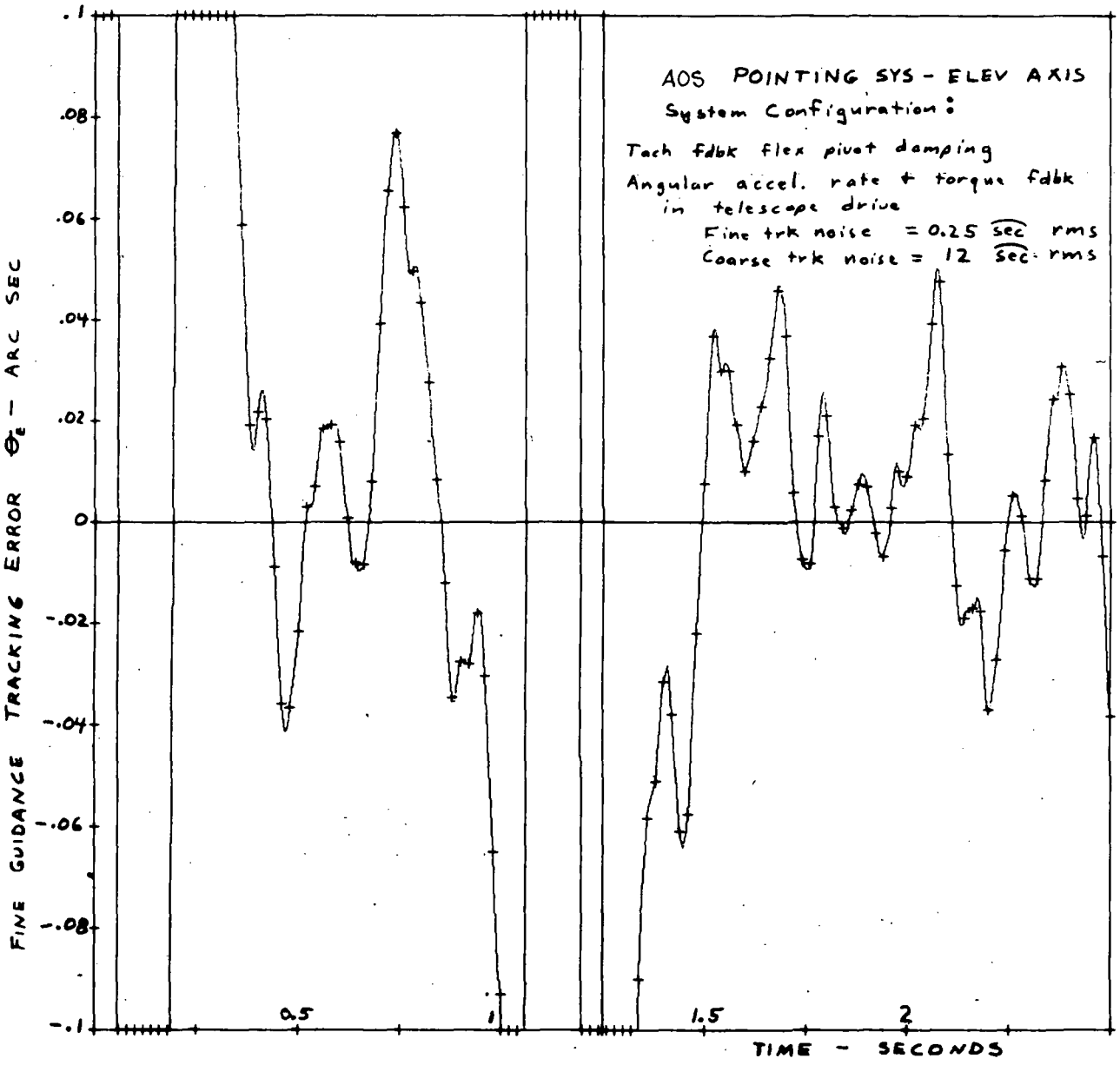

Figure 7-20 Fine Guidance Error Response to Sensor Noise for Average Star Brightness (Using f/10 Optics)

during this transient period. It will, therefore, be necessary to block the optical path to the experiment for a period of 1/2 second following RCS firing. This can be accomplished by operating a

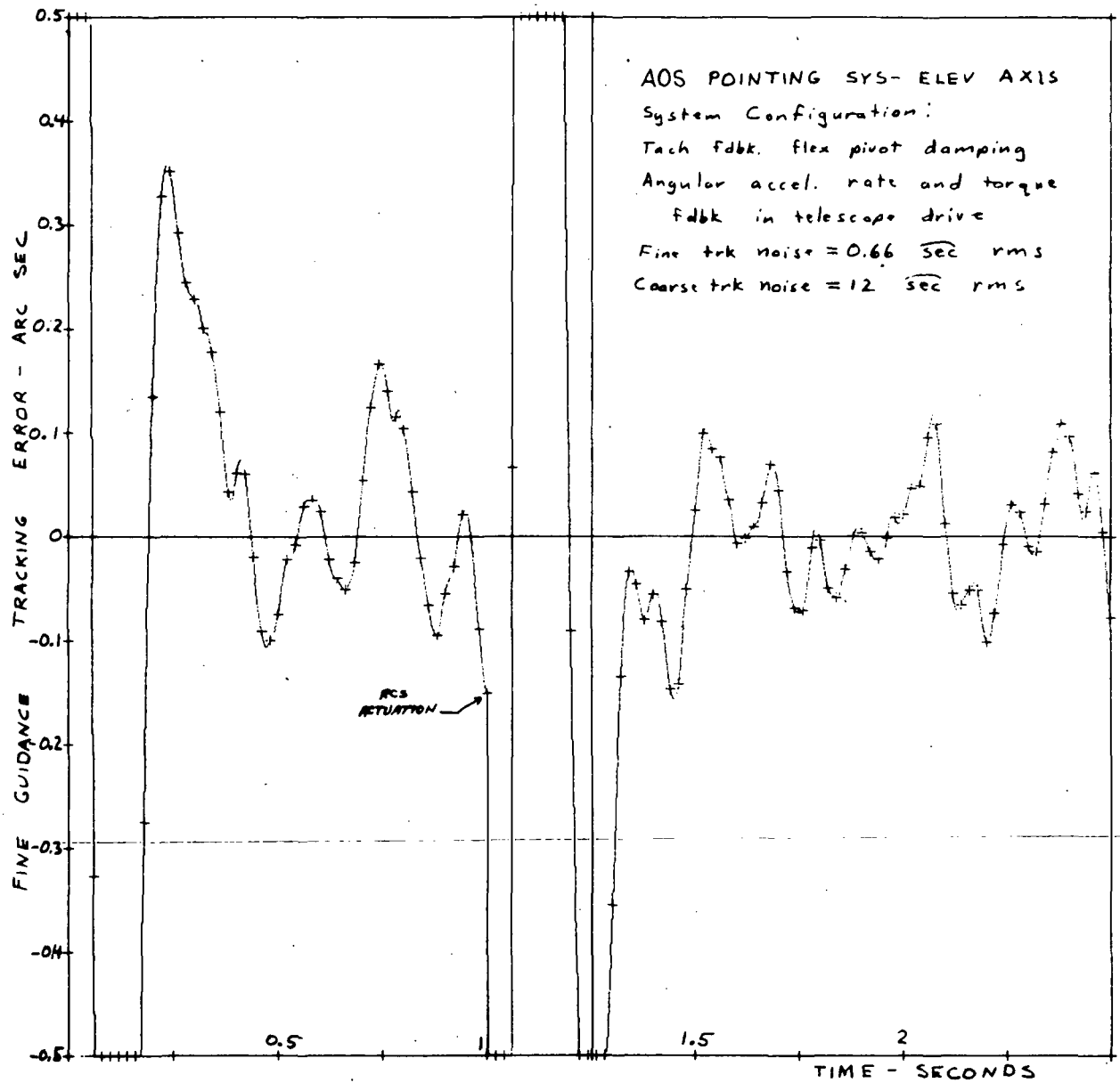

Figure 7-21 Fine Guidance Error Response to Sensor Noise for Minimum Star Brightness (Using f/10 Optics)

shutter mechanism with an "RCS Fire" signal furnished by the shuttle attitude control system.

The possibility of smaller shuttle motion suggests certain areas for further study. Since the errors will decrease with smaller vehicle rates, the shutter mechanism may not be necessary if the rate decrease is sufficient. Also, a small shuttle-vehicle angular error deadband would make it possible to lock the telescope to the vehicle during star observations. The effect of this on the fine guidance tracking error should be studied. The combination of improved shuttle vehicle attitude control and the use of the angular accelerometer in the sensing loops should easily meet the required pointing accuracy.

7.4 IMAGE ROLL CONTROL

As explained in Section 7.2.3, rotations of the shuttle about the telescope line of sight produce target error motion proportional to the angle of the guide star from the center of the field of view. The roll attitude must be controlled to less than 5 arc-seconds in order to maintain the required accuracy in the fine guide pointing servo. Pointing error sensing for the roll track loop is provided by a roll star tracker mounted on the telescope assembly, orthogonal to the coarse guidance star sensor. Accuracy and bandwidth requirements are such that the coarse tracker design can also be used for the roll star tracker.

The operation of the roll sensor servo is very similar to that of the telescope pointing servo described in Section 7.2.2. The roll gimbal is driven with a brushless dc torque motor, and is bearing-mounted to the shuttle. Rate feedback compensation is obtained from a rate gyro, or possibly from an angular accelerometer. The computer results of Section 7.3 indicate that an angular accelerometer considerably improves the pointing accuracy, although further tests are necessary to confirm the computer results. Final design selection of the rate sensor can be made only after all factors, such as bandwidth, accuracy, cost, reliability, etc. are better defined. This definition can be made only after shuttle performance has been explicitly determined.

REFERENCES

1. Culver, R. C., The Use of Positive Feedback to Control Spring Mass Systems. Presented to American Astronautical Society Symposium, Denver, Colorado, July 1968. Ball Brothers Research Corporation Report No. M68-03, Boulder, Colorado.

2. Highman, C. O., A Scanning Mirror System for the Apollo Telescope Mount Ultraviolet Spectroheliometer, Presented at the Fifth Aerospace Mechanisms Symposium, Goddard Space Flight Center, Greenbelt, Maryland, June 15-16, 1970.

3. Tou, Julius T., Digital and Sampled-Data Control Systems, Chapter 9, McGraw-Hill Book Co., New York, 1959.

4. Leigh, Philip G., Use of the Angular Accelerometer for Stabilization and Control, Systron-Donner Corporation, Concord, California.

Section 8
AOS SYSTEM CONSIDERATIONS

8.1 DATA HANDLING REQUIREMENTS

Scientific and housekeeping data from the AOS will be made available to the payload specialist wherever possible in real time. The Shuttle is projected to have on-board computer capability for data processing. The capability at the present time is projected to be 10,000 32-bit words reserved exclusively for payloads. Further definition will be needed to determine the actual requirement for all the science packages that may fly with the AOS, but the approximate requirement will be:

- 3,000 words for control system computations
- 1,000 words for data display computations
- Remaining 6,000 words for experiment data computation and buffers

The experiment computation requirement is purely a best guess at this time since the exact nature of the principal investigator's data output is not known.

The Shuttle-provided shuttle-to-ground link of 256 kbps maximum is a more than adequate rate for the AOS; however, formatting and interfacing require further definition.

8.1.1 Instrument Data - Electronic Output

The SAL instruments will employ SEC vidicons with signal conditioning output circuits. These detectors will produce data that

will be partially processed in real time and stored on the Shuttle. The data could be telemetered to the ground as well; however, on-board storage with rapid recall is recommended. The rapid recall will enable the payload specialist to make real-time comparisons and evaluations for optimum utilization of observation time.

The payload specialist also should be able to recall data, especially housekeeping data, in the event of equipment failure. If this should occur, alternate modes of operation can then be determined.

Real time data display of the electrical outputs will be provided for both the imaging and spectral instrumentation. The imaging instrument outputs will be fed into a scan converter and be displayed on a viewer. A scan converter will be necessary since data acquisition will be over extended time periods. The scan converter will display the information in "pictorial" form, showing the payload specialist the observed field.

Spectral data is better displayed by viewing an analog output produced by an oscilloscope. Two methods of display are possible. One is simply to accumulate the data and display it on a storage display. The other is to store the data in a computer memory and display it on a CRT by repeated cycling of the memory. This latter method is preferred since the AOS will have on-board computer capability. Storage-type CRT's do not permit recall or extended storage for observing programs in excess of 30 minutes with reasonable resolution.

8.1.2 Instrument Data---Photographic

The AOS instruments will also use electronographic cameras as detectors. These use as a recording medium either film or emulsions.

Near real time information by film examination will be possible. The major problem with data handling will be developing. At present, the only quick developing techniques that could be found were those used by Kodak and Polaroid. The Kodak system, called BIMAT, is a dry developing process and currently is only applicable to polyester film.

These methods will be used to obtain "quick look" data only. Since resolution is limited, their use in applications leading to detailed analysis is not recommended. These applications should use the photographic methods discussed in Section 5. These methods employ films and emulsions that require special processing and are better done in ground-based facilities.

8.2 POWER REQUIREMENTS

The baseline power made available to payloads from the Shuttle is 3 kw average with 6 kw peak for a total of 50 kw hours. Under study is a power system with 6 kw average and peak and total power as yet undetermined. Table 8-1 identifies the approximate AOS power requirements. It does not include power for other science packages or for the Sortie Lab for operation of computers and other equipment.

The hardware listed in Table 8-1 can be specifically designed with low power components, decreasing the average power by approximately 30 percent. Without low power design, the operating life based on a total power capability of 50 kwh is 65 hours. With low-power components designed into the hardware, the approximate operating life is 100 hours. Without an increase in power available from the Shuttle and assuming a 7-day mission in which 60 percent of the time will be observing time, a power capability of 50 kwh is marginal. Further study leading to increasing the power available from the Shuttle is therefore recommended.

Table 8-1
AOS POWER REQUIREMENTS

	Avg Pwr (w)	Pk Pwr (w)
Telescope Guidance		
Coarse Servo	30	280
Intermediate Servo	5	20
Tertiary Mirror Servo	5	20
Optical Bench Roll Control Servo	10	30
Instrument Operation		
SEC Detector Packages (2 ea.)	50	50
Electronographic Camera	25	25
Optical Bench Positioning	15	15
Peripheral Equipment		
Pointer Control and Monitoring Panel	10	10
Optical Bench Control Panel	10	10
Instrument Data Display Panel	120	120
Telescope		
Thermal Control	500	1,000
	780	1,580

8.3 WEIGHT

The expected weights of the major AOS components are tabulated below:

Item	Weight (lbs./kg.)
Telescope	710/323
Telescope Mount	480/218
Optical Bench	374/170
Echelle Spectrograph w/Detectors	175/80
Imaging Spectrograph w/Detectors	175/80
Lyman Spectrometer	100/45
Pointing Control and Monitoring Panel	200/90
Experiment Data Display Panel	150/68
Optical Bench Control Panel	150/68
TOTAL	2514/1142

Table 8-2 is an itemized listing of the weights and inertias of the movable structures of the AOS.

8.4 GENERAL SYSTEM CONSIDERATIONS

8.4.1 Shuttle Parameters

The telescope pointing and stabilization model used in the study should be considered an idealized model in that it does not take into account random inputs from the Shuttle, which were not available. The model did use the original Shuttle stabilization number of ±0.5° in each axis. Available shuttle data now indicates that stabilization to ±30 arc-seconds may be attainable. This and other new Shuttle performance data must be considered in the design of the telescope pointing and stabilization system.

Table 8-2
WEIGHT AND MOMENTS OF INERTIA

PRELIMINARY MASS PROPERTIES 10/12/72 H. V. ROYER

ITEM	DWG NO	C. G. COORDINATE (INCHES)			WEIGHT (POUNDS)	MOMENTS OF INERTIA (SLUG-FEET SQUARED)			PRODUCTS OF INERTIA (SLUG-FEET SQUARED)		
		X	Y	Z	WT	IXX	IYY	IZZ	PXY	PYZ	PXZ
PORTION ABOUT ELEVATION											
MAIN MIRROR		-42.800	0.000	59.250	187.500	8.040	4.185	4.185			
MOVABLE MIRROR & FRAME		-7.000	0.000	59.250	21.250	0.033	0.022	0.033			
MIRROR MECHANISMS		-7.500	0.000	59.250	12.000	0.016	0.016	0.016			
PEDESTAL		-29.000	0.000	59.250	18.000	0.056	0.452	0.452			
LWR BULKHEAD		-48.000	0.000	59.250	56.800	3.387	1.693	1.693			
PIVOT POINT BLKD		0.000	0.000	59.250	38.750	3.926	1.963	1.963			
BLKD SECONDARY MIRROR 300MM		48.750	0.000	59.250	19.450	1.962	0.981	0.981			
BLKD SECONDARY MIRROR 200MM		64.750	0.000	59.250	19.450	1.962	0.981	0.981			
SECONDARY MIRROR 300MM		48.750	0.000	59.250	20.350	0.079	0.041	0.041			
UPPER BLKD		87.000	0.000	59.250	9.700	0.981	0.490	0.490			
STRUCTURE (INVAR)		20.750	0.000	59.250	135.000	15.725	53.178	53.178			
MYLAR INSULATION		20.750	0.000	59.250	8.000	0.923	3.194	3.194			
HEATERS		20.750	0.000	59.250	30.000	3.535	10.804	10.804			
SPIDER		60.000	0.000	59.250	15.000	0.658	0.329	0.329			
ELEVATION BEARINGS		0.000	0.000	59.250	20.500	0.292	0.292	0.584			
ELEVATION MOTOR , MOVEABLE		0.000	25.500	59.250	30.000	0.441	0.441	0.872			
STAR SENSOR PACKAGE		72.000	26.000	59.250	19.500	0.054	0.078	0.040			
ELECTRONICS PACKAGE		72.000	-26.000	59.250	19.500	0.054	0.078	0.040			
WIRING,ETC		0.000	-20.000	59.250	30.000	0.431	0.863	0.863			
SUM		-0.240	0.232	59.250	710.749	55.049	311.385	324.529	0.008	-0.000	0.000
AZIMUTH PORTION											
YOKE		0.000	0.000	36.500	204.000	5.401	10.233	11.744			
ELEVATION MOTOR , FIXED PART		0.000	25.500	0.000	30.000	0.441	0.441	0.872			
YOKE BASE		0.000	0.000	12.000	74.400	3.328	3.328	6.270			
MAIN BARREL		0.000	0.000	-20.000	168.000	16.721	16.721	11.621			
OUTER DOOR & BLKD		0.000	0.000	16.500	65.000	1.356	1.356	2.712			
MOVABLE PART OF AZIMUTH DRIVE		2.500	6.000	0.000	59.800	1.538	1.538	3.063			
MOVABLE PART OF OUTER B/R		0.000	6.000	-0.500	18.000	0.755	0.755	1.509			
MOVABLE PART OF INNER B/R		0.000	6.000	-38.500	18.000	0.755	0.755	1.509			
INSTRUMENT PACKAGE & SHELF		0.000	6.000	-25.000	110.000	0.696	2.763	2.458			
FIXED PART EL BEARINGS		0.000	0.000	0.000	20.500	0.292	0.292	0.584			
WIRING,ETC		0.000	-20.000	0.000	30.000	0.431	0.863	0.863			
SUM		0.187	1.754	3.258	797.699	137.681	137.215	91.157	0.137	-5.456	-0.105
TOTAL ABOUT AZIMUTH		-0.014	1.037	29.640	1508.449	447.309	703.005	375.889	0.198	-12.374	-2.048
FIXED PORTION											
FIXED PART OF OUTER B/R		0.000	6.000	-0.500	18.000	0.755	0.755	1.509			
FIXED PART OF INNER B/R		0.000	6.000	-38.500	18.000	0.755	0.755	1.509			
FIXED PART OF AZIMUTH DRIVE		2.500	6.000	0.000	59.800	1.538	1.538	3.063			
INNER SHELL & FLGS		-20.000	6.000	0.000	205.000	15.858	15.858	17.408			
INNER AIR-LOCK		-46.500	6.000	0.000	98.000	3.311	3.311	6.623			
SUM		-21.332	6.000	-1.760	398.800	27.712	52.061	54.462	-0.000	-0.000	-3.233
GRAND TOTAL		-4.471	2.075	23.074	1907.249	543.840	853.156	462.976	-7.005	-22.985	40.301

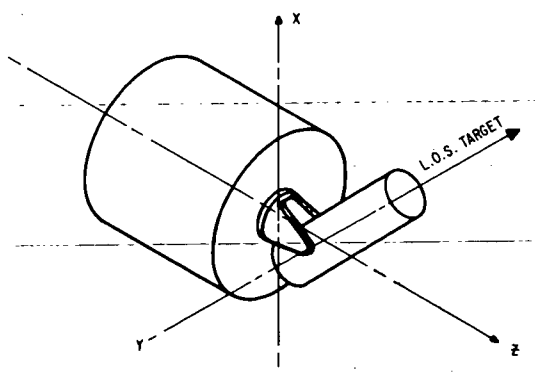

The guide star acquisition technique proposed for the AOS assumes that real-time shuttle attitude information will be available and can be interfaced with the AOS orientation system. The accuracy of this information relative to errors that may exist between orbiter position and the AOS position in the orbiter bay are not yet defined. This must also be incorporated in the follow-on AOS design and the acquisition mode then must be re-evaluated.

As previously mentioned, the present total power capability from the Shuttle is marginal for AOS operation. It is recommended that, if at all possible, this capability be increased.

8.4.2 Launch and Recovery

During the launch and recovery phases of the AOS, it will be necessary to have the telescope gimbals in a stored and locked position in order to prevent damage from the "g" loading and vibration environment. In addition to locking the telescope structure to the Sortie Lab, the tertiary mirror gimbal system must also be locked. These locking mechanisms will be remotely controlled from the Pointing Control and Monitoring panel. Figure 8-1 is a conceptual layout of the tertiary mirror gimbal and lock.

Locks will also be provided on the optical bench assembly and the fine sensor drive mechanism. Figure 8-2 is a conceptual layout of the fine sensor drive and lock mechanism. As stated in Section 7, the fine sensor must be positioned in a spherical focal plane; hence the need for a curved elevation rack.

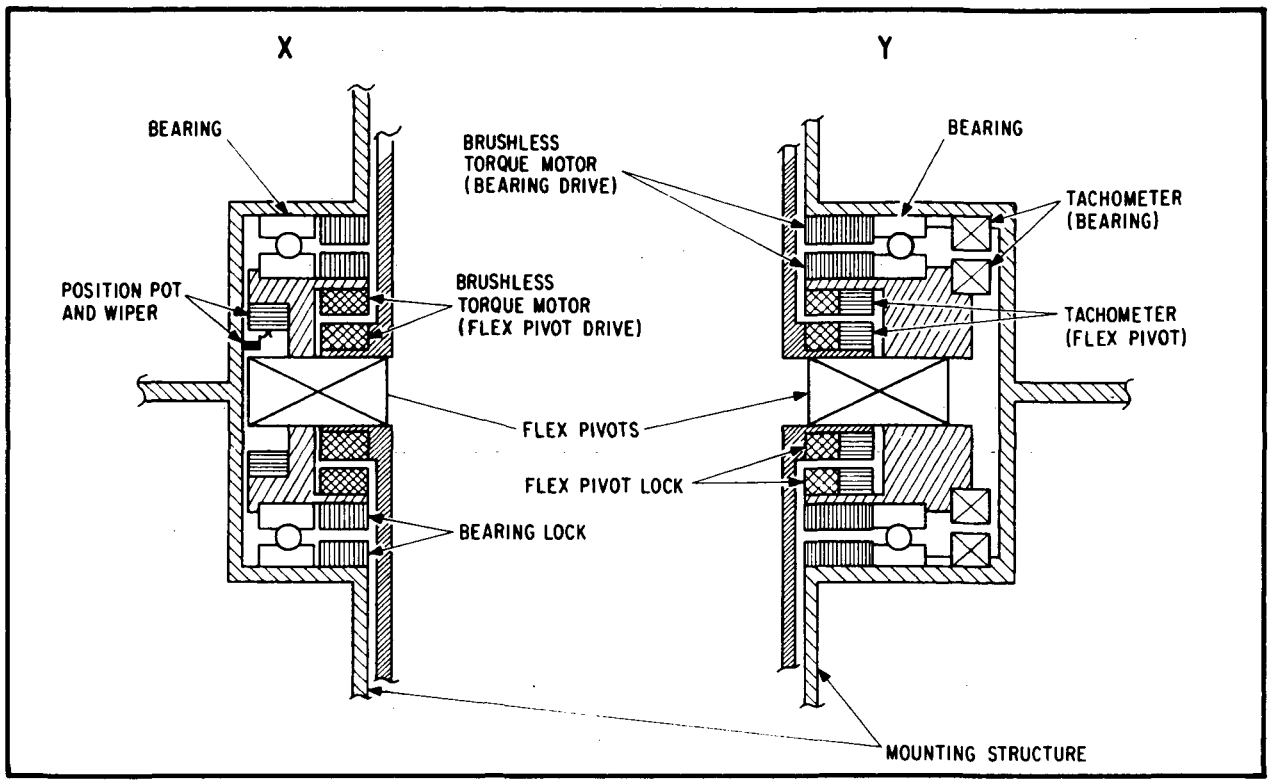

Figure 8-1 Tertiary Mirror Gimbal Conceptual Layout

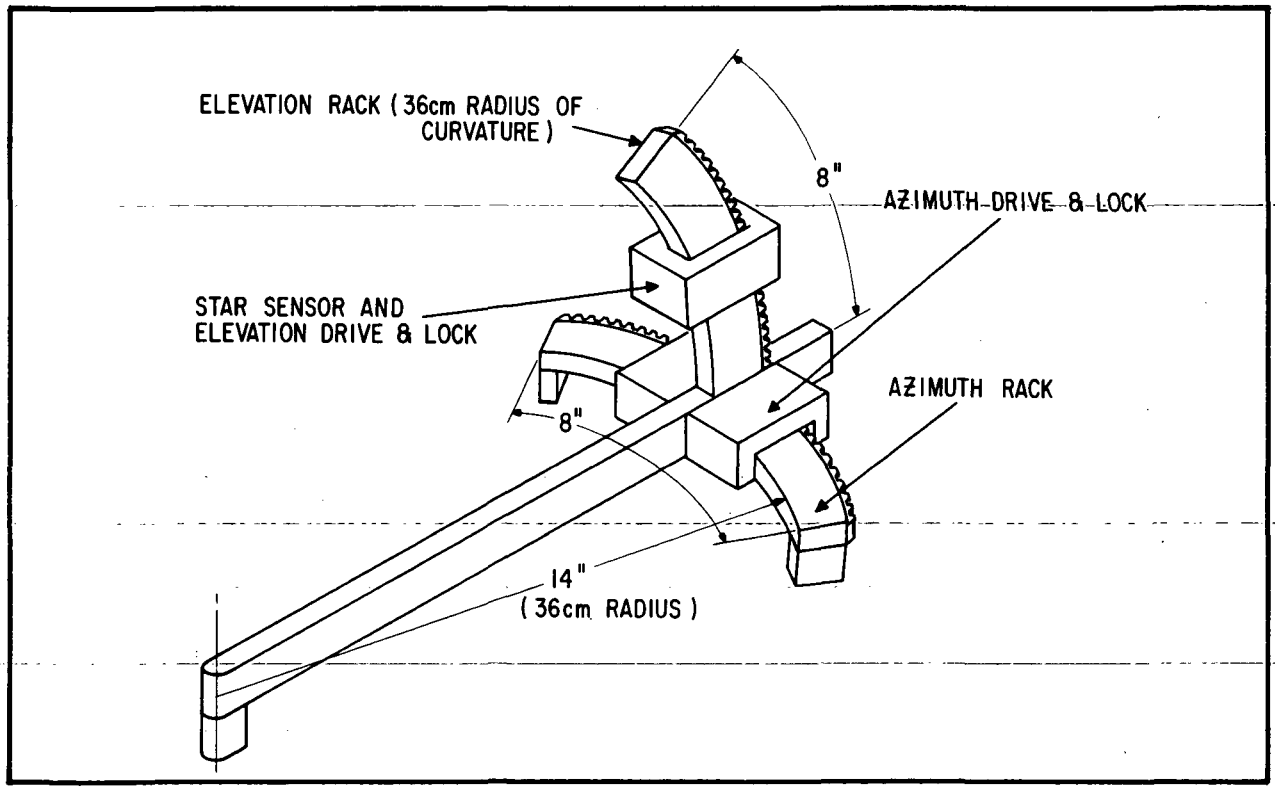

Figure 8-2 Fine Sensor Drive Mechanism Conceptual Layout

8.5 EXTENDED STUDY AREAS

As a result of this study certain areas have been identified where further study is recommended. The AOS study has resulted in a laboratory concept and has identified and defined the basic parameters for a preliminary design. The areas of preliminary design that have not been fully explored and must be examined before the AOS concept is committed are discussed in the following sections.

8.5.1 Filter Wheel Mechanization

The requirement for a filter has been only briefly examined, although such a subsystem probably will be required to more fully complete the AOS. The need for this subsystem must be established and then a concept developed for its implementation.

8.5.2 Optical Bench Mechanization

The feasibility of an optical bench as described in Section 10 has been established by this study. However, implementation of this concept needs further examination, and this must be done before airlock design can commence. The optical bench has been identified as a major AOS component which has not been fully defined by this study.

8.5.3 Polarization Instrumentation

If polarization experiments are to be done on the SAL, further study is required to conceptually define the mounting at the telescope prime focus (i.e. at the rear of the telescope operating without a tertiary mirror). If mounting in the airlock is desired, the study should define the degree of polarization error that can be tolerated as a result of the testing mirror and possibly the airlock window.

8.5.4 Fine Sensor Mount

The AOS study has presented only one concept for mounting the fine sensor and moving it in the spherical focal plane. Mounting and positioning methods should be examined further.

8.5.5 Pointing and Stabilization

The AOS study has presented in detail a pointing and stabilization method. It is felt that this approach will be functional, but due to the lack of shuttle vibrational and dynamic performance parameters the model used is not complete. When such data becomes available this approach should be further examined and extended into the area of brea board testing. The concept as stated herein is sound if hardware such as the accelerometer used in the model performs according to expect-ation and bearing frictions are reduced to the expected levels. These should be verified before commitment by breadboarding. In addition, it is recommended that further study be done to identify the coordinat transformations required to position the optical bench in roll. Due to the economic limits of this study, image roll correction was not fully investigated.

8.5.6 Telescope Baffling

The AOS study, because of the initial ground rules, has not attempted to define the baffling required. Baffle definition is highly dependen on mission inputs, which were not known. When they are known an investigation into required baffling should be made.

8.5.7 Radiation

The effects of radiation on films, emulsions, and active detector surfaces was totally ignored in this study. This problem also is mission-dependent and should be further investigated.

8.5.8 Contamination

The effects of contamination on optical surfaces were given a cursory examination in this study. Further examination should be made when final RCS propellants and their location as well as other sources of contamination from the shuttle have been defined.

8.5.9 Orbital Parameters

The missions flown by the AOS will undoubtedly be varied. Each mission will require examination to define the optimum orbit for the shuttle. Observing time, for example, may be drastically affected by orbit selection. Radiation, the effect of the South Atlantic anomaly, etc. are all mission-dependent data that are a function of the orbit chosen.

8.5.10 Secondary Mirror Mount

The choice of operating the telescope in either the f/10 or f/25 configuration is a mission-dependent decision. If it must operate at both f/10 and f/25 during a single mission, a means of automatically changing secondary mirrors must be devised. Further study is necessarry to determine the required mechanization.

Possible mechanisms are a "flippable" mount or an insertion mount. Particular attention must be given to alignment and thermal tolerancing during design of the mechanism.

8.6 AOS GROWTH CAPABILITY

The AOS was baselined to be flown in a Sortie Lab module, that may not be available for early shuttle missions. Should this occur it is still possible that the AOS, in an abbreviated design, could be

flown interfacing directly with the shuttle. The extent of abbreviation will depend largely on the space available within the orbiter cabin.

The AOS provides for a modular set of basic instruments to be mounted at the telescope focal plane, but access to the focal plane is not limited to this set. With time and follow-on funding, other instrument systems such as special purpose systems should be considered for addition to the AOS. These could include instruments such as those with special purpose detectors or instruments for polarization studies that would mount at the telescope Cassegrain focus.

The total SAL capability can be obtained by ongoing implementation rather than by delivery of all instrumentation by a single date. This approach, coupled with the SAL concept of limiting design to current technological levels, reduces peak funding and total cost.

In the spirit of reducing total costs of scientific operations in space, the following suggestion, while outside the scope of this study, should be considered. Scientific disciplines (such as astronomy) which require attachment of dedicated instrumentation to and perhaps through a laboratory wall might be assigned a dedicated bulkhead which actually constitutes the (interchangeable) aft wall of the laboratory. In this way a very few laboratories can be used with many scientific payloads, without interference among those disciplines which have special requirements for equipment such as telescope mounting gimbals and airlocks.

REFERENCES

1. Space Shuttle Program Overview, MSC, 8 Nov 1972.

Section 9
OPERATION

The successful operation of the AOS is dependent on the presence of payload and mission specialists. Since the mission duration is to be over extended periods of time, a crew of four such specialists will be required. Two will be in attendance at all times while at least one additional person is in rotation. A schedule of alternating four-hour rest periods with eight-hour attendance periods will permit a continuous operation with two men. The effects of such a schedule on each man should be further evaluated before implementation.

9.1 OPERATION

9.1.1 Acquisition

Target acquisition is predicated on having the payload or mission specialist as part of the servo loop. He will execute the following procedure to acquire the desired target:

a. Activate the system and remove all launch locks on the gimbal axes.

b. Determine the need for stellar source calibration. If required, orient the telescope toward the calibration source and perform the calibration.

c. Select either the calibration source or the offset guide star coordinate data and enter it into the computer from the pointing control and monitoring panel.

d. Command the telescope to slew to the guide star.

e. Select the offset data required to offset the telescope from the guide star to the target source and enter this into the coarse position servo logs. This entry is made via the pointing control and monitoring panel.

f. View the telescope focal plane either through the optical viewer or on the scan converter display on the experiment data display panel.

g. Using the "joy stick" control on the pointing control and monitoring panel and visual observation of the image at the focal plane, precisely position the tertiary mirror servo to place the image at the spectrograph entrance.

h. Initiate automatic tracking.

9.1.2 Instrument Operation

The payload specialist will install the desired instrument on the optical bench. After closing the airlock and completing the acquisition phase, he will align and focus the instrument and telescope by positioning the optical bench and monitoring the output of the instrument on the experiment data display panel.

He will then monitor and evaluate the data as necessary until it is determined that the desired result has been achieved or another target is in order.

9.2 MAINTENANCE

On-board maintenance during a mission hopefully will be at a minimum. However, the payload and mission specialists should be able to do minor repairs and alignments. They should be provided with a minimum set of tools and instruments for necessary rework. They will have equipment for minor cleaning operations, quick-look developing, and tools for fastening the instruments in place. Any disorder that is extensive in nature should not be repaired on board the spacecraft.

9.3 DATA HANDLING

The payload specialist will be responsible for the recording and stowage of all data gathered during the flight. When he has determined that the instrument is operating properly, he will activate the shuttle-provided tape recorder or will change sensitive plates as needed.

Prior to re-entry, he will secure all systems and lock all gimbals. He will store all equipment, plates, and data tapes accumulated during the flight.

Page Intentionally Left Blank

Section 10
AOS PERIPHERAL EQUIPMENT

10.1 POINTER CONTROL AND MONITORING PANEL

Operation of the three servo control mechanisms of the AOS will be done from this panel. The panel will have either keyboard, tape, or card computer access capability for programming target coordinate information into the computer. The panel will have either digital or analog displays of the error signals from each axis as well as a display to which the various housekeeping functions can be individually switched and monitored.

The panel will have a "joy stick" or some similar control that will be used as a high-resolution control to permit the payload specialist to precisely position the telescope optical axis (via tertiary mirror position and telescope coarse servo loop). This will be done while viewing the output of the focal plane viewer (SEC vidicon system) located on the experiment data display panel.

Located on this panel also will be the main power control and monitoring circuits for the telescope. Power delivered to the telescope heaters, control servos, and associated electronics will be monitored to detect malfunctions.

It is anticipated that each telescope gimbal axis must be locked during launch and recovery and during a change in shuttle attitude. The locks will be electrically actuated and controlled from the pointer control and monitoring panel.

10.2 EXPERIMENT DATA DISPLAY PANEL

The payload specialist will be able to monitor data output and view

the field at the telescope focal plane on the experiment data display panel. The panel will be a composite of commercial display monitors supported by specifically designed interface electronics. It will consist primarily of a scan conversion system and a storage tube display.

The scan converter will take the output from either the SEC vidicon used to view the telescope focal plane or the SEC vidicons used to collect data. Scan conversion will be required because the SEC scan rate is expected to be much slower than the rate required for visual viewing on the display. This is especially true if long SEC integration times are needed while observing faint objects in the field.

The storage tube display will be used to display data, in pulse height form, of the line spectra at the exit of the imaging spectrograph mounted on the optical bench.

It appears that both the scan conversion system and the storage tube display system can be of commercial quality, appropriately modified to withstand the shuttle environment. This design approach will reduce the overall cost.

10.3 OPTICAL BENCH

The optical bench (Figure 10-1) is the platform on which the desired instrument is mounted. It will have the capability of being remotely positioned to align the entrance aperture and also to position the aperture precisely at the telescope focal plane. It is a three-point mounted bench positioned by motor-driven lead screws. Mechanical registration surfaces will be provided for mechanical positioning of the experiment packages and final positioning will be

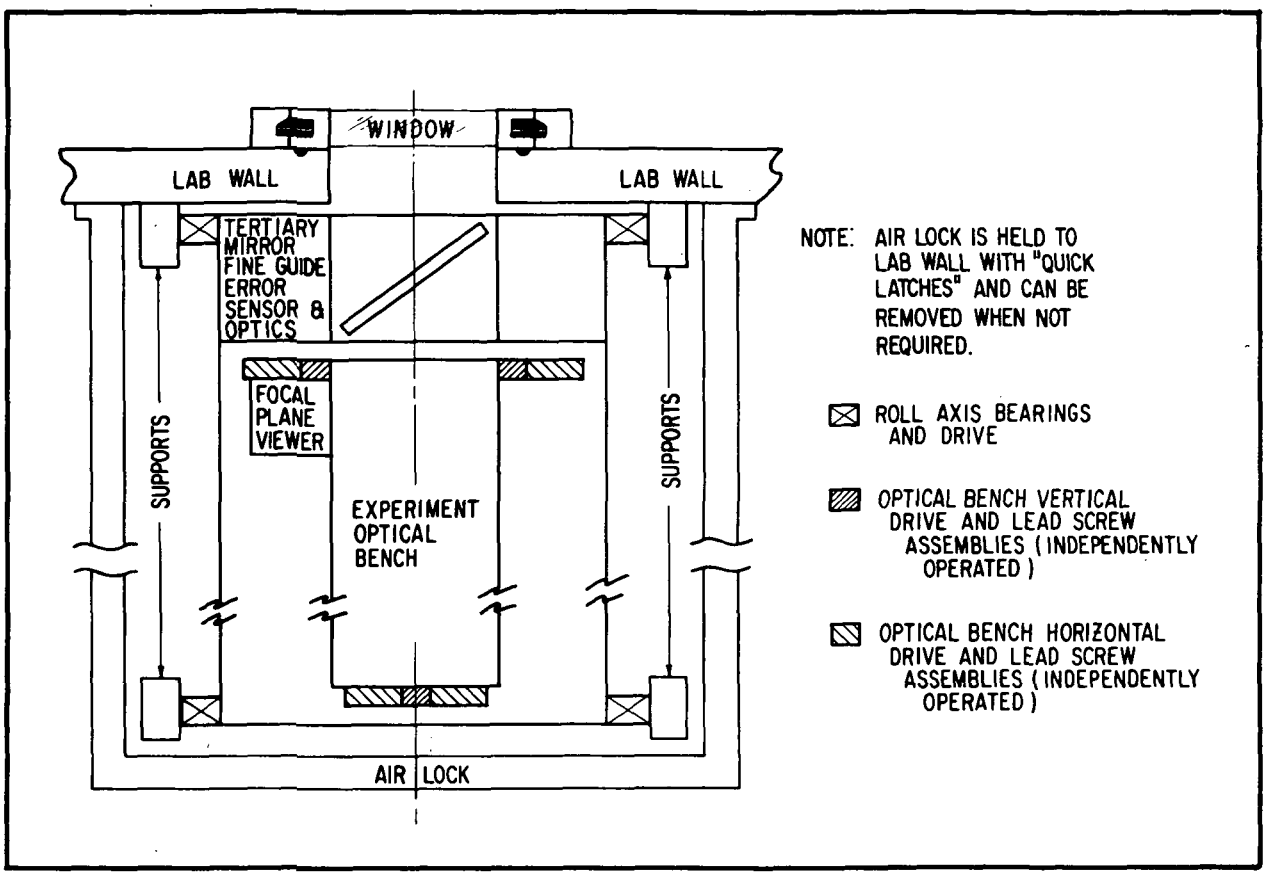

Figure 10-1 Optical Bench Assembly

made by moving the bench with its various drives and monitoring the data display panel. Position readout encoders on each drive assembly will be monitored on the optical bench control panel.

The horizontal drive assembly will permit motion in the horizontal direction to be either translational (all horizontal drive assemblies operating simultaneously) or rotational (independent operation). Translation motion will be used for focal plane positioning and entrance aperture alignment (two orthogonal directions translation). Rotational motion will permit experiment optical axis alignment with the telescope optical axis.

The vertical drive assembly will permit motion in the vertical direction to be either translation (all vertical drive assemblies operating simultaneously) or rotational (independent operation). Translation motion will be used to position the entrance aperture on the focal point of the target of interest and rotational motion will be used to align the experiment optical axis to the telescope optical axis.

The entire optical bench assembly will be mounted inside a limited-motion set of roll bearings. The roll motion will be servo controlled and will have the capability of roll null positioning by insertion of bias into the roll control loop. This will permit the payload specialist to set in the desired roll position and that position will be automatically maintained. Error signals for the roll control servo will be derived from a star tracker that is orthogonally mounted to the telescope axis.

10.4 FOCAL PLANE VIEWER

The focal plane viewer is an SEC vidicon detector with a folding mirror that can be inserted by remote control into the optical path. The output of the SEC is monitored on the experiment data display panel. The SEC vidicon will have imbedded on its sensitive surface fiducial markings that will be precisely related to the optical bench registration surfaces. Once image positioning has been completed as determined from the display, the folding mirror will be withdrawn from the optical path permitting energy to be delivered to the experiment.

10.5 AIRLOCK

The entire optical bench assembly will be contained within the airlock, envisioned to be a cylinder approximately 3 1/2 feet in diameter and 5 feet long.

Optical access to the airlock is to be through a quartz window that can be remotely opened from the optical bench control panel. Experiment access is to be through a sealing door in the side of the cylinder.

The airlock will mount to the aft bulkhead of the sortie lab. This bulkhead will be designed to mount the telescope coarse azimuth drive assembly outside the sortie lab and the airlock inside the lab.

The airlock is considered to be a growth element of the AOS. By limiting the spectral range to the quartz window cutoff, the AOS could operate without the airlock until it was economically feasible to add the airlock.

10.6 OPTICAL BENCH CONTROL PANEL

The optical bench control panel will house all the actuator switches and readout displays required to monitor the position of each drive assembly on the optical bench. It will also house all the controls required to operate the airlock.

Control of the optical bench will be accomplished by joint operation with the data display panel. The payload specialist will receive visual inputs from the data display panel and will make corresponding optical bench adjustments.

10.7 OTHER PERIPHERAL EQUIPMENT

It is difficult to anticipate precisely the nature and extent of additional needed equipment. However, it is expected that limited test equipment and tools will be required.

Certain basic pieces of laboratory equipment should be carried on board. These will likely be electrical test instruments, spare parts, hand tools and specialized equipment for *in situ* alignment and checkout. Further mission definition is needed to identify this equipment. It should be stored on board in the peripheral equipment storage rack.

Section 11
AOS SCHEDULE AND COST

The AOS program schedule and cost estimates presented here include Phase B - Definition, Phase C - Design, and Phase D - Fabrication and Test.

11.1 PROGRAM PLANNING AND SCHEDULE

The total program including phases B through D, as shown in Figure 11-1, extends over a 44.5 month period. Of this total period, 10.5 months are required for phase B and 16 months for phase C, with the fabrication and test (phase D) of the AOS system hardware extending over a two year period. Based upon an assumed October 1, 1974, authority to proceed on phase B, we anticipate the following major milestone schedule:

Preliminary Requirements Review*	December 2, 1974
Preliminary Design Review*	May 14, 1975
Phase C Authority to Proceed	June 2, 1975
Critical Design Review*	June 9, 1976
Phase D Authority to Proceed	June 11, 1976
High Fidelity Training Model Delivery	December 15, 1976
Flight/Prototype Qualification Complete	October 19, 1977
Flight/Prototype Refurbishment Complete	January 6, 1978
Flight/Prototype System Delivery	March 3, 1978

*It is recommended that the major reviews, preliminary requirements, preliminary design, and critical design, be held at the contractor's facility to minimize total program cost.

SCHEDULE - ASTRONOMICAL OBSERVATORY FOR SHUTTLE

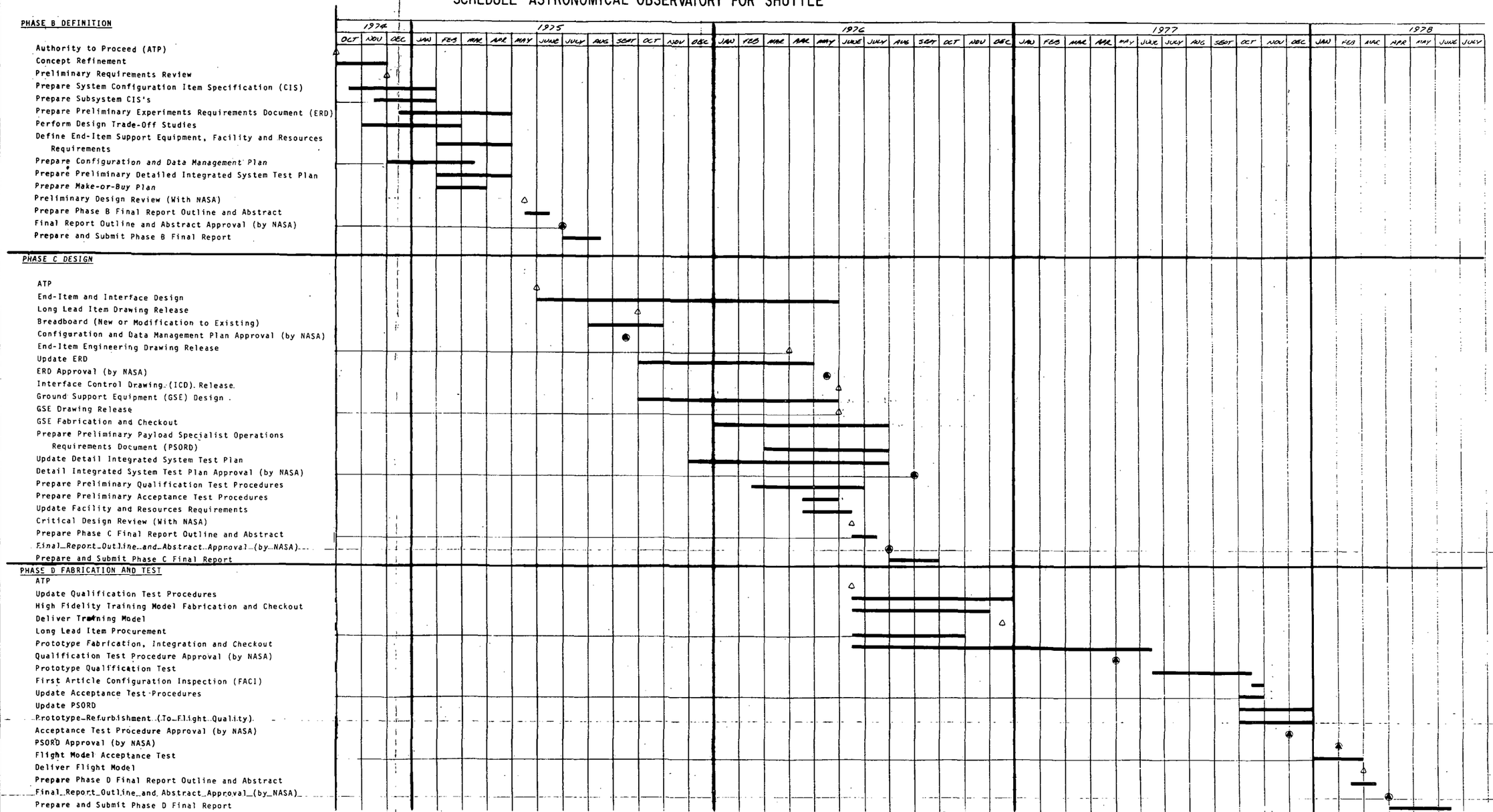

Figure 11-1 Program Schedule

11.1.1 Phase B - Definition

Program, system and subsystem definition will occur during Phase B. System concepts derived during this phase A study will be refined, thus forming the basis for the system and subsystem and item configuration specifications. Interface and experiment requirements defined during phase B will be used to prepare a preliminary experiment requirements document.

The configuration and data management, make or buy, and preliminary system test plans will be prepared during this phase. Upon completion, the configuration and data management plan will be submitted to the NASA for approval. Except for the final report, the preliminary design review essentially completes the definition phase.

11.1.2 Phase C - Design

Detail design of each end item of the AOS system will be completed with the engineering drawing release scheduled to occur 10 months after the start of this phase. Interface control drawing and ground support equipment (GSE) drawing release are scheduled two months later.

Fabrication and checkout of the GSE has been scheduled during this phase so that it can be ready for use as test equipment during the fabrication and test (phase D) of the end item hardware. Design of the GSE with this objective in mind is expected to result in significant cost savings, by avoiding duplication of test equipment where possible.

Documents and plans prepared during this phase include the preliminary payload specialist operations requirements document and preliminary qualification and acceptance test procedures.

The major milestone of this phase is successful completion of the critical design review. The final report describing the activities and results of this phase will be submitted September 30, 1976.

11.1.3 Phase D - Fabrication and Test

Authority to proceed with this phase is scheduled to occur simultaneously with completion of the critical design review. The major milestone of this phase will be reached with delivery of the refurbished flight/prototype system on March 3, 1978. The refurbishment requirement is discussed in a subsequent paragraph.

A high fidelity training model of selected major components of the AOS system would be fabricated of wood and metal from released engineering drawings. It would be identical in form, fit, weight and center of gravity to the flight/prototype end item hardware. Electrical connectors, panel switches, knobs and selected indicators that will be used on the flight hardware will be provided on the training model. In certain instances, it may be desirable to provide active indication on the panel with actuation of certain panel controls. It is expected that this training model would be beneficial for several reasons: fit check, human factors, and its availability 14.5 months before system hardware delivery.

Four months have been allocated for informal functional, vibration, thermal, and acoustic prequalification testing and for formal qualification testing. Program planning has been predicated on the premise that the AOS hardware will be qualified on a system basis rather than on a subsystem component level. Due to system volume requirements, use of the NASA environmental test or other aerospace contractor test facilities will be required.

To minimize total program cost, it is recommended that the prototype hardware, after successful completion of the qualification testing, be refurbished as the flight hardware. The refurbishment effort will be completed prior to flight acceptance testing, which is scheduled for completion on March 3, 1978. The final report which will be submitted on June 15, 1978, will bring the fabrication and test phase to a close. It is expected that prior to this time contractor and NASA personnel will have discussed arrangements for post-delivery (phase E) support. This report does not include estimates for any phase E activity.

11.2 PROGRAM COST ESTIMATES

The basis for the cost estimates provided herein is the work breakdown structure (WBS) as shown in Figure 11-2. The WBS includes phases B, C, and D and depicts work packages to the third level where necessary.

To enable the reader to get an idea of the AOS program cost, the WBS first level sub-total costs and total estimated cost are presented in Table 11-1. For convenience, the table is arranged so that the estimated cost for each phase can be easily identified.

To further reduce costs, only one each echelle spectrograph, imaging spectrograph, and Lyman spectrometer (all f/10) have been specified for the initial procurement. The total spectral range of each instrument is achieved by interchanging gratings (in flight if desired).

PHASE B DEFINITION

System Engineering Definition & Management (1000)	System Engineering Definition (1100)	System Definition (1110)	• System Performance Requirements • Power Systems • Packaging • Interface • Command & Data Management
		Analysis (1120)	• Tradeoff • Stress • Mass Properties • Thermal • Material & Contamination Control
	Program Management and Administration (1200)	Program Management (1210)	
		Administration Support (1220)	
		Configuration & Data Management (1230)	• Configuration Item Spec (CIS) • Experiment Requirements Doc. (ERD) • Configuration Management Plan • Reliability Plan • Final Report
		Publications Support (1240)	
Subsystem Definition (2000)	Telescope Stab. & Control (2100)	Analysis (2110)	
		Electrical (2120)	
		Mechanical (2130)	
	Tertiary Mirror Control (2200)	Analysis (2210)	
		Electrical (2220)	
		Mechanical (2230)	
	Optical Bench Control (2300)	Analysis (2310)	
		Electrical (2320)	
		Mechanical (2330)	
	Echelle Spectrograph (2400)	Optics (2410)	
		Electronics (2420)	• Logic • Housekeeping • Power Cond. & Distribution • Control & Data Mgmt.
		Mechanical (2430)	
	Imaging Spectrograph (2500)	Optics (2510	
		Electronics (2520)	• Logic • Housekeeping • Power Cond. & Distribution • Control & Data Mgmt.
		Mechanical (2530)	
	Lyman∝Spectrograph (2600)	Optics (2610)	
		Electronics (2620)	• Logic • Housekeeping • Power Cond. & Distribution • Control & Data Mgmt.
		Mechanical (2630)	
	Peripheral Equip. (2700)	Display (2710)	
		Optical Bench Control (2720)	
		Pointing & Stab. Monitor (2730)	
		Special Align. & Tools (2740)	
		Special Test Equip. (2750)	
		Mechanical (2760)	
	Telescope (2800)	Optics (2810)	• Primary Mirror • Secondary Mirror • Tertiary Mirror
		Alignment (2820)	
		Mechanical (2830)	
	Sensors (2900)	Coarse Star (2910)	
		Fine Guide Error(2920)	
		Roll Star (2930)	

PHASE C DESIGN

System Engineering Design & Mgmt.(3000)	System Engineering Design (3100)	System Design (3110)	• Power Cond. & Distribution • Packaging • Interface Coordination • Command & Data Management • Stress • Mass Properties • Thermal • Materials & Contamination Control • EMC • GSE Software
		Analysis (3120)	
		Reliability & Safety (3130)	
	Program Management & Administration(3200)	Program Mgmt.(3210)	
		Administrative Support (3220)	
		Config. & Data Mgmt. (3230)	• CIS's • ERD • PSORD • QTP • ATP • Final Report
		Publications Support (3240)	
Subsystem Design (4000)	Telescope Stab. & Control (4100)	Analysis (4110)	
		Electrical (4120)	
		Mechanical (4130)	
		Breadboard (4140)	
	Tertiary Mirror Control (4200)	Analysis (4210)	
		Electrical (4220)	
		Mechanical (4230)	
		Breadboard (4240)	
	Optical Bench Control (4300)	Analysis (4310)	
		Electrical (4320)	
		Mechanical (4330)	
		Breadboard (4340)	
	Echelle Spectrograph (4400)	Optics (4410)	
		Electronics (4420)	• Logic • Housekeeping • Power Cond. & Distribution • Control & Data Management
		Mechanical (4430)	
	Imaging Spectrograph (4500)	Optics (4510)	
		Electronics (4520)	• Logic • Housekeeping • Power Cond. & Distribution • Control & Data Management
		Mechanical (4530)	
	Lyman∝Spectrograph (4600)	Optics (4610)	
		Electronics (4620)	• Logic • Housekeeping • Power Cond. & Distribution • Control & Data Management
		Mechanical (4630)	
	Peripheral Equip. (4700)	Experiment Data Display Panel(4710)	• Electrical (4711) • Mechanical (4712)
		Optical Bench Control Panel (4720)	• Electrical (4721) • Mechanical (4722)
		Pointing Control & Monitor Panel(7730)	• Electrical (4731) • Mechanical (4732)
		Special Align. & Tools (4740)	
		Special Test Equip. (4750)	
	Telescope (4800)	Optics (4810)	• Primary Mirror • Secondary Mirror • Tertiary Mirror
		Alignment (4820)	
		Mechanical (4830)	
	Sensors(4900)	Coarse Star (4910)	
		Fine Guide Error(4920)	
		Roll Star (4930)	

PHASE D FABRICATION & TEST

Ground Support Equipment (5000)	GSE Design (5100)	Special Tooling (5110)	
		Special Test Equipment (5120)	
		Handling Fixtures (5130)	
		Shipping Containers (5140)	
		Breadboard (5150)	
	GSE Fabrication & Checkout (5200)	Special Tooling (5210)	
		Special Test Equipment (5220)	
		Handling Fixtures (5230)	
		Shipping Containers (5240)	
		Design Support (5250)	
		Quality Assurance (5260)	
High Fidelity Training Model (6000)	Fab & C/O (6010)		
	Design Support (6020)		
Flight/Prototype Fabrication and Test (7000)	Telescope Stab. & Control (7100)	Fabrication & C/O (7110)	
		Design Support (7120)	
		Quality Assurance (7130)	
	Tertiary Mirror Control (7200)	Fab & C/O (7210)	
		Design Support (7220)	
		Quality Assurance (7230)	
	Optical Bench Control (7300)	Fab & C/O (7310)	
		Design Support (7320)	
		Quality Assurance (7330)	
	Echelle Spectrograph (7400)	Fab & C/O (7410)	
		Design Support (7420)	
		Quality Assurance (7430)	
	Imaging Spectrograph (7500)	Fab & C/O (7510)	
		Design Support (7520)	
		Quality Assurance (7530)	
	Lyman∝Spectrograph (7600)	Fab & C/O (7610)	
		Design Support (7620)	
		Quality Assurance (7630)	
	Peripheral Equipment (7700)	Experiment Data Display Panel (7710)	• Fab & Checkout • Design Support • Quality Assurance
		Optical Bench Control Panel (7720)	• Fab & Checkout • Design Support • Quality Assurance
		Pointing Control & Monitor Panel (7730)	• Fab & Checkout • Design Support • Quality Assurance
		Special Tods & Test Equipment (7740)	• Fab & Checkout • Design Support • Quality Assurance
	Telescope (7800)	Fab & C/O (7810)	
		Design Support(7820)	
		Quality Assurance (7830)	
	Sensors (7900)	Coarse Star(7910)	• Fab & Checkout • Design Support • Quality Assurance
		Fine Guide Error(7920)	• Fab & Checkout • Design Support • Quality Assurance
		Roll Star (7930)	• Fab & Checkout • Design Support • Quality Assurance
Flight/Prototype Integration & Test (8000)	System Integration (8100)	Integration (8110)	
		Checkout (8120)	
		Design Support(8130)	
	System Pre-Qual.Test (8200)	Vibration (8210)	
		Thermal (8220)	
		Acoustic(Subcontract)(8230)	
	Qualification Test (8300)	Qual Test Performance(8310)	
		Design Support (8320)	
		Production Support(8330)	
		Quality Assurance(8340)	
Flight/Prototype Refurbishment (9000)	Design Support(9100)		
	Production (9200)	Refurbish Activity(9210)	
		Acceptance Test (9220)	
		Quality Assurance(9230)	

Figure 11-2 Work Breakdown Structur

Table 11-1

AOS PROGRAM ESTIMATED COST

Program Phase	WBS Level	WBS Level Description	Estimated Cost	Phase Subtotal
B	1000	System Engineering Definition & Management	225,200	
	2000	Subsystem Definition	345,300	570,500
C	3000	System Engineering Design & Management	408,300	
	4000	Subsystem Design	1,028,000	
	5000	Ground Support Equipment	127,300	
	6000	High Fidelity Training Model	36,200	1,599,800
D	7000	Flight/Prototype Fabrication & Test	4,542,500	
	8000	Flight/Prototype Integration & Test	609,100	
	9000	Flight/Prototype Refurbishment	312,400	5,464,000
		Total Estimated Cost		7,634,300